INFORMATION TO USERS

This manuscript has been reproduced from the microfilm master. UMI films the text directly from the original or copy submitted. Thus, some thesis and dissertation copies are in typewriter face, while others may be from any type of computer printer.

The quality of this reproduction is dependent upon the quality of the copy submitted. Broken or indistinct print, colored or poor quality illustrations and photographs, print bleedthrough, substandard margins, and improper alignment can adversely affect reproduction.

In the unlikely event that the author did not send UMI a complete manuscript and there are missing pages, these will be noted. Also, if unauthorized copyright material had to be removed, a note will indicate the deletion.

Oversize materials (e.g., maps, drawings, charts) are reproduced by sectioning the original, beginning at the upper left-hand corner and continuing from left to right in equal sections with small overlaps. Each original is also photographed in one exposure and is included in reduced form at the back of the book.

Photographs included in the original manuscript have been reproduced xerographically in this copy. Higher quality 6" x 9" black and white photographic prints are available for any photographs or illustrations appearing in this copy for an additional charge. Contact UMI directly to order.

UMI

A Bell & Howell Information Company
300 North Zeeb Road, Ann Arbor, MI 48106-1346 USA
313/761-4700 800/521-0600

Reproduced with permission of the copyright owner. Further reproduction prohibited without permission.

University of California, Santa Barbara

Millimeter-Wave On-Wafer Waveform and Network Measurements Using Active Probes

A Dissertation submitted in partial satisfaction
of the requirements for the degree of

Doctor of Philosophy
in
Electrical and Computer Engineering
by
Ruai Yong Yu

Committee in charge:
Professor Mark Rodwell, Chairperson
Professor John Bowers
Professor Steve Long
Professor Umesh Mishra

October 1994
(May 1995)

UMI Number: 9542057

UMI

300 North Zeeb Road
Ann Arbor, MI 48103

The Dissertation of Ruai Yong Yu is approved

Stephen I. Long

John Bow

Committee Chairperson

October 1994

Acknowledgments

I would like to thank my thesis advisor professor Mark Rodwell who has always been inspirational and encouraging during the course of this thesis project. His exceptional technical insight into the subject matter is indispensable to the success of the project. I would also like to thank other committee members, professors John Bower, Steve Long, and Umesh Mishra, for their invaluable guidance and constant encouragement.

I am indebted to my colleagues in the research group: Michael Case, Masayuki Kamagawa, Joe Pusl, Eric Carmen, Yoshiyuki Konishi, Kirk Gibony, Scott Allen, Madukar Reddy, Uddullak Batachaya, Raja Pullela, and Bipul Agarwal. The completion of the thesis project would not have been possible without their help and support. I would also like to extend my gratitude to people from other research groups who have contributed to the project: Allen Mar and Tom Reynolds from professor Bower's group, and Rob Lynch and Rudy Stuber from the machine shops.

I would like to acknowledge the financial support from all the funding agencies of this project. These include: the National Science Foundation, the Air Force Office of Scientific Research, Hughes Aircraft Company, and the Wiltron Company.

Finally, my special thank goes to my wife Monique, whose understanding, patience, and continuos support have given me the courage and strength necessary to complete this difficult journey.

VITA

January 7, 1964:	Born, Guangzhou, The People's Republic of China
December 1988:	B.S.E.E., San Francisco State University
June 1988 - Sept. 1989:	Dessign Engineer, Ampex Corporation
March 1991:	M.S., Electrical Engineering, University of California, Santa Barbara
Oct. 1989 - Jan. 1994:	Research Assistant, Electrical and Computer Engineering Department, University of California, Santa Barbara

PUBLICATIONS

1. Ruai Y. Yu, Michael Case, Masayuki Kamegawa, Mani Sundaram, M.J.W. Rodwell, and A.C. Gossard; "275 GHz 3–Mask Integrated GaAs Sampling Circuit." Electronics Letters, vol. 26, no. 13, June 21, 1990, pp. 949–951.

2. Michael Case, Ruai Y. Yu, Masayuki Kamegawa, Mani Sundaram, M.J.W. Rodwell, and A.C. Gossard; "Accurate 225 GHz Sampling Circuit Implemented in a 3–Mask Process." IEEE Device Research Conference, Santa Barbara, CA, June 25–27, 1990.

3. Michael Case, Masayuki Kamegawa, Ruai Y. Yu, Kirk Giboney, M.J.W. Rodwell, J. Bowers, and Jeff Franklin; "62.5 ps to 5.5 ps Soliton Compression on a Monolithic Nonlinear Transmission Line." IEEE Device Research Conference, Santa Barbara, CA, June 25–27, 1990.

4. Michael Case, Masayuki Kamegawa, Ruai Y. Yu, M.J.W. Rodwell, and Jeff Franklin; "Impulse Compression Using Soliton Effects in a Monolithic GaAs Circuit." Applied Physics Letters, vol. 58, no. 2, January 14, 1991, pp. 173–175.

5. Eric Carman, Kirk Giboney, Michael Case, Masayuki Kamegawa, Ruai Y. Yu, Kathryn Abe, M.J.W. Rodwell, and Jeff Franklin; "28–39 GHz Distributed Harmonic Generation on a Soliton Nonlinear Transmission Line." IEEE Microwave and Guided-Wave Letters, vol. 1, no. 2, February 1991, pp. 28–31.

6. Michael Case, Eric Carman, Masayuki Kamegawa, Kirk Giboney, Ruai Y. Yu, Kathryn Abe, M.J.W. Rodwell, and Jeff Franklin; "Impulse Generation and Frequency Multiplication Using Soliton Effects in Monolithic GaAs Circuits." IEEE/OSA Topical Meeting on Picosecond Electronics and Optoelectronics, Salt Lake City, Utah, March 13–15, 1991.

7. Masayuki Kamegawa, Kirk Giboney, Judy Karin, Michael Case, Ruai Y. Yu, M.J.W. Rodwell, and J.E. Bowers; "Picosecond GaAs Photodetector Monolithically Integrated with a High Speed Sampling Circuit." IEEE/OSA Topical Meeting on Picosecond Electronics and Optoelectronics, Salt Lake City, Utah, March 13–15, 1991.

8. M.J.W. Rodwell, Masayuki Kamegawa, Michael Case, Ruai Y. Yu, Kirk Giboney, Eric Carman, Judy Karin, Scott Allen, and Jeff Franklin; "Nonlinear Transmission Lines and their Applications in Picosecond Optoelectronic and Electronic Measurements." Engineering Foundation Conference on High Frequency/High Speed Optoelectronics, Palm Beach, Florida, March 18–22, 1991.

9. Masayuki Kamegawa, Kirk Giboney, Judy Karin, Michael Case, Ruai Y. Yu, M.J.W. Rodwell, and J.E. Bowers; "Picosecond GaAs Monolithic Optoelectronic Sampling Circuit." IEEE Photonics Technology Letters, vol. 3, no. 6, June 1991, pp. 567–569.

10. M.J.W. Rodwell, Masayuki Kamegawa, Ruai Y. Yu, Michael Case, Eric Carman, and Kirk Giboney; "GaAs Nonlinear Transmission Lines for Picosecond Pulse Generation and Millimeter-Wave Sampling." IEEE Transactions on Microwave Theory and Techniques, vol. 39, no. 7, July 1991, pp. 1194–1204.

11. Masayuki Kamegawa, Yoshiyuki Konishi, Michael Case, Ruai Y. Yu, and M.J.W. Rodwell; "Coherent Broadband Millimeter-Wave Spectroscopy Using Monolithic GaAs Circuits." LEOS Summer Topical Meeting on Optical Millimeter-Wave Interactions, Newport Beach, CA, July 24–26, 1991.

12. Ruai Y. Yu, Masayuki Kamegawa, Michael Case, M.J.W. Rodwell, and Jeff Franklin; "A < 2.5 ps Time-Domain Reflectometer for mm-Wave Network Analysis." IEEE/Cornell Conference on Advanced Concepts in High Speed Semiconductor Devices and Circuits, Cornell, NY, August, 1991.

13. Ruai Y. Yu, Masayuki Kamegawa, Michael Case, M.J.W. Rodwell, and Jeff Franklin; "A 2.3 ps Time-Domain Reflectometer for Millimeter-Wave Network Analysis." IEEE Microwave and Guided-Wave Letters, vol. 1, no. 11, Nov. 1991, pp. 334–336.

14. Yoshiyuki Konishi, Masayuki Kamegawa, Michael Case, Ruai Y. Yu, M.J.W. Rodwell, and D.B. Rutledge; "Broadband Millimeter-Wave GaAs Transmitters and Receivers Using Planar Bow-Tie Antennas." NASA Symposium on Space Terahertz Technology, 1992.

15. M.J.W. Rodwell, Scott Allen, Masayuki Kamegawa, Kirk. Giboney, Judy Karin, Michael Case, Ruai Y. Yu, and J.E. Bowers; "Picosecond Photodetectors Monolithically Integrated with High-Speed Sampling Circuits." AFCEA DOD Fiber Optics Conference, March 24–27, 1992

16. Eric Carman, Michael Case, Masayuki Kamegawa, Ruai Y. Yu, and M.J.W. Rodwell; "V-Band and W-Band Broadband, Monolithic Distributed Frequency Multipliers." IEEE/MTT International Microwave Symposium, Albuquerque New Mexico, June 2–4, 1992.

17. Eric Carman, Michael Case, Masayuki Kamegawa, Ruai Y. Yu, Kirk Giboney, and M.J.W. Rodwell; "Electrical Soliton Devices as >100 GHz Signal Sources." Ultrafast Phenomena VIII Conference, Antibes, France, June 8–12, 1992.

18. Michael Case, Eric Carman, Ruai Y. Yu, and M.J.W. Rodwell; "Picosecond Duration, Large-Amplitude Impulse Generation Using Electrical Soliton Effects." Applied Physics Letters, vol. 60, no. 24, June 15, 1992, pp. 3019–3021.

19. Eric Carman, Michael Case, Masayuki Kamegawa, Ruai Y. Yu, Kirk Giboney, and M.J.W. Rodwell; "V-Band and W-Band Broadband, Monolithic Distributed Frequency Multipliers." IEEE Microwave and Guided-Wave Letters, vol. 2, no. 6, June 1992, pp. 253–254.

20. Michael Case, Eric Carman, Ruai Y. Yu, and M.J.W. Rodwell; "Picosecond Duration, Large Amplitude Impulse Generation Using Electrical Soliton Effects on Monolithic GaAs Devices." IEEE Device Research Conference, Boston, MA, June 22–24, 1992.

21. Ruai Y. Yu, Joe Pusl, Yoshiyuki Konishi, Michael Case, Masayuki Kamegawa, and M.J.W. Rodwell; "A Time-Domain Millimeter-Wave Vector Network Analyzer." IEEE Microwave and Guided Wave Letters, vol. 2, no. 8, Aug. 1992, pp. 319–321.

22. Ruai Y. Yu, Joe Pusl, Yoshiyuki Konishi, Michael Case, Masayuki Kamegawa, and M.J.W. Rodwell, "8-96 GHz On-Wafer Network Analysis." IEEE GaAs IC Symposium, Miami Beach, Florida, Sept. 5–7, 1992

23. Yoshiyuki Konishi, Masayuki Kamegawa, Michael Case, Ruai Y. Yu, M.J.W. Rodwell, and D.B. Rutledge; "Picosecond Spectroscopy Using Monolithic GaAs Circuits." Applied Physics Letters, Dec. , 1992.

24. Yoshiyuki Konishi, Masayuki Kamegawa, Michael Case, Ruai Y. Yu, and M.J.W. Rodwell; "An Accurate, High Resolution 30-250 GHz Free-Space Vector Transmission Measurement System Using Monolithic GaAs ICs." The 17th International Conference on Infrared and Millimeter Waves, Pasadena, California, Dec. 14-18, 1992

25. Yoshiyuki Konishi, Masayuki Kamegawa, Michael Case, Ruai Y. Yu, and M.J.W. Rodwell; "Millimeter-Wave Free-Space Electromagnetic Measurements." Ultrafast Electronics & Optoelectronics, San Francisco, California, Jan. 25-27, 1993

26. Y. Konishi, S.T. Allen, M. Reddy, R. Yu, and M.J.W. Rodwell; "AlAs/GaAs Schottky-Collector Resonant-Tunnel-Diodes and Traveling-Wave RTD Pulse Generators." Ultrafast Electronics & Optoelectronics, San Francisco, California, Jan. 25-27, 1993

27. Ruai Y. Yu, Mahdukar Reddy, Joe Pusl, Scott Allen, Michael Case, and M.J.W. Rodwell; "Full Two-Port On-Wafer Vector Network Analysis to 120 GHz Using Active Probes." IEEE MTT-S International Microwave Symposium, Atlanta, Georgia, June 14-18, 1993

28. M.J.W. Rodwell, M. Case, R. Yu, S. Allen, M. Reddy, U. Bhattacharya, K. Giboney : "Ultrashort Pulse Generation Using Nonlinear Microwave Transmission Lines", Invited presentation during the 1993 IEEE International Microwave Symposium, Workshop on Picosecond and Femtosecond Electromagnetic Pulses: Analysis and Applications.

29. M.J.W. Rodwell, R. Yu, M. Reddy, S. Allen, M. Case, U. Bhattacharya: "mm-Wave Network Analysis using Nonlinear Transmission Lines", Invited Presentation at the 14th Biennial IEEE/Cornell University Conference on Advanced Concepts in High Speed Semiconductor Devices and Circuits, Cornell, August 2-4, 1993

30. M.J.W. Rodwell, S. Allen, M. Case, R. Yu, M. Reddy, U. Bhattacharya, K. Giboney: "GaAs Nonlinear Transmission Lines for Picosecond and Millimeter-Wave Applications" Invited presentation at the 1993 European Microwave Convention, Madrid, September 8-10.

31. R. Y. Yu, M. Reddy, J. Pusl, S.T. Allen, M.G. Case, and M.J.W. Rodwell, "Millimeter-Wave On-Wafer Waveform and Network Measurements Using Active Probes", NASA/IEEE 5th international symposium on Space Terahertz technology, Ann Arbor, Michigan, May 1994

32. M. Schlectweg, W. Reinh ert, A. Bangert, J. Braunstein, P.J. Tasker, R. Bosch, W. H. Haydl, W. Bronner, A. Hulsmann, K. Kohler, J. Seibel, R. Yu, and M.J.W. Rodwell, "High Performance MMICs in Coplanar-Waveguide Technology for Commercial V-Band and W-band applications", 1994 IEEE Microwave and Millimeter-Wave Monolithic Circuits Symposium, May 22-25, San Diego

33. M.J.W. Rodwell, R. Yu, M. Reddy, S. Allen, U. Bhattacharya, "Active Probes For On-Wafer millimeter-Wave Network Analysis", Invited Paper, IEEE Conference on Precision Electromagnetic Measurements, June 1994 , Boulder, Co.

34. Y. Konishi, M. Kamegawa , M. Case, R. Yu, S.T. Allen, and M. J. W. Rodwell, "A Broadband Free-Space Millimeter-Wave Vector Transmission Measurement System", IEEE Trans. MTT, vol. 42, No. 7, July 1994, pp. 1131-1139

35. R. Y. Yu, Y. Konishi, S.T. Allen, and M. J. W. Rodwell, "A traveling-wave resonant tunnel diode pulse generator", IEEE Microwave and Guided Wave Letters, Vol. 4, No. 7, July 1994, pp. 220-222

36. M.J.W. Rodwell, R. Yu, S. Allen, U. Bhattacharya, M. Reddy, 'Nonlinear Wave Propagation Devices for Ultrafast Electronics", Invited Paper, Conference on Ultra-Wideband Short-Pulse Electromagnetics, Weber Research Institute, Polytechnic University, Brooklyn, NY.

37. M.J.W. Rodwell, S. T. Allen, R. Y. Yu, M. G. Case, M. Reddy, E. Carman , J. Pusl, M. Kamegawa, Y. Konishi, and R. Pullela, "Active and Nonlinear Wave Propagation Devices in Ultrafast Electronics and Optoelectronics", Invited Paper, IEEE Proceedings, Vol. 82, No. 7, July 1994, pp. 1037-1058.

38. R. Y. Yu, M. Reddy, J. Pusl, S.T. Allen, M.G. Case, and M.J.W. Rodwell, "Millimeter-Wave On-Wafer Waveform and Network Measurements Using Active Probes" *To be published,* IEEE Trans. MTT, accepted August 1994.

ABSTRACT

Millimeter-Wave On-Wafer Waveform and Network Measurements
Using Active Probes
By
Ruai Y. Yu

Recent advances in III-V technology has led to successful development of transistors with maximum frequency of oscillation over 400 GHz and integrated circuits (ICs) with bandwidth in excess of 100 GHz. However, current coaxial based instrumentation bandwidth is limited to below 70 GHz; device and circuit measurements at higher frequencies can only be obtained with waveguide based instruments which have limited operation bandwidth and require extra effort with measurement setup. Non-linear transmission lines (NLTLs) permit generation of electrical transients in the order of 1 ps. This dissertation describes the theory, design, and fabrication of NLTL-based broadband instrumentation as well as measurements of high frequency integrated circuits with these instruments.

Fast electrical transients generated with NLTLs provide the strobe signals for high speed sampling circuit, resulting in sampling circuit bandwidth of 275 GHz. These fast electrical transients contain significant Fourier harmonic power, hence can be used as high frequency stimulus signal sources for device and IC characterization. Combining high-speed sampling circuits, broadband directional devices, and NLTL stimulus signal sources, GaAs integrated circuits for time-domain reflectometry and network analysis are designed and fabricated. Active probes incorporating high frequency quartz probe tips and instrument ICs show step response of 3.5 ps. Major system level limitations on measurement accuracy and reproducibility include phase noise, calibration standard accuracy, sampling circuit noise, quantization errors, and probe crosstalk. Reduction of these noise sources with careful system design allow on-wafer waveform measurements with 3 ps timing resolution and network measurements to 200 GHz.

TABLE OF CONTENTS

1. Introduction 1
  1.1 Electrical measurement techniques 2
  1.2. Optoelectronic Measurement Techniques 7
  1.3. The Active Probe Measurement System 10

2. Sampling Circuits: Design, Fabrication, and Measurements 13
  2.1 Equivalent-Time vs. Real-Time Sampling 14
  2.2 Sampling Circuit Principle of Operation 22
  2.3 The Nonlinear Transmission Line Gated Sampling Circuit 33

3. The Active Probe 57
  3.1 The Network Analyzer Integrated Circuit 60
    3.1.1 Network Analyzer IC Design and Fabrication 60
    3.1.2. Network Analyzer IC Simulation 68
    3.1.3 NWA IC Characterization 73
  3.2 The Bias Tee 77
  3.3 Probe Tip Design and Fabrication 81
  3.4 Bond Wire Connection Bandwidth 84
  3.5 Hybrid Assembly and Mechanical Design 87
  3.6 Active Probe Bandwidth Measurements 91

4. Network Analyzer System Design 94
  4.1 The Synthesizer Phase Noise 96
  4.2. Sampling Circuit Noise 101
  4.3 System Calibration 108
  4.4 Quantization Noise 112
  4.5 Probe Crosstalk 113

5. Millimeter-Wave On-Wafer Measurements 115

5.1. Waveform Measurements 116

5.2. Network Measurements 119

5.2.1 First Generation Results 122

5.2.2. Second Generation Results 125

5.2.3. Third Generation Results 131

5.3. Network Measurements With Alternative System Configurations 143

6. Summary and Future Directions 150

Bibliography 161

Appendix A. MWSPICE Netilists for the Sampling Circuits and the NWA ICs 168

Appendix B. Detailed Process Flow Sheets 171

Appendix B.1. Process Flow Sheets For Sampling Circuits and Netwok Aanlyzer ICs 171

Appendix B.2. Process flow sheets for fabrication of quartz probe tips 184

Appendix B.3. Quartz probe tipe lapping procedure 192

Appendix C. Example C Programs for System Control and Measurement De-embedding for the Active Probe Measurement System 194

Appendix D. Machine Drawings of the Active Probe System 237

LIST OF FIGURES

Figure 1.1. Operation of equivalent-time sampling techniques. 3
Figure 1.2. Block diagram of a conventional microwave network analyzer; channel 2 is identical to channel 1. 4
Figure 1.3. Block diagram of a conventional spectrum analyzer. 6
Figure 1.4. Photoconductive detector connected to a coplanar-waveguide transmission line: (a) for subpicosecond electrical pulse generation and sampling, and (b) photoconductive pulse generation circuit. 7
Figure 1.5. Pump-probe experiments: a photoconductor generates a subpicosecond impulse driving a device under test, while a second photoconductor samples the resulting output signal. 8
Figure 1.6. Conceptual diagram of the active probe. 11

Figure 2.1. Real-time sampling process: (a) time domain band-limited input signal; (b) input signal spectrum; (c) gate function in time domain; (d) gate function spectrum; (e) sampled signal in time domain; (f) sampled signal spectrum. 15
Figure 2.2. Equivalent-time sampling process: (a) band-limited input signal spectrum; (b) gate function spectrum; (c) sampled signal spectrum. 18
Figure 2.3. Gate function with finite pulse width: (a) time domain, and (b) frequency domain. 21
Figure 2.4. Circuit diagram of a 1-diode sampling bridge. 22
Figure 2.5. Operation of an ideal DC restorer circuit: (a) circuit diagram, (b) diode I-V characteristic, (c) input signal waveform, and (d) output signal waveform. 24
Figure 2.6. Operation of a realistic DC restorer circuit: (a) circuit diagram, (b) input signal waveform, and (c) output signal waveform. 25
Figure 2.7. Waveform of the diode conduction current for the DC restorer circuit shown in Figure 2.5. 26

Figure 2.8. Equivalent circuit of a 1-diode sampling circuit: (a) diode model, and (b) circuit diagram. 27
Figure 2.9. Sampling gating function $g(t)$. 28
Figure 2.10. (a) A triangular sampling strobe pulse train, and (b) the corresponding diode conduction current. 29
Figure 2.11. Circuit diagram of a 2-diode sampling circuit. 30
Figure 2.12. Input signal path circuit diagrams: (a) equivalent circuit; (b) simplified equivalent circuit. 31
Figure 2.13. (a) NLTL circuit diagram, (b) equivalent circuit, and (c) layout, where C_d is the diode capacitance and R_d its series resistance, $C_L = \tau / Z_l$ is the line capacitance and $L = Z_l \tau$ the line inductance. 34
Figure 2.14. SPICE simulation of NLTL wavefront compression and shock-wave formation. 35
Figure 2.15. A fabricated Schottky diode (a) top view, and (b) cross sectional view of AA'. 36
Figure 2.16. Cross-sectional view of a Schottky diode with parasitic resistances and capacitance. 37
Figure 2.17. Conceptual diagram of the CPW/CPS balun/differentiator. 39
Figure 2.18. Equivalent circuits of the balun/differentiator. 40
Figure 2.19. Circuit diagrams of (a) modified strobe generation circuit, and (b) matching network formed by C1, C2 and Lslot. 41
Figure 2.20. Diagram illustrating effect of the CPS round-trip delay to the amplitude and duration of the strobe pulses: (a) input step, (b) round-trip delay less than input falltime, (c) round-trip delay greater than input falltime, and (d) round-trip delay equals input falltime. 42
Figure 2.21. Broadening of strobe pulses by sampling diode parasitics: (a) equivalent circuit, (b) strobe pulse waveforms with and without the sampling diode obtained from SPICE simulation. 43
Figure 2.22. SPICE simulation illustrating effect of diode bias on strobe pulse

width: (a) smaller diode reverse-bias, and (b) larger diode reverse-bias 44
Figure 2.23. Sampling circuit (a) circuit diagram, and (b) layout 47
Figure 2.24. Circuit diagram of the strobe signal generation circuit for MWSPICE simulation. 49
Figure 2.25. Strobe generation circuit simulation results: (a) voltage across the sampling diodes, (b) reflection back to the input, and (c) sampling diode conduction current pulse. 52
Figure 2.26. Circuit diagram of RF signal circuit for MWSPICE simulation. 53
Figure 2.27. Signal line step response from MWSPICE simulation. 54
Figure 2.28. NLTL output measured by an NLTL-gated sampling circuit, both using hyperabrupt diode technology. Inset: two periods of the waveform. 56

Figure 3.1. Probe tip of a commercial microwave wafer probe. 58
Figure 3.2. Conceptual diagram of the active probe: (a) bottom view, and (b) top view. 59
Figure 3.3. Block diagram of the NWA IC 61
Figure 3.4. Illustration of an attenuator as the directional device 62
Figure 3.5. Circuit diagram of the NWA IC. 64
Figure 3.6. Layout of the NWA IC. 66
Figure 3.7. Photograph of a fabricated network analyzer IC. 67
Figure 3.8. NWA IC Strobe generation circuit for MWSPICE simulation 69
Figure 3.9. MWSPICE simulation results for the NWA IC strobe generation circuit: (a) dynamic range, (b) reflection, and (c) diode aperture time. 71
Figure 3.10. NWA IC RF signal line equivalent circuit for MWSPICE simulation. 72
Figure 3.11. MWSPICE simulation result for the NWA IC RF signal line equivalent circuit. 72
Figure 3.12. Observed NWA IC waveforms: incident wave, and (incident +

reflected) waves with the IC open-circuited or connected to a terminated 40 GHz microwave wafer probe. 74
Figure 3.13. Reflection coefficient displayed in time with the NWA IC open-circuited. 76
Figure 3.14. Conceptual circuit diagram of a bias tee 77
Figure 3.15. Circuit diagrams of two implementations of bias tees: (a) with high impedance line, and (b) with 2 dB 50 Ω attenuator. 79
Figure 3.16. Layout of the bias tee with 2-dB attenuator 79
Figure 3.17. Measured S-parameters of a bias tee: (a) insertion loss, and (b) return loss. 80
Figure 3.18. Computed total (skin plus radiation) losses for coplanar waveguide probe tips on quartz and alumina substrates. 82
Figure 3.19. Illustrating the necessity of angle-lapped probe tips: (a) before lapping, and (b) after lapping. 83
Figure 3.20. Angle lapping process: (a) top view of the lapping fixture, (b) cross sectional view of AA', and (c) final shape of lapped probe tips. 84
Figure 3.21. Scanning-electron micrograph of a fabricated quartz coplanar-waveguide probe tip. 85
Figure 3.22. Computed ribbon connection bandwidth for 2-mil wide ribbons of different lengths. 87
Figure 3.23. Hybrid assembly of the active probe. 89
Figure 3.24. (a) Photograph showing the active probe hybrid assembly, and (b) photograph of an active probe compared to a commercial passive microwave probe. 90
Figure 3.25. Mechanical setup of the active probe. 91
Figure 3.26. Step response of active probes for (a) waveform measurements, and (b) network measurements. 93

Figure 4.1. Basic network measurement system configuration. 95
Figure 4.2. Phase noise sideband overlap due to downconversion of frequency

spectrum by the sampling circuits: (a) spectrum at the sampling circuit input with RF fundamental frequency f_0, (b) spectrum at the sampling circuit output with IF fundamental frequency Δf, and (c) spectrum at the sampling circuit output with IF fundamental frequency $\Delta f'$ where $\Delta f' > \Delta f$. 98

Figure 4.3. Measured relative phase noise spectral density of 2 microwave synthesizers operating under the same 10 MHz fundamental frequency reference. 99

Figure 4.4. Effect of signal averaging on signal spectra: (a) without averaging, and (b) with averaging 101

Figure 4.5. 2-diode sampling circuit: (a) equivalent circuit diagram, and (b) simplified equivalent circuit diagram. 102

Figure 4.6. Impedance scaling by switching action: (a) circuit comprising components being scaled by switching, and (b) its Thevenin equivalent circuit. 103

Figure 4.7. Equivalent circuit diagram of the sampling circuit shown in Fig. 4.5(b). 104

Figure 4.8. Equivalent circuit for the sampling circuit shown in Fig. 4.5(b) when C1 is an open at the sampling rate 104

Figure 4.9. Equivalent circuit for the sampling circuit input. 105

Figure 4.10. Signal power spectrum at sampling circuit input 107

Figure 4.11. Measured signal to background noise at sampling circuit output 108

Figure 4.12. Conceptual diagram illustrating calibration for network measurements. 109

Figure 5.1. Waveform measurement setup 117

Figure 5.2. Waveform measurements with the active probe: (a) 0.7-ps NLTL output risetime, and (b) traveling-wave resonant tunnel diode pulse generator output risetime and the inset shows two periods of the waveform. 118

Figure 5.3. System setup for network measurements using active probes 120

Figure 5.4. Photograph of two active probes and a commercial passive microwave probe measuring a DUT. 121
Figure 5.5. Step response of the first generation of active probes. 123
Figure 5.6. S11 measurements of (1) short, (2) load, (3) open, and (4) 23 Ω resistor from 8-96 GHz (a) initial measurements, and (b) measurements performed 30 minutes later 124
Figure 5.7. Step response of the second generation of active probes 126
Figure 5.8. 2-port measurements of a 1.6 ps transmission line with LRL calibration 127
Figure 5.9. 2-port S-parameter measurements (taken at three different times with 30 minute time intervals) of a nominal 50 Ω 25-ps transmission line: (a) dB plot of the magnitude of S21, (b) calculated and measured phase of S21, and (c) dB plot of the magnitude of S11. 129
Figure 5.10. 2-port measurements (taken at three times with 30 minute time intervals) of a nominal 6-dB attenuator: (a) dB plot of the magnitude of S21, and (b) dB plot of the magnitude of S11. 130
Figure 5.11. Return losses of two 2400-µm long quartz CPW lines: one is periodically loaded with air bridges and one is not loaded. 132
Figure 5.12. Measured return loss of a 2400-µm long quartz CPW line loaded periodically with 5 times smaller air bridges than that shown in Fig. 5.11. 133
Figure 5.13. Step response of the third generation of the active probes. 134
Figure 5.14. 2-port S-parameter measurements (taken at 30 minute time intervals) of a 1-ps through line calibration standard: (a) magnitude and phase of S21, and (b) magnitude of S11 136
Figure 5.15. Measured and calculated S11 magnitude of a 50 Ω load in series with a 7.5 pH inductor (two measurements were taking 30 minutes apart). 137
Figure 5.16. S-parameter measurements (taken at 30 minute time intervals) of a 40-ps 50 Ω transmission line: (a) magnitude of S21, and (b)

magnitude of S11. 138
Figure 5.17. S-parameter measurements of a 3-stage low noise amplifier: (a) gain, and (b) return losses. 140
Figure 5.18. S-parameter measurements of a 5-stage traveling-wave amplifier: (a) gain, and (b) return losses. 141
Figure 5.19. S-parameter measurements of a medium power amplifier: (a) gain, and (b) return losses. 142
Figure 5.20. Schematics of an alternative 2-port measurement set-up using lock-in amplifiers to measure the IF signals. 144
Figure 5.21. 2-port measurements of a 1-ps through line (two measurements taken 30 minutes apart): (a) dB plot of the transmission magnitude, (b) calculated and measured transmission phase, and (c) dB plot of the return loss magnitude 147
Figure 5.22. 2-port measurements of a 25-ps transmission line (three measurements taken with 30 minute time intervals): (a) dB plot of the transmission magnitude, and (b) calculated and measured transmission phase 148
Figure 5.23. Schematics of a second alternative network measurement setup using a single microwave synthesizer and a mechanical delay 149

Figure 6.1. Schematic diagrams of (a) the 1-ps through line and the 50 Ω match load on a commercial calibration standard substrate, and (b) the offset DUT and the offset 50 Ω match load. 154
Figure 6.2. Schematic diagram of an active probe fabricated with beam lead technology. 155
Figure 6.3. Comparision of stimulus and measured signal spectrums of the frequency-domain ((a) and (b)) and time-domain network analyzers ((c) and (d)): (a) & (c) stimulus signal spectrum, and (b) & (d) measured DUT response and spurious signal spectrum. 158

Chapter 1

Introduction

Recent advancements in III-V technology have led to significant improvements in transistor and monolithic millimeter-wave integrated circuit (MMIC) bandwidths. High-electron-mobility field-effect transistors (HEMTs) with power-gain cutoff frequencies (f_{max}) above 450 GHz and amplifiers operating have been reported [1-3], enabling demonstration of monolithic 120 GHz amplifiers [4-6]. In contrast, current coaxial-based instrument bandwidths have been limited to 60 GHz. Sampling oscilloscopes can measure broadband waveforms to 50 GHz [7] and network analyzers can perform network measurements to 60 GHz [8]. Network analyzers from 75-120 GHz have been reported [9,10], but these systems require waveguide connections, hence are narrow band. 1 THz vector network analyzers have also been reported [11], but these network analyzers can perform only quasi-optical transmission measurements and are waveguide-based. As with all waveguide-based network analyzers, a long setup time is required for broadband measurements due to the need for multiple waveguide fixtures to cover a broad frequency band.

Inadequate instrumentation results in great difficulties in characterization of high frequency devices and in design of MMICs. To measure f_{max} of a transistor, for example, the transistor maximum available gain (Gmax) is measured from DC to 60-120 GHz, and extrapolated to obtain f_{max}=450 GHz. Circuit design of MMICs demands accurate transistor and passive element models which cannot be determined with great confidence from extrapolation of measurements made at lower frequencies. In addition, while device models can be, to certain extent, extrapolated from measurements at lower frequencies, MMIC measurements cannot. State-of-the-art devices and MMICs present a pressing need for high frequency instruments.

1.1 Electrical measurement techniques

Conventional high frequency instruments include sampling oscilloscopes, time-domain reflectometer (TDR), network analyzers, and spectrum analyzers. Sampling oscilloscopes measure the time-domain response of a device under test (DUT). Sampling oscilloscopes capable of capturing transient time waveforms are commercially available only to 8 GHz, and higher frequency sampling oscilloscopes operate exclusively with equivalent-time sampling techniques. The equivalent-time sampling technique can be illustrated in both time and frequency domains (Fig. 1.1). In the time-domain description, a periodic waveform (with period $T_0 - \Delta T$) is sampled with a train of sampling pulses spaced T_0 apart. In real-time, the input waveform is sampled once in each (or multiple) period, and the input waveform can be reconstructed in equivalent-time. In frequency domain description, the sampling circuit strobe signal spectrum (at f_0 and its Fourier harmonics) convolves with the input signal spectrum (at $f_0 + \Delta f$ and its Fourier harmonics). The input signal spectrum is, in effect, down-converted into much lower IF frequencies (Δf and its harmonics) and can be reconstructed with low-pass filtering. Note that the equivalent-sampling technique is applicable only for periodic signals. To achieve high frequency operation, sampling circuits implemented with Schottky diodes have long been used in the sampling oscilloscopes [12-14]. The bandwidth of these sampling circuits is limited by sampling diode parasitics and by duration of the strobe pulses used to switch the sampling diodes into forward conduction. Since 1966, 20-30 ps silicon step recovery diodes (SRDs) [12] have been used for strobe pulse generation [13,14], limiting the sampling circuit bandwidths to ≈20-40 GHz. Network analyzers, frequency counters, and frequency synthesizers also use diode sampling circuits for signal measurement or frequency downconversion. The bandwidths of these instruments are therefore also limited by the sampling circuit bandwidth. Incorporating a high-speed step function generator, the sampling oscilloscope can also be used for TDR measurements.

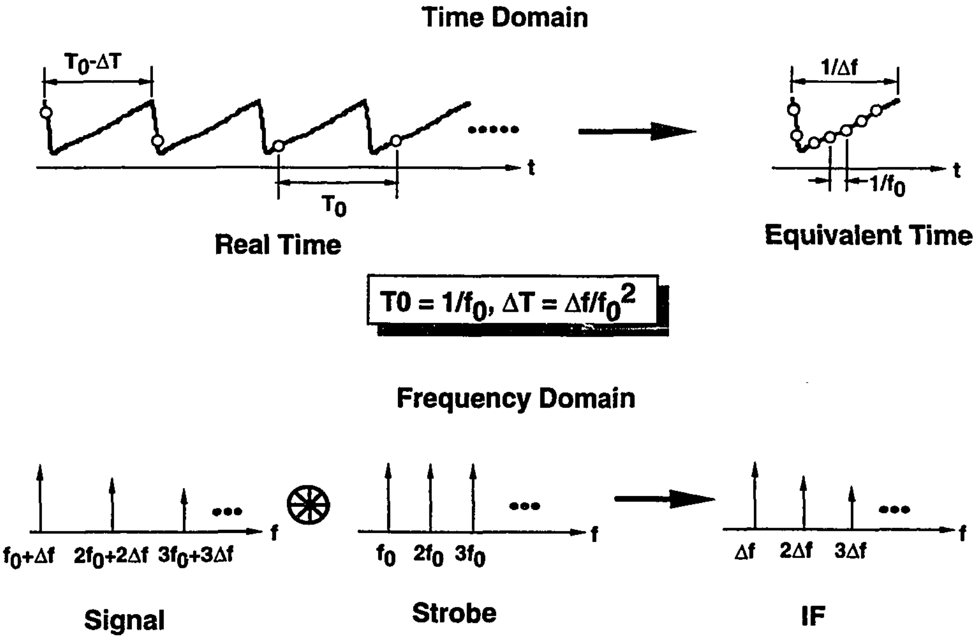

Figure 1.1. Operation of equivalent-time sampling techniques.

Network analyzers measure the S-parameters of a DUT. The block diagram of a conventional network analyzer is shown in Fig. 1.2. A swept-frequency stimulus signal is applied, through a directional coupler, to the device under test (DUT). A pair of sampling circuits monitor the forward and reverse waves at microwave frequencies, and downconvert these waves to signals at 20 MHz IF frequency. Amplitude and phase measurements are then made at 20 MHz. For 2-port measurements, an identical channel is placed at the output port of the DUT. The bandwidth of the network analyzer is limited by the sampling circuit bandwidth and the frequency range of the stimulus signal source. As discussed above, the sampling circuit bandwidth is limited by the sampling diode parasitics and by the duration of the strobe signal pulses. In addition, for on-wafer network analysis, the swept-frequency stimulus signals used in commercial network analyzers are not readily generated and delivered to the DUT at millimeter-wave (mm-wave) frequencies.

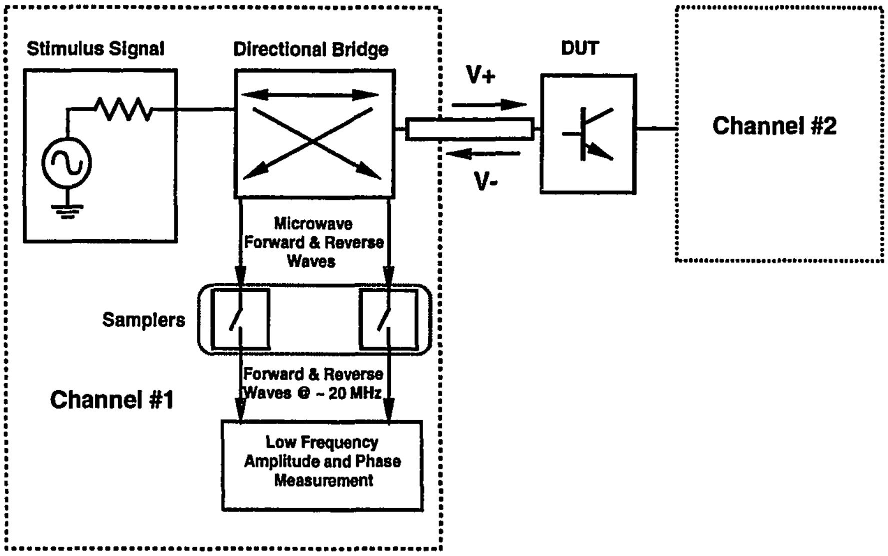

Figure 1.2. Block diagram of a conventional microwave network analyzer; channel 2 is identical to channel 1.

Spectrum analyzers measure the power spectrum of a signal. The block diagram of a typical microwave spectrum analyzer is shown in Fig. 1.3. The basic idea is to send the signal through a band-pass filter having a center frequency adjustable over the range in which the analysis is to be made. The bandwidth and shape of the response of the filter determines the resolution by which the various components of the signal spectrum can be determined. It is difficult to design narrow-band filter which is tunable over a wide frequency range. Instead, practical spectrum analyzers use a an architechture similar to superheterodyne radio receivers (Fig. 1.3). The input signal is first adjusted to a suitable level for the subsequent mixer by a calibrated input attenuator. A preselector in the form of a electronically tuned filter is connected in front of the mixer. The purpose of the preselector is to suppress the image frequency response which is generated by the mixer: if the IF frequency f_i is lower than the signal and local oscillator frequencies f_s and f_l, respectively, the mixer produces f_i either by $f_i = f_{s1} - f_l$ or $f_i = f_l - f_{s2}$ where $f_{s2} < f_l < f_{s1}$. The input signal frequency range is covered by sweeping the voltage- controlled oscillator (VCO). Both the VCO and the preselector are controlled by the same sweep signal generator so that precise tracking of the VCO and the preselector frequencies can be obtained. The sweep generator also drives the x-axis input of the CRT display. The bandwidth of the spectrum analyzers are limited by the achievable bandwidths of the VCO, the tunable filter, and the broadband mixer. Sampling circuits are also used as mixers for single frequency downconversions such as in phase-lock-loop applications. Because the sampling circuit strobe pulse train contains multiple harmonic signals (Fig. 1.1), many image frequency signals will be generated for a broadband input signal. This places more stringent demands on the performance of the preselector. Additionally, typical sampling circuits have only 10-100 KHz IF signal bandwidths and have high noise figures. For these reasons, sampling circuits are not suitable for application in spectrum analyzers.

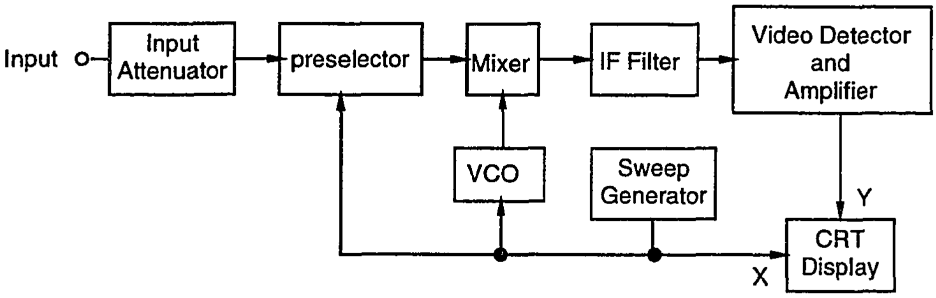

Figure 1.3. Block diagram of a conventional spectrum analyzer.

A bandwidth limitation common to all coaxial instruments arises from the coaxial connectors and cables used to connect the DUTs to the instruments. These coaxial connectors and cables are currently limited to 110 GHz [15]. For on-wafer measurement, the wafer probes contribute additional limit to the overall instrument bandwidths. Current commercial coaxial wafer probes are bandwidth limited to ≈ 65 GHz.

With external frequency multipliers, mixers, waveguides, and waveguide adopters, the bandwidth of spectrum analyzers and network analyzers can be extended to higher frequencies, as discussed above. However, the frequency coverage of waveguide based instruments is limited to the 1.5:1 waveguide bandwidth, and the DUT needs to be mounted in waveguide fixtures.

1.2. Optoelectronic Measurement Techniques

The highest bandwidth signal generation and sampling measurement systems reported have been based on optoelectronic techniques [16,17]. The shortest electrical pulses on record have been generated by photoconductors. A photoconductor is a gap between two ohmic contacts on a semiconductor (Fig. 1.4(a)). A pulsed laser illuminates the photoconductor and generates electron-hole pairs which increases the gap conductance $G(t)$ in proportion to the laser intensity. The photoconductor is incorporated into a biased transmission line to generate electrical pulses and to deliver the pulses to a load. For small illumination intensities, the output voltage is proportional to the optical power, while for high intensities, gap conductance is greatly increased and the photo conductor behaves as a laser pulse-gated switch. The impulse response of the photo conductor is determined by the gap capacitance and by the carrier recombination life time, the latter minimized with ion implantation techniques [18] or low-temperature growth [19].

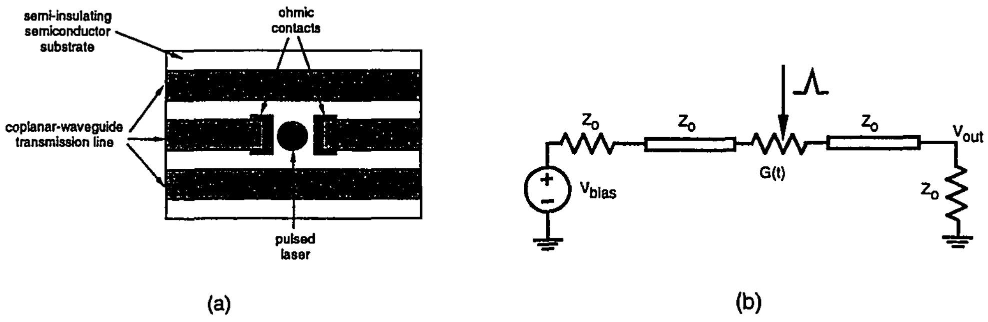

Figure 1.4. Photoconductive detector connected to a coplanar-waveguide transmission line: (a) for subpicosecond electrical pulse generation and sampling, and (b) photoconductive pulse generation circuit.

Photoconductors are also used for signal measurements (Fig. 1.5) [19-21]. A laser-illuminated photoconductor generates a train of impulses, driving the device under test. A second photoconductor operates as a laser-gated switch, generating a sampled (DC) voltage proportional to the device output at the time of arrival of the optical pulse. Adjusting an optical delay stage varies the sampling pulse arrival time, producing a measurement of the device output voltage waveform as a function of time. Comparing the Fourier spectra of the incident and transmitted pulses, transmission-frequency measurements of materials or devices are made. Photoconductors integrated with on-wafer broadband antennas are used to generate and radiate, then receive and sample, subpicosecond electromagnetic pulses; by passing the radiation through test samples, material absorption spectra have been measured at low THz frequencies [22]. Photoconductor switches have also been incorporated into wafer probes [20,21], eliminating the need for fabricating the photoconductive switches with the DUTs. Incorporating fiber input into the optoelectronic wafer probes, Feuer et. al have obtained calibrated 1-port S-parameter measurements to 125 GHz [21].

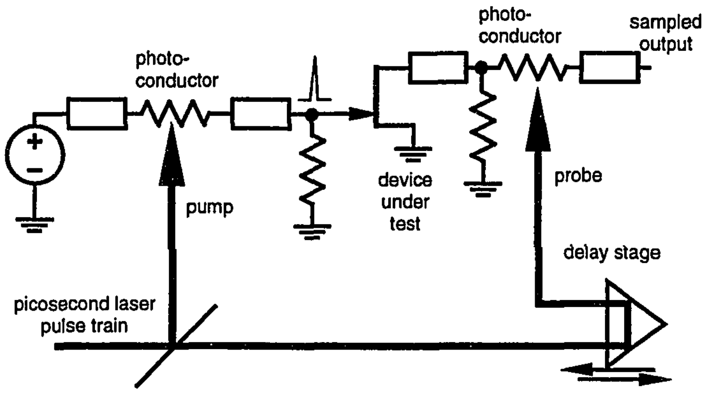

Figure 1.5. Pump-probe experiments: a photoconductor generates a subpicosecond impulse driving a device under test, while a second photoconductor samples the resulting output signal.

Subpicosecond electrical transients are also measured by electrooptic sampling [23-25]. Both lithium niobate and III-V compound semiconductors exhibit small anisotropic variations in their optical refractive indices in response to applied electric fields [26]. Electric fields associated with nearby conductors can be measured by measuring the change in polarization of an optical pulse passing through the crystal. As with photoconductive sampling (Fig. 1.5), electrooptic sampling measures electrical waveforms by using pairs of synchronized optical pulses for signal generation (using a photoconductor) and electro-optic signal measurement. Using electrooptic sampling, Keil has measured 150 fs risetime step-functions [17].

Optoelectronic measurement techniques have several potential advantages over electrical methods. First, the fastest electrical signal generation and detection systems to-date have been implemented with optoelectronic techniques, although this advantage has progressively diminished (recently, Allen et. al. have achieved electrical transients of 0.68 ps and sampling circuits of 725 GHz using nonlinear transmission line technology [27]). Second, high frequency electrical wafer probes are implemented with 50 Ω coplanar-waveguides to control the line impedance from the coaxial transitions (connectors) to the IC bond pads and to reduce parasitics. The low characteristic impedance of such lines limits their use to DUT input/output connections. In contrast, electrooptic probing of ICs is a noncontact technique which introduces no parasitic impedances, permitting its use for internal-node probing of ICs. Third, while the probe pitch of high frequency electrical wafer probes are limited to ≈ 100 μm, the spatial resolution of electrooptic sampling can be as small as a few μm in diameter, ultimately limited by the optical wavelength.

Against this, optoelectronic techniques have several serious disadvantages. Application of the optoelectronic measurement techniques are limited by the lasers' size and the complexity of the measurement system. All the optics in the experiment require careful alignment, hence long experimental set-up time. Photoconductor signal generators and detectors for measurements are normally integrated onto the DUTs, making its application as general instruments impractical. Although photoconductor switches have also been integrated into wafer probes, they suffer from the same probe tip parasitics as the electrical probes, and their speed advantage over their electrical counterparts therefore diminishes. Optoelectronic techniques have also been used for S-parameter measurements, but these rely on time-gating to separate incident and reflected waves. Truncation of response time waveform of a DUT can result in large measurement errors. Laser systems have much larger amplitude and phase noise than precision microwave sources, and accuracy is therefore sacrified. Finally, the pulse repetition rate of mode-locked lasers is adjustable only by mechanical adjustment of the cavity. This prevents taking measurements over a frequency scan. Microwave synthesizers using transistor oscillators are readily and precisely frequency-tuned.

1.3. The Active Probe Measurement System

Nonlinear transmission line (NLTL) pulse generators [28] can attain transition times more than a factor of 30 shorter than the Silicon SRDs [29,30]. The pulse trains generated by NLTLs have significant spectral content to sub-mm-wave frequencies and can serve as convenient stimulus signal sources for network measurements. Using NLTLs as strobe pulse generators, sampling circuits with mm-wave bandwidths can be fabricated. Combining the mm-wave NLTL stimulus signal sources and sampling circuits, integrated circuits for mm-wave network analysis can be implemented. To eliminate the bandwidth limitations arising from coaxial cables and connectors, the instrumentation ICs (sampling circuits and network analyzer ICs) are mounted directly on wafer probes (Fig. 1.6) a short distance from the probe tips. Millimeter-wave signals between the DUT and the instrument IC then only propagate on the low-loss coplanar-waveguide (CPW) quartz probe tip and through the gold ribbons used to connect the probe tip to the instrument IC. With proper probe tip design and careful probe hybrid assembly, signal connection bandwidths much higher than 120 GHz are attainable. With appropriate system design, active probes can provide convenient solutions to broadband on-wafer waveform and network measurements to 200 GHz.

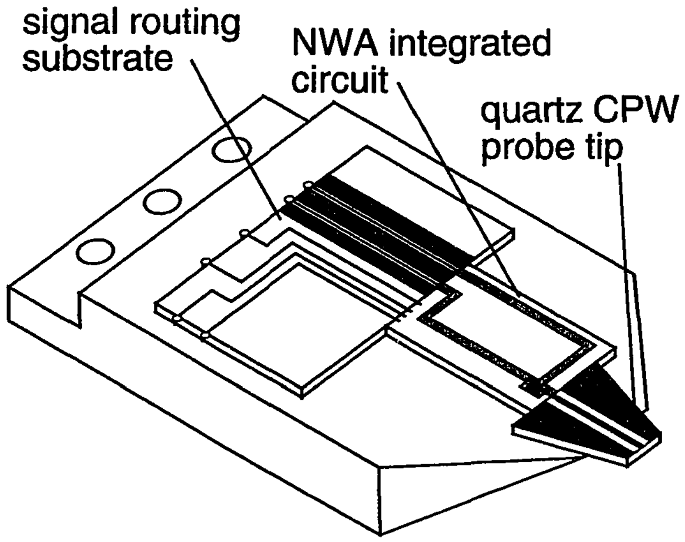

Figure 1.6. Conceptual diagram of the active probe.

Shakouri et. al. have also fabricated active probes incorporating NLTL-gated sampling circuits [30]. Probe heads (probe tips and sampling circuits) have been monolithically fabricated on GaAs substrates with micro-machining, minimizing probe tip parasitics and resulting in probe bandwidths of 500 GHz. However, to-date, only waveform measurements have been reported.

The work described in this dissertation focuses on network measurements, although waveform measurement examples are also given to illustrate the usefulness of the active probes. The dissertation describes the design and fabrication of the mm-wave sampling circuits, the network analyzer ICs, and the active probes. Bandwidth limitations are then analyzed. System design considerations for accurate and reproducible mm-wave network analysis are discussed. Both waveform and network measurement results obtained with the active probes are presented. Finally, some future directions for improvement of the current active probe systems are given.

Chapter 2

Sampling Circuits: Design, Fabrication, and Measurements

Since the advent of the first vacuum tube based sampling circuit in 1950 [31], sampling circuits have been used in such diverse broadband electronic instruments as sampling oscilloscopes, network analyzers, frequency counters, frequency synthesizers, and vector volt-meters. In these instruments, the sampling circuits are used either for signal measurements by repetitive sampling, or for frequency downconversion prior to subsequent signal detection. The performance of these instruments is largely determined by the sampling circuits. Progress in sampling circuit technology has been relatively slow. The first microwave diode sampling circuit was reported in 1957 with a bandwidth of 600 MHz [32]. Since 1966, silicon step recovery diodes (SRDs) have been used as strobe pulse generators [13,14] in diode sampling circuits. The 20-30 ps SRD risetimes have limited the sampling circuit bandwidths to ≈20-40 GHz. More recently, nonlinear transmission line (NLTL) pulse generators have been developed [28,29]. These enable generation of transient signals with picosecond transition times. Using NLTLs as the strobe signal generators, sampling circuits useful even at sub-mm-wave frequencies are attainable. This chapter describes the operation and design principles of ultra-high frequency sampling circuits. Fabrication and bandwidth measurements of the sampling circuits are also given.

2.1 Equivalent-Time vs. Real-Time Sampling

There are two major sampling schemes employed in various instruments incorporating sampling circuits: real-time sampling and equivalent-time sampling. The preferred sampling scheme depends upon the type of input (RF) signals and on the application. Real time and equivalent time sampling are best described in frequency domain.

Fig. 2.1 illustrates the real-time sampling processes of a band-limited signal. Consider a band-limited signal $f(t)$ having no spectral components above $2\pi B$ rad/sec. We shall sample this signal using a periodic gate function $g(t)$. Without loss of generality, we assume that the sampling pulses are rectangular in shape, τ seconds in width, of unit amplitude, and occurs at intervals of T seconds. Denoting the sampled signal by $f_s(t)$, we can write

$$f_s(t) = f(t)g(t) \qquad (2.1)$$

Since $g(t)$ is periodic, it can be represented by a Fourier series

$$g(t) = \sum_{n=-\infty}^{+\infty} G_n e^{jn\omega_0 t} \qquad (2.2)$$

where $\omega_0 = 2\pi / T$. Combining Eqs. (2.1) and (2.2), we have

$$f_s(t) = f(t) \sum_{n=-\infty}^{+\infty} G_n e^{jn\omega_0 t} \qquad (2.3)$$

Taking the Fourier transform of both sides of (2.3) and after some algebraic manipulation, the spectral density of $f_s(t)$, denoted by $F_s(\omega)$, is

$$F_s(\omega) = G_0 F(\omega) + \sum_{n=-\infty, n\neq 0}^{+\infty} G_n F(\omega - n\omega_0) \qquad (2.4)$$

where $F(\omega)$ is the spectral density of $f(t)$. If $\omega_0 > 2\pi B$, the spectrum (Fourier transform) of the sampled signal $f_s(t)$ is, within a constant factor, exactly the same as that of $f(t)$ within the original bandwidth. In addition, the spectrum of the sampled signal repeats periodically in frequency every ω_0 radians per second. These replicas of

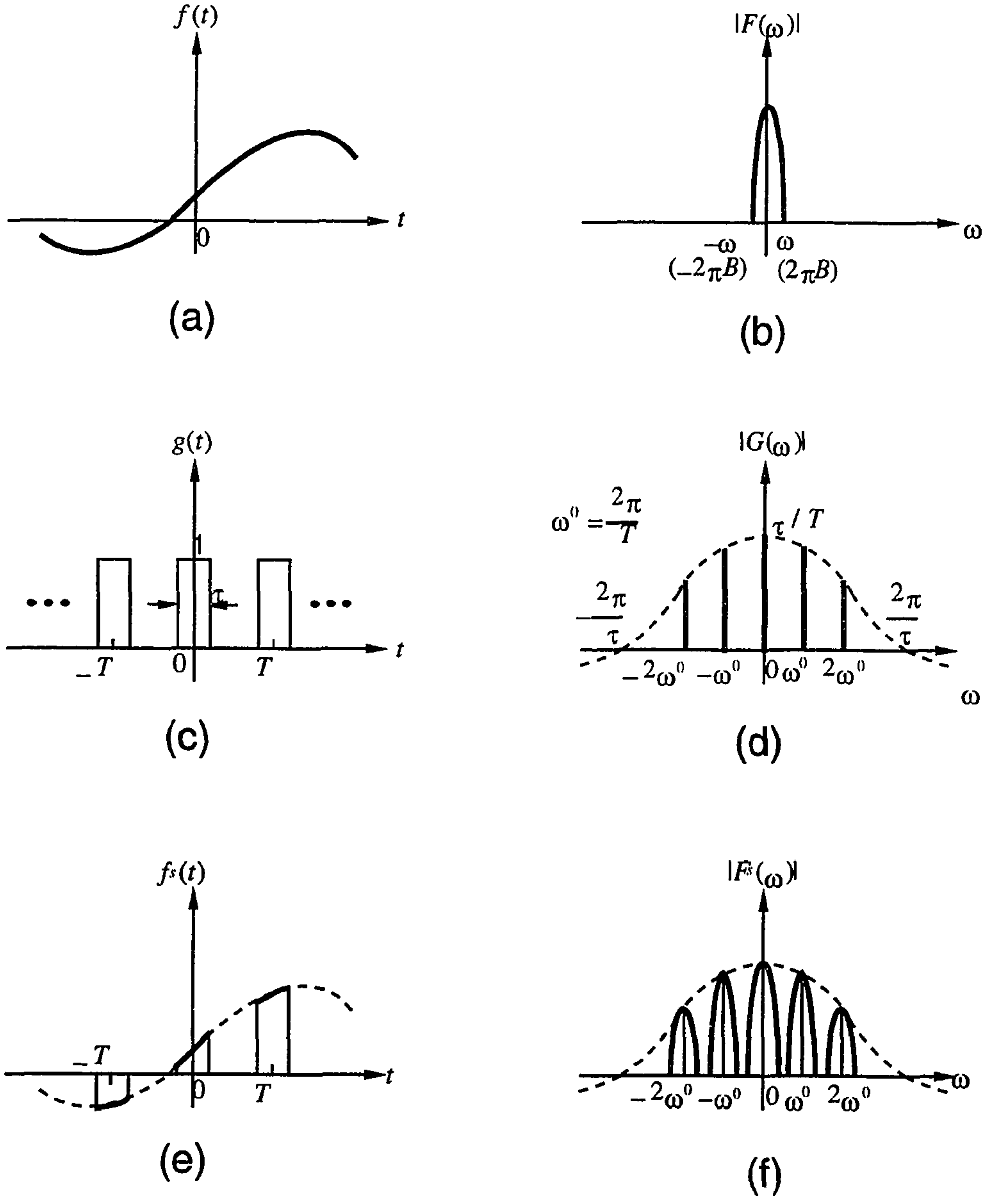

Figure. 2.1. Real-time sampling process: (a) time domain band-limited input signal; (b) input signal spectrum; (c) gate function in time domain; (d) gate function spectrum; (e) sampled signal in time domain; (f) sampled signal spectrum.

the original spectral density are weighted by the amplitudes of the Fourier series coefficients of the sampling waveform, as shown in Fig. 2.1. The spectral density of the original function $f(t)$ can be retrieved simply by using a low-pass filter on $F_s(\omega)$.

As the sampling rate ω_0 decreases, there exists a point beyond which a reduction in sampling rate will result in overlap between spectral densities, a phenomenon known as aliasing. From Fig. 2.1 (f), it can be seen that this point is attained when

$$2\pi / T = 2\omega_0 \text{ or } T = 1/(2B) \qquad (2.5)$$

At this point, all replicas of the original spectral density are just tangent to each other and an ideal low-pass filter of bandwidth $2\pi B$ rad/sec can be used to recover $f(t)$ from the sampled signal $f_s(t)$. If the sampling interval T becomes slightly larger than that given in Eq. (2.5), the terms $\sum_{n=-\infty}^{+\infty} G_n F(\omega - n\omega_0)$ in Eq. (2.4) overlap in frequency and the original signal cannot be retrieved by filtering the sampled signal $f_s(t)$. To permit recovery of $f(t)$ from $f_s(t)$, we must require that

$$T < 1/(2B) \qquad (2.6)$$

This is the well-known Nyquist sampling theorem; a real-valued band-limited signal having no spectral components above a frequency of B Hz is determined uniquely by its values at uniform intervals spaced no greater than $1/(2B)$ seconds apart. $T = 1/(2B)$ is the Nyquist interval; its reciprocal is the Nyquist sampling frequency.

For real-time sampling, the signal being sampled $f(t)$ need not be periodic. Provided that $f(t)$ is band-limited to B Hz and the gate function has a sampling frequency of $1/T > 2B$, $f(t)$ can be reconstructed from $f_s(t)$ by low-pass filtering.

For microwave and millimeter-wave signals whose bandwidth B is in the tens or hundreds of GHz, the Nyquist criteria leads to very high sample rate. Acquisition and storage of the signal samples at such rates is not feasible.

If the signal to be sampled is periodic, an equivalent-time sampling can be employed, and the gate function sampling frequency can be much less than (usually a subharmonic of) the fundamental frequency of the signal being sampled.

The operation of the equivalent-time sampling scheme is illustrated in Fig. 2.2. The signal being sampled $f(t)$ is a periodic function with fundamental frequency $m\omega_0$ (Fig. 2.2(a)), where m is an integer. We assume that $f(t)$ is band-limited to its k^{th} harmonic, hence has signal bandwidth of $km\omega_0$. The gate function $g(t)$ has fundamental frequency $\omega_g = \omega_0 + \omega_{IF}$, where ω_0 is a subharmonic of the signal fundamental frequency $m\omega_0$ and ω_{IF} is a subharmonic of the fundamental intermediate frequency (IF) $m\omega_{IF}$. For simplicity, the gating function $g(t)$ is drawn as a train of impulses. The effect of a finite gating pulse duration on the sampled signals will be discussed subsequently. As shown in Fig. 2.2, the spectrum $F(\omega)$ of the periodic function $f(t)$ has components at $m\omega_0$, $2m\omega_0$, $\cdots$, and $km\omega_0$; the gate function $g(t)$ has spectral components, denoted by $G(\omega)$, at ω_g, $2\omega_g$, $\cdots$, mω_g, etc. Because $f(t)$ is periodic, it can be represented by a Fourier series

$$f(t) = \sum_{n=-k}^{+k} F_n e^{jn(m\omega_0)t} \tag{2.7}$$

Similarly, the gate function is

$$g(t) = \sum_{l=-\infty}^{+\infty} G_l e^{jl\omega_g t} \tag{2.8}$$

The sampled signal, denoted by $f_s(t)$, is

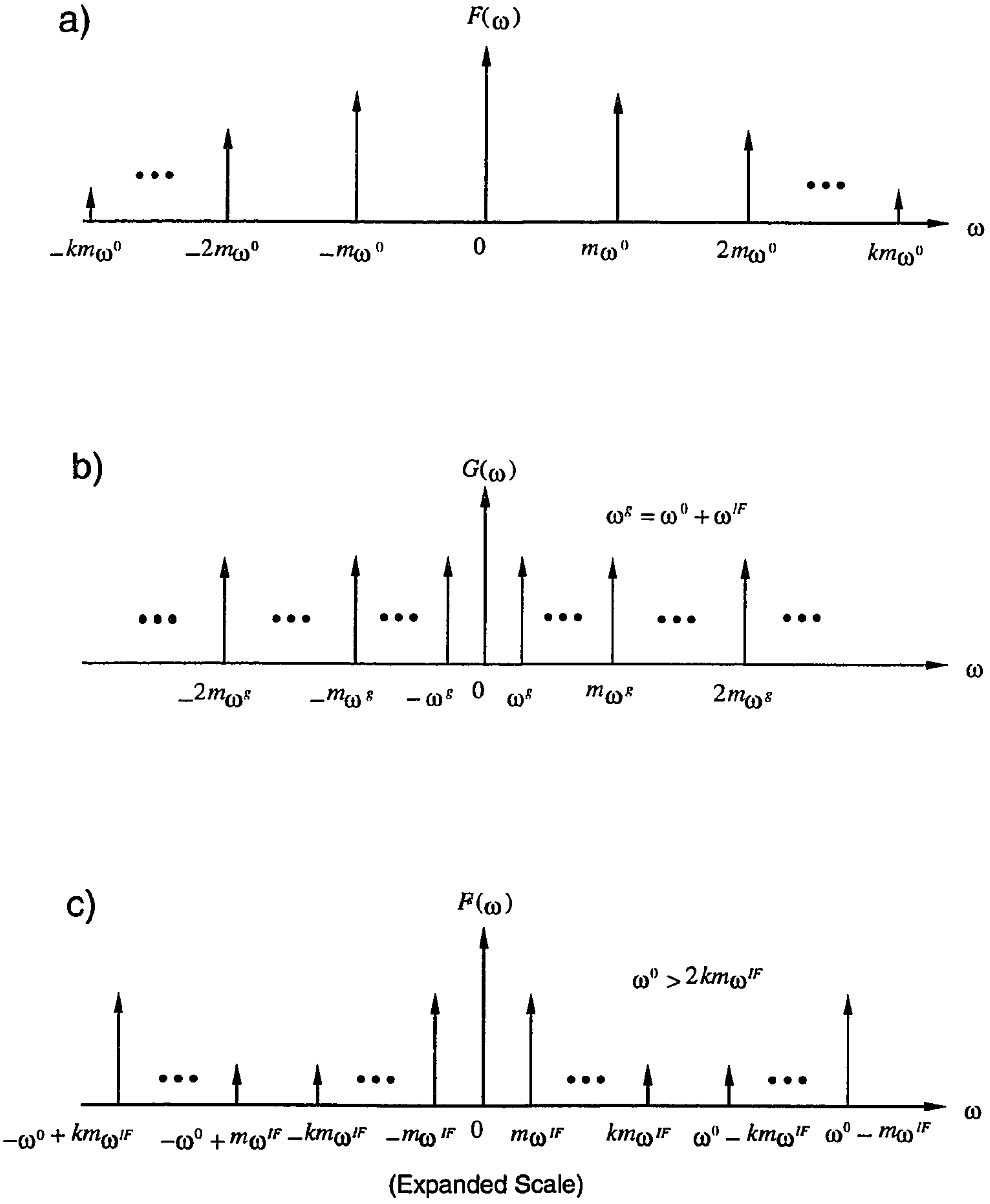

Figure. 2.2. Equivalent-time sampling process: (a) band-limited input signal spectrum; (b) gate function spectrum; (c) sampled signal spectrum.

$$\begin{aligned} f_s(t) &= f(t)g(t) \\ &= \sum_{l=-\infty}^{+\infty} G_l \sum_{n=-k}^{+k} F_n e^{j(n(m\omega_0)+l\omega_g)t} \end{aligned} \tag{2.9}$$

Taking Fourier transforms of both sides of Eq. (2.9), we have

$$F_s(\omega) = 2\pi \sum_{l=-\infty}^{+\infty} G_l \sum_{n=-k}^{+k} F_n \delta(\omega - (n(m\omega_0) + l\omega_g)) \tag{2.10}$$

When $l = -nm$, $n(m\omega_0) + l\omega_g = n(m\omega_0) - n(m\omega_0) - n(m\omega_{IF}) = -n(m\omega_{IF})$, and Eq. (2.10) can therefore be rewritten as:

$$\begin{aligned} F_s(\omega) &= 2\pi \sum_{n=-k}^{+k} G_{nm} F_n \delta(\omega - n(m\omega_{IF})) \\ &+ 2\pi \sum_{l=-\infty, l\neq nm}^{+\infty} G_l \sum_{n=-k}^{+k} F_n \delta(\omega - (n(m\omega_0) + l\omega_g)) \end{aligned} \tag{2.11}$$

In Eq. 2.11, the first summation term represents the spectral components of $F(\omega)$ being downconverted to harmonics of $m\omega_{IF}$ and being scaled by spectral components of $g(t)$ at frequencies of $l = -nm$. Now examine the second summation term. For $n \cdot l > 0$, the spectral frequencies are either greater than $m\omega_0$ or smaller than $-m\omega_0$; for $n \cdot l < 0$, the spectral frequencies are either greater than $\omega_0 - k(m\omega_{IF})$ or less than $-\omega_0 + k(m\omega_{IF})$. Consequently, to avoid overlap of the spectral components in the first summation term with those in the second summation term, we must impose

$$(\omega_0 - k(m\omega_{IF})) - (-\omega_0 + k(m\omega_{IF})) > 2k(m\omega_{IF})$$

$$\text{or} \qquad \omega_0 > 2k(m\omega_{IF}) \tag{2.12}$$

where $k(m\omega_{IF})$ can be considered as the IF signal bandwidth. If Eq. 2.12 is satisfied, the spectral components of the original signal $f(t)$ can be recovered from $F_s(\omega)$, the IF frequency spectrum, by low pass filtering to bandwidth $k(m\omega_{IF})$. If the sampling pulse train $g(t)$ is not a train of impulses, the coefficients G_n will be unequal. In this case, appropriate filtering of $f_s(t)$ will correct (equalize) the spectrum of the IF signal.

To reconstruct the original signal $f(t)$ from its IF spectrum $F_s(\omega)$ after equivalent-time sampling, the fundamental frequency of the gate function (which is a subharmonic of the fundamental frequency of the signal being sampled) must be greater than twice the IF signal bandwidth. This conclusion can be considered as the sampling theorem for equivalent-time sampling.

When the gating function $g(t)$ is a train of impulses,

$$g(t) = A\sum_{n=-\infty}^{+\infty}\delta(t-nT)$$

where A is the amplitude of the impulses and T is the period. Its Fourier spectrum is:

$$G(\omega) = A\omega_g\sum_{n=-\infty}^{+\infty}\delta(\omega-n\omega_g)$$

Eq. 2.11 becomes, after low-pass filtering,

$$F_s(\omega)|_{LPF} = 2\pi A\omega_g\sum_{n=-k}^{+k}F_n\delta(\omega-n(m\omega_{IF}))$$

Except for a scaling factor and frequency downconversion to $m\omega_{IF}$, $F_s(\omega)|_{LPF}$ is identical to the spectral density of the original signal $f(t)$. Consequently, $f(t)$ can be reconstructed by low-pass filtering and it has a period of $1/(m\omega_{IF})$.

If the sampling pulse width is finite (Fig. 2.3 (a)), the spectrum of the gate function is (Fig. 2.3(b))

$$G(\omega) = A\tau\omega_g\sum_{n=-\infty}^{+\infty}\frac{\sin(n\omega_g\tau/2)}{n\omega_g\tau/2}\delta(\omega-n\omega_g) \qquad (2.13)$$

where τ is the sampling pulse width. As shown in Fig. 2.3(b), the n^{th} spectral component of $G(\omega)$, i.e.,$G_n = [\sin(n\omega_g\tau/2)]/[n\omega_g\tau/2]$, has its maximum at $n=0$ and has nulls at $n\omega_g\tau/2 = k\pi$ or $n = kT/\tau$, where k is an integer. The first null in G_n occurs at $n = T/\tau$, and G_n decreases as $\sin x/x$ for $0 \le n \le T/\tau$. As indicated in Eq. (2.11), the spectral components of the original signal (F_n) is scaled (attenuated) by G_{nm}. Consequently, finite pulse duration of the gate function $g(t)$ constitutes one of the bandwidth limitations of a sampling circuit. This will be discussed in the next section. To minimize spectrum attenuation due to G_{nm} (hence maximize sampling circuit bandwidth), we need to have $\tau << T / km$ so that spectrum attenuation in the band of frequencies of interest is negligible.

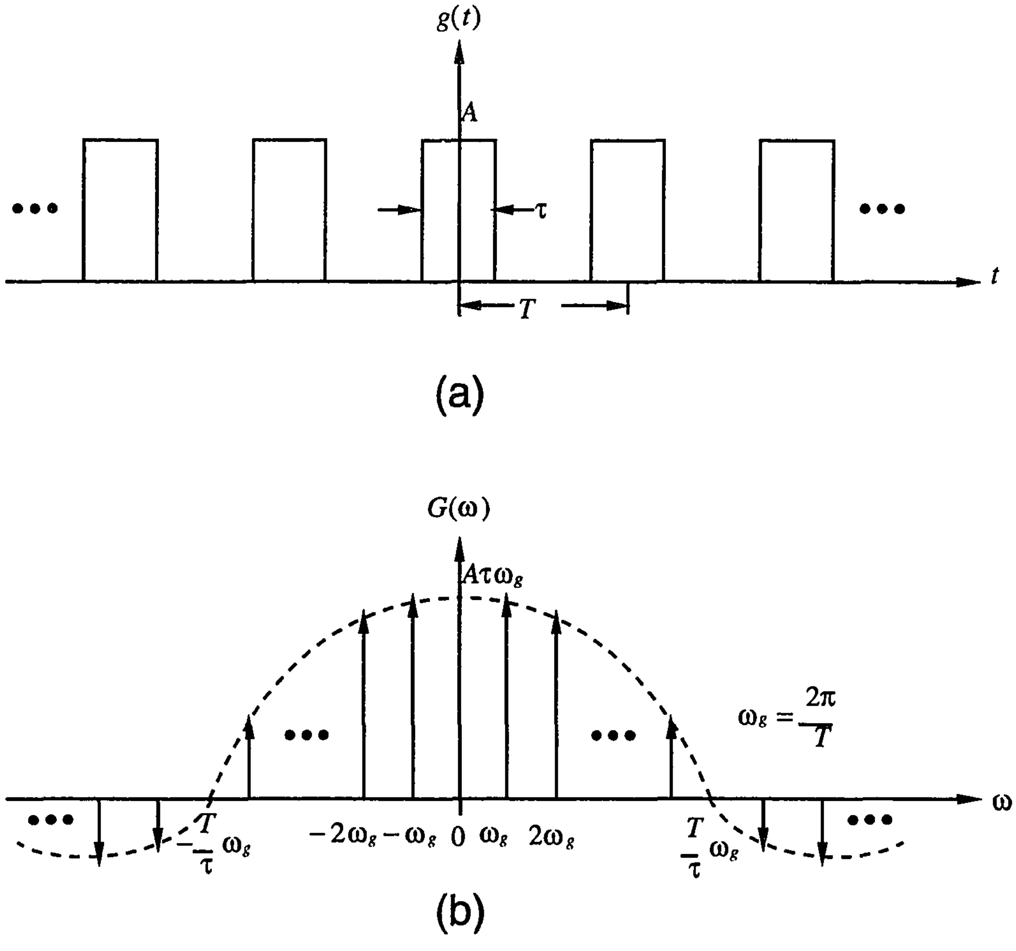

Figure 2.3. Gate function with finite pulse width: (a) time domain, and (b) frequency domain.

Although the above discussion assumes a rectangular sampling pulse shape for $g(t)$, the analysis can be generalized to an arbitrary sampling pulse shape. A finite sampling pulse width places a limit on the sampling circuit bandwidth.

2.2 Sampling Circuit Principle of Operation

Owing to their high cut-off frequencies (low device parasitics), Schottky diodes have long been employed in switching applications such as sampling circuits. To understand the operation of the diode sampling bridges, first examine the 1-diode sampling circuit shown in Fig. 2.4.

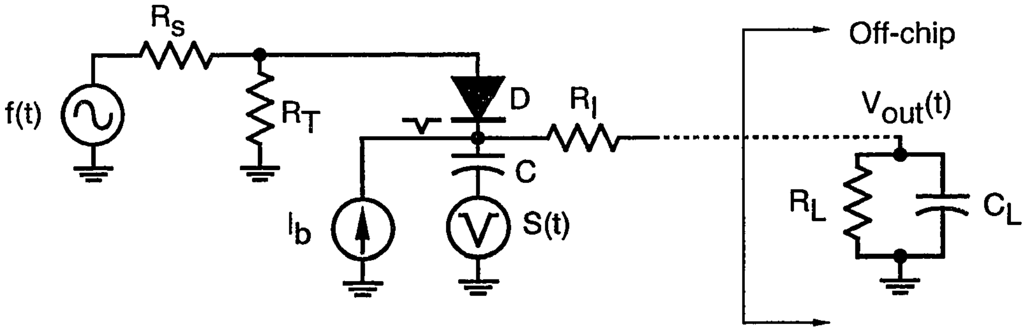

Figure 2.4. Circuit diagram of a 1-diode sampling bridge.

In the 1-diode sampling circuit (Fig. 2.4), $f(t)$ is the input RF signal to be sampled, R_s is the input source resistance, R_t is the termination resistor (normally, $R_s=R_t=50\Omega$), D is the sampling diode, I_b is the current source used to reverse bias the sampling diode, $S(t)$ is the sampling strobe voltage signal, C is the coupling capacitor, $V_{out}(t)$ is the sampled output voltage, R_L is the load resistor (usually off-chip), C_L is the capacitance of the cables connecting the sampling circuit to the oscilloscope which measures the sampled output voltage, and R_I is the on-chip isolation resistor used to isolate the cable capacitance from the coupling capacitor. Because C_L is usually much greater than the C, we will neglect C_L from the subsequent sampling circuit analysis, and its effect on the sampling circuit IF signal bandwidth will be discussed in Chapter 4. Further, we assume that the sampling capacitor C is so large that the AC voltage across the capacitor, in response to the application of the strobe pulse train, is practically zero. For physical realization of the sampling circuits, the diode reverse bias current sources need not be implemented, and the circuit can instead be self-biased. The self-bias concept can be understood by examining the operation of a DC restorer circuit (Fig. 2.5(a)). For simplicity, we assume that the diode has a current voltage characteristic as shown in Fig. 2.5(b). Assume initially, $S(t)$ is at V_1 and $V_{out}(t)$ is at zero volts. When $S(t)$ switches from V_1 to $-V_2$, $V_{out}(t)$ attempts to follow. However, according to the diode I-V curve shown in Fig. 2.5(b), $V_{out}(t)$ is clamped at $-V_{on}$. When $S(t)$ switches from $-V_{on}$ back to V_1, the diode is turned-off, and $V_{out}(t)$ will swing from $-V_{on}$ to $V_1 + V_2 - V_{on}$. For a pulse train $S(t)$ (Fig. 2.5(c)), the steady-state $V_{out}(t)$ is then as shown in Fig. 2.5(d). The diode is reverse-biased most of the time at the voltage $V_1 + V_2 - V_{on}$. For $T_{on} << T_{off}$, the output DC voltage (V_{dc}) is equal to the diode reverse-biased voltage $V_1 + V_2 - V_{on}$.

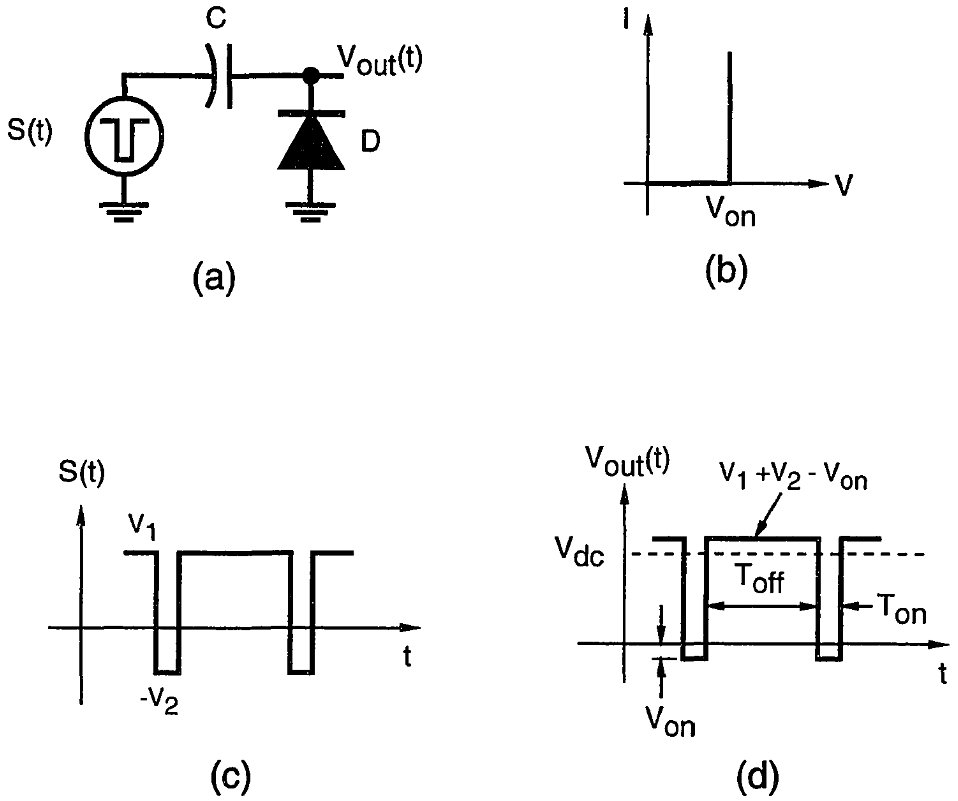

Figure. 2.5. Operation of an ideal DC restorer circuit: (a) circuit diagram, (b) diode I-V characteristic, (c) input signal waveform, and (d) output signal waveform.

A more realistic DC restorer circuit is shown in Fig. 2.6(a). This circuit can be obtained from the 1-diode sampling circuit shown in Fig. 2.4 with $f(t) = 0$, $I_b = 0$, $C_L = \infty$, and $R = R_l + R_L$. Again, assume a diode I-V curve shown in Fig. 2.5(b). When $S(t)$ is at V_1 (at $t = t_0$), the diode is off. A current now flows through R and causes $V_{out}(t)$ to fall exponentially with a time constant $R \cdot C$ between t_0 and t_1. At $t = t_1$, $S(t)$ switches from V_1 to $-V_2$, $V_{out}(t)$ attempts to follow. The diode conducts heavily to quickly charge the capacitor, and $V_{out}(t)$ is clamped at $-V_{on}$. At $t = t_2$, $S(t)$

switches to V_1, $V_{out}(t)$ follows, and the cycle repeats itself. In steady state, the charge lost on the capacitor during the time interval t_0 to t_1 is recovered during the interval t_1 to t_2, and an equation relating the peak diode conduction current and the average output voltage (the diode self-bias voltage) can be derived.

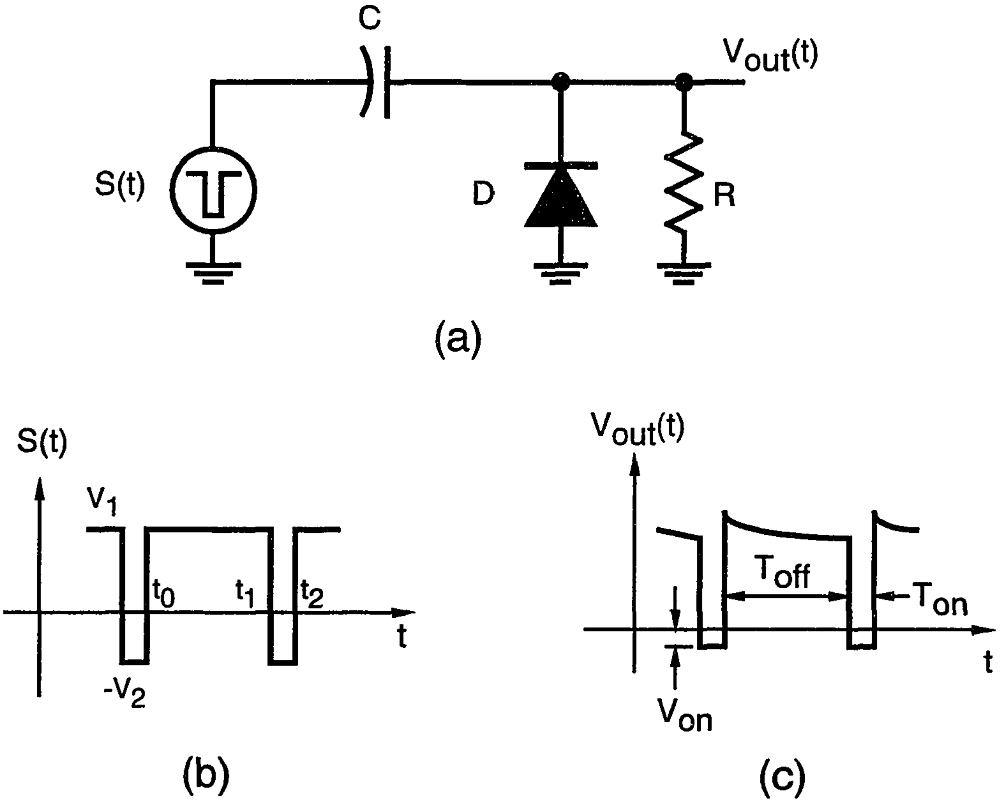

Figure 2.6. Operation of a realistic DC restorer circuit: (a) circuit diagram, (b) input signal waveform, and (c) output signal waveform.

For the nonlinear transmission line (NLTL) gated sampling circuits discussed in the next section, the capacitor discharging $R \cdot C$ time constant is much larger than the interval when the sampling diode is off (T_{off} in Fig. 2.6(c)), and $V_{out}(t)$ resembles that shown in Fig. 2.5(d). The diode conduction current $I_s(t)$, in this case, is as shown in Fig. 2.7.

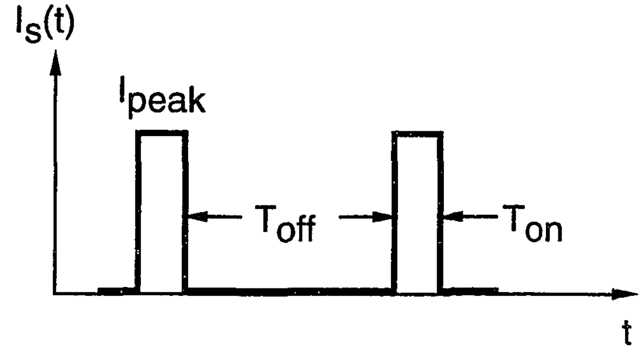

Figure 2.7. Waveform of the diode conduction current for the DC restorer circuit shown in Figure 2.5.

According to the charge equilibrium requirement $Q_{charged} = Q_{discharged}$, we can write (approximately),

$$I_{peak} \cdot T_{on} \approx \frac{V_{sb}}{R_L} T_{off} \tag{2.14}$$

where I_{peak} is the peak diode conduction current. Since V_{sb}, T_{on}, and T_{off} are determined by the waveform characteristics of $S(t)$, a particular I_{peak} can be obtained with a R_L calculated using Eq. (2.14).

To relate the sampling operation in the diode sampling circuit with the sampling theory discussed in Sec. 2.1, examine the equivalent circuit diagram (Fig. 2.8(b)) for the 1-diode sampling circuit shown in Fig. 2.4. The model for the sampling diode is shown in Fig. 2.8(a), where R_{ds} is the diode series resistance, C_d is the diode junction capacitance, and g_d is the diode conductance. Using this diode model, neglecting C_L, and eliminating I_b from Fig. 2.4, we have the equivalent circuit for the 1-diode sampling circuit shown in Fig. 2.8(b), where $R = R_{ds} + R_s \| R_l$.

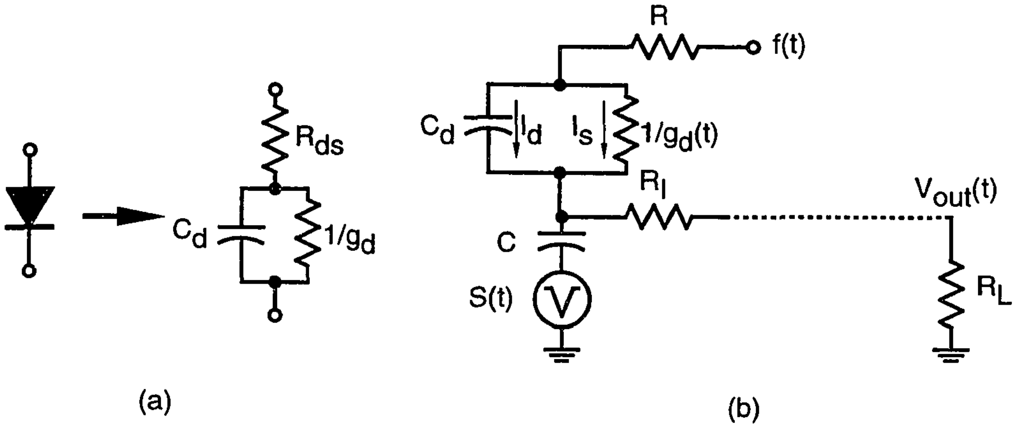

Figure 2.8. Equivalent circuit of a 1-diode sampling circuit: (a) diode model, and (b) circuit diagram.

In Fig. 2.8(b), $g_d(t) = \partial I_s / \partial V_d = I_s(t) / V_T$ where V_T is the thermal voltage. Using the diode current waveform shown in Fig. 2.7, $g_d(t)$ will be I_{peak} / V_T during T_{on} and zero during T_{off}. For normal operation of the sampling circuit, C is designed to be much larger than C_d. Upon application of a strobe pulse, a large displacement current I_d quickly charges up the diode junction capacitor C_d to turn-on the diode while this displacement current contributes practically no change to the voltage of the coupling capacitor C. However, when the diode is on, the diode conduction current I_s charges/discharges the coupling capacitor which in turn produces a change in the output voltage $V_{out}(t)$.

For the NLTL-gated sampling circuit discussed later in this chapter, C is large such that $V_{out}(t) \approx 0$ for each occurrence of the strobe pulse $S(t)$. In this case, we can write:

$$I_s(t) = \frac{f(t)}{R + 1/g_d(t)} = f(t) \cdot g(t) \qquad (2.15)$$

where $g(t) = f(t)/(R + 1/g_d(t))$ is the gate function for the sampling operation as discussed in the last section. For the diode conduction current waveform shown in Fig. 2.7, $g(t)$ will be as shown in Fig. 2.9. We can observed that the gating time T_{on} is the same as the diode-on time.

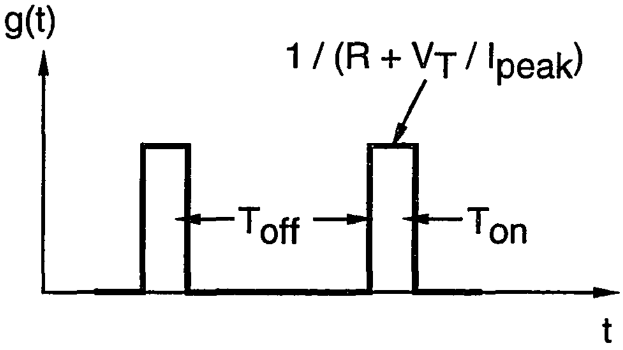

Figure 2.9. Sampling gating function $g(t)$.

Having obtained the expression for the output signal current $I_s(t)$ which charges/discharges the coupling capacitor (Eq. (2.15)), the output voltage can be found to be:

$$V_{out}(t) = V_{bs} + \frac{1}{C}\int_0^{T_{IF}} I_s(t)dt \qquad (2.16)$$

where V_{bs} is the diode self-bias voltage and T_{IF} is the IF signal periods. The IF signal period (or the IF signal bandwidth) will be discussed in Chapter 4. If $f(t) = 0$,

$V_{out}(t) = V_{bs}$, hence the sampling diode self-bias voltage can be measured with zero input signals.

The analysis so far assumes a rectangular strobe pulse train and an ideal diode I-V curve (Fig. 2.5(b)), hence the resulting diode on-time is the same as the strobe pulse width (Fig. 2.6 and Fig. 2.7). For a more realistic strobe signal $S(t)$ (such as the triangular pulse train shown in Fig. 2.10(a)) and diode I-V characteristic (i.e. the diode is on over a finite diode voltage range), it is apparent that the diode aperture time can be much smaller than the full-width-half-maximum (FWHM) of the strobe voltage pulses (Fig. 2.10).

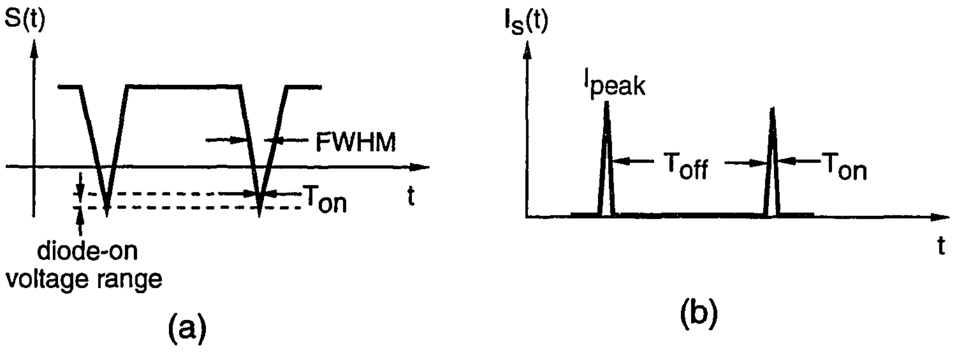

Figure 2.10. (a) A triangular sampling strobe pulse train, and (b) the corresponding diode conduction current.

The disadvantage of the 1-diode sampling circuit is that as the voltage at the anode of the diode goes beyond the diode turn-on voltage, a fraction of the strobe signal $S(t)$ is coupled back to the input signal generator because the diode voltage is clamped at ≈0.8 V after turn-on. This effect, called kick-out, is analogous to spurious LO-RF coupling in mixers, and is suppressed by using a balanced circuit such as the 2-diode sampling circuit shown in Fig. 2.11.

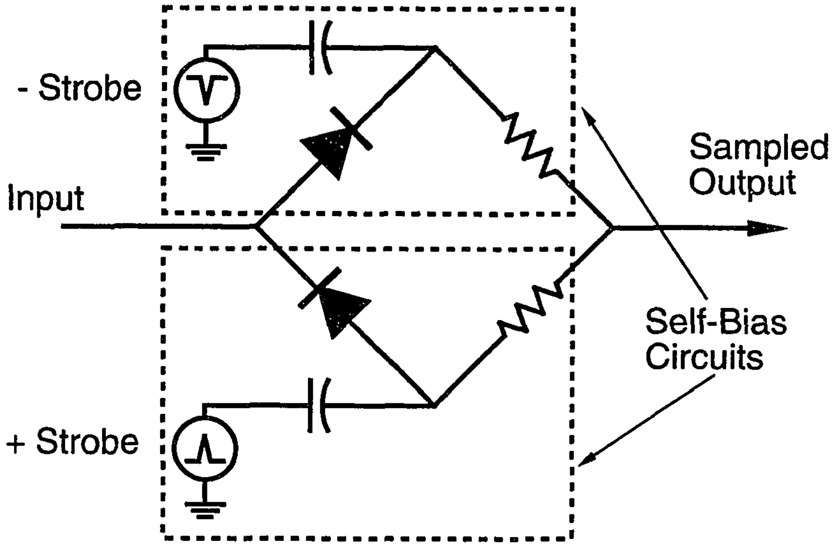

Figure 2.11. Circuit diagram of a 2-diode sampling circuit.

The operation of the 2-diode sampling circuit is similar to the 1-diode sampling circuit. The advantage of this circuit is that the circuit is balanced and hence the net kick-out voltage on the signal line is minimized. In addition, the two-diode sampling bridge generates a pair of common mode signals which can be fed to a summing amplifier, thereby rejecting any spurious differential mode signals.

Important figures of merit for sampling circuits are the sampling efficiency, bandwidth, and dynamic range. Noise figure of the sampling circuits is also important for certain low-noise applications such as sampling circuits used in active probes for network analysis and as mixers for front-end receivers in wireless communications. We will defer the discussion of the sampling circuit noise figure to Chapter 4. The sampling efficiency is defined as the ratio of the voltage on the sampling capacitor e_{sample} to the input voltage e_{in}:

$$\eta = \frac{e_{sample}}{e_{in}}$$

The bandwidth of the sampling circuit is defined to be the frequency at which η is $1/\sqrt{2}$ times its low-frequency value (- 3 dB point). As discussed earlier, the bandwidth of the sampling circuit is inversely proportional to the time for which the sampling diode is on (t_g). It can be shown that the bandwidth of a sampling circuit is approximately [33]

$$BW(GHz) = \frac{350}{t_g(ps)} \tag{2.17}$$

where t_g is the FWHM of the diode aperture time. In the form of Eq. 2.17, t_g is analogous to the 10-90% risetime of the step response of a single-time-constant circuit.

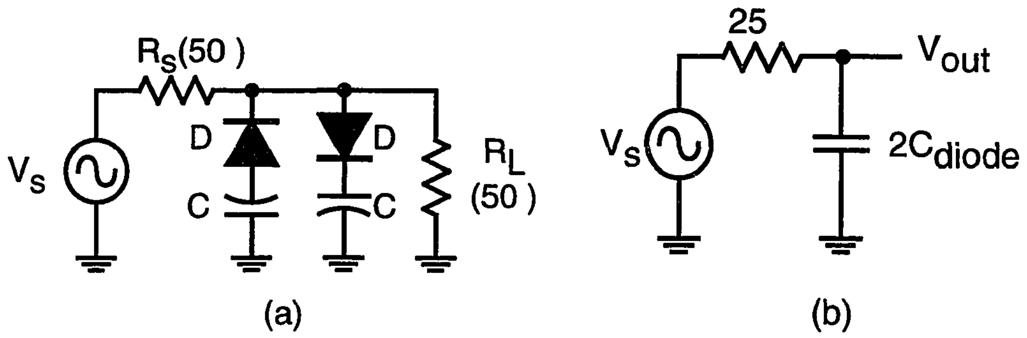

Figure 2.12. Input signal path circuit diagrams: (a) equivalent circuit; (b) simplified equivalent circuit.

Another bandwidth limitation arises from the sampling diode capacitances. For the 2-diode sampling bridge shown in Fig. 2.11, an equivalent circuit for the input signal path is shown in Fig. 2.12(a). Because the sampling diodes are reverse biased most of the time, they are voltage dependent capacitors. Since the diode capacitance (C_{diode}) is much less than the coupling capacitance C, the coupling capacitors can be replaced by short circuits and an simplified equivalent circuit for the input signal path is shown in Fig. 2.12(b). The risetime for the step response of the circuit in Fig. 2.12(b) is then $t_{signal} = 2.2 \times 25\Omega \times 2C_{diode}$. Since C_{diode} is voltage dependent, t_{signal} is best determined using SPICE simulation.

As discussed earlier, the finite pulse width of the sampling pulses places a single-time-constant-like limitation on the bandwidth of the sampling circuit. Assuming these bandwidth limitation effects are linear and time-invariant, the overall bandwidth of the sampling circuit is the convolution of these two effects. Using approximate, sum-of squares convolution (exactly appropriate only if all constituent responses are Gaussian), the approximate risetime in the step response of the sampling circuit is

$$t_r \cong \sqrt{t_g^2 + t_{signal}^2} \tag{2.18}$$

and the approximate -3-dB bandwidth of the sampling circuit is

$$BW(GHz) = \frac{350}{t_r(ps)} \tag{2.19}$$

The dynamic range of the sampling circuit is defined as the ratio of the maximum measurable and minimum resolvable signal amplitudes. The minimum resolvable signal amplitude is limited by the noise figure of the sampling circuit and any other sources of noise. The maximum measurable signal amplitude is limited by the self-bias of the sampling diodes, which is in turn limited by the strobe pulse amplitude that is coupled to the sampling diodes.

2.3 The Nonlinear Transmission Line Gated Sampling Circuit

As with most of the integrated circuits (ICs), IC design is a iterative process of hand analysis, simulation and layout because layout parasitics must be included in the models for circuit simulation, and the final circuit layout must function properly with these parasitics. Hence, this section describes collectively the design, simulation, layout, and fabrication of the nonlinear transmission line (NLTL) gated sampling circuits.

Sampling circuits gated by 20-30 ps Silicon SRDs are band-limited to 20-40 GHz. At the time of this thesis research, nonlinear transmission lines have allowed generation of transient signals of 5-6 volt amplitudes and 1-2 picosecond transition times [28]. More recently, 0.48 ps transitions have been attained by Scott Allen et. al. [27]. With these NLTLs, sampling pulses with a factor of 20-40 shorter than obtainable with the Silicon SRDs can be generated, and NLTL-gated sampling circuits incorporating ≈2-4 THz Schottky sampling diodes can attain much higher bandwidth than obtainable with Silicon SRD-gated sampling circuits.

The operation of the NLTL has been studied extensively and described thoroughly in a number of publications [28,29,34,35,36]. For the sake of completeness of this dissertation, a very brief description is given below. The NLTL is an electrical pulse (wavefront) compressor. The NLTL (Fig. 13) is a high impedance transmission line periodically loaded by reverse-biased Schottky diodes acting as voltage-variable capacitors. The wave propagation velocity varies as the inverse square root of the total (diode plus transmission line) capacitance per unit length and hence increases as the diode reverse bias voltage is increased. For a negative-going step function (wavefront) input, the initial portions of the wavefront, near zero volts,

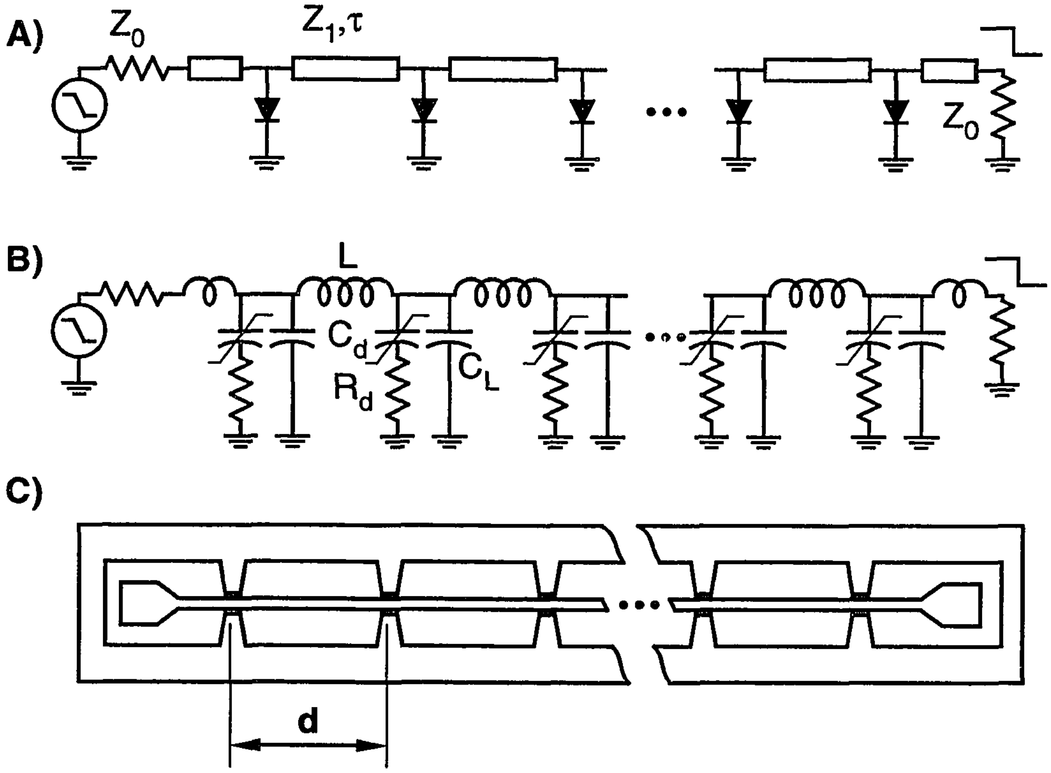

Figure 2.13. (a) NLTL circuit diagram, (b) equivalent circuit, and (c) layout, where C_d is the diode capacitance and R_d its series resistance, $C_L = \tau / Z_l$ is the line capacitance and $L = Z_l \tau$ the line inductance.

propagate more slowly than the final, more negative, portions of the wavefront. The wavefront transition time (falltime) will progressively decrease with propagation distance. An asymptotic (minimum) compressed falltime is eventually reached (Fig. 14) at which the NLTL compression is balanced by various bandwidth limits in the structure. The two dominant bandwidth limits are the varactor diode cut-off frequency $f_D = 1/2\pi R_d C_d$ (defined using the average diode capacitance $\Delta Q/\Delta V$) and the periodic-line (Bragg) cut-off frequency $f_{per} = 1/\pi\sqrt{L(C_d + C_L)}$. The NLTLs employed in this work use hyperabrupt varactor diodes. Hyperabrupt varactors have larger capacitance variation than uniform-doped diodes, thereby increasing the NLTL compression rate, decreasing the required NLTL length and hence both the skin loss and the die area. When driven by a sinewave, the NLTL output is a sawtooth waveform with picosecond transition time. Its output therefore has a Fourier spectrum with power at high harmonics of its drive frequency.

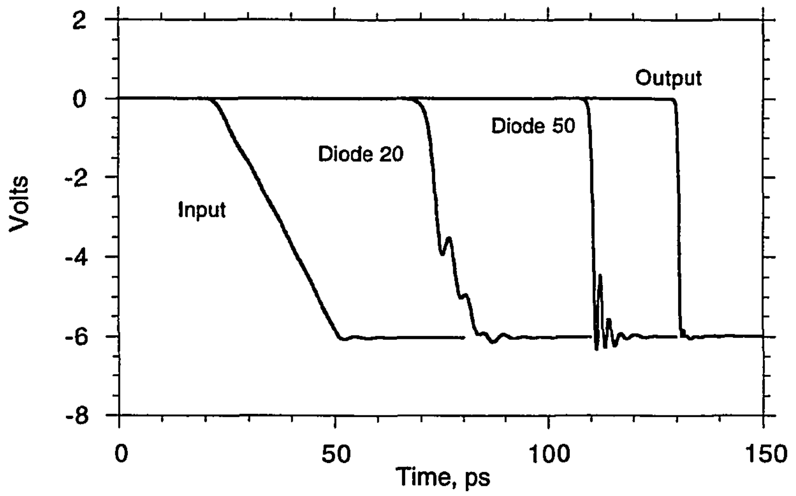

Figure 2.14. SPICE simulation of NLTL wavefront compression and shock-wave formation.

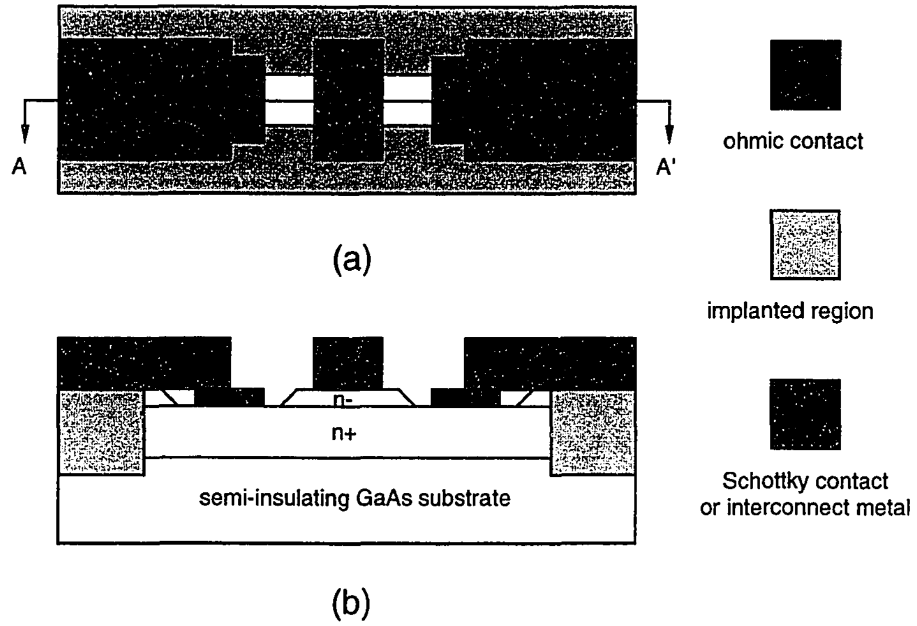

Figure 2.15. A fabricated Schottky diode: (a) top view, and (b) cross sectional view of AA'.

A simple 3-mask process has been used to fabricate these sampling circuits. Schottky diodes for both the NLTL and the sampling bridge are formed on GaAs molecular beam epitaxy material with a 425 nm n- active layer (2 x 10^{17} /cm^3). A buried 1 μm n$^+$ layer (6 x 10^{18} /cm^3) provides the diode cathode connection, second-layer interconnections, and 7Ω per square resistors. Ohmic contacts to the n$^+$ layer are formed by 0.5 μm $NH_4OH\,/\,H_2O_2\,/\,H_2O$ recess etch, a self-aligned AuGe/Ni/Au liftoff, and subsequent alloying. Proton implantation at 180 keV, 1.7 x 10^{15} /cm^2 and 110 keV, 4 x 10^{14} /cm^2 (masked by 1.7 μm Au on 1.0 μm polyimide) provides >50 MΩ per square isolation, defining resistors and diode contact areas. Interconnections are formed with an 800 Å Ti/80 Å Pt/11000Å Au liftoff; Schottky contacts result where the liftoff intersects unimplanted material. The top view and cross-sectional view of a

Schottky diode fabricated with this process are shown in Fig. 2.15, illustrating various features just described. Detailed process flow sheets are attached in Appendix B.1.

The important diode figures of merit include diode nonlinearity (important for shockwave formation on the NLTL), breakdown voltage (which determines the NLTL shockwave amplitudes), and cut-off frequency (important for both high speed NLTLs and sampling circuits). These have been thoroughly discussed in Michael Case's Ph. D. thesis [35]. In this dissertation, a discussion on the diode parasitic resistances and capacitances is given because these diode parasitics play an important role in determining the sampling circuit bandwidths.

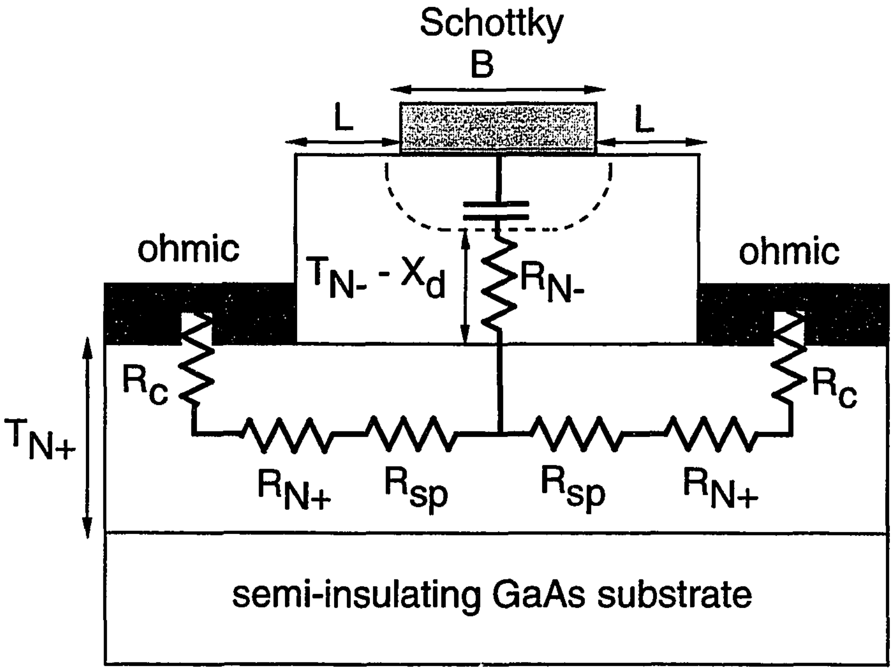

Figure 2.16. Cross-sectional view of a Schottky diode with parasitic resistances and capacitance.

A cross sectional view of the ion-implant isolated Schottky diode with parasitic capacitances and resistances is shown in Fig. 2.16. R_{N^-} is the undepleted N^- layer resistance and is

$$R_{N^-} = \rho_{N^-} \cdot \frac{(T_{N^-} - x_d)}{WB} \qquad (2.17)$$

where B is the length of the Schottky contact, w is the width of the Schottky contact, T_{N^-} is the N^- layer thickness, x_d is the depletion layer thickness, and ρ_{N^-} is the N^- layer resistivity. R_{sp} is the spreading resistance and is

$$R_{sp} = \frac{1}{6}\left(\frac{\rho_{N^+}}{T_{N^+}} \cdot \frac{1}{2} \cdot \frac{B}{W}\right) = \frac{1}{12} \cdot \rho_{S,N^+} \cdot \frac{B}{W} \qquad (2.18)$$

where ρ_{N^+} is the N+ layer resistivity, T_{N^+} is the N^+ layer thickness, and $\rho_{S,N^+} = \rho_{N^+} / T_{N^+}$ is the sheet resistivity of the N^+ layer. R_{N^+} is the N^+ layer resistance and is

$$R_{N^+} = \rho_{S,N^+} \frac{L}{2W} \qquad (2.20)$$

R_C is the ohmic contact resistance and is

$$\frac{\sqrt{\rho_{S,N^+}\rho_C}}{2W} = \frac{\rho'_C}{2W} \qquad (2.21)$$

where ρ_C is the vertical ohmic contact resistivity in units of $\Omega \cdot length^2$ and $\rho'_C = \sqrt{\rho_{S,N^+}\rho_C}$ is the ohmic contact resistivity in units of $\Omega \cdot length$. Finally, the diode capacitance is

$$C_d = \varepsilon \cdot \frac{A}{x_d} = \varepsilon \cdot \frac{BW}{x_d} \qquad (2.22)$$

where $A = BW$ is the area of the Schottky contacts and $\varepsilon = 13\varepsilon_0$ is the dielectric constant of GaAs. Since x_d is voltage dependent, C_d is voltage dependent. For design of sampling circuits where reverse-biased diodes are used as capacitors, a large-signal (average) capacitance is defined as

$$C_{ls} = \frac{\Delta Q}{\Delta V} = \frac{A}{V_{high} - V_{low}} \int_{x_d(V_{high})}^{x_d(V_{low})} qN_D(x_d)dx_d \tag{2.23}$$

where V_{high} and V_{low} is, respectively, the high and low voltage of the diode voltage swing, and $N_D(x_d)$ is the doping density of the N^+ layer at x_d.

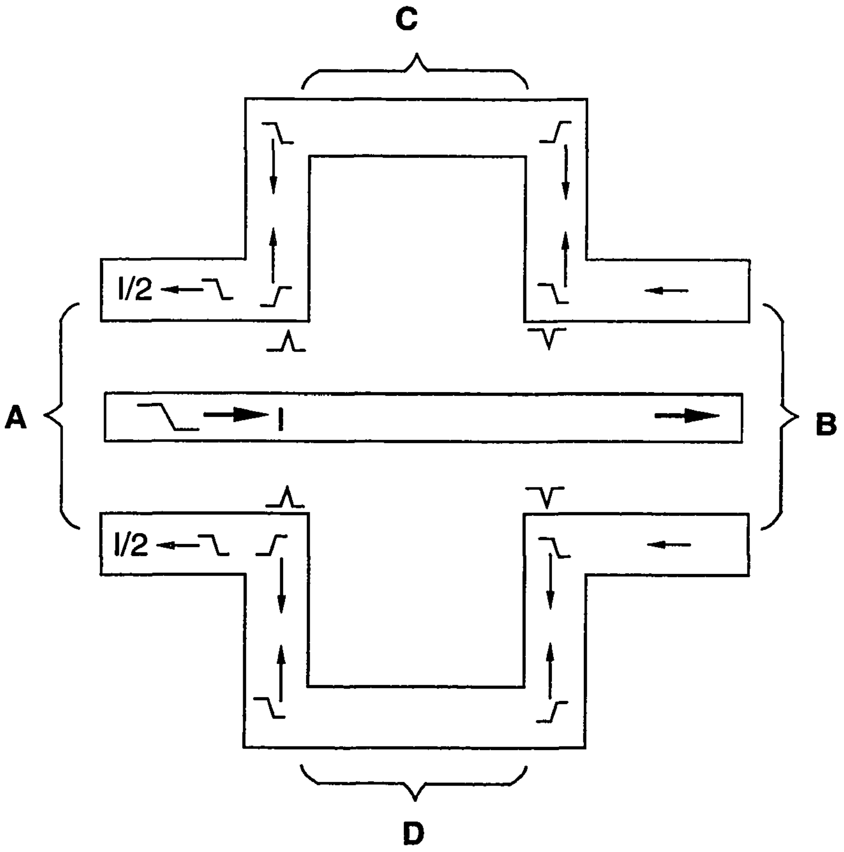

Figure 2.17. Conceptual diagram of the CPW/CPS balun/differentiator.

From a sinusoidal input, the NLTL generates a sawtooth waveform with picosecond falltimes. A circuit known as the balun/differentiator is used to convert the sawtooth waveform into a train of sampling (strobe) pulses. One such circuit is implemented with coplanar waveguides (CPW) and coplanar stripes (CPS) (Fig. 2.17). Four transmission lines can be identified in the circuit: lines A and B are CPW lines, and lines C and D are CPS lines. When a negative going step is applied on line A traveling towards line B, the return currents in the ground planes of the CPW lines (A and B) travel as a CPS mode on the CPS lines (C and D). Because the two CPS lines are short circuited, the forward traveling step functions are reflected back with reversed polarities, and pulses (the sum of the forward and reflected step functions) are generated at the launch points of the CPS lines. The polarities of these pulses, with respect to the center of the CPS lines, are as shown in Fig. 2.14. This, in effect, differentiates the step function into pulses, hence the name of the circuit. Balun is a contraction for balanced-unbalanced converter, and it represents the feeding (excitation) of the balanced (CPS) mode by the unbalanced (CPW) mode in the circuit.

Both the amplitude and duration of these sampling (strobe) pulses are important as the amplitude limits the dynamic range of the sampling circuits and the duration limits the bandwidth of the sampling circuits. First examine the amplitude of the sampling pulses. Fig. 2.18(a) is the equivalent circuit for the circuit shown in Fig. 2.17, and Fig. 2.18(b) is the circuit including the source ($R_s = 50\Omega$) and termination ($R_l = 50\Omega$) resistors in the CPW line.

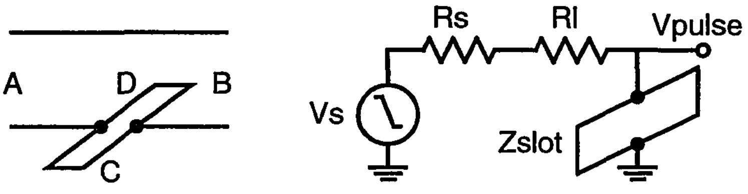

(a) (b)

Figure 2.18. Equivalent circuits of the balun/differentiator.

The amplitude of the sampling pulse at the CPS slots is

$$V_{pulse} = \frac{Z_{slot}/2}{2R_s + Z_{slot}/2} V_s$$

It is difficult to obtain $Z_{slot} >> 100\ \Omega$. If we choose $Z_{slot}/2$ be $50\ \Omega, V_{pulse}$ then becomes one-third of V_s, a significant reduction in the pulse amplitude. In addition, the shorted high-impedance (100Ω) CPS lines are inductive and cause large reflections back to the strobe pulse generator V_s. The inductance of the parallel shorted CPS lines (L_{slot}) is approximately $\tau_{slot} \cdot Z_{slot}/2$, where τ_{slot} is the electrical length of the CPS lines. A modified circuit (Fig. 2.19(a)) reduces both these difficulties. The addition of $C2$ bypasses Rl at high frequencies and a larger input signal step (high frequency signal) can therefore be coupled to the CPS differentiator. Moreover, as shown in the equivalent circuit (Fig. 2.19(b)) for the network consisting of $C1$, $C2$, Rl, and Z_{slot} in Fig. 2.19(a), the π network comprising $C1$, $C2$, and L_{slot} provides a broadband match for the strobe circuit. Assuming $C1{=}C2{=}C/2$, C can be calculated from $\sqrt{L_{slot}/C} = 50\Omega$. For example, for τ_{slot}=1.5 ps and Z_{slot}=100Ω, L_{slot} is 75 pH, hence C=30 fF and $C1{=}C2$=15 fF. The optimal values of $C1$ and $C2$ which generate large sampling pulses while maintaining acceptable reflection levels are best determined from SPICE simulations.

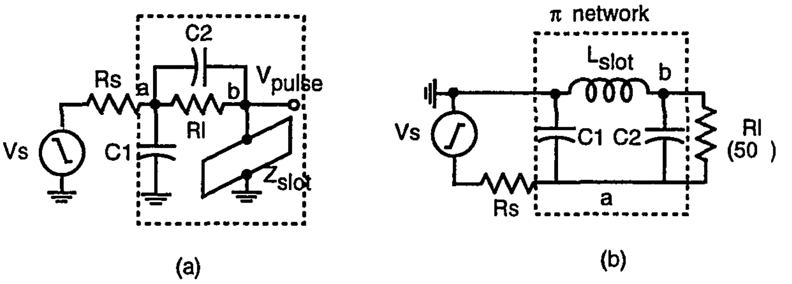

Figure 2.19. Circuit diagrams of (a) modified strobe generation circuit, and (b) matching network formed by C1, C2 and Lslot.

The duration of the strobe pulses are limited by several effects: the length (delay) of the CPS line, broadening of the strobe pulses due to sampling diode capacitance, and the sampling diode reverse bias. Fig. 2.20 illustrates the effect of the length (delay) of the CPS slot on the strobe pulse duration and amplitude: when 2τ (the round-trip delay of the CPS line) is less than T_f (fall time of the input step), the pulse amplitude V' is less than the input step amplitude V, and T_f' (the full-width-half-maximum duration of the strobe pulses) is less than T_f. When 2τ is greater than T_f, V'=V and $T_f' > T_f$ while when 2τ is equal to T_f, V'=V and $T_f' = T_f$. Consequently, a large amplitude and small pulse width is obtained with the CPS slot round-trip delay equal to the input step falltime.

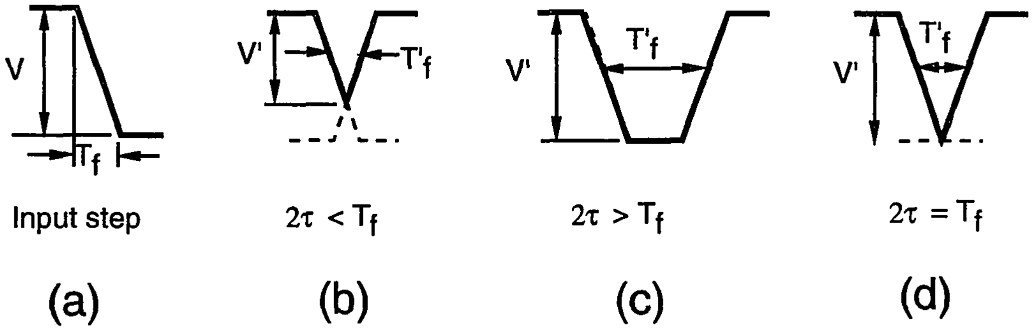

Figure 2.20. Diagram illustrating effect of the CPS round-trip delay to the amplitude and duration of the strobe pulses: (a) input step, (b) round-trip delay less than input falltime, (c) round-trip delay greater than input falltime, and (d) round-trip delay equals input falltime.

The pulse broadening effect by the sampling diode parasitics can be understood by investigating the circuit shown in Fig. 2.21(a). This circuit is similar to the strobe generation circuit shown in Fig. 2.19(a) except that the sampling diode is added as the load to the circuit. In Fig. 2.21(a), D is an ideal diode, and C_d and R_d is, respectively, the parasitic capacitance and resistance of the sampling diode. With a CPS round-trip delay of 3 ps, the strobe pulse signals with and without the sampling diode were obtained with SPICE simulation, and the results are shown in Fig. 2.21(b). It can be observed that the strobe pulse is broadened by the sampling diode parasitics. However, the sampling diode $R_d \cdot C_d$ time constant is less than 0.1 ps, its broadening effect on a 3 ps pulse is therefore not significant (Fig. 2.21(b)).

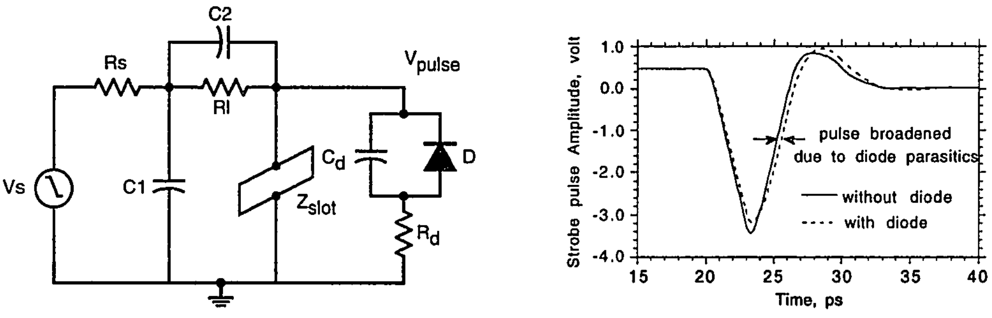

(a) (b)

Figure 2.21. Broadening of strobe pulses by sampling diode parasitics: (a) equivalent circuit, (b) strobe pulse waveforms with and without the sampling diode obtained from SPICE simulation.

Finally, the pulse width is affected by sampling diode reverse bias. An external diode reverse bias can be used to vary the sampling diode aperture time. For a given strobe signal and load resistance, a larger reverse bias voltage shortens the sampling diode aperture time while the diode conduction current amplitude is reduced, as illustrated in Fig. 2.22. However, according to Eq. (2.16), a smaller diode conduction current amplitude gives rise to a smaller output sampled voltage. As a result, with external diode reverse bias, there is a trade-off between short sampling diode aperture time and small sampling circuit conversion loss.

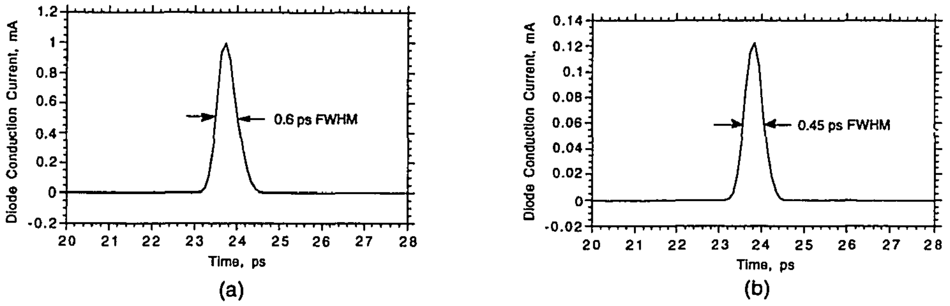

Figure 2.22. SPICE simulation illustrating effect of diode bias on strobe pulse width: (a) smaller diode reverse-bias, and (b) larger diode reverse-bias

As discussed in last section, the overall rise time of the sampling circuit is

$$T_{overall} = \sqrt{t_g^2 + t_{signal}^2} \quad \text{and} \quad BW(GHz) = \frac{350}{T_{overall}(ps)}$$

where t_g is the pulse duration and t_{signal} is the RF signal path rise time due to sampling diode parasitics.

A complete sampling circuit diagram is shown in Fig. 2.23(a). Most of the circuit elements shown have been described earlier. $D1$ and $D2$ are the sampling diodes, and $C3$ and $C4$ are the coupling capacitors. $R8$ provides the termination for the strobe CPW line. $C1$ and $C2$ are the compensation capacitors used to enhance the dynamic range of the sampling circuit as well as to provide a broadband impedance match for the strobe line. $R1$, $R2$, and $R3$ form a 25-dB attenuator on the signal CPW line to prevent overloading of the sampling diodes for large input signals such as the NLTL output signals. $R6$ and $R7$ provides the termination for the input CPW. The balun/differentiator is implemented using the CPS mode of the input signal CPW ground planes. A 30 ps falltime strobe step-function is input to a NLTL, which compresses the falltime to ≈ 2 ps. Coupled through $R8$, $C1$, and $C2$, the strobe step-function is applied between the CPW ground planes, and propagates on them in both directions as a CPS mode. 170 μm (1.5 ps) from the sampling diodes, a short circuit (on the left) and $R2$ and $R3$ (on the right) reflect the CPS mode, generating $\approx$ 3 ps FWHM symmetric positive and negative impulses at the sampling diodes. Due to self-bias, the sampling diode reverse bias is close to the impulse peak amplitude, and the aperture times are consequently much less than 3 ps, as discussed in the last section (Fig. 2.10).

To simplify the fabrication process, only 3 mask steps were used in the first generation of sampling circuits fabricated at UCSB. These circuits were fabricated at 3 μm minimum device dimensions. This complicates the sampling circuit layout, as the circuit requires both signal crossovers and capacitors. Shown in Fig. 2.23(b) is the layout of the sampling circuit shown in Fig. 2.23(a). Instead of using thin-film dielectric capacitors, sampling circuit coupling and compensation capacitors ($C1$-$C4$) are implemented using reverse-biased diodes, while their buried layers provide the wiring crossovers, eliminating the need for air bridges. This reduces inductive parasitics due to air bridges but introduces crossover resistive parasitics due to the diode buried layer resistances (R_{N^-}, R_{N^+}, R_{sp}, and R_C). Where crossed by the strobe line, the N$^+$ layers of $C1$ and $C2$ provide continuity for the input signal CPW ground planes, that of $C3$ connects the input signal CPW ground planes where crossed by the first IF output, and the second IF output crosses beneath the CPW ground plane using the N$^+$ layer of $C4$.

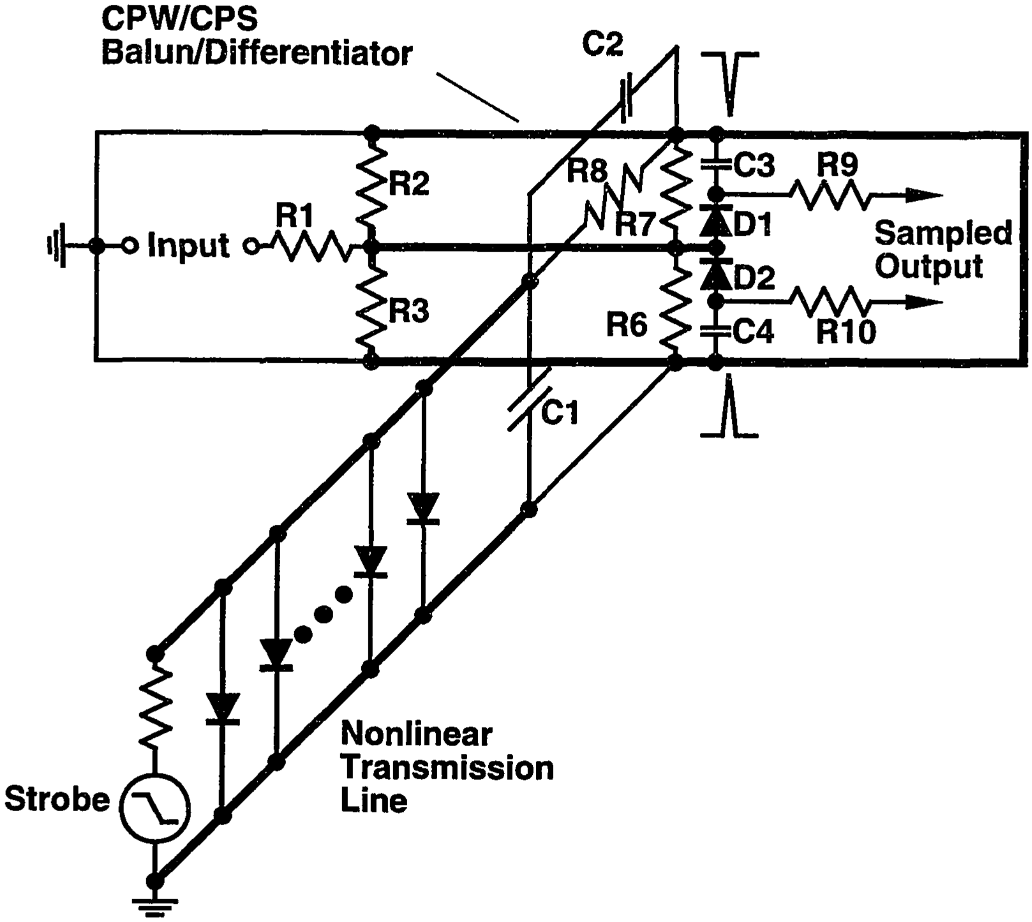
CPW/CPS
Balun/Differentiator
C2
R2
R1
Input
R8
R7
C3
R9
D1
D2
Sampled
Output
R3
R6
C4
R10
C1
Strobe
Nonlinear
Transmission
Line

(a)

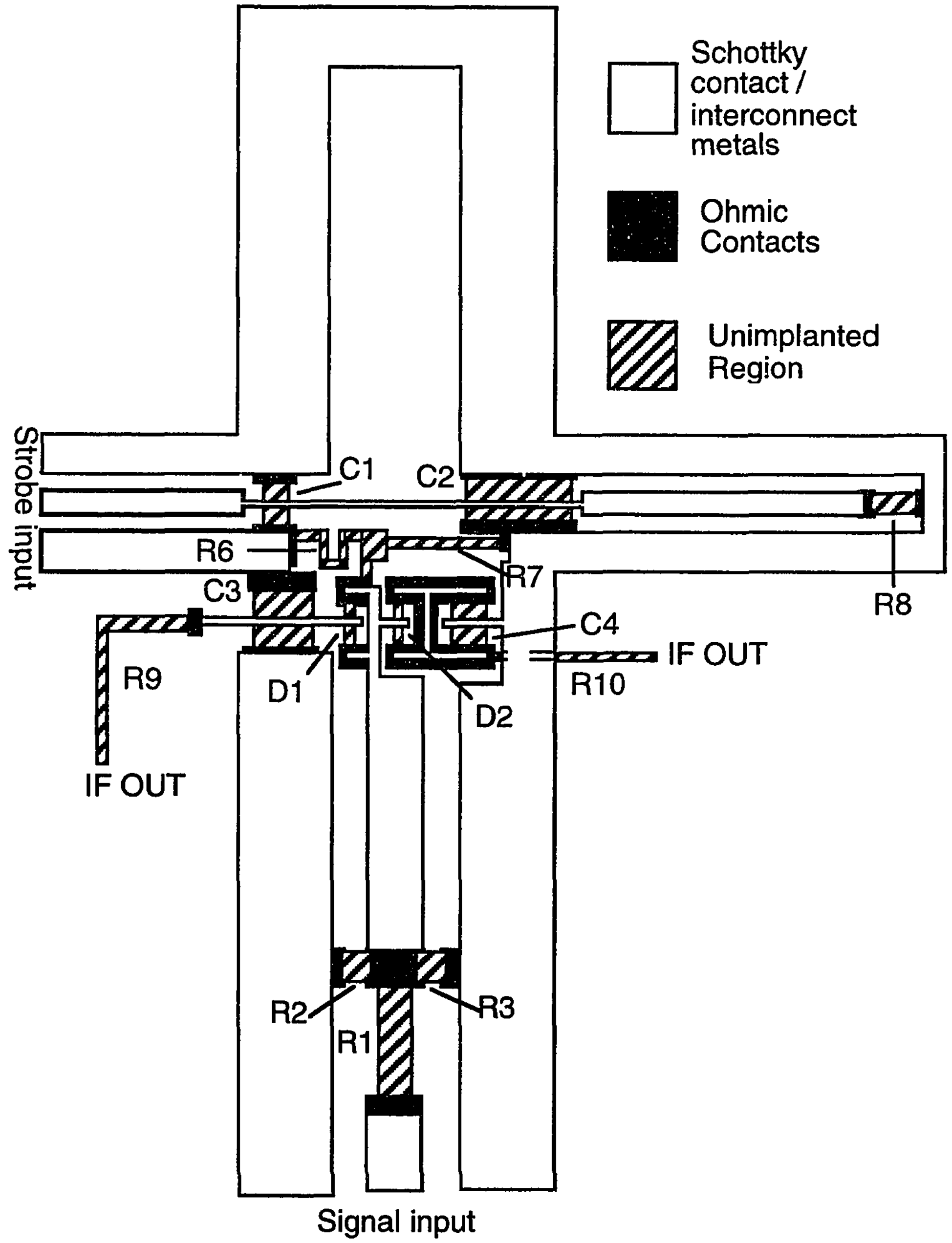

(b)

Figure 2.23. Sampling circuit (a) circuit diagram, and (b) layout.

To minimize the diode capacitance (hence maximize the bandwidth of the sampling circuits), the sampling diodes have minimum geometry of 3 μm x 3 μm Schottky contact area. The reverse biased diodes used to implement the coupling capacitors are 10 times larger than the sampling diodes. For the 25 dB attenuator formed by *R*1 (50 Ω), *R*2 (5 Ω), and *R*3 (5 Ω), the sum of *R*2 and *R*3 presents a reasonably low impedance termination for the CPS balun/differentiator.

So far the sampling circuit design has been based on hand analysis. For more accurate analysis of circuit behavior incorporating diode models and layout parasitics, circuit simulation tools must be utilized. One suitable simulation program is MWSPICE from EESOF, as it adds many transmission line models to the standard SPICE circuit simulator. Based on the epi-layer structure and the doping profiles of the GaAs material, diode parameters necessary for circuit simulation, such as the diode saturation current, zero bias junction capacitance, series resistance, breakdown voltage, diode ideality factor, etc., can be calculated. These diode model parameters are obtained from a program written by Michael Case and are shown in the MWSPICE netlist in Appendix A.1.

The most important figures of merits of the sampling circuits are dynamic range and bandwidth. Because the sampling diodes must remain off between two strobe pulse, the maximum measurable input voltage can be estimated as the difference between the diode anode voltages and the diode-on voltage (≈ 0.8 V). The bandwidth of the sampling circuits can be evaluated by examining both the sampling diode on time and the RC time constant roll-off on the input signal line due to sampling diode parasitics. The sampling diode on time is determined by the duration of the diode conduction current pulse.

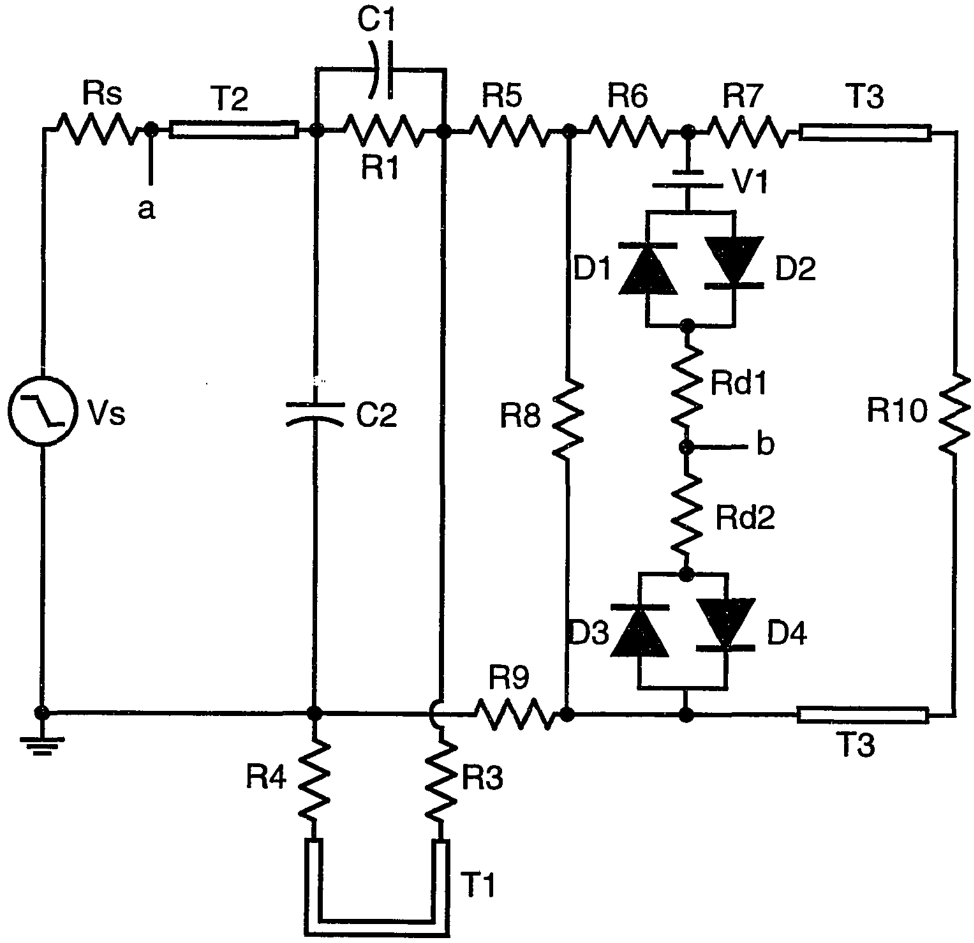

Figure 2.24. Circuit diagram of the strobe signal generation circuit for MWSPICE simulation.

Fig. 2.24 shows the circuit for strobe pulse generation, which includes all the resistive parasitics arising from the use of Schottky diodes as wiring crossovers. *Vs* is the input step function generated by the NLTL. *Rs* is the source resistance (50 Ω). *R*1 is the termination resistor of the strobe line. *C*1 and *C*2 are the compensation capacitors, and *R*3, *R*5, *R*4, and *R*9 are their parasitic resistances, each of which is the sum of R_{N^-}, R_{N^+}, R_{sp}, and R_C (Fig. 2.16) in the diode. *R*8 is due to the termination of the input signal line (200 Ω). Because the sampling diode parasitic capacitance draws a large displacement current when the strobe pulse is applied to the diode while only the diode conduction current contributes to the signal sampling as discussed in the last section, each sampling diode is replaced by a pair of diodes ($D1$ and $D2$, $D3$ and $D4$), one of which represents the voltage dependent diode capacitance only (with zero diode saturation current) and the other has zero capacitance. This separates, in SPICE, the conduction current from the displacement current. $Rd1$ and $Rd2$ are the diode series resistances. Because the coupling capacitors are charged only when the sampling diodes are on, and because the sampling diode on time (< 1 ps) is smaller than the coupling capacitor RC charging time (> 5 ps), it takes many input signal cycles to charge the coupling capacitors to the steady-state diode bias levels, hence exceedingly long simulation time is required. One way to deal with this problem is to replace the coupling capacitors by a DC voltage source $V1$ whose voltage is chosen to set the diode bias to an appropriate diode current level (such as 1 mA peak conduction current). In reality, the peak diode conduction current is set with appropriate load resistance R_L, as discussed in the last section. Transmission lines $T1$ and $T3$ are the CPS lines (3-ps round-trip delay) for the balun/differentiator, and transmission line $T2$ is for monitoring the reflection of the pulse back to the source (it separates the incident signal from the reflected signal).

Many component values in the circuit (such as $C1$, $C2$, and $R1$) are adjusted to achieve best sampling circuit performance. The optimal values for all the circuit elements are shown in the MWSPICE netlist in Appendix A.1. Fig. 2.25 shows the simulation results. Fig. 2.25(a) is the voltage pulse across the sampling diodes (node b in Fig. 2.24). The sampling diodes are reverse biased by at least 0.8 V, hence the maximum input voltage can be as big as 1 V peak before the sampling diodes are inadvertently turned on by the input signal. Fig. 2.25(b) shows the reflection of the strobe pulses back to the strobe signal generator (node a in Fig. 2.24). As described earlier, selection of *C2* represents trade-off between strobe pulse amplitude and reflection back into the NLTL. The chosen 120 fF gives a large strobe pulse amplitude while maintaining a small reflection. Fig. 2.25(c) shows the conduction current pulse width whose FWHM contributes a limitation to the bandwidth of the sampling circuits (Section 2.2). The resulting FWHM is 0.6 ps. Circuit performance sensitivity to variations of the circuit component values must be evaluated for successful implementation of circuits. It was verified, through MWSPICE simulation, that as much as 20% variations in circuit component values do not result in significant degradation in circuit performance.

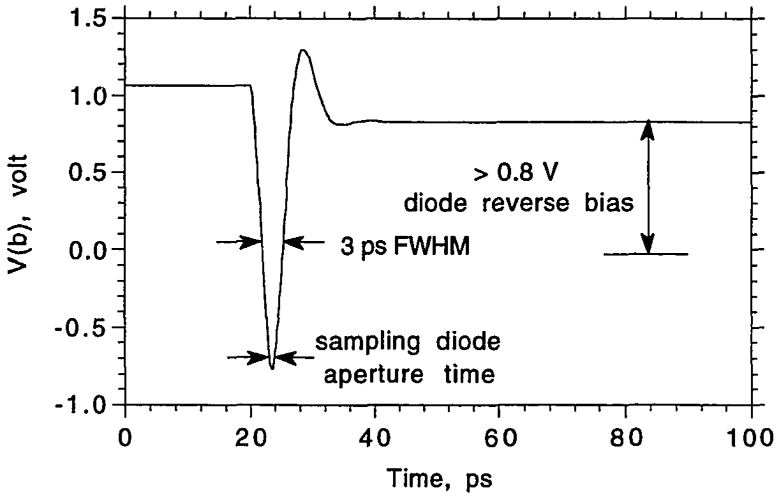

(a)

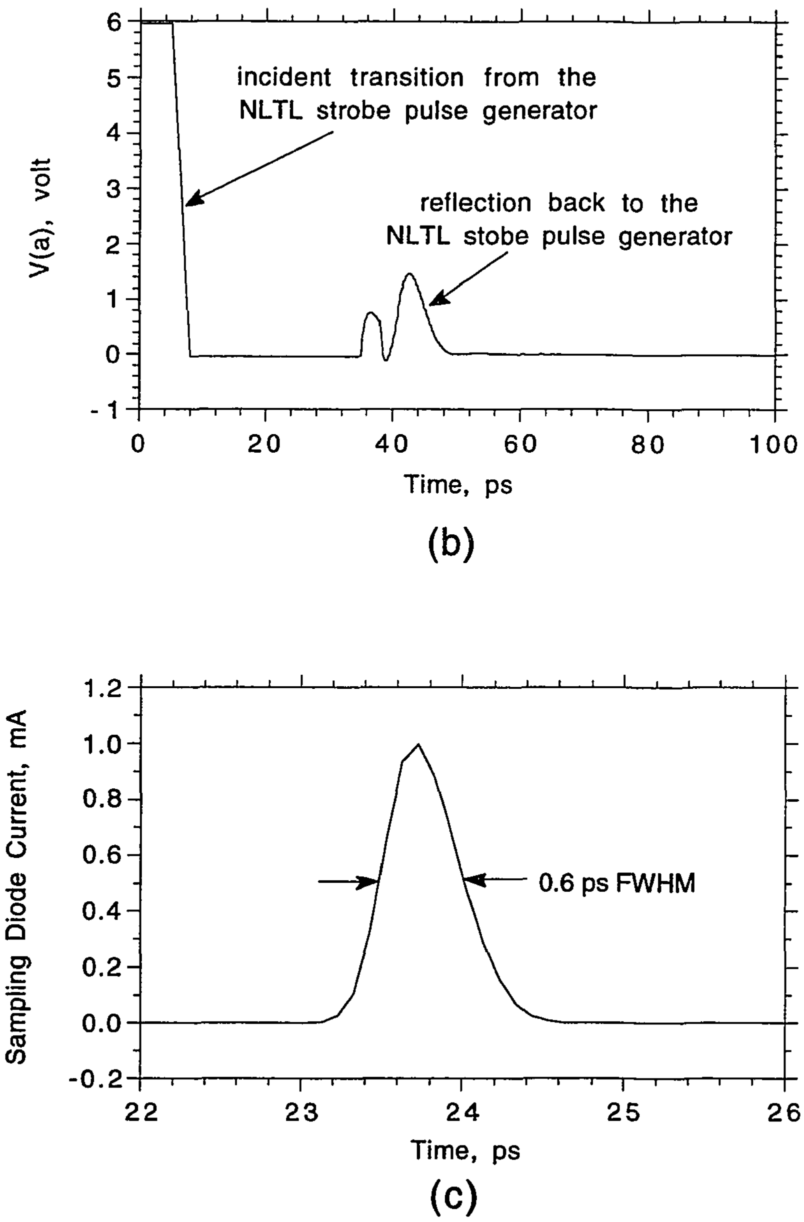

Figure 2.25. Strobe generation circuit simulation results: (a) voltage across the sampling diodes, (b) reflection back to the input, and (c) sampling diode conduction current pulse.

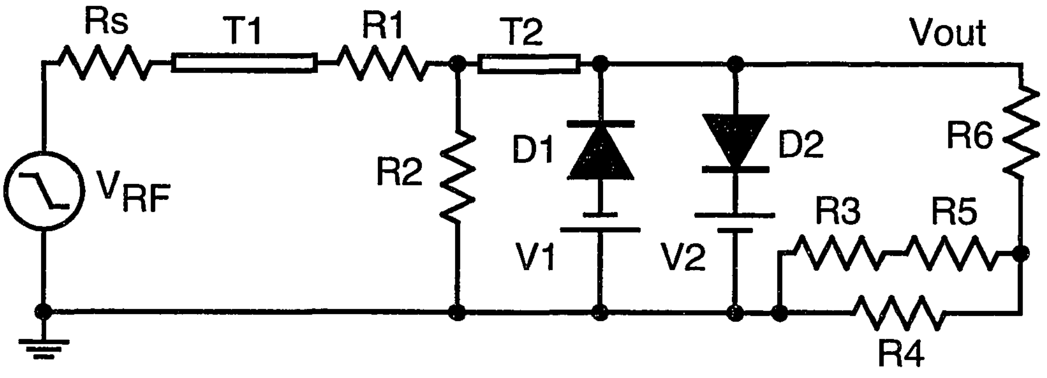

Figure 2.26. Circuit diagram of RF signal circuit for MWSPICE simulation.

As discussed previously, another bandwidth limit arises from the RC time constant produced by the sampling diode parasitics on the input signal line. Fig. 2.26 shows the circuit diagram for MWSPICE simulation of the signal line bandwidth, where *Rs* is the source resistance, *R*1 (50 Ω) and *R*2 (2.5Ω) form the 25-dB attenuator, *R*3-*R*5 are the resistances on the signal CPW ground planes introduced by implementing capacitors as reverse-biased diodes, and *R*6 is the termination resistor. *V*1 and *V*2 are DC diode reverse bias voltages established by self-biasing. Transmission line *T*2 models the 1.5 ps signal delay from the 25-dB attenuator to the sampling diodes. The MWSPICE netlist for this circuit is attached in Appendix A.2. Fig. 2.27 shows the step response $V_{out}(t)$ of the signal line circuit. Because the 25-dB attenuator has a very small output impedance, and because *R*3-*R*6 do not terminate the line in 50 Ω, significant reflections can be observed between the 25-dB attenuator and the sampling diodes, and the 3-ps between reflections corresponds to the round-trip delay between the sampling diodes and the 25-dB attenuator. SPICE simulation indicates 1 ps falltime. Consequently, the overall time constant of the sampling circuits estimated from simulation is

$$T_{overall} = \sqrt{t_g^2 + t_{signal}^2} = \sqrt{0.6^2 + 1^2} = 1.17ps$$

and the corresponding -3-dB bandwidth is

$$BW(GHz) = \frac{350}{T_{overall}(ps)} = 300GHz$$

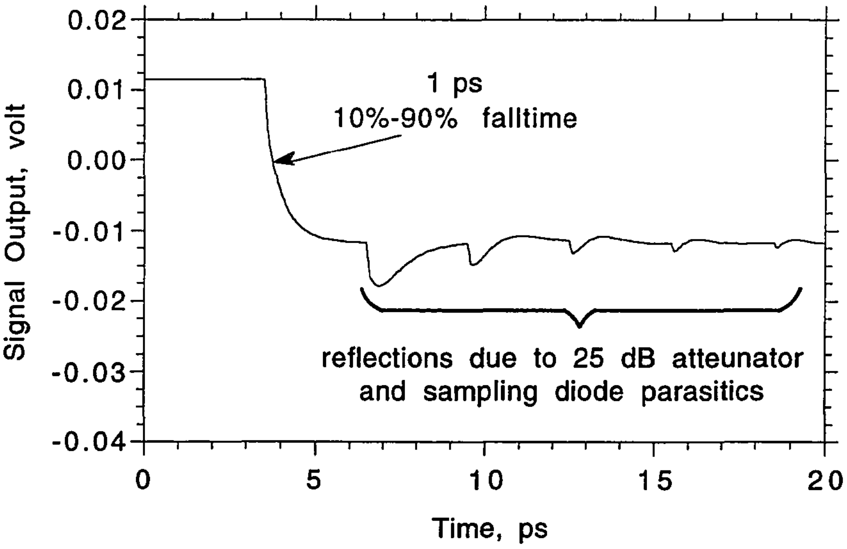

Figure 2.27. Signal line step response from MWSPICE simulation.

Because calibrated picosecond step function generators are not available for step response measurements of the sampling circuits, NLTLs are used instead as the input test signal generators, and the combined step responses of the NLTLs and the sampling circuits can be measured. Because of sampling circuit conversion losses, and because of DC offset voltages arising from imperfect bridge balance, the sampling circuits are calibrated with known DC input voltages. The sampling circuits are linear in the input range of -6 to 0 volt (the shockwave voltage amplitude) and sampling circuit conversion loss ($\Delta V_{out} / \Delta V_{in}$) is about 0.026 or -32 dB (which includes the 25 dB input attenuation). In measuring the sampling circuit rise(fall) time, a second NLTL is used to generate the ≈ 2ps test signals. Synchronized microwave synthesizers drove the strobe NLTL at 9 GHz, 25 dBm and the test signal NLTL at 9 GHz+90 Hz, resulting in a IF output fundamental frequency of 90 Hz. Because the strobe fundamental frequency is 10^8 times greater than the IF fundamental frequency, the criteria for equivalent sampling without spectral density overlaps (Eq. 2.12) is satisfied. Although the microwave synthesizers share a common 10 MHz crystal reference, they have significant phase fluctuations (or timing jitter) [37]. Synthesizer phase noise measurement [38] indicate $\sigma_{jitter} = 0.3ps$ RMS timing jitter, hence the 10%-90% time constant contributed by the timing jitter is

$$T_{jitter,10-90\%} = 2.2\sigma_{jitter} = 0.66ps$$

The measured falltime then is the convolution of $T_{jitter,10-90\%}$, the test signal falltime T_{NLTL}, and the sampling circuit falltime $T_{sampler}$ and is

$$T^2_{measured} = T^2_{sampler} + T^2_{NLTL} + T^2_{jitter,10-90\%}$$

Fig. 2.28 shows the NLTL output waveform measured by the sampling circuits, and the inset of Fig. 2.28 shows two periods of the waveform. The waveform is a 5 volt step function with 1.8 ps 10-90% falltime. Assuming a equal falltime contribution from the test signal NLTL and the sampling circuit, $T_{sampler}$ is ≈ 1.26 ps, corresponding to 275 GHz -3 dB bandwidth (very close to the estimated value of 300 GHz). A step response with 24% peak-peak ringing is observed, owing to the relatively clean layout design.

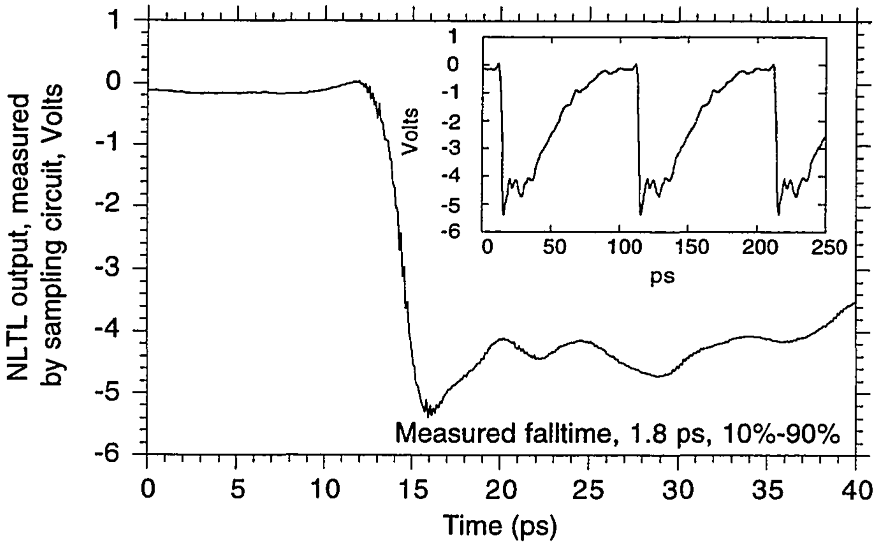

Figure 2.28. NLTL output measured by an NLTL-gated sampling circuit, both using hyperabrupt diode technology. Inset: two periods of the waveform.

Chapter 3

The Active Probe

Conventional microwave on-wafer measurements are performed using microwave wafer probes. The commercial microwave wafer probe from Cascade Microtech Inc. [39] or Tektronix [7] (Fig. 3.1) consists of a alumina probe tip carrying a coplanar waveguide (CPW) mounted on a gold-plated brass probe body. A microwave coaxial connector directly contacts the CPW probe tip and provides the connection between the CPW probe tip and the measuring instrument. The microwave signals travel, between the DUT and the instrument, on the CPW probe tip and the coaxial connectors and cables. The ground planes of the CPW probe tip are strapped together with a gold sheet (not shown) to minimize propagation of slot-line modes, and microwave absorbers (not shown) are incorporated around the probe tip to reduce electro-magnetic interference (EMI) from nearby instruments or other probes. For more reliable probe to DUT contacts and extended probe tip life, $\approx 10\ \mu m$ thick Ni bumps are plated at the contact points of the CPW tip (gold is too soft to provide a durable contact point). The CPW probe tips are typically > 1.5 cm in length to provide sufficient flexibility so that the probe tips do not break when contacting the DUT. CPW have skin and radiation losses which increase with frequency and length of the CPW. The long (> 1.5 cm) probe tips in commercial microwave wafer probes, therefore, have high losses and limit the useful bandwidth of these probes. In addition, the coaxial connectors and cables were band-limited to $\approx$ 60 GHz until March of 1993, when 110 GHz coaxial connectors were introduced [15], albeit with a limit set of necessary components.

Nevertheless, broadband on-wafer measurements are currently limited to about 75 GHz [56]. Although commercial W-band (75-120 GHz) probes were introduced in 1993 [9,10], these have waveguides rather than coaxial connectors and hence are narrow band. With state-of-the-art transistors achieving power gain cutoff frequencies (f_{max}) in excess of 400 GHz, the lack of high frequency instrumentation has presented great difficulties in device measurements, device model extraction, and circuit design and circuit characterization.

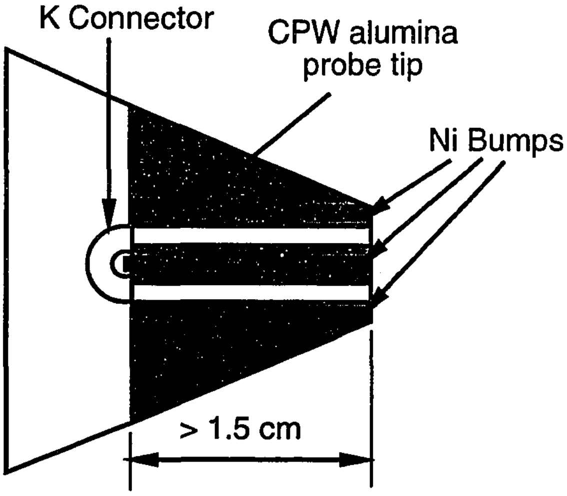

Figure 3.1. Probe tip of a commercial microwave wafer probe.

The NLTL-gated sampling circuits of Chapter 2 attain -3-dB bandwidths of 275 GHz, while > 500 GHz bandwidth sampling circuits have recently been fabricated [29,30]. With such wideband sampling circuits used for instrumentation, the connection between the device under test (DUT) and the sampling circuit becomes the dominant bandwidth limitation. To achieve a higher signal connection bandwidth, we mount the instrument IC (the sampling circuit for waveform measurements or the network analyzer IC for network measurements) directly on the probe and adjacent to the probe tip (Fig. 3.2). High frequency signals must therefore only propagate, between the instrument IC and the DUT, on a short, low-loss probe tip, and across a single set of ribbon bonds connecting the probe tip and the instrument IC. As described earlier, the millimeter-wave frequency signals from the DUT are down-converted by the sampling circuits to IF frequencies of less than 2 MHz, where they can easily be delivered to other instruments for subsequent signal processing. The only microwave connectors and cables needed are for delivering the drive signal for the NLTL which generates the strobe signals for the sampling circuit and the drive signal for the NLTL which generates the broadband stimulus signal for network analysis. These drive signals are between 7-14 GHz, hence can be handled with standard SMA connectors and cables. The bandwidth of the active probes are then limited by the instrument IC, the low loss probe tip, and the bond wires connecting the IC and the probe tip.

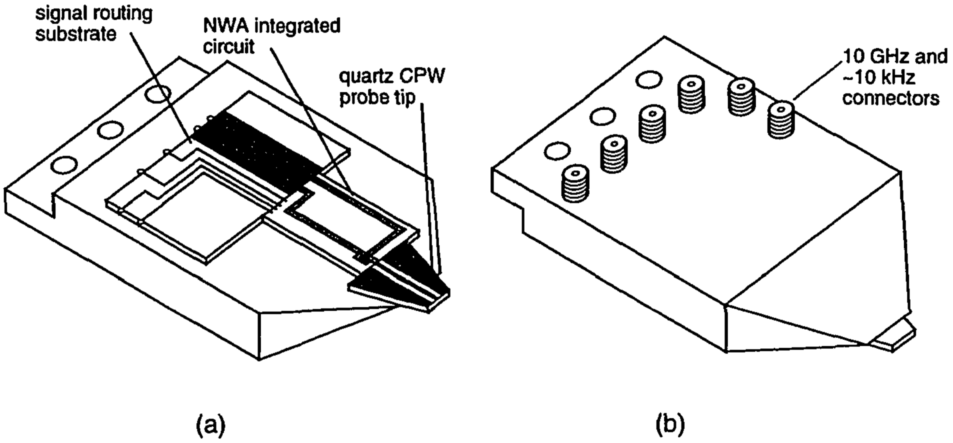

Figure 3.2. Conceptual diagram of the active probe: (a) bottom view, and (b) top view.

3.1 The Network Analyzer Integrated Circuit

In conventional microwave network analyzers, swept-frequency signal sources are used to provide the stimulus signal for the device under test (Fig. 1.1). Commercial coaxial frequency synthesizers are available to 50 GHz, and the frequency range can be extended to much higher frequencies with frequency multipliers. However, these millimeter-wave frequency multipliers have waveguide outputs, hence are narrow band. Because NLTLs generate sawtooth waveforms, from sinusoidal inputs, with ≈ 2 ps falltimes, significant harmonic power is available at frequencies up to approximately 200 GHz. Therefore, NLTLs can serve as convenient broadband (7-200 GHz) stimulus signal sources for network analysis. Incorporating the NLTL stimulus signal generator, the high speed sampling circuits, and a directional device, integrated circuits for network analysis are fabricated.

3.1.1 Network Analyzer IC Design and Fabrication

The block diagram of a network analyzer (NWA) IC is shown in Fig. 3.3. The NWA IC consists of a directional sampler, an attenuator, and two NLTLs. The directional sampler independently measures the forward and reverse waves of the DUT. An NLTL generates the strobe pulses to operate the directional sampler. A second NLTL generates the sawtooth stimulus signal. The stimulus signal is coupled through an attenuator and through the directional sampler, and then drives the DUT. The attenuator is used to attenuate the ≈ 5 V NLTL output signal to levels suitable for linear characterization of transistors and circuits.

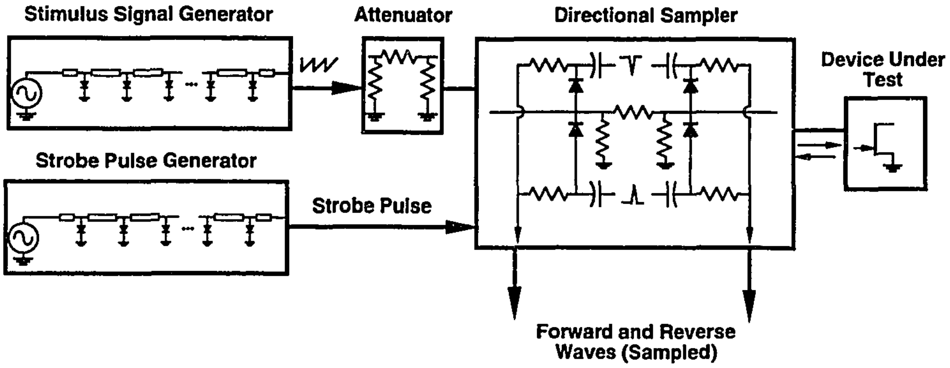

Figure 3.3. Block diagram of the NWA IC.

Commercial vector network analyzers use directional couplers to obtain independent measurements of the forward and reverse waves. Directional couplers rely on phase cancellation of propagating waves on coupled transmission lines to achieve isolation between the incident and the isolated port. Transmission line length within directional couplers are generally at least $\lambda / 4$ where λ is the guided wavelength on the directional coupler. Broadband (such as 7-200 GHz required in the NWA IC) directional couplers are difficult to implement in monolithic form, as the required coupler length is prohibitively long. A directional coupler for the 7-200 GHz bandwidth of the NWA IC would be very large; the propagation velocity of a coplanar line on GaAs is $c / \sqrt{7}$, and hence $\lambda / 4$ is 4 mm at 7 GHz. Instead, we use an attenuator as the directional element, because an attenuator is very small when fabricated in monolithic form. Operation of the attenuator as a directional device is illustrated in Fig. 3.4. The input (V_{in}) and output (V_{out}) port voltages of the attenuator can be expressed in terms of the incident ($V_{incident}$) and reflected ($V_{reflected}$) waves as:

$$V_{in} = \frac{1}{\alpha} V_{incident} + \alpha V_{reflected} \tag{3.1}$$

$$V_{out} = V_{incident} + V_{reflected} \tag{3.2}$$

where $\alpha < 1$ is the attenuation factor of the attenuator. $V_{incident}$ and $V_{reflected}$ can then be solved from the linear equations 3.1 and 3.2 and expressed in terms of the port voltages of the attenuator as:

$$V_{incident} = \frac{\alpha}{1-\alpha^2}(V_{in} - \alpha V_{out}) \tag{3.3}$$

$$V_{reflected} = \frac{1}{1-\alpha^2}(V_{out} - \alpha V_{in}) \tag{3.4}$$

Given parasitic elements in the attenuator, the exact coefficients in equations 3.3 and 3.4 become frequency dependent, but standard network analysis calibration procedures can be used to obtain accurate measurements of these coefficients at all frequencies of operation. The S-parameters of the DUT can then be determined after this calibration.

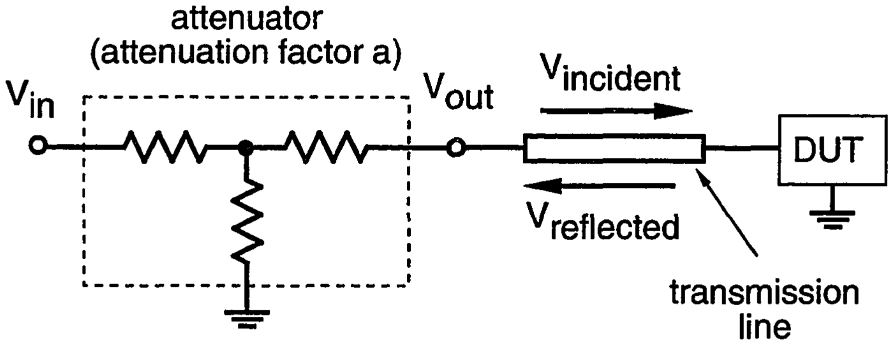

Figure 3.4. Illustration of an attenuator as the directional device.

The selection of the attenuation factor α represents a compromise between the system dynamic range and the system accuracy. As discussed in chapter 2, the sampling circuits used to measure the input and output port voltages of the attenuator have a finite dynamic range. The system dynamic range is mainly determined by the sampling circuit at the input of the attenuator, as the input voltage of the attenuator is the sum of a large signal $V_{incident} / \alpha$ and a much smaller signal $\alpha V_{reflected}$ (Eq. 3.1). Given that $V_{incident} / \alpha$ is set by the sampling circuit linear dynamic range, the smaller the α, the bigger the minimum detectable $V_{reflected}$ because the minimum resolvable signal of the sampling circuit is set by its noise figure. As a result, smaller α gives rise to smaller system dynamic range. But if α is close to unity, the measurement accuracy will be degraded. This can be seen by the following argument. Assuming $\alpha = \alpha_0 + \Delta\alpha$, where α_0 is the nominal value of α and $\Delta\alpha << \alpha_0$ is the measurement error in α. From Eq. 3.3, we have

$$V_{incident} = \frac{\alpha_0 + \Delta\alpha}{(1+\alpha_0+\Delta\alpha)(1-\alpha_0-\Delta\alpha)}[V_{in} - (\alpha_0 + \Delta\alpha)V_{out}] \qquad (3.5)$$

Because $\Delta\alpha << \alpha_0$, we can rewrite Eq. 3.5, approximately, as

$$\begin{aligned} V_{incident} &= \frac{\alpha_0}{(1+\alpha_0)(1-\alpha_0-\Delta\alpha)}(V_{in} - \alpha_0 V_{out}) \\ &= \frac{\alpha_0}{(1-\alpha_0^2)(1-\dfrac{\Delta\alpha}{1-\alpha_0})}(V_{in} - \alpha_0 V_{out}) \\ &= \frac{1}{1-\left(\dfrac{\Delta\alpha}{1-\alpha_0}\right)} V_{0,incident} \end{aligned} \qquad (3.6)$$

where $V_{0,incident} = \frac{\alpha_0}{1-\alpha_0^2}(V_{in} - \alpha_0 V_{out})$ is the nominal value of $V_{incident}$. If $\Delta\alpha = 0$, we have $V_{incident} = V_{0,incident}$ as expected; if $\Delta\alpha \neq 0$, then the term $\Delta\alpha / (1-\alpha_0)$ in the denominator of Eq. 3.6 represents the error in $V_{incident}$. If $\alpha_0 \approx 1$, then $\Delta\alpha / (1-\alpha_0)$ $>>$ $\Delta\alpha$ and the measurement is very sensitive to $\Delta\alpha$. Consequently, large errors will be introduced into measurements of $V_{incident}$. Similar arguments apply to measurements of $V_{reflected}$ (Eq. 3.4). A good compromise between large system dynamic range and high measurement accuracy is obtained with $\alpha = 1/2$, or -6 dB.

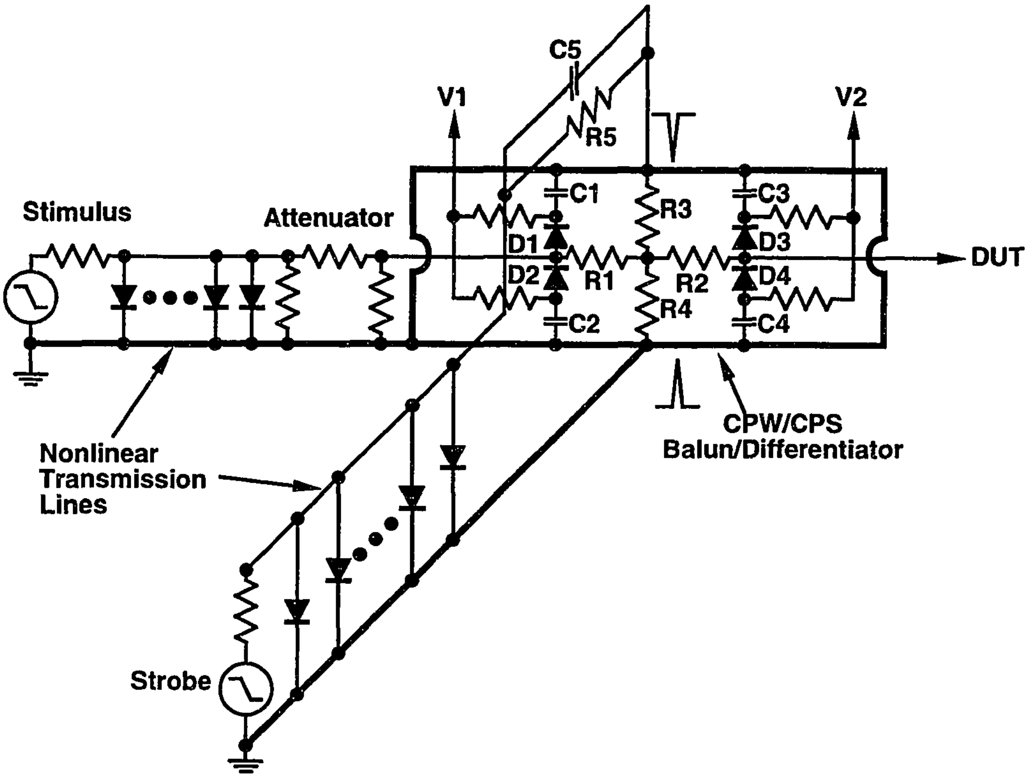

Figure 3.5. Circuit diagram of the NWA IC.

The complete circuit diagram of the NWA IC is shown in Fig. 3.5. $R1-R4$ form the 6-dB 50 Ω attenuator used as the directional device. A pair of 2-diode sampling bridges ($D1-D4$, $C1-C4$) are placed at the input and output ports of the attenuator to monitor its port voltages. Symmetric positive and negative impulses are generated by a balun/differentiator implemented using the CPS mode of the input signal coplanar waveguide. Coupled through $R5$ and $C5$, the strobe step-function is applied between the CPW ground planes, and propagates on them in both directions as a CPS mode. 120 μm from the sampling diodes, a short circuit on each side of the CPW ground planes reflects the CPS mode, generating ≈ 2 ps impulses at the sampling diodes. A 5-V amplitude and ≈ 2 ps falltime sawtooth stimulus signal is generated by another NLTL. The stimulus signal amplitude is attenuated to 120 mV at the DUT port by a 25-dB 50 Ω attenuator and the directional samplers' 6-dB attenuator, thereby providing a signal sufficiently small for linear characterization of transistor circuits.

The NWA IC is implemented in a six-mask process. The first three masks, namely, ohmic contact metal, proton implant isolation, and Schottky and interconnect metal, are identical to those used to fabricate the 3-mask sampling circuits described in Chapter 2. Due to the complexity of the directional sampling circuits, three more mask steps are added to simplify the circuit layout. The fourth mask step is used to fabricate MIM capacitors, and the fifth and sixth mask steps are used to fabricate air bridges for wiring cross-overs and for forming the top plates of the MIM capacitors. Detailed process flow sheets of the 6-mask process are attached in Appendix B.1.

Adaptation of parallel plate dielectric capacitors and electroplated air bridges for signal cross-overs simplifies the circuit layout and minimizes circuit parasitics. The corresponding layout for the NWA IC circuit (Fig. 3.5) is shown in Fig. 3.6, with circuit components labeled as in the circuit diagram (Fig. 3.5). The coupling capacitors ($C1-C4$) are implemented with Si3N4 films, and the small compensation capacitor ($C5$) was implemented using reverse-biased diode. As described in Chapter 2, the compensation capacitor $C5$ permits high differentiator efficiency while maintaining a low reflection termination to the NLTL. Air bridges $AB1$ and $AB2$ provide the short circuits for the balun/differentiator, while air bridges $AB3$ and $AB4$ provide continuity for the stimulus signal CPW ground planes. A photograph of the NWA IC is shown in Fig. 3.7.

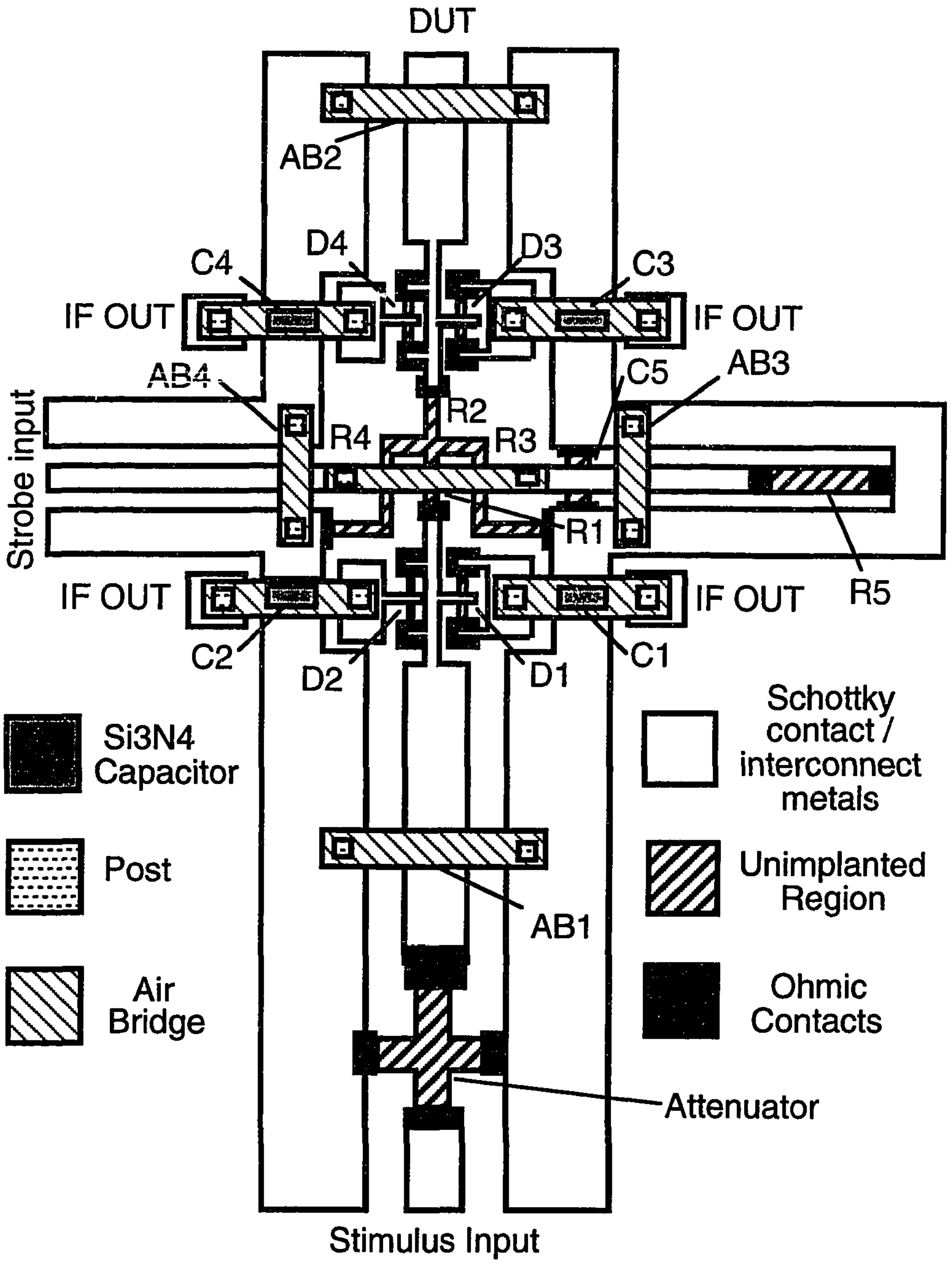

Figure 3.6. Layout of the NWA IC.

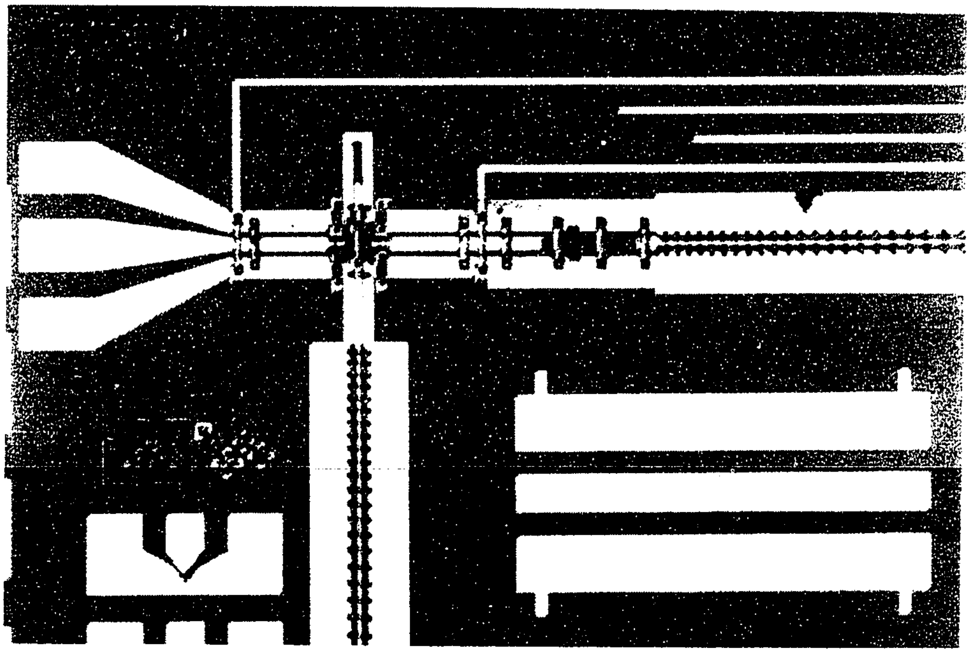

Figure 3.7. Photograph of a fabricated network analyzer IC.

3.1.2. Network Analyzer IC Simulation

As with the design of sampling circuits, MWSPICE is used to obtain optimal component values and verify final circuit design. In contrast to the 2-diode sampling bridge, the directional sampling circuit has a pair of 2-diode sampling bridges, and hence there two sets of sampling diode capacitances loading the signal transmission line. To reduce diode capacitances, diode areas are reduced from 3 μm x 3 μm to 2 μm x 3 μm. In addition, a 6-dB 50 Ω attenuator is inserted between the two sampling bridges. However, through the use of silicon nitride capacitors and air bridges for wiring crossovers, most of the resistive parasitics in the 3-mask sampling circuit is eliminated. Again, both the strobe signal generation circuit and the RF input signal circuit are analyzed. Fig. 3.8 shows the strobe generation circuit used for MWSPICE simulation. All the optimal circuit component values are included in the netlist in Appendix A.3. In Fig. 3.8, Vs is the step function generated by the strobe NLTL, and Rs is its source resistance (50 Ω). The 15 ps transmission line ($T3$) is used for monitoring, in the simulation, the magnitude of the reflection from the differentiator. $R1$ is the strobe NLTL termination resistor. $C2$ is the compensation capacitor and $RC2$ is its parasitic resistance arising because $C2$ is implemented as a reversed biased diode. $D1 - D8$ model the conduction currents and junction capacitances of the four sampling diodes in the two 2-diode sampling bridges, and $Rd1 - Rd4$ are the diode series resistances. As discussed in sections 2.2 and 2.3, because it takes many simulation cycles to reach steady state diode bias voltages, $V1$ and $V2$ are used instead, in the simulation, to set the diode bias voltages for a specified peak conduction current (≈ 1 mA). In reality, the external resistor R_L is set to give about 1 mA through self-bias. The 1-ps short circuited transmission line (*T*1) models the CPS slots used to differentiate the step function to form impulses.

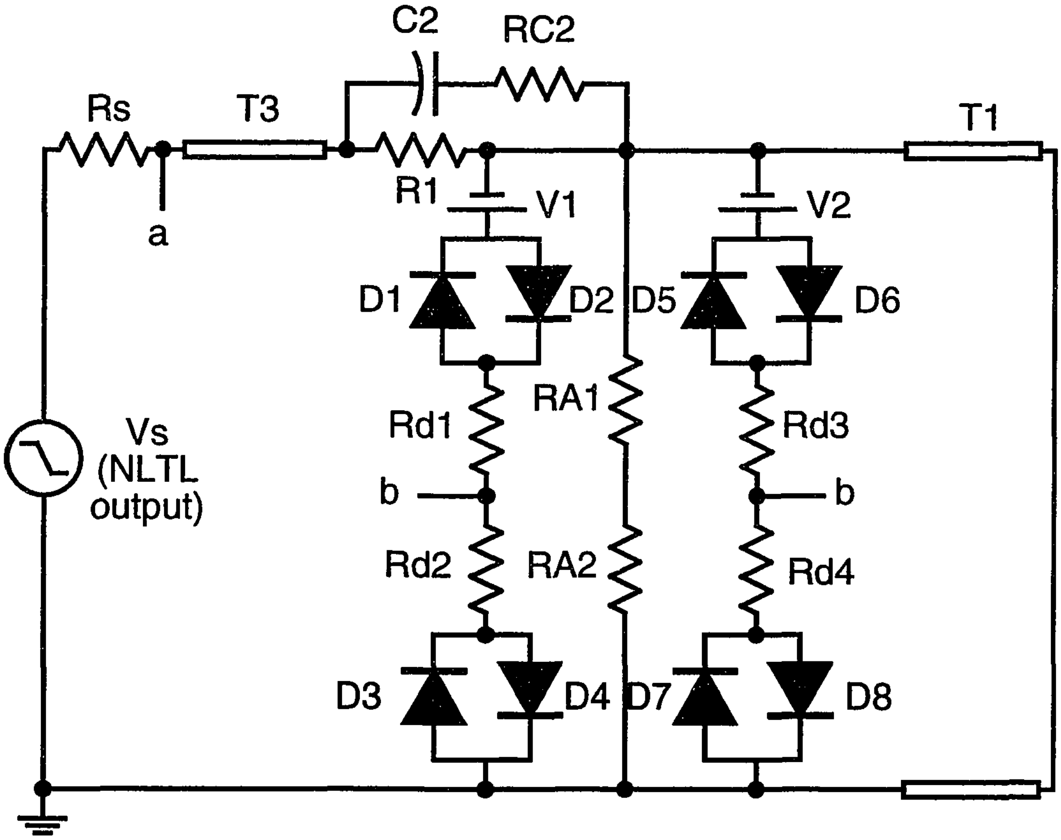

Figure 3.8. NWA IC Strobe generation circuit for MWSPICE simulation.

The simulation results are presented in Fig. 3.9. Fig. 3.9 (a) shows the voltage across the sampling diodes (node b in Fig. 3.8). A dynamic range of 1.1 V can be observed. Fig. 3.9(b) shows the reflection on the strobe signal line (node a in Fig. 3.8) due to diode parasitics. The reflections are small due to the matching network $C2\|R1$. Fig. 3.9(c) shows the diode conduction current pulse, whose duration determines the sampling aperture time. The FWHM of the current pulse (t_g) is approximately 0.4 ps.

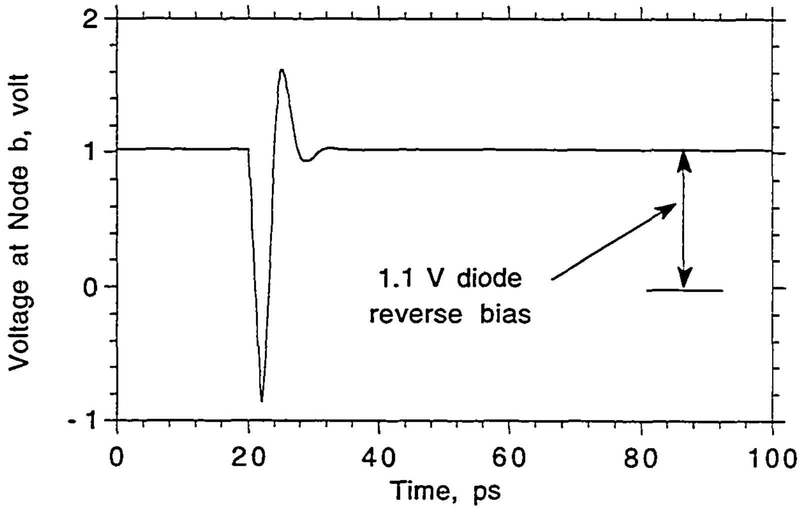

(a)

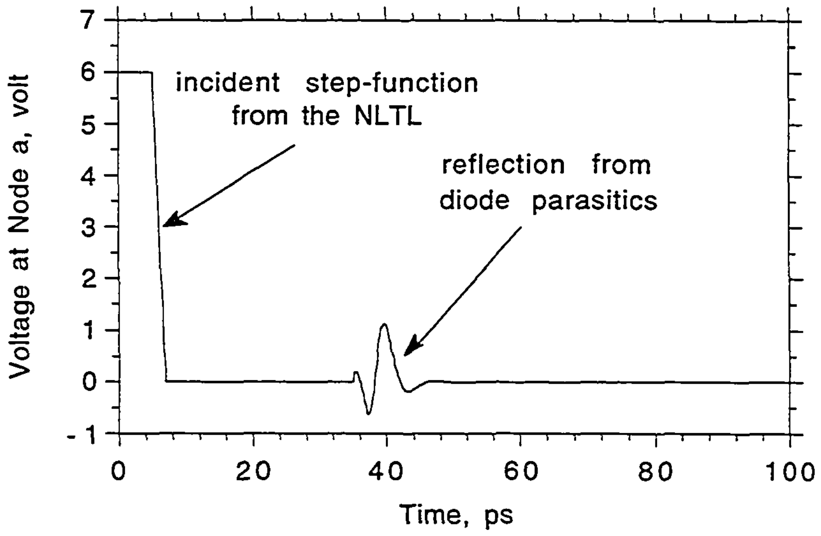

(b)

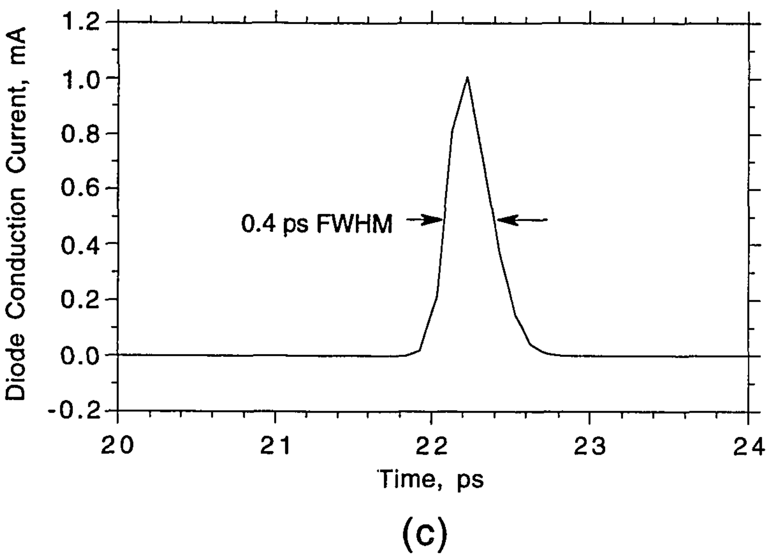

Figure 3.9. MWSPICE simulation results for the NWA IC strobe generation circuit: (a) dynamic range, (b) reflection, and (c) diode aperture time.

Fig. 3.10 shows the circuit diagram of the RF input signal circuit used for MWSPICE simulation. V_{RF} is the RF signal source and Rs its source resistance. $D1 - D4$ are the sampling diodes, and $V1 - V4$ are DC voltage sources used to reverse bias the diodes. $R1 - R3$ form the 6-dB 50 Ω attenuator. R_T is the termination resistor. All component values are in the netlist attached in Appendix 1.4. As opposed to the sampling circuits, the RF signal source (the NLTL stimulus signal source) is incorporated on the NWA IC, hence the V_{RF} for the simulation is set to have a ≈ 2 ps falltime, as is typical of the NLTL. The simulated output voltage (Vout) is shown in Fig. 3.11. The falltime (t_{signal}) is 2.1 ps. Consequently, the overall time constant is

$$T_{overall} = \sqrt{t_g^2 + t_{signal}^2} = 2.14 \text{ ps}$$

and the corresponding -3-dB bandwidth is

$$BW(GHz) = \frac{350}{T_{overall}(ps)} \approx 165GHz$$

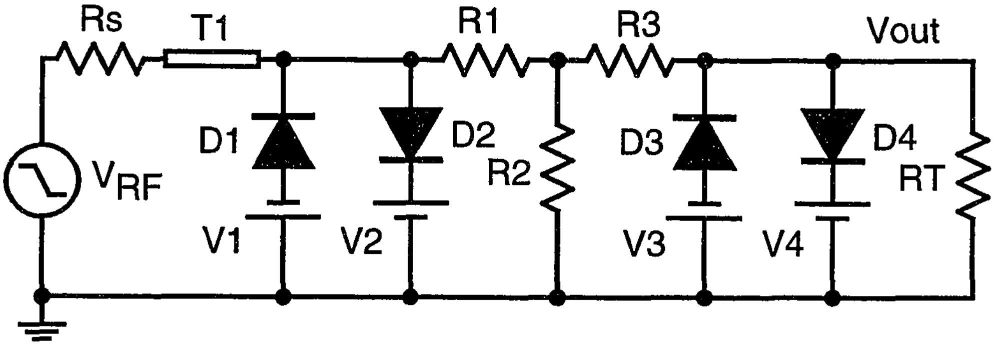

Figure 3.10. NWA IC RF signal line equivalent circuit for MWSPICE simulation.

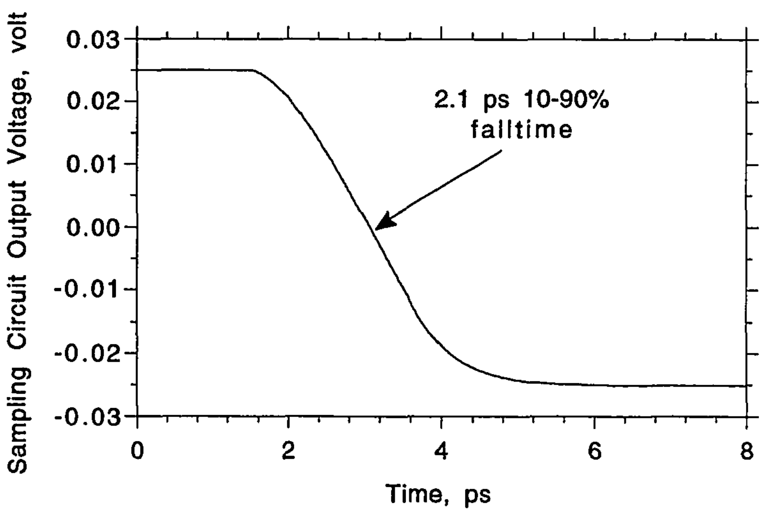

Figure 3.11. MWSPICE simulation result for the NWA IC RF signal line equivalent circuit.

3.1.3 NWA IC Characterization

The experimental configuration for characterization of the NWA ICs is similar to that for the sampling circuits. The main difference in characterization of the NWA ICs and the sampling circuits is that in addition to its bandwidth (as for the sampling circuit), directivity is another performance parameter for the NWA ICs. As an initial indication of the NWA IC directivity, the output waveforms of the NWA IC under different circuit termination (such as a 50 Ω load and an open circuit) are observed. In measuring the NWA IC performance, synchronized microwave synthesizers drove the strobe NLTL at 14 GHz, 27 dBm and the stimulus signal NLTL at 14 GHz + 140 Hz, 25 dBm, resulting in a 140 Hz IF output. Significant high frequency ringing (≈ 200 GHz) is observed on the measured waveforms due to either parasitic microstrip modes propagating between the CPW signal line and the wafer chuck or parasitic coupling between different circuit nodes through dielectric slab modes in the GaAs substrate. A piece of 0.5"-thick microwave absorber (ferite-filled plastic) inserted between the NWA IC and the wafer chuck suppresses the propagation of both slab and microstripe modes, and suppresses the high frequency ringing. The resulting NWA IC waveforms both under an open circuit termination and a 40 GHz 50Ω CPW probe as a load are shown in Fig. 3.12. The waveform under the 50 Ω load is very similar to the incident waveform because the reflected wave is small. The distinct two-step response under open circuit termination clearly indicates the reflection from the open circuit with the 7.6 ps delay of the reflected step corresponding to the expected round-trip time between the directional sampler and the NWA IC test port. The falltime of the transitions was measured to be 2.3 ps, corresponding to a 150 GHz NWA IC bandwidth.

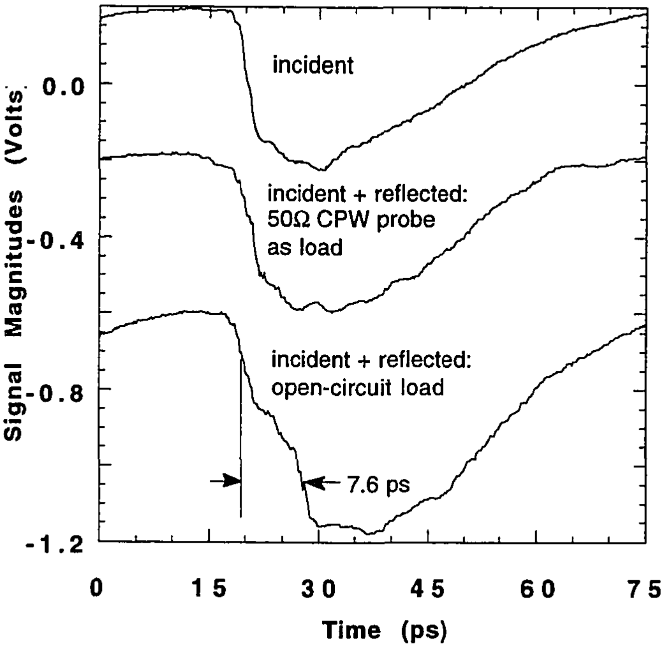

Figure 3.12. Observed NWA IC waveforms: incident wave, and (incident + reflected) waves with the IC open-circuited or connected to a terminated 40 GHz microwave wafer probe.

Before building the active probes, the directivity of the NWA ICs should be measured. The true (calibrated) NWA IC directivity measurement can be done with three calibration standards. However, calibration standards covering the DC to beyond 70 GHz frequency band are only available in wafer form. As a result, to obtain fully calibrated measurements of the NWA IC before packaging, one would have to wire-bond the calibration standards, one at a time, to the NWA IC and perform the 1-port calibration procedure. This is expensive and time consuming for rough checking of the NWA IC functionality. Instead, we coupled to the NWA IC through microwave wafer probes, and we are therefore constrained to coaxial calibration standards for this experiment. In addition, because the computer program which performs the 1-port calibration procedure was not yet developed, we used a partial calibration procedure described below. This rough procedure has many sources of errors arising from the use of 40 GHz coaxial calibration standards to cover a 10-200 GHz frequency band and from the partial calibration procedure which does not account for the source reflection coefficient of the NWA IC. Nevertheless, the result from this partial calibration procedure should suffice to indicate proper functionality of the NWA ICs.

To demonstrate calibrated measurement with the NWA IC before constructing probes, a partially-calibrated measurement was performed on an open-circuit termination. The sampling diode and layout parasitics load the 6-dB attenuator ($R1 - R4$ in Fig. 3.5), and its attenuation $H(\omega)/2$ then varies with frequency. Hence, in frequency domain,

$$V_{in}(\omega) = 2V_{incident}(\omega)/H(\omega) + H(\omega)V_{reflected}(\omega)/2 \tag{3.5}$$

$$V_{out}(\omega) = V_{incident}(\omega) + V_{reflected}(\omega) \tag{3.6}$$

By measuring $V_{in,50\Omega}(\omega)$ and $V_{out,50\Omega}(\omega)$ with the test port loaded by a 40 GHz coplanar microwave probe and 50 Ω coaxial termination, $V_{reflected}(\omega) \approx 0$, and

$$H(\omega) = \frac{2V_{out,50\Omega}(\omega)}{V_{in,50\Omega}(\omega)} \tag{3.7}$$

The reflection coefficient of an arbitrary load is then found from Eqs. 3.5 - 3.7 to be

$$\Gamma(\omega) = \frac{2V_{out}(\omega) - H(\omega)V_{in}(\omega)}{H(\omega)\left(V_{in}(\omega) - H(\omega)V_{out}(\omega)/2\right)} \tag{3.8}$$

After calibration with the 50 Ω load, $V_{in}(\omega)$ and $V_{out}(\omega)$ were measured with an open-circuit termination. Ideally, $|\Gamma(\omega)|$ should be unity for an open circuit termination. There are a number of difficulties and sources of errors in the above procedure, the most significant of which is the 40 GHz coplanar-probe bandwidth. It is instructive to examine Γ in the time domain. The resulting Γ(ω) was numerically low-pass-filtered by a 190 GHz 3-dB bandwidth Gaussian filter (2.2 ps FWHM impulse response) to bandlimit high-frequency noise, and the inverse Fourier transformed to obtain Γ(t). Consequently,

$$\Gamma(\omega)|_{filtered} = \Gamma(\omega) \cdot G(\omega)$$

and

$$\Gamma(t)|_{filtered} = \Gamma(t) \otimes g(t)$$

where $G(\omega)$ is the Gaussian filter response and $g(t)$ is its time domain waveform (also Gaussian form). As a result, $\Gamma(t)|_{filtered}$ should contain a reflection of Gaussian pulse shape at 7.6 ps (the round-trip delay) from the incident signal (occurring at $t = 0$). The resulting $\Gamma(t)|_{filtered}$ for an open-circuit at the NWA IC test port is shown in Fig. 3.13, with a major reflection of $0.38 \cdot (1/ps)$ peak amplitude, and 2.6 ps FWHM duration observed at the expected 7.6 ps round-trip delay. The product of magnitude and reflection duration yields a DC reflection coefficient of $(1.06)(0.38/ps)(2.6ps) = 1.05$ with the factor of 1.06 arising from an assumed Gaussian pulse shape.

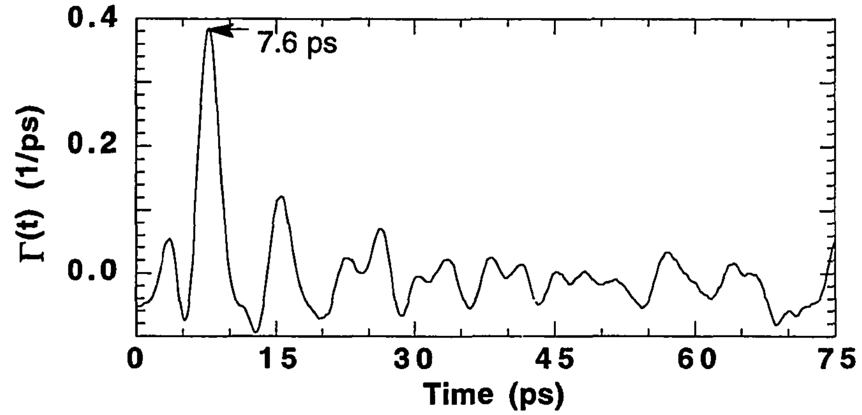

Figure 3.13. Reflection coefficient displayed in time with the NWA IC open-circuited.

The rudimentary calibration procedure above does not correct for the NWA IC source reflection coefficient and uses a 40 GHz microwave wafer probe and termination as a calibration standard over a 14 GHz - 190 GHz bandwidth. These substantial errors introduce the additional structure seen in Γ(t) (Fig. 3.13). In particular, we ascribe the second peak in Γ(t) at 15.2 ps (2×7.6 ps) to the uncorrected NWA IC source reflection coefficient. The procedure has however served to verify that the NWA ICs function as intended. Probes can therefore be fabricated.

3.2 The Bias Tee

To measure transistors and other active devices, instruments must incorporate bias tees for device biasing. The first generation of NWA ICs incorporated such bias tees. Fig. 3.14 shows the conceptual circuit diagram of a bias tee, where C1 provides the DC blocking capacitance for the RF signal, and L and C2 provide isolation between the DC and RF ports.

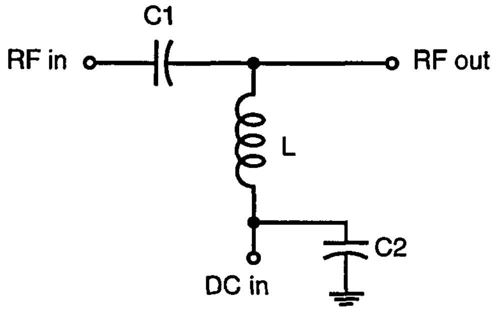

Figure 3.14. Conceptual circuit diagram of a bias tee.

It is difficult to monolithically fabricate broadband inductors, and two alternative and more practical implementations of the bias tees are considered (Fig. 3.15). In Fig. 3.15(a), the inductor is implemented with a high impedance transmission line. Because the high impedance line behaves as an inductor only when less than $\lambda / 4$ in length, the line must be very short if the bias tee is to operate at 200 GHz. The line is then too short to provide sufficient inductive isolation at ≈ 10 GHz. The advantage of this implementation is that inductive or transmission line bias tees have very little power loss. The second implementation shown in Fig. 3.15(b) uses a large resistor (R3) to isolate the DC signal from the RF signal. The resistor network comprising $R1$, $R2$ and $R3$ forms a 50 Ω attenuator to maintain a 50 Ω environment for the RF signal path. This configuration is inherently broadband and can be implemented in a relatively compact circuit layout. To minimize RF power losses, a small attenuation (2 dB) is used for the attenuator, and the resulting resistance values are $R1 = R2 = 5.73\Omega$ and $R3 = 215\Omega$. The major drawbacks of this implementation are that significant DC power dissipation arises in the large resistor $R3$. The small resistances of $R1$ and $R2$ are also hard to implement accurately because the ohmic contact resistance constitutes a major portion of the total resistance, with such ohmic contact resistance a poorly-controlled process parameter. The layout of this bias tee is shown in Fig. 3.16. Because $R3$ is large (215 Ω) and the sheet resistance of the N^+ layer of the GaAs substrate is small (≈ 7 Ω per square), the bias tee layout is not very clean, and layout parasitics (such as capacitances between $R3$ and the CPW center conductor and ground planes) are introduced. S-parameters of the bias tees measured with the active probes are shown in Fig. 3.17. It can be observed that the measured insertion loss is 3.5 dB at lower frequencies (bigger than the designed 2-dB due to process variations of the resistor values) and increases at higher frequencies due to layout parasitics; the return loss is better than -10 dB below 100 GHz, but degrades to -5 dB around 150 GHz. As a result, these bias tees do not perform well in the expected frequency range of operation of the active probes, and hence were not implemented in the latter generation of the NWA ICs.

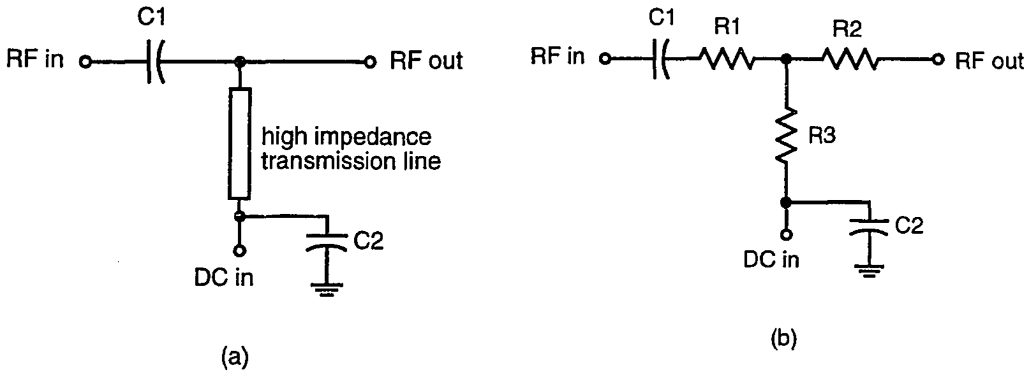

Figure 3.15. Circuit diagrams of two implementations of bias tees: (a) with high impedance line, and (b) with 2 dB 50 Ω attenuator.

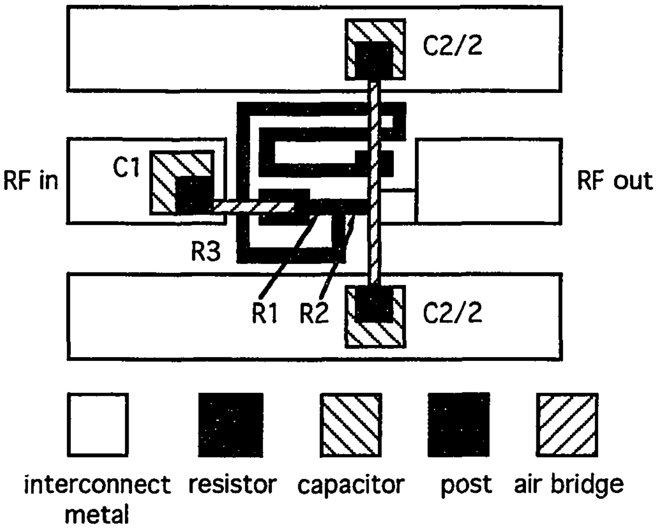

Figure 3.16. Layout of the bias tee with 2-dB attenuator.

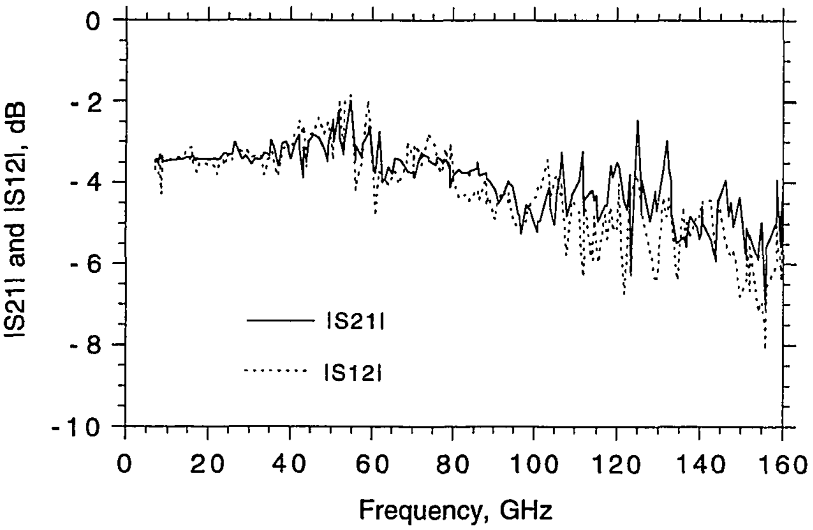

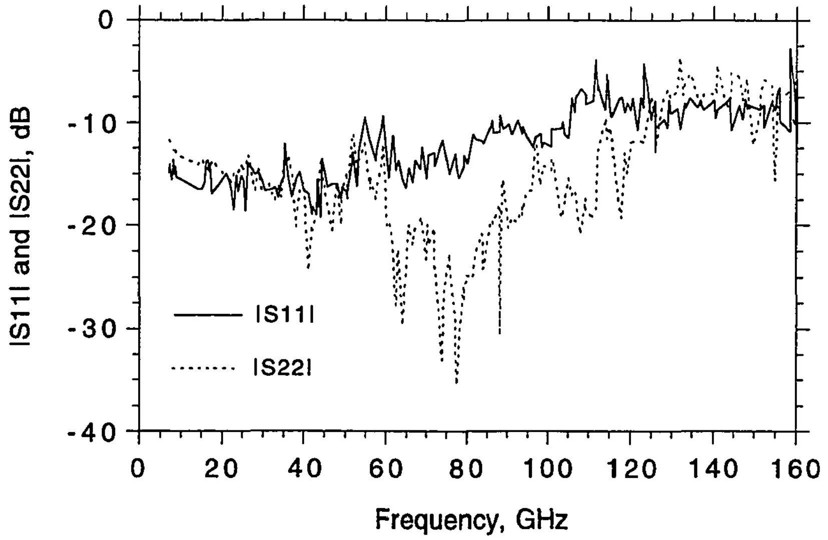

Figure 3.17. Measured S-parameters of a bias tee: (a) insertion loss, and (b) return loss.

3.3 Probe Tip Design and Fabrication

One of the bandwidth limits of the active probes arises from the CPW probe tip. The long (> 1.5 cm) alumina probe tips in the commercial microwave probes have high attenuation. Signal attenuation on the CPW probe tips arises from skin and radiation losses. For a given line impedance, skin loss is [40]:

$$\alpha_{skin} = \frac{\sqrt{\pi f \mu_0 / \sigma}\sqrt{(1+\varepsilon_r)/2}}{4\eta_0 d \mathrm{K}(k)\mathrm{K}(k')[1-(w/d)^2]} \times \left\{ \frac{2d}{w}\left[\pi + \ln\left(\frac{4\pi w(1-w/d)}{t(1+w/d)}\right)\right] + 2\left[\pi + \ln\left(\frac{4\pi d(1-w/d)}{t(1+w/d)}\right)\right]\right\} \tag{3.8}$$

where f is the frequency in Hz, ε_r=13 the substrate dielectric constant, d the CPW ground-ground spacing, w the center conductor width, t the metal thickness, μ_0 the permeability of vacuum, σ the metal (gold) conductivity, η_0=377 Ω the free space impedance, $k = w/d$, $k'^2 = 1 - k^2$, and $\mathrm{K}(k)$ the complete elliptic integral of first order. Radiation loss is [41]:

$$\alpha_{rad} = \left(\frac{\pi}{2}\right)^5 \frac{1}{\sqrt{2}} \frac{(1-\varepsilon_r)^2}{\sqrt{1+\varepsilon_r}} \frac{f^3 d^2}{c^3 \mathrm{K}(k)\mathrm{K}(k')} \tag{3.9}$$

where c is the speed of light. The total attenuation is then:

$$\alpha_{total} = \alpha_{skin} + \alpha_{rad} \tag{3.10}$$

As apparent from Eqs. 3.8 and 3.9, both α_{skin} and α_{rad} increase with ε_r. In addition, for a given CPW characteristic impedance ($w/d \approx$ constant), α_{skin} is inversely proportional to d, while α_{rad} is proportional to d^2. Consequently, with appropriate scaling of line dimensions, CPWs on substrates with lower ε_r can attain lower attenuation. Further, for a given substrate, d can be chosen such that α_{total} is minimized at a particular frequency. One way to do this is to differentiate Eq. 3.10 with respect to d, the resulting expression is then set to zero and d can be solved for a given frequency. The resulting mathematics are arduous. Instead, Eq. 3.8 and 3.9 were solved for minimum attenuation using mathematical optimization software. This was done by Joe Pusl using the program Eureka on a Macintosh. Fig. 3.18 shows the computed attenuation-frequency characteristics of CPW of different dimensions on alumina (ε_r=9.8) and on quartz (ε_r=3.8) substrates. For the same d, CPWs on quartz substrates have lower attenuation due to smaller ε_r. For a given substrate (ε_r), CPWs with a larger d have smaller attenuation at lower frequencies and larger attenuation at higher frequencies, indicating that skin losses dominate at lower frequencies while radiation losses dominate at higher frequencies. At 200 GHz, d=100 μm results in a minimum attenuation of 0.57 dB/mm on a quartz substrate. For the 2 mm-long quartz probe tips used in the current probes, the calculated round-trip attenuation is 2.3 dB at 200 GHz.

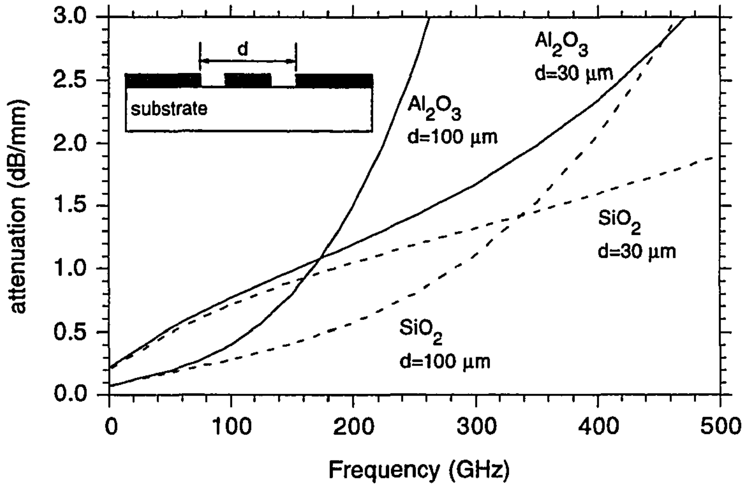

Figure 3.18. Computed total (skin plus radiation) losses for coplanar waveguide probe tips on quartz and alumina substrates.

A four-mask process is used to fabricate the quartz probe tips. CPW lines are first patterned on a quartz substrate with a lift-off of electron-beam evaporated 300 Å Ti / 1 μm Au. A standard air bridge process is then used to fabricate air bridges to connect the ground planes of the CPW, thereby suppressing the propagation of parasitic slotline modes [24]. 10-μm thick Ni is electro-plated at the contact points. The most critical process steps for successful quartz probe tip processing is the initial cleaning and the use of HMDS before each photoresist application to achieve good adhesion. A detail process flow is attached in Appendix. B.2.

The probe tips are initially fabricated on 2"x2" quartz substrates. To separate the tips, they are sawn with diamond blades. Because the probe tips have finite thickness, when the tip is in on contact with a wafer, the contact areas are invisible to the probe user (Fig. 3.19(a)). To achieve accurate placement of probes (critical for accurate measurements), the tip contact points are made visible with a lapping process (Fig. 3.19(b)).

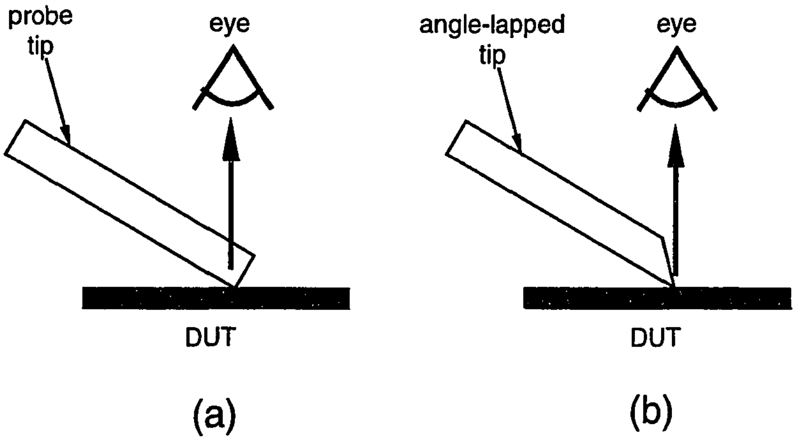

Figure 3.19. Illustrating the necessity of angle-lapped probe tips: (a) before lapping, and (b) after lapping.

The lapping process in illustrated in Fig. 3.20. A few pieces of quartz are first mounted around the periphery of the brass lapping fixture (Fig. 3.20(a)) with crystal wax to separate the brass fixture from the lapping powder. The probe tips (usually five at a time) are then mounted into the 45° slot (Fig. 3.20(b)) and the mounting side of the tips is aligned almost flush with the edge of the slot. The tips are lapped until the tip contact ends are approximately 2 mil thick (Fig. 3.20(c)). The lapping rate is approximately 3 mils per 100 laps. Finally, the probe tips are polished until the lapped surface is shiny. A more detailed lapping procedure is attached in Appendix. B.3. The probe tip after completion of all fabrication steps is shown in Fig. 3.21.

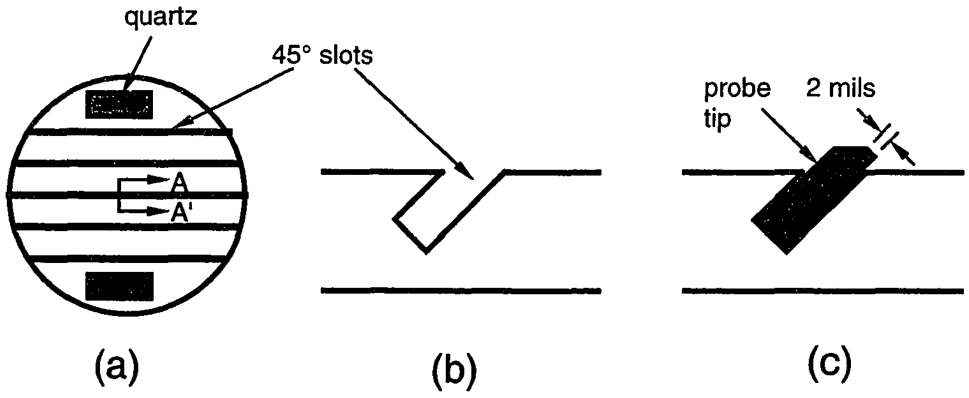

Figure 3.20. Angle lapping process: (a) top view of the lapping fixture, (b) cross sectional view of AA', and (c) final shape of lapped probe tips.

3.4 Bond Wire Connection Bandwidth

The last element in the high frequency path is the connection element between the low loss probe tip and the NWA IC. Gold ribbons are generally used as the wider ribbons have lower inductances than round wires. In addition, with the current bonding

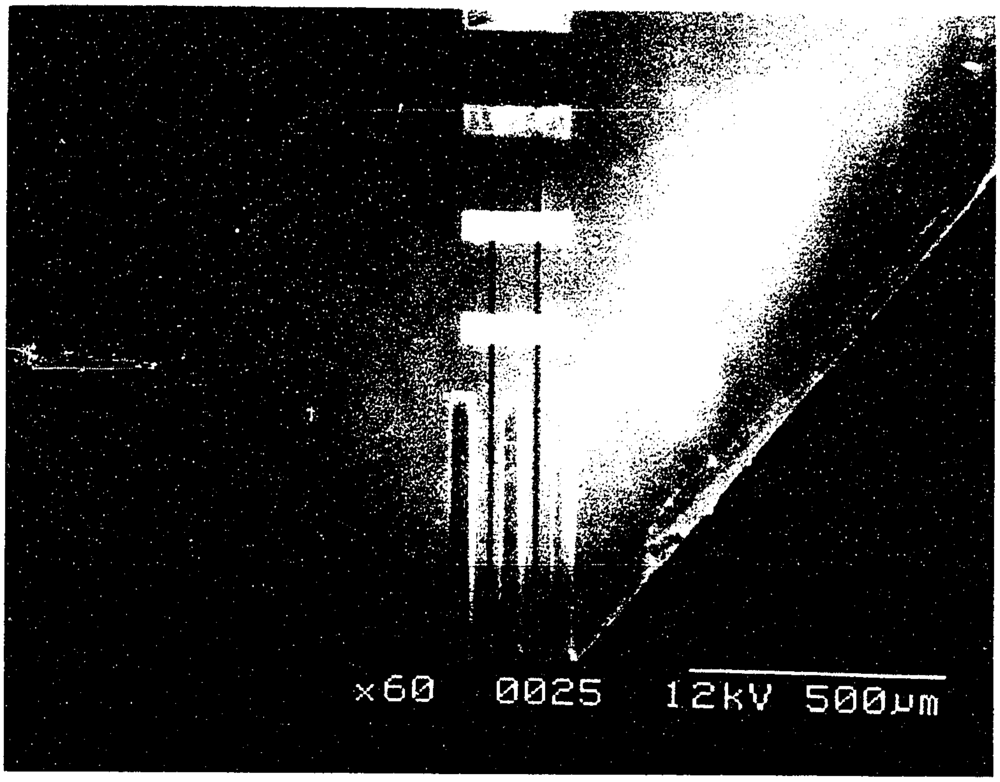

Figure 3.21. Scanning-electron micrograph of a fabricated quartz coplanar-waveguide probe tip.

machines available at UCSB, it is much easier to accurately place and bond very short ($\approx$ 100 μm) ribbons than round wires. For connecting the CPWs on planar substrates, ribbon bonding have less bonding point parasitics because wire bonding usually forms large gold balls at the bonding points. The inductance of gold ribbon of thickness t, width w, and length l can be calculated as [42]:

$$L = 5.08\times 10^{-3} l \left[\ln\left(\frac{l}{w+t}\right) + 1.19 + 0.22\times\left(\frac{w+t}{l}\right) \right] \quad \text{nH/mil}$$

So for a $t\times w\times l$=0.25 mil × 2 mil × 4 mil ribbons, L=40 pH. The circuit includes one bond in the center (signal) conductor and two parallel bonds for the ground connection, hence the total inductance of the ribbon bonds is 60 pH ($1.5\times L$).

The ribbon bond inductance can also be estimated with Touchstone simulations. Fig. 3.22 shows the $|S21|$ of two 2-mil-wide ribbons of different lengths (150 μm and 225 μm), and the $|S21|$ curves are also fitted with a model having an inductor in series with a resistor. The inset of Fig. 3.22 shows the 2-port network used for simulation. An inductance of 65 pH is estimated for the 150 μm ribbon and 120 pH for the 225 μm ribbon. The -3-dB bandwidth is $\approx$ 240 GHz for a 150 μm ribbon and $\approx$ 130 GHz for a 225 μm ribbon. A total bond length of 150 μm for connecting CPWs corresponds to a single ribbon length of 100 μm, and 225 μm total bond length corresponds to 150 μm single bond length. As a result, to achieve greater than 200 GHz connection bandwidth, the single ribbon length should be kept less than 100 μm.

The calculated bond wire inductance can be experimentally verified by using the NWA IC to measure the magnitude of the reflection from the wire bond. Ribbon bonds are incorporated into the output of the MWSPICE simulation circuit for the RF input signal line (Fig. 3.10). The length and inductance of the ribbon bonds are estimated by applying an NLTL generated incident wave and fitting the output voltage waveform (sum of the incident and reflected waves) to the measured waveform. The falltime of the input waveform is chosen to give an output incident edge that matches the measured incident edge, and the length (hence inductance) of the ribbons is then adjusted to give a reflection which matches the measured reflection. A 60 pH inductance ($\approx$ 150 μm long ribbon) is then determined, which is very close to the inductance calculated by Eq. 3.10 and estimated by Touchstone simulation for a 150 μm long ribbon. Therefore the experimental data agrees with two analytical models. Consequently, the ribbon connection limits the probe bandwidth to $100\Omega / (2\pi \cdot 60pH)$=265 GHz.

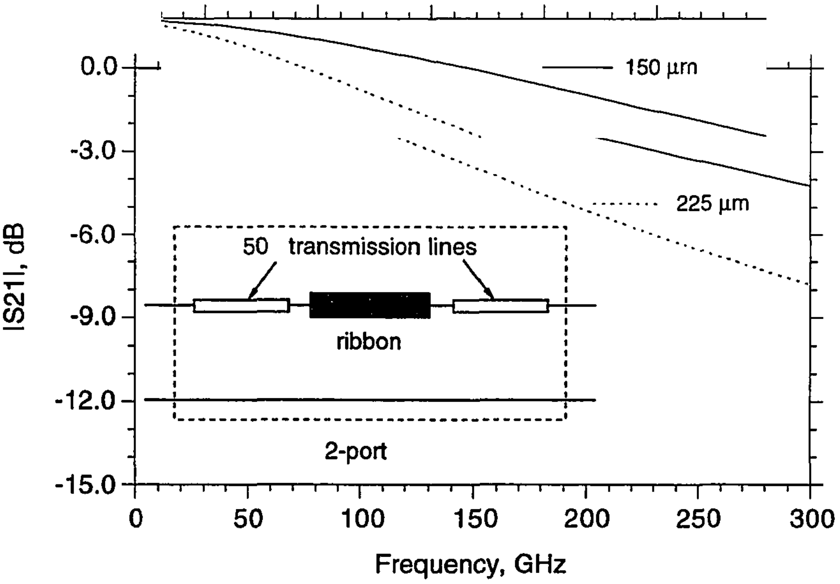

Figure 3.22. Computed ribbon connection bandwidth for 2-mil wide ribbons of different lengths.

3.5 Hybrid Assembly and Mechanical Design

The active probe bandwidth is limited by the NWA IC, the low-loss quartz probe tip, and by the ribbon bond parasitic inductance. The minimum length of the probe tips is set by the area needed for reliable mounting of the probe tips and ease of handling during hybrid assembly. This length (currently 2 mm) in turn sets the probe tip bandwidth. NWA IC bandwidth is independent of the hybrid assembly. The ribbon length (hence the connection bandwidth) is determined by the hybrid assembly design and process. To ensure low parasitic ribbon bonds, their lengths must be minimized. This requires that the surface of the NWA IC be flush with the probe tip, hence the GaAs IC and the quartz probe tip substrate must be equal thickness. Furthermore, the bonding pads on both the NWA IC and the probe tip must be as close to the edge as possible. The NWA IC thickness is determined by the IC substrate vendor, and is extremely controllable. Quartz substrates with very precise dimensions (currently < ± 0.3 mil) can also be purchased with a higher price. To have the bonding pads close to the edge, the metal pads should be extended beyond the cutting marks in the mask layout so that the sawing blade cuts through the metal. To obtain smooth cutting edges and prevent peeling of metal bond pads, thin blades (i.e. 1 mil blades) and appropriate cutting speeds should be used. One company which has provided satisfactory sawing service is Halcyon Microelectronics Inc. in Erwindale, CA. The probe bodies were machined from brass and then gold plated. The detailed machine drawings of the probe bodies are attached in Appendix D.

The hybrid assembly of the active probes are shown in Fig. 3.23. In fabricating the active probes, the glass beads for the two k-connectors are first soldered into place. The signal routing substrate is then epoxied on the probe body. The Au sliding contacts of the k-connectors are installed and connections to the CPWs on the signal routing substrates are made with Silver epoxy paint. The NWA IC and the quartz probe tip are then mounted consecutively on the probe with epoxy. As alignments are needed for mounting all these pieces on the probe body, they must be done under the microscope. Having mounted all the pieces, electrical connections are provided with ribbon bonds. The ribbons are first cut into appropriate lengths, and the pick-up tool is used to pick-up and place the ribbon on the right position. The ribbon is then tapped at its ends with the 1 mil bonding tip with a bonding machine setting of: power = 100; time = 150. Practice and patience are the keys to high quality bonding. Fig. 3.24(a) shows a photograph of the hybrid assembly of an active probe, while Fig. 3.24(b) shows the comparative sizes of the active probe and a commercial passive probe.

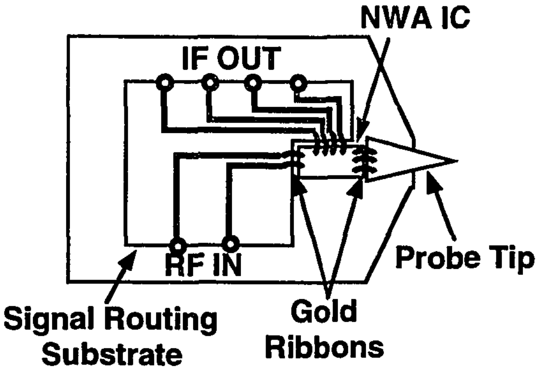

Figure 3.23. Hybrid assembly of the active probe.

Fig. 3.25 shows the mechanical setup for the active probes. Because the probe tips are very short (2 mm), they do not flex when the probe is brought into contact with the DUT. Instead, the necessary mechanical flexure for reliable probe-DUT contacts is provided through elastic materials (i.e. a rubber joint) placed at the interface between the probe and its supporting arm. With this elastic mounting, probe planarization is

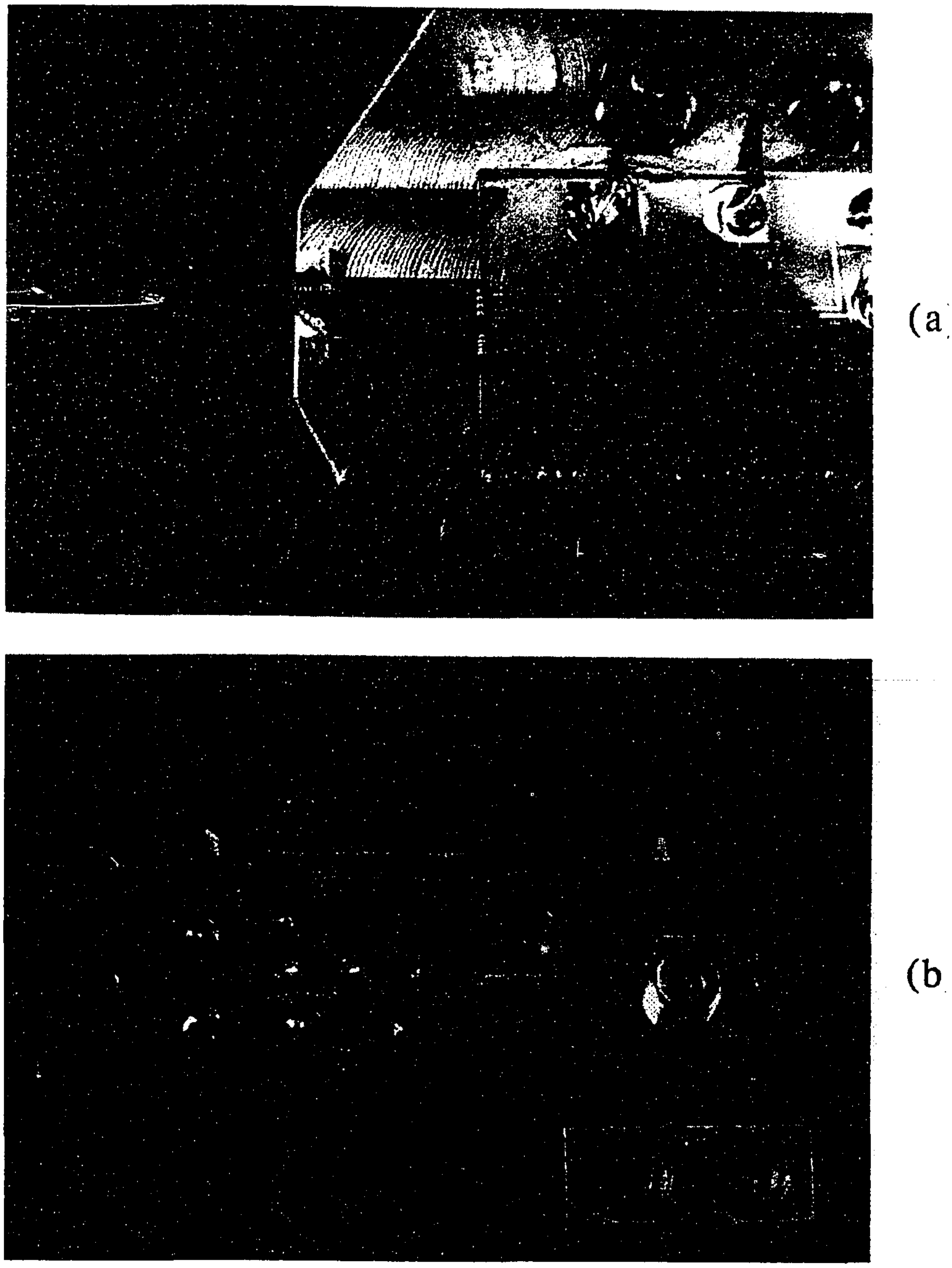

Figure 3.24.(a) photograph showing the active probe hybrid assembly, and (b) photgraph of an active probe compared to a commercial passive microwave probe.

also made less critical. Hundreds of contacts have been made without significant wear in the probe tips. A strain relief device for the cables is mounted on the probe arm so that accidental pulling of the cables does not displace and break the probes.

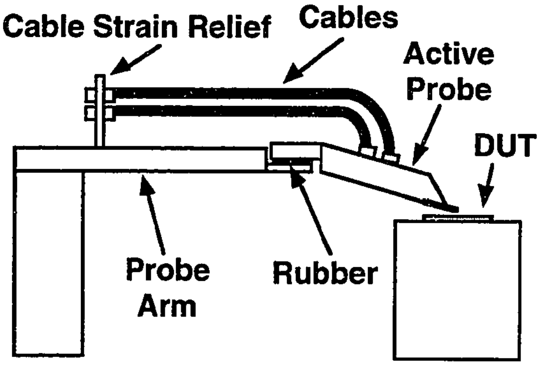

Figure 3.25. Mechanical setup of the active probe.

3.6 Active Probe Bandwidth Measurements

When the active probes are used for waveform measurements, the bandwidth (BW) of the probes can be determined by falltime measurements with the probes measuring signals which have much smaller falltimes than that of the probes. In contrast, when the active probes are used for network measurements, the stimulus signal for the DUT is supplied through the probes, thus the probe falltime measurements should include the contribution from the probe's NLTL stimulus signal generator. Fig. 3.26(a) shows the step response of the active probes with the probes measuring an NLTL with a 0.7 ps falltime [29]. If the measured 2.7 ps is deconvolved from the 0.7 ps input signal falltime, a probe falltime of 2.6 ps is estimated, corresponding to a probe -3-dB bandwidth of 135 GHz for waveform measurements. To determine the uncorrected (pre-calibration) bandwidth of the active probe for network measurements, we measured the falltime of the reflection from an open circuit load with the active probe providing its own stimulus signal (Fig. 3.26(b)). The measured 3 ps reflection falltime, corresponding to an active probe -3-dB BW (before calibration) of 110 GHz for network measurements, includes the convolved contributions of the NLTL pulse generator falltime, the capacitance charging time of the two sampling circuits, the probe tip losses, and the inductance of bond wires connecting the probe tip to the NWA IC. As with conventional VNAs, measurements can be obtained significantly beyond the uncorrected -3-dB BW after calibration. The corrected system bandwidth is limited by various system noises and these noise sources will be discussed in the next chapter. The probe step responses presented here are for the most current probes. Step responses of earlier probes will be discussed in Chapter 5.

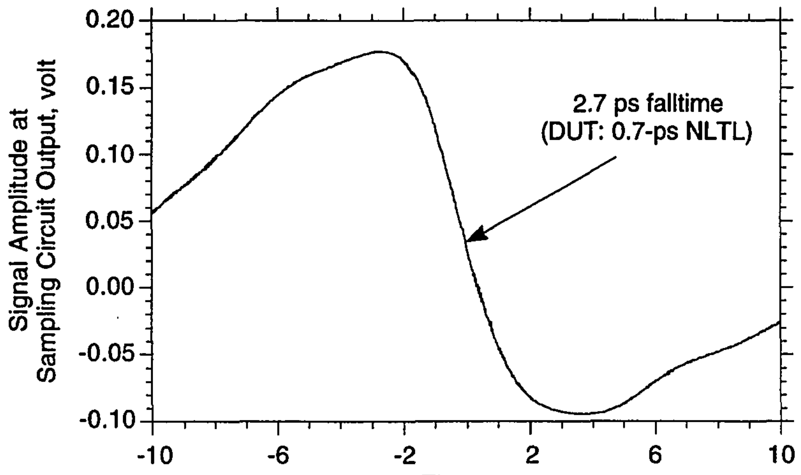

(a)

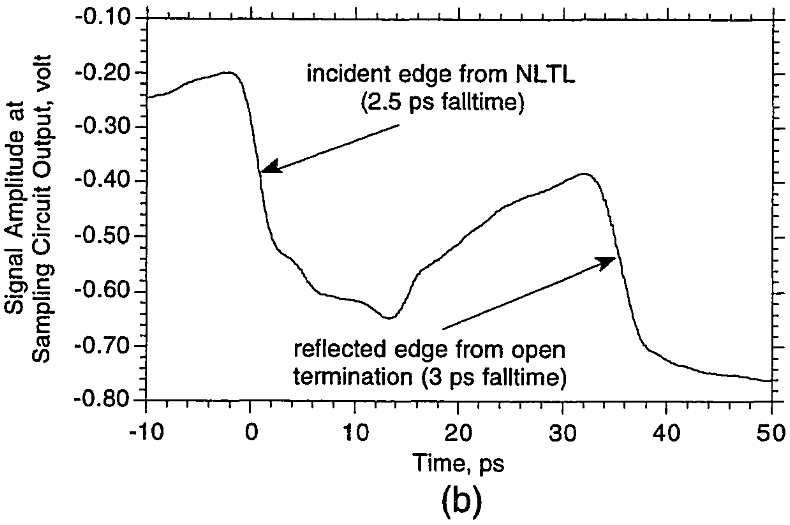

Figure 3.26. Step response of active probes for (a) waveform measurements, and (b) network measurements.

Chapter 4

Network Analyzer System Design

The active probes can be used for both waveform measurements and network measurements. If the frequency response of the active probe is accurately known, the useful bandwidth for waveform measurements can be much larger than the -3-dB bandwidth of the active probe, as the actual signal response can be obtained with deconvolution of the active probe response from the measured signal response. Because coherent signal sources are not readily available at millimeter-wave frequencies, an NLTL is used to generate the stimulus signal for approximate measurement of the active probe bandwidth.

For transition measurements of signal waveforms, the -3-dB bandwidth of the active probes can be considered a good measure of the useful bandwidth for waveform measurements. For network measurements, the system bandwidth can only be defined for a given measurement accuracy and reproducibility, and the system bandwidth depends not only on the -3-dB bandwidth of the active probes, but also on other system level issues such as system noise, calibration methods used, and accuracy of the calibration standards. As a result, the network analysis system bandwidth can be either much smaller or much larger than the -3-dB bandwidth of the active probes. Therefore, careful and ingenuous system design is essential for broadband network analysis systems.

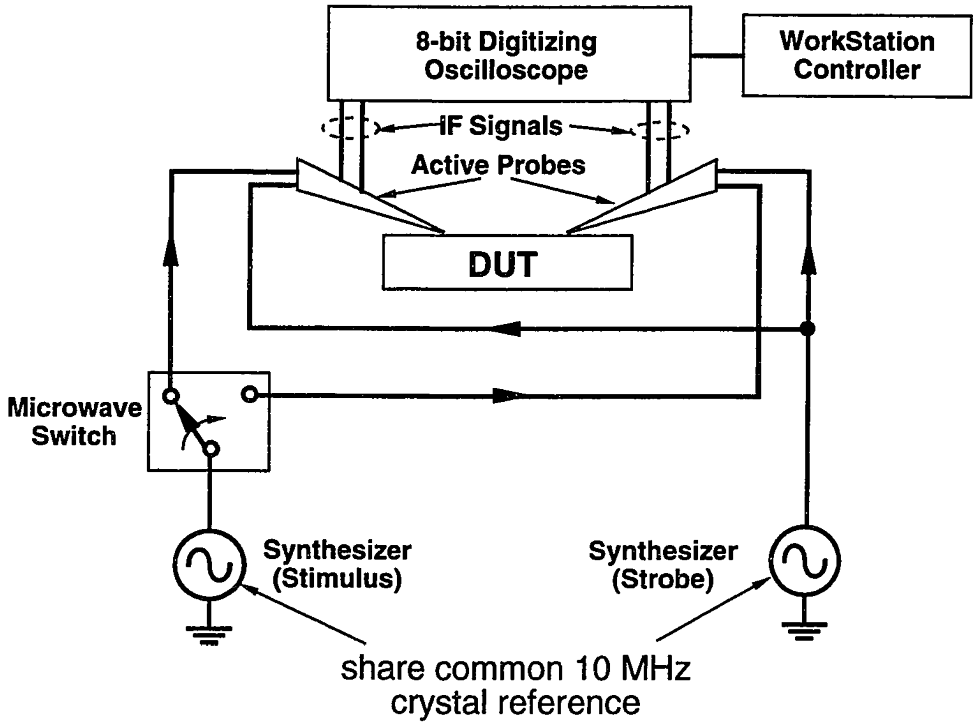

Figure 4.1. Basic network measurement system configuration.

To understand the origin of various system noise sources, let us examine the measurement system configuration shown in Fig. 4.1. In Fig. 4.1, a microwave synthesizer provides the ≈ 10 GHz drive signal for the NLTL to generate the stimulus signal on the active probe. The drive signal is switched between the two active probes through a computer-controlled microwave switch to provide the stimulus signal to either port 1 or to port 2. A second microwave synthesizer with the same phase reference provides the drive signals for the sampling circuit strobe NLTLs on the active probes. The active probes generate the millimeter-wave stimulus signals for the DUT, and the millimeter-wave response signals from the DUT are downconverted by the active probes to 10-500 KHz IF signals. The IF signals are digitized by a digitizing oscilloscope and transferred to a workstation controller for data processing via a GPIB interface. Raw S-parameters are calculated from these measurements after Fourier transformation of the time waveforms. The corrected S-parameters of the DUT are obtained from calibration procedures. In the experimental configuration of Fig. 4.1, the dominant noise sources are the relative phase flutuation (phase noise) of the two microwave synthesizers, the quantization noise due to finite resolution of the digitizing oscilloscope, the sampling circuit noise figure, the errors in calibration standards, and electromagnetic crosstalk between the active probes.

4.1 The Synthesizer Phase Noise

Although the two microwave synthesizers share a common 10 MHz frequency standard (Fig. 4.1), they have significant relative phase fluctuation. This phase fluctuation produces phase noise sidebands about each harmonic of the RF fundamental frequency. We will ascribe, without loss of generality in the signal/noise analysis, this timing fluctuation to the RF synthesizer which provides the drive signal to the stimulus NLTLs on the active probes. Given zero phase and amplitude noise, the RF synthesizer output is $V_0 \cos(\omega_{RF} t)$, and the measured signal at the sampling circuit input will be $r(t) = r(t - n \cdot 2\pi / \omega_{RF})$, some periodic waveform with repetition frequency ω_{RF}. With phase noise, the RF synthesizer output is $V_0 \cos[\omega_{RF}(t - J(t))]$, where $J(t)$ is the randomly-varying timing jitter and $< J(t) >= 0$. $J(t)$ has a power spectral density of

$S_J(\omega)=\int_{-\infty}^{+\infty}<J(t)J(t+\tau)>e^{-j\omega\tau}d\tau$. The single-sideband phase noise spectral density of the RF synthesizer is $L(\omega)=\omega_{RF}^2 S_J(\omega)$. The sampling circuit input signal is now $r(t-J(t))$, and the power spectral density of $r(t)$ can be written as [37]:

$$S_R(\omega)=\sum_{n=0}^{+\infty}R_n(\delta(\omega-n\omega_{RF})+n^2\omega_{RF}^2 S_J(\omega-n\omega_{RF})) \tag{4.1}$$

This assumes $n\omega_{RF}\sigma_J \ll 1$, where σ_J is the standard deviation of $J(t)$; R_n is the signal power in the n$^{\text{th}}$ harmonic of ω_{RF}. From Eq. 4.1, it is apparent that $J(t)$ has produced phase noise sidebands $n^2\omega_{RF}^2 S_J(\omega-n\omega_{RF})$ about each harmonic of ω_{RF}.

The sampled IF output is the product $i(t)=r(t)S(t)$, where $S(t)$ is a sampling pulse train at repetition frequency $\omega_{LO}=\omega_{RF}-\omega_{IF}$. To simplify the analysis, and without loss of generality, the sampling pulses are assumed to be impulses, and the power spectrum of the sampled signal is then

$$S_I(\omega)=G_S\sum_{n=0}^{+\infty}R_n(\delta(\omega-n\omega_{IF})+n^2\omega_{RF}^2 S_J(\omega-n\omega_{IF})) \tag{4.2}$$

plus terms at higher frequencies ($2\omega_{RF}$, $2\omega_{LO}$, $\omega_{RF}+\omega_{LO}$, etc.) which are removed by low-pass filtering. G_S is the sampling circuit conversion power gain (or loss).

The measurement system determines the vector amplitude at frequency $n\omega_{RF}$ of $r(t)$ (R_n in Eq. 4.2) by measuring the amplitude at frequency $n\omega_{IF}$ of $i(t)$. As evident from Eq. 4.2, because $i(t)$ is downconverted to a low scan rate ω_{IF}, the phase noise sidebands $S_I(\omega)$ are now separated by a much smaller ω_{IF} compared to ω_{RF}, and a given Fourier component of the input signal is then detected against a noise background set by the collective phase modulation sidebands of all other Fourier components.

A graphical illustration of phase noise sideband overlaps due to sampling circuit frequency downconversion is shown in Fig. 4.2. Sampling of the RF signals (at ω_{RF} and its harmonics) downconverts the RF signal spectrum (Fig. 4.2(a)) to much lower

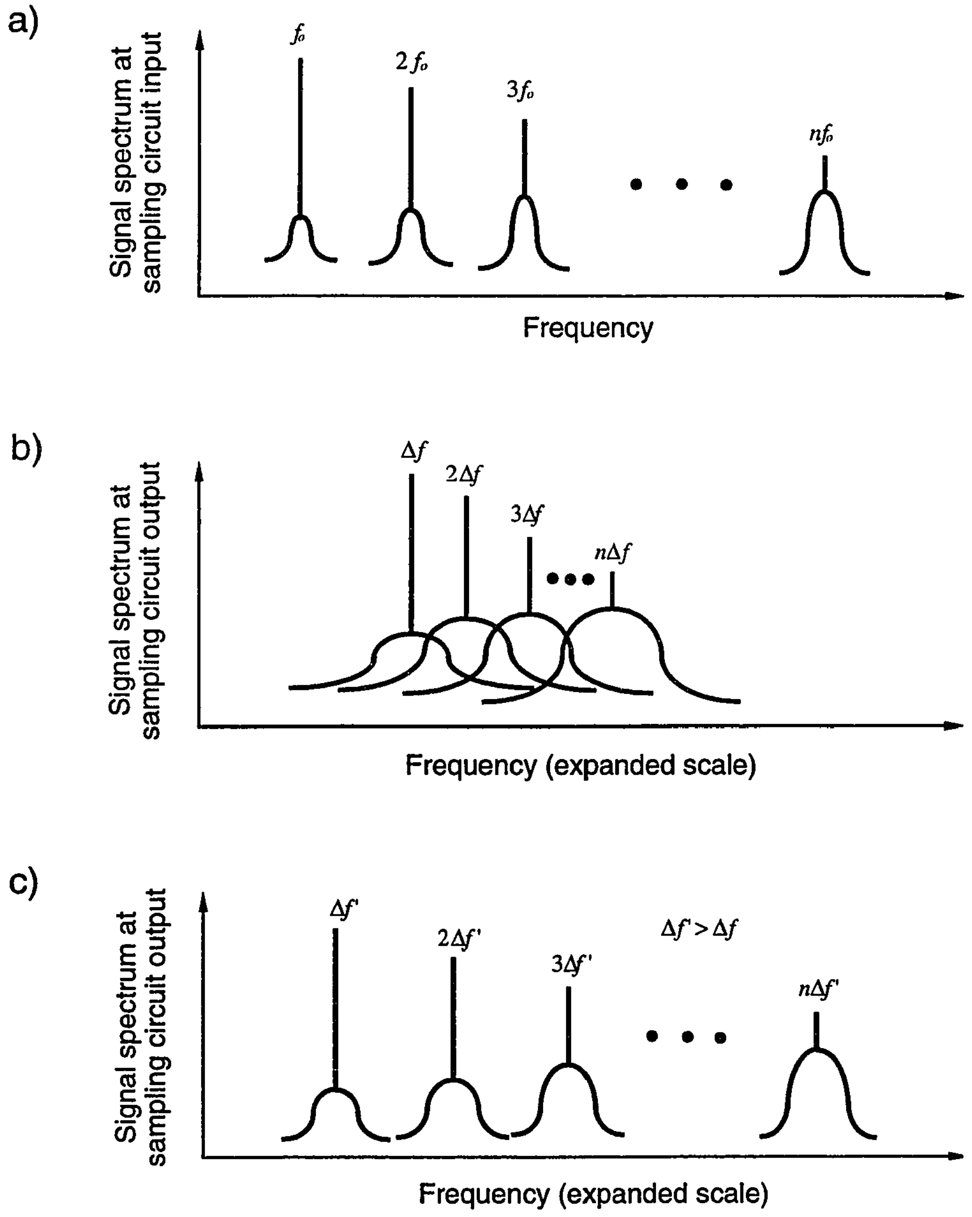

Figure 4.2. Phase noise sideband overlap due to downconversion of frequency spectrum by the sampling circuits: (a) spectrum at the sampling circuit input with RF fundamental frequency f_0, (b) spectrum at the sampling circuit output with IF fundamental frequency Δf, and (c) spectrum at the sampling circuit output with IF fundamental frequency $\Delta f'$ where $\Delta f' > \Delta f$.

IF frequencies (ω_{IF} and its harmonics, Fig. 4.2(b)). Depending on the bandwidth of the phase noise sidebands and the IF fundamental frequency, significant overlap of phase noise sidebands can occur. To reduce this effect, the IF fundamental frequency should be larger than the phase noise bandwidth (Fig. 4.2(c)).

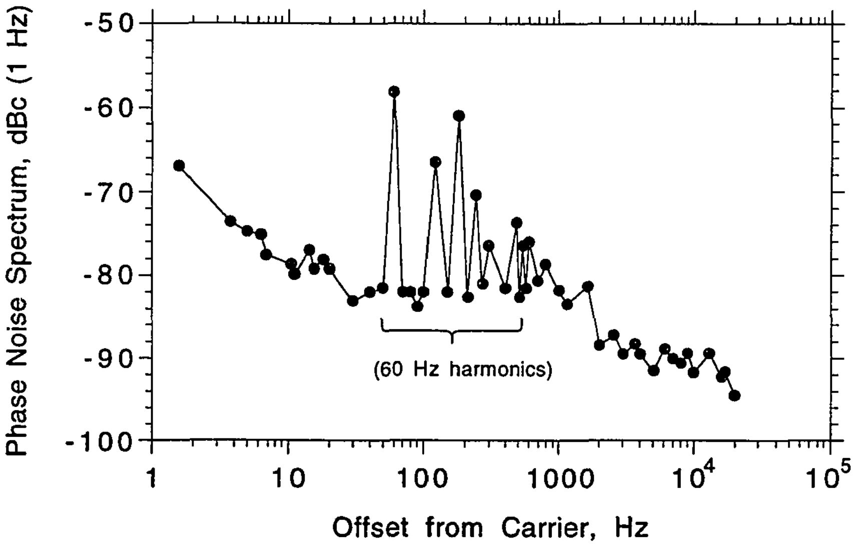

Figure 4.3. Measured relative phase noise spectral density of 2 microwave synthesizers operating under the same 10 MHz fundamental frequency reference.

Shown in Fig. 4.3 is the measured synthesizer single-sideband phase noise spectral density in unit of dBc (1 Hz). We emphasize that the pulse noise spectral density is the relative phase noise measured with the synthesizers operating from the same crystal oscillator fundamental frequency reference, which is the relevant quantity for the experimental configuration shown in Fig. 4.1. As shown in Fig. 4.3, the phase noise is significant at frequencies close to the carrier frequency, and phase modulation due to power line harmonics contributes large phase noise components at 60 Hz and its first several harmonics. The phase noise spectrum decreases rapidly for f>10 KHz (≈ 15 dB from its low frequency spectrum), therefore, IF frequencies of > 10 KHz should be used.

For an NLTL drive frequency of 10 GHz and an IF fundamental frequency of 10 KHz, the IF signal bandwidth required to measure a 300 GHz signal is 300 KHz. The sampling circuit output impedance is ≈ 40 KΩ (as calculated from the sampling circuit equivalent circuits discussed in the next section). A 1-meter long coaxial cable has 100 pF cable capacitances, hence the resulting IF bandwidth is only 40 KHz. To extend the IF signal bandwidth to beyond 300 KHz, much shorter cables (≈ 10 cm) must be used. An IF signal buffer circuit was fabricated and mounted on the probe arm to allow the use of very short cables.

Another way to combat the effects of phase noise (and other random noise terms) is to use signal averaging. The effect of signal averaging on signal spectrum is illustrated in Fig. 4.4. With no signal averaging, the signal spectral lines are detected against the phase noise background (Fig. 4.4(a)). With M signal averages, and assuming the signal period is T_{IF}, it can be shown that the effective IF detection bandwidth is a bandwidth $\Delta f \approx 1/(MT_{IF}) = f_{IF}/M$ placed around each signal harmonic, where f_{IF} is the IF fundamental frequency. Now the signal spectral lines are detected against the smaller band-pass filtered noise. Note that M / f_{IF} represents the minimum time required to obtain M averages of a signal with fundamental frequency f_{IF}. If we keep this ratio constant (constant data acquisition time or constant filter width), higher f_{IF} will result in a smaller noise background for detection of each spectral line because phase noise sideband overlap is reduced.

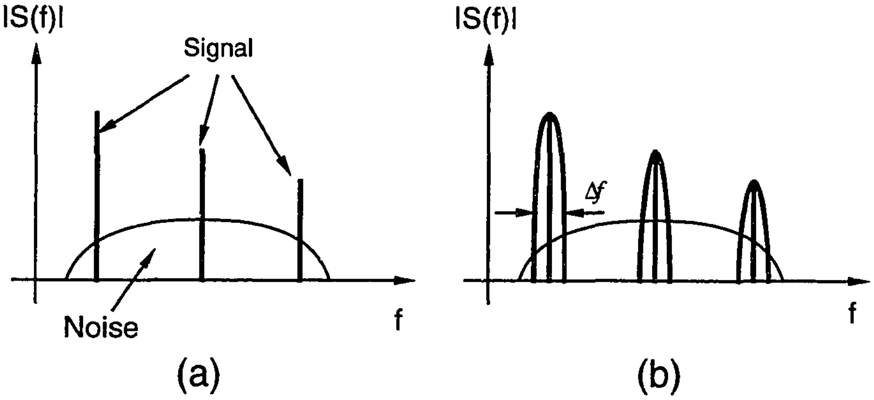

Figure 4.4. Effect of signal averaging on signal spectra: (a) without averaging, and (b) with averaging.

4.2. Sampling Circuit Noise

In addition to phase noise arising from the relative timing jitter between the two microwave synthesizers, the sampling circuits used in the NWA IC also contribute noise to the measurement system. Fig. 4.5 (a) shows an equivalent circuit for the sampling circuit. Because this circuit is balanced (symmetrical), it can be simplified to a single-channel equivalent circuit shown in Fig. 4.5(b), and this simplified equivalent circuit will be used for noise analysis.

In Fig. 4.5(b), the sampling diode is modeled with a switch. R_{on} is the diode on resistance and is the sum of the diode series resistance R_s and the diode junction resistance $R_j = kT / I_{pulse}$, where I_{pulse} is the average strobe-pulse conduction current passing through the sampling diodes. R_j has an associated short-circuit shot-noise current with spectral density $2qI_{pulse}$ (A^2/Hz), and hence an available noise power of $kT / 2$ (W/Hz). For brevity, we will (pessimistically) assume an available noise power of kT (W/Hz) for R_j so that R_j can be treated as a physical resistor. T_{on} is the sampling aperture time duration, and $T_{on} + T_{off} = 1/f_{LO}$ where f_{LO} is the sampling frequency. C_1 is the coupling capacitor, and C_2 is the capacitance of the cable connecting the sampling circuit output to the summing circuit. R_I is the isolation resistor used to isolate the cable capacitance from the coupling capacitor, hence preventing loading for the sampling RF and LO circuits by the IF cable capacitance. R_L is the load resistance.

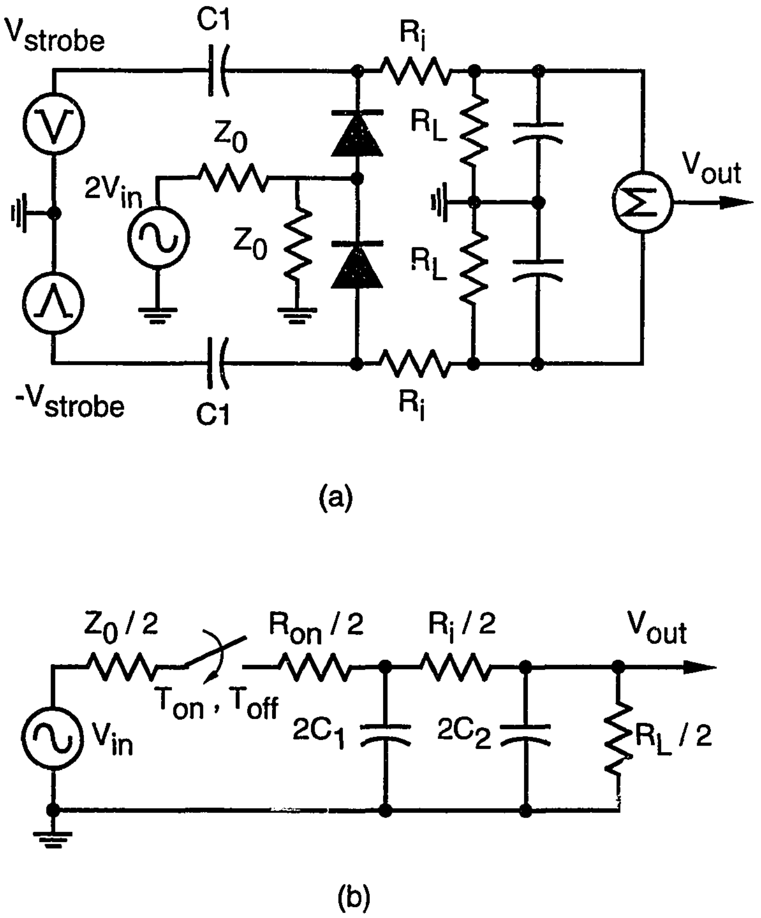

Figure 4.5. 2-diode sampling circuit: (a) equivalent circuit diagram, and (b) simplified equivalent circuit diagram.

Sampling circuit analysis is similar to that applied to switched-capacitor filters [43,44]. First consider the circuit shown in Fig. 4.6, we will find the Thevenin equivalent circuit. If C_1 is a short-circuit at the sampling rate, the voltage across C_1 has only a DC component. The short-circuit current is then

$$I_{SC}=\frac{V_{in}}{Z_0/2+R_{on}/2}\cdot\frac{T_{on}}{T_{on}+T_{off}}=\frac{V_{in}}{Z_0/2+R_{on}/2}\cdot D \qquad (4.3)$$

where $D=\frac{T_{on}}{T_{on}+T_{off}}$ is the duty cycle when the sampling diode is on. The open-circuit voltage is Voc=Vin. Consequently, the Thevenin resistance is

$$R_{th}=\frac{V_{OC}}{I_{SC}}=(Z_0/2+R_{on}/2)\cdot D$$

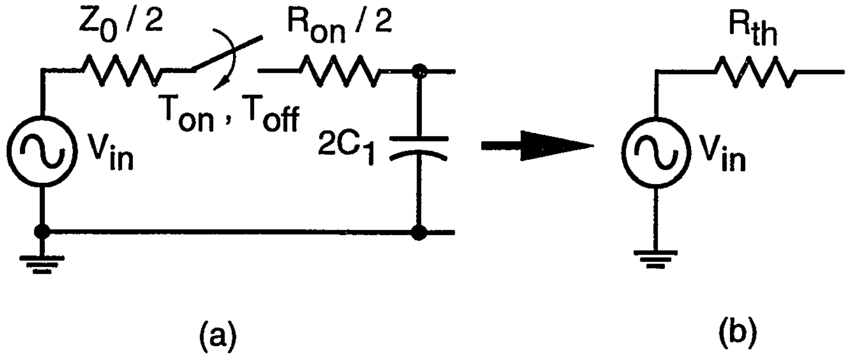

Figure 4.6. Impedance scaling by switching action: (a) circuit comprising components being scaled by switching, and (b) its Thevenin equivalent circuit.

If C_1 is not a short at the sampling rate, V_{OC} is no longer equal to V_{in}, and I_{SC} is no longer described by Eq. 4.3. The circuit in this case becomes much more difficult to analyze by hand. Continuing with the case where C_1 is a short-circuit, we combine the

Thevenin equivalent circuit in Fig. 4.6(b) with the remaining of the circuit in Fig. 4.5(b) and obtain the circuit shown in Fig. 4.7.

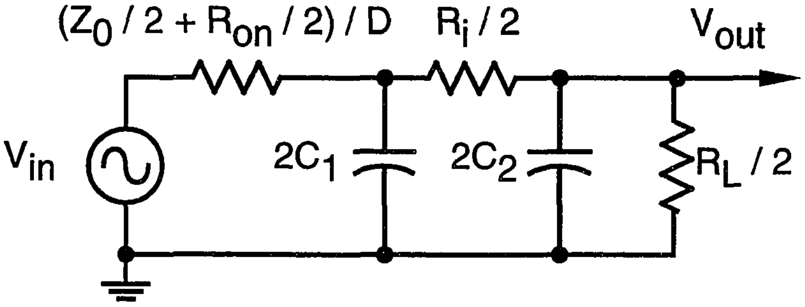

Figure 4.7. Equivalent circuit diagram of the sampling circuit shown in Fig. 4.5(b).

Because $C_2 >> C_1$, if C_1 is a short at the sampling rate, the voltages at the two nodes of R_l do not change as the diode is switched on and off. As a result, the current through R_l has only a DC component, thus R_l is not scaled by $1 / D$. However, on the other limiting case where C_1 is an open-circuit while C_2 is a short-circuit at the sampling rate, we have the circuit shown in Fig. 4.8. This circuit is similar to the circuit in Fig. 4.6 and, by similar analysis, R_l is now also scaled by $1 / D$.

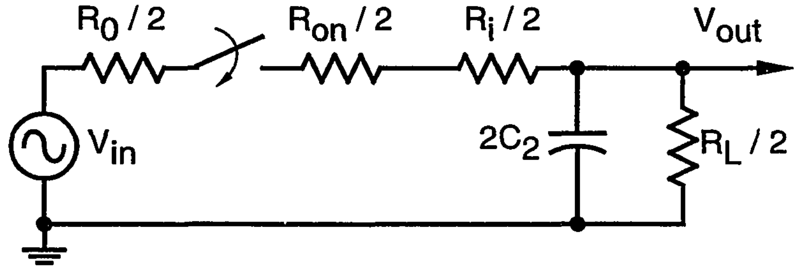

Figure 4.8. Equivalent circuit for the sampling circuit shown in Fig. 4.5(b) when C1 is an open at the sampling rate.

For the circuit in Fig. 4.7 (where C_1 is sufficiently large to be a short-circuit at the LO frequency), we can write

$$V_{out} = V_{in} \frac{R_L / 2}{R_L / 2 + R_l / 2 + (Z_0 / 2 + R_{on} / 2) / D}$$

and the available noise power spectral density at the sampling circuit output is

$$\frac{d < V_{n,out}^2 >}{df} = 4KTR_{out} = 4KT \cdot (R_L / 2) / / [R_l / 2 + (Z_0 / 2 + R_{on} / 2) \cdot D]$$

where $R_{out} = (R_L / 2) \| [R_l / 2 + (Z_0 / 2 + R_{on} / 2) \cdot D]$ is the equivalent resistance at the circuit output node.

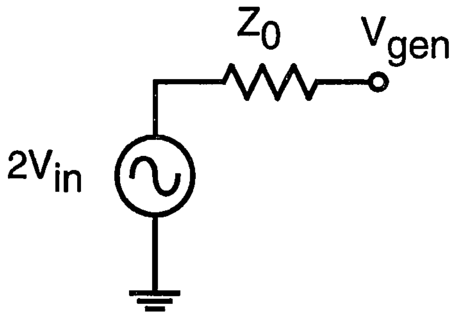

Figure 4.9. Equivalent circuit for the sampling circuit input.

For the generator circuit shown in Fig. 4.9, we can write $V_{gen} = 2V_{in}$ and the available thermal noise power spectral density at the circuit input is

$$\frac{d < V_{n,gen}^2 >}{df} = 4KTZ_0$$

The sampling circuit noise figure is then

$$F = \left(\frac{V_{gen}^2}{\dfrac{d < V_{n,gen}^2 >}{df}} \right) \cdot \left(\frac{V_{out}^2}{\dfrac{d < V_{n,out}^2 >}{df}} \right)^{-1}$$

$$= \frac{2}{Z_0 R_L} \left(R_l + \frac{Z_0 + R_{on}}{D} \right) \left(R_L + R_l + \frac{Z_0 + R_{on}}{D} \right) \qquad (4.4)$$

Eq. 4.4 is valid only when C1 is a short at the sampling rate. This requires

$$2\pi R_{eq}(2C_1) >> 1 / f_{LO} \qquad (4.5)$$

where

$$R_{eq} = \left(\frac{Z_0 / 2 + R_{on} / 2}{D} \right) \| (R_l / 2) \qquad (4.6)$$

is the equivalent resistance seen by C_1.

For the sampling circuit with 3μm x 3 μm sampling diodes, $R_s \approx 18\Omega$, $C_{diode} \approx$ 12 fF, and C_1=10 x C_{diode}=120 fF. In addition, R_L=1 MΩ, R_l=1 KΩ, and Z_0=50 Ω. $D \approx$ 0.5 ps / 100 ps = 0.005. The average diode current I_{avg} = 0.8 μA and the peak diode current $I_{peak} = I_{avg} / D$ = 160 μA. The diode junction resistance is then R_j = 163 Ω. Consequently, $(R_{on} + Z_0) / D$ = 46.2 KΩ. Because $1 / (2\pi R_{eq} C_1)$= 1.35 GHz, C_1 is adequately a low impedance at the sampling frequency (≈ 10 GHz), and Eq. 4.4 can be used to estimate the sampling circuit noise figure. In this case, F=1.98 x 10^3 or 33 dB.

In measuring the noise figure of the sampling circuit, the sampling circuit is first calibrated with DC voltages to obtain the sampling circuit conversion gain (loss). An NLTL shockwave input signal is then applied to the sampling circuit, and the input signal power spectrum is obtained with Fourier transformation of the measured output time waveform followed by proper conversion back to the circuit input. Fig. 4.10 shows the input signal power spectrum.

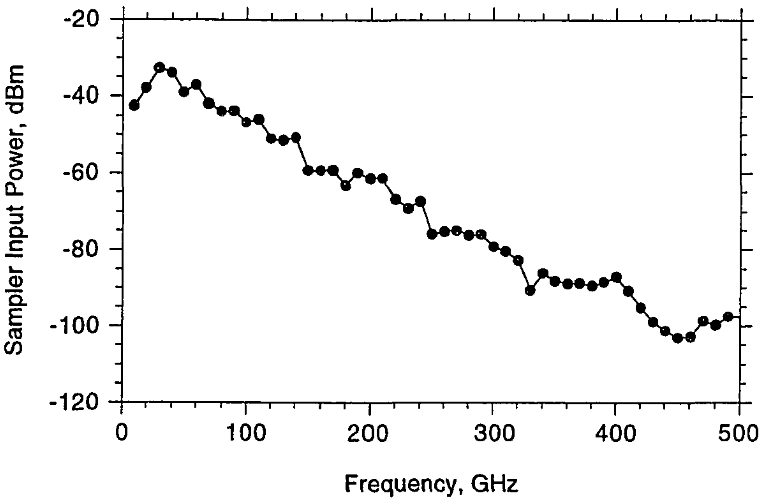

Figure 4.10. Signal power spectrum at sampling circuit input.

The sampling circuit output signal to background noise ratio is then measured with a spectrum analyzer where background noise includes the sampling circuit noise and generator noise. Fig. 4.11 shows the sampling circuit output signal to background noise ratio. The noise figure of the sampling circuit is

$$F = \frac{(S/N)|_{in}}{(S/N)|_{out}}$$

or in unit of dB, $F = S_{in,dBm} - KT - (S/N)|_{out,dB}$. At room temperature, KT=-174 dBm (1 Hz), and consequently, F = 65 dB ± 5 dB. The much higher measured noise figure compared to the predicted 33 dB is not understood. The input-referred equivalent noise power is therefore -109 ± 5 dBm (1 Hz).

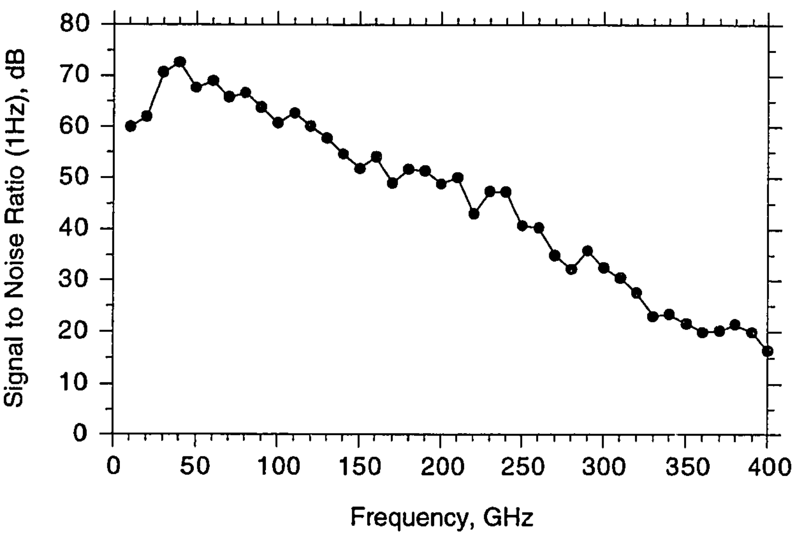

Figure 4.11. Measured signal to background noise at sampling circuit output.

4.3 System Calibration

Network measurement accuracy, hence bandwidth, is largely determined by how well the measurement system can be calibrated. A well-calibrated system can perform accurate measurement to bandwidths significantly higher than the -3-dB bandwidth of the system hardware (as in most of the commercial network analyzers), while a poorly-calibrated system can fail to function at bandwidths much lower than the -3-dB bandwidth of the system. As a result, proper calibration methods and well-defined calibration standards are essential for accurate millimeter-wave network analysis.

The concept of calibration (or de-embedding) is illustrated in Fig. 4.12. Non-idealities between the measuring ports and the DUTs, arising from cable and connector losses and reflection, finite measurement port directivity and reflection, etc., are modeled by two error 2-port networks. The S-parameter matrices of the error 2-port networks are obtained by measurements of several calibration standards. The calibration mathematical procedure is carried out by first converting the S-parameter matrices of the error 2-port networks and the measured DUT's 2-port network to transmission (also called Cascade) parameter matrices [45]. The measured DUT 2-port matrix (M) is then related to the actual DUT transmission matrix (A) as:

$$M = XAY$$

where X and Y are the transmission matrixes of the error 2-port networks. Knowing the error 2-port transmission matrixes, the actual transmission matrix of the DUT can be determined by:

$$A = X^{-1}MY^{-1}$$

and the corresponding actual S-parameter matrix can be obtained by conversion of the transmission parameter matrix to an S-parameter matrix.

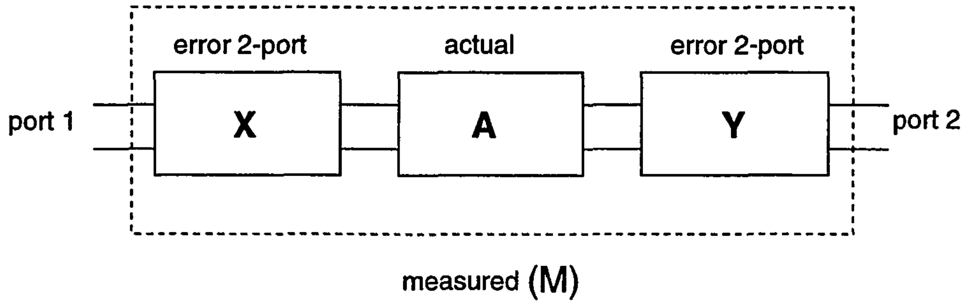

Figure 4.12. Conceptual diagram illustrating calibration for network measurements.

Over the last two decades, various researchers have done extensive studies on network measurement calibration methods [45-51]. The major results will be stated here without proof. Because all the S-parameters (hence the transmission parameters) are ratio quantities, only seven error terms need to be determined for X and for Y. While there are 7 unknowns, measurements of three 2-port standards yield 12 sets of equations. Due to this redundancy, it is not necessary to know all the parameters of all the calibration standards.

Over the years, many calibration methods have been proposed and experimented with, and each of these methods has its own drawbacks and merits. The most common calibration methods for on-wafer measurements are Short-Open-Load-Through (SOLT), Line (or Through)-Reflect-Line (LRL or TRL), and Line-Reflect-Match (LRM). With SOLT, all parameters of the calibration standards must be accurately defined. Because it is difficult to fabricate and accurately model the SOLT calibration standards up to millimeter-wave frequencies, SOLT calibration generally yields less accurate measurement results at high frequencies. In addition, 4 calibration standards are needed in SOLT as the SOL standards are first used to calibrate each measurement port (3 S-parameters each for X and Y) and the Through standard is used to measure the 7th unknown in the two error 2-port matrices. However, if only one measurement port is available, SOL calibration provides a convenient way to calibrate the 1-port measurement system.

Both LRL and LRM calibration methods require two-port calibrations even if only 1-port measurements are desired. With LRL calibration, the impedance of the transmission line standards provides the impedance standard (usually 50 Ω), and the line length must by accurately known. The reflect standards (usually a short or an open) need not be accurately defined, except that they must be identical for both ports. The transmission line parameters, such as the propagation constant and loss coefficient, can be determined from the calibration procedures. To avoid ill-conditioned matrix solutions in the calibration mathematical calculations, the difference of the line lengths mush be such that the signal phase delay at a given frequency stays within the range of 18 ° to 162°. As a result, a transmission line standard can only cover an ≈ 8:1 frequency range. For broadband network analysis, many lines are required to cover the whole frequency range of interest. The advantage of LRL over SOLT is that the reflect standard and the transmission line parameters need not be accurately defined.

The LRM calibration technique addresses some of the limitations of the LRL calibration method. In LRM, the transmission line standard is assumed to have zero return loss (perfect 50 Ω impedance) and have zero dispersion and attenuation, which is still a good approximation to 200 GHz for a short (1-ps) 50 Ω through line. A 50 Ω match load is used to provide the impedance standard. Again, the reflect standard needs not be accurately defined. Only three measurements of calibration standards are needed for the LRM calibration and the spacing of the standards can be made suitable for fixed probe configuration.

All three calibration methods have been implemented and experimented with our network measurement system. The computer codes implementing the calibration mathematical processes for each of these calibration methods are written in C and are attached in Appendix C. The measurement results are presented in the next chapter. The calibration standards for SOL and LRM are those purchased from Cascade Microtech Inc., while the transmission line standards for LRL are fabricated at UCSB. SOL provides a convenient 1-port measurement calibrations. However, because the SOL calibration method relies on the accuracy of all the calibration standards and these standards are not verified above 75 GHz, 1-port measurements are performed only to 96 GHz. With LRL calibration method, the impedance standard is provided with the transmission line impedance, which may become inaccurate at millimeter-wave frequencies due to dispersion effects. Moreover, the measurement accuracy is limited by the system's ability to accurately determine the transmission line loss coefficient and propagation constants. For calibration at very high frequencies (> 100 GHz), the transmission lines are short and the line losses small, hence it becomes very difficult to accurately determine the line loss coefficient at these frequencies. For our network measurement system, we were only able to determine the line parameters accurately to ≈ 100 GHz. LRM calibration method offers the best performance in 2-port measurements. Accurate and reproducible measurements on the calibration standards are obtained to ≈ 200 GHz. However, measurements of other known DUTs (such as an open circuit) have larger errors above 100 GHz. We attribute this fact to the inaccuracy in the 50 Ω calibration standard, and we will give more discussion in next chapter and propose ways to improve the calibration standard accuracy in Chapter 6.

4.4 Quantization Noise

The current network measurement system uses an 8-bit digitizing oscilloscope to acquire and digitize the NWA IC output waveforms (Fig. 4.1). Since the stimulus (incident) time waveforms are approximately sawtooth waveforms, their spectral content decreases as $1/\pi n$ (normalized to the peak to peak amplitude of the time waveform), where n is the n^{th} harmonic of the fundamental frequency, hence the resolution for the signal Fourier components at higher frequencies are much less than 8-bit, severely limiting the accuracy, directivity, and dynamic range of the VNA at higher frequencies. For a uniform quantizer (quantization levels spaced evenly, such as the digitizing oscilloscope) with resolution a, assuming the quantization errors distribute uniformly over a, the mean-square quantization error for each signal sample is $\sigma_q^2 = a^2 / 12$. Assuming the quantization noise is uncorrelated from sample to sample (usually a good assumption and used in most of the signal processing literature for treatment of quantization noise), it can be shown that the quantization noise is white and also has a variance of $a^2 / 12$ for each signal spectral line. In other words, associated with each signal spectral line, there is a RMS noise signal of $a / \sqrt{12}$. For a sawtooth waveform at 8 GHz fundamental drive frequency and with 1-volt signal swing, for example, the signal amplitude at 200 GHz (25th harmonic) is $1 / 25\pi$ volt. For a 8-bit quantizer, the RMS noise signal amplitude is $(1 / 2^8) / \sqrt{12}$ and the signal/quantization error ratio is then 21 dB at 200 GHz. Because the NWA IC measures the sum of the incident and reflected signals, the quantization error becomes particularly severe when measuring reflections from DUTs with ≈50 Ω impedance where the small reflected signal is much smaller in magnitude than the large incident signal. To improve the system directivity, the approximate incident and reflected signals (as described by Eq. 3.3 and Eq. 3.4) are obtained by a difference circuit before data acquisition by the digitizing oscilloscope.

4.5 Probe Crosstalk

For 2-port on-wafer network measurements, two active probes are employed. For LRM, LRL, or SOLT calibrations, the 1-ps through line is about 200 μm long. Currently, the NWA ICs and the probe tips on the active probes are exposed to air. When the probes are brought within 200 μm of each other, some degree (≈ -40 dB) of electromagnetic coupling is observed. The probe crosstalk cannot be eliminated by calibrations because the magnitude of the coupling depends upon probe placement (and is non-systematic). Better shielding of the NWA ICs and probe tips should reduce this effect.

To summarize this chapter, for the current network measurement system, the dominant sources of error are the inaccuracy in the calibration standards at millimeter-wave frequencies and the quantization errors arising from the 8-bit digitizing oscilloscope. Compared to these errors, the sampling circuit noise contribution is of minor importance. In addition, the signal/phase noise ratio can be kept much lager than the signal/quantization noise ratio with the use of IF buffer circuits to increase the IF signal bandwidth to MHz range, allowing much higher IF signals hence adequate separation of phase noise sidebands. Several other system configurations which attempt to address some of the system limitations have been experimented with. These alternative system configurations and their drawbacks and merits will be discussed in the next chapter.

Chapter 5

Millimeter-Wave On-Wafer Measurements

While frequency-domain measurements, such as S-parameter measurements (also called network measurements), reveal steady-state response of a device under test (DUT), time-domain measurements offer additional insight into the transient behavior of the DUT. Depending on the information desired about the DUT, measurements in one or both domains are required. For example, component values in high-frequency transistor models are generally obtained by fitting these models to S-parameter measurements, while reflection measurements for microwave packages are best obtained with time-domain reflectometry (TDR) measurements, as these measurements separate, in time, the reflections due to various parasitic transitions and impedance mismatch along the signal path in the packages and the nature of these parasitics can therefore been investigated and modeled. In addition, waveform measurements for a DUT yield useful information about its time-domain characteristics (such as the transition time, over shoot and ringing in a waveform). The high-speed network analyzer (NWA) ICs described in chapter 3 are in reality time-domain reflectometers. These ICs contain high-speed sampling circuits. The active probes incorporating these ICs are thus inherently time-domain instruments and can be used for waveform and TDR measurements. Under steady-state and small signal conditions, measurements in frequency domain are mathematically related to those in time-domain by Fourier transforms. Consequently, active probes can also be used for network measurements. In this chapter, both waveform and network measurement results with the active probes are presented.

5.1. Waveform Measurements

The basic measurement setup for waveform measurements using active probes is shown in Fig. 5.1. The strobe NLTL on the active probe is driven at f_0 with a microwave frequency synthesizer. A second synthesizer provides the $nf_0 + \Delta f$ input signal to the device under test through a commercial microwave wafer probe. The DUT output waveform is measured by the active probe and downconverted by the NWA IC to an IF frequency of Δf. The IF signal is subsequently measured with a low-frequency digitizing oscilloscope. Shown in Fig. 5.2(a) is the waveform of a 0.7-ps NLTL [29] measured by an active probe. The measured falltime is 2.7 ps, and the deconvolved probe falltime is then 2.6 ps, corresponding to a probe -3-dB bandwidth of 135 GHz. Fig. 5.2(b) shows the output waveform of a traveling-wave resonant tunnel diode (TWRTD) pulse generator [52]. The TWRTD pulse generator is excited at 40 GHz plus 1 KHz and the strobe NLTL on the active probe is driven at 10 GHz. A 3.5 ps, 400 mV transition is measured. If a probe response time of 2.6 ps is deconvolved from the measured 3.5 ps, a TWRTD pulse generator transition time of 2.5 ps is estimated.

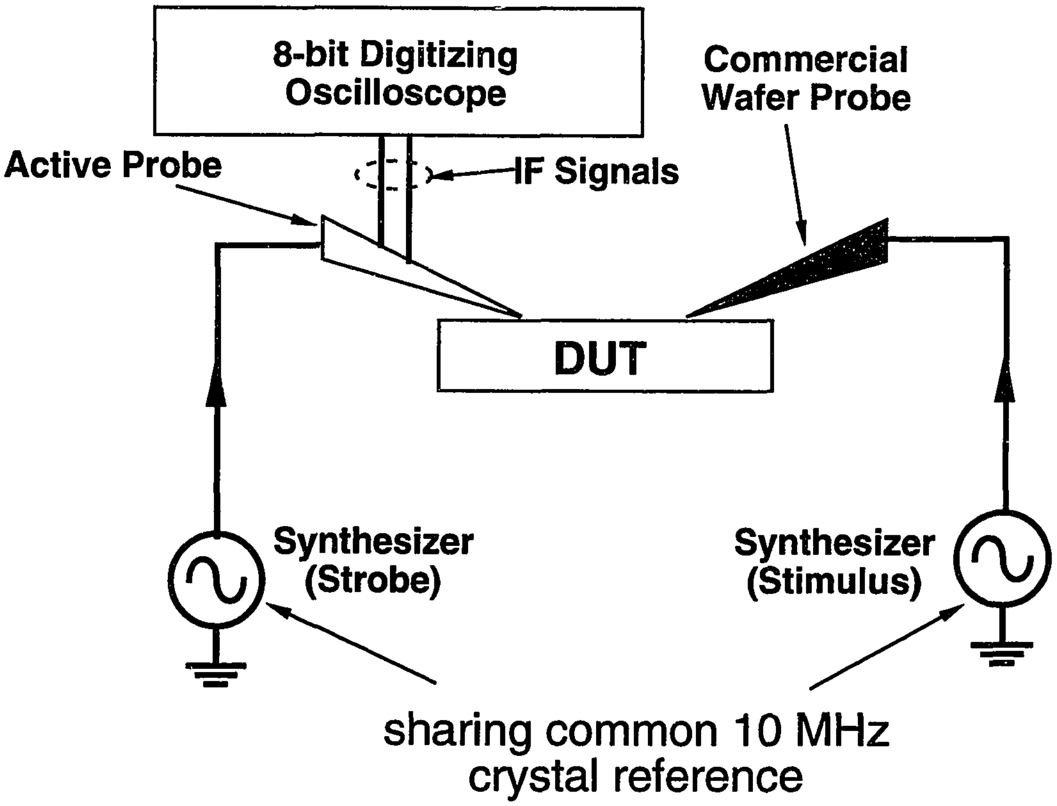

Figure 5.1. Waveform measurement setup.

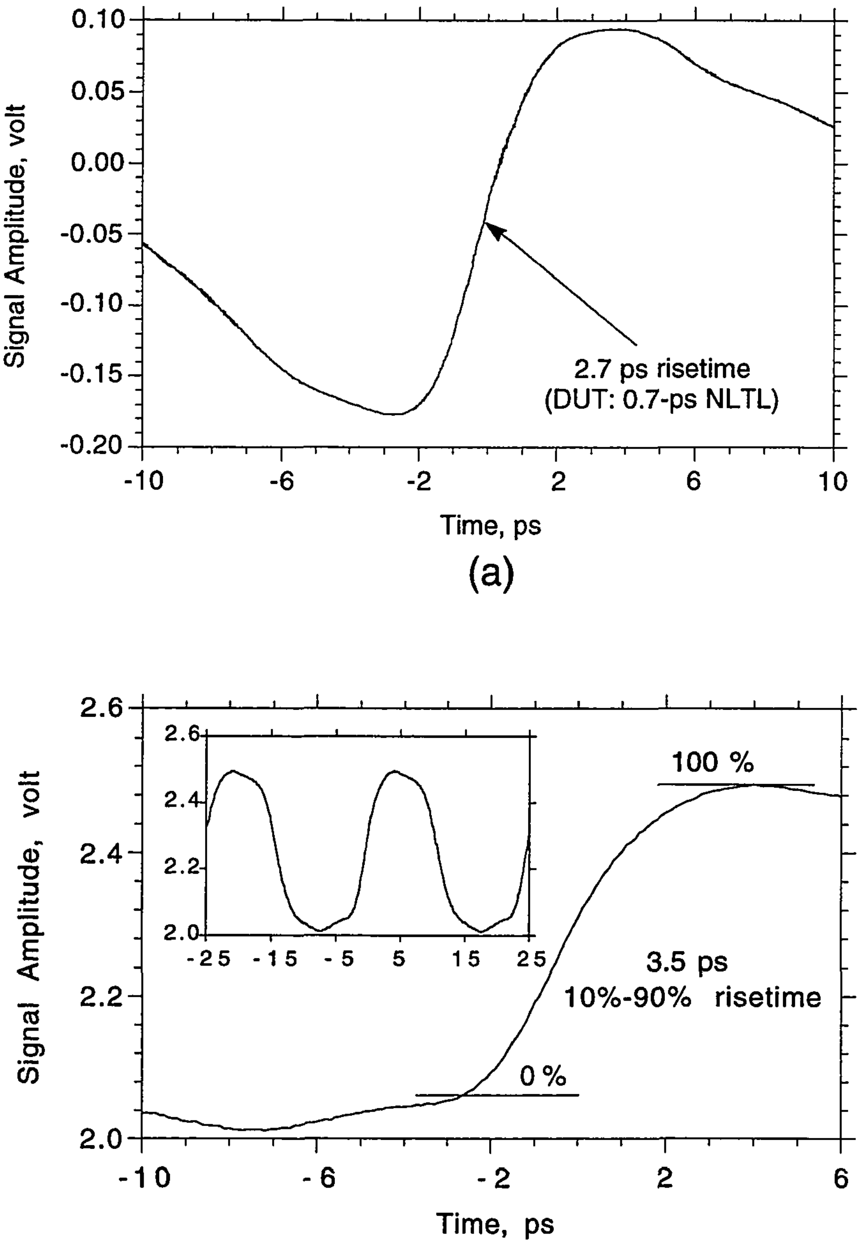

Figure 5.2. Waveform measurements with the active probe: (a) 0.7-ps NLTL output risetime, and (b) traveling-wave resonant tunnel diode pulse generator output risetime and the inset shows two periods of the waveform.

5.2. Network Measurements

The system configuration for network measurement using the active probes is shown in Fig. 5.3. A synthesizer provides the 7-14 GHz drive signals for the NLTL to generate the stimulus signal on the active probe. The drive signal is switched between the two active probes through a computer-controlled microwave switch to provide the stimulus signal to either port 1 or to port 2. A second synthesizer with the same phase reference provides the drive signals for the sampling circuit strobe NLTLs on the active probes. The active probes generate the 7-200 GHz stimulus signals for the DUT, and the response signals from the DUT, also in the 7-200 GHz bandwidth, are downconverted by the active probes to 10-500 KHz IF signals. The IF signals first pass through buffering and summing circuits, are then digitized with a digitizing oscilloscope, and are transferred to a workstation controller for data processing via a GPIB interface. The buffering and summing circuits, as described in Chapter 4, allow higher IF signal frequencies (hence reducing phase noise aliasing) and reduce the effects of quantization noise on the system directivity and dynamic range. One period of the output waveform is digitized with M points. The digitizing oscilloscope's sampling frequency is then $M\Delta f$ where Δf is the IF fundamental frequency. It is very important to ensure that $M\Delta f > 2B_{IF}$ where B_{IF} is the IF signal circuit bandwidth, otherwise aliasing will seriously distort the sampled signal spectrum. Raw S-parameters are calculated from these measurements after Fourier transformation of the time waveforms. Since the active probes function correctly over a stimulus drive frequency range of 7-14 GHz, a complete octave in frequency, S-parameter measurements are possible over the entire frequency spectrum from 7-200 GHz. Fig. 5.4 shows a photograph of two active probes and a conventional microwave probe measuring a DUT.

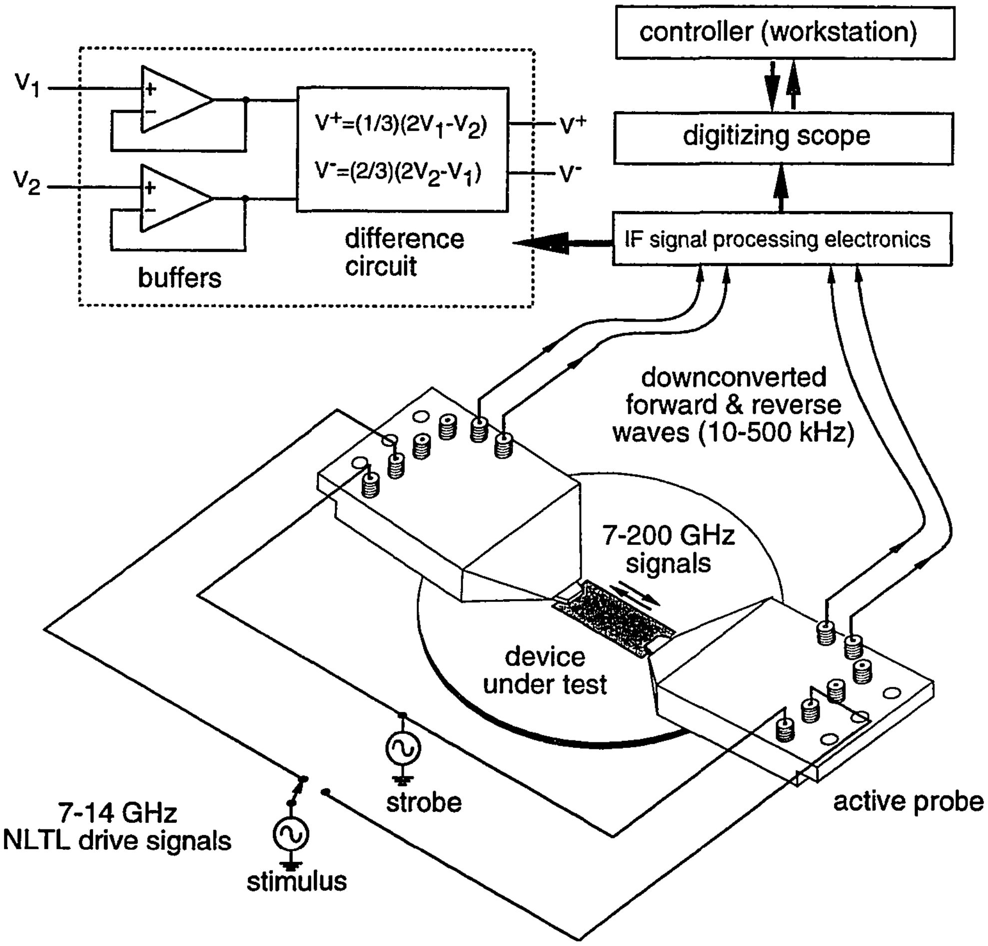

Figure 5.3. System setup for network measurements using active probes.

Three generations of active probes have been fabricated, with each generation exhibiting performance improvement over its predecessor. System level design is also improved in the course of improving the active probes. The system configuration

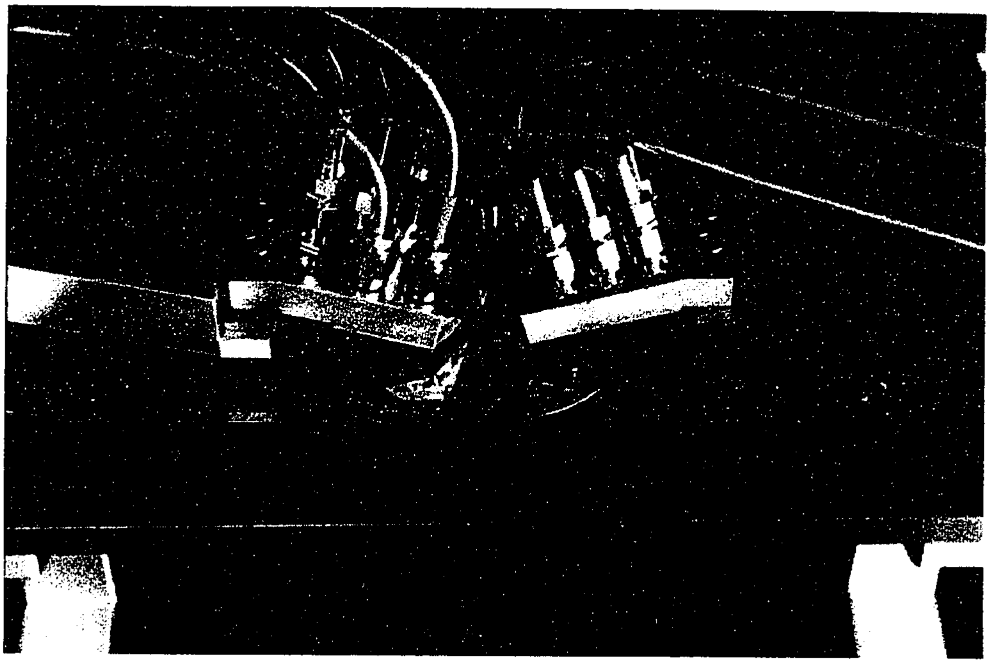

Figure 5.4. Photograph of two active probes and a commercial passive microwave probe measuring a DUT.

shown in Fig. 5.3 reflects the most current system setup, and certain system components are absent from that shown in Fig. 5.3 for earlier generations of the network measurement setup. The major network measurement results for the three generations of active probes will be presented in the subsequent sub-sections, and the experimental conditions will be specified. Alternative network measurement system configurations have also been explored, and these will be discussed in section 5.3.

5.2.1 First Generation Results

In the first generation of active probes, the NWA ICs included bias tees, and the probe tips were fabricated on alumina and are 5 mm long. Due to layout parasitics of the bias tees, the bias tees had very poor high-frequency performance, and the active probes did not show distinct differences in output waveforms when the probes were under different load (such as a 50 Ω and an open circuit). As a result, the active probes had very little directivity and could not be used for network analysis. As a rudimentary fix, the bias tee on the NWA IC was bypassed with a gold ribbon. Having done this, the active probes behaved as expected. However, because the probe tips were long (5 mm) and fabricated on alumina, they had high losses, as discussed in Chapter 3. In addition, the gold ribbon used to bypass the malfunctioning bias tee introduced additional parasitics in the millimeter-wave signal path. Consequently, the active probes showed slow step response (Fig. 5.5). In Fig. 5.5, the output waveform of the active probe under a short circuit is presented. The input signal was a shockwave generated by an NLTL on the NWA IC. The incident signal had a falltime of ≈ 2.8 ps, while the risetime of the reflected edge was degraded to ≈ 7 ps. The 94 picosecond delay between the incident and reflected edges corresponded to the signal round-trip delay between the directional sampling circuit and the DUT. The -3-dB bandwidth of these active probes was then 50 GHz.

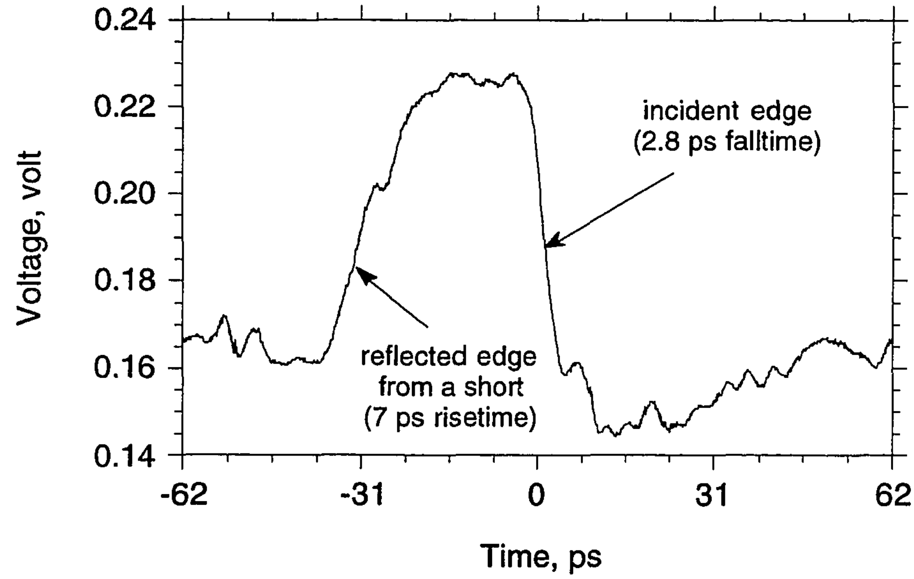

Figure 5.5. Step response of the first generation of active probes.

The SOL calibration technique was first implemented because of its simplicity. The mathematical procedures was coded in C, and an example program is attached in Appendix C. The short standard was implemented with a big metal pad, the open standard was implemented with the active probe in air, and the 50 Ω standard was purchased from Cascade Microtech Inc.

Only 1-port measurements were performed with the first generation of probes. The measured setup was similar to that shown in Fig. 5.3 except that only one channel was present and the IF signal processing electronics were not used. The NLTLs on the active probe were driven with 2 microwave synthesizers at 8 GHz. The IF fundamental frequency was 100 Hz (hence significant phase noise aliasing arose). The active probe output waveforms were averaged 32 times before being digitized by the digitizing oscilloscope to reduce the phase noise. The measurement results are shown in Fig. 5.6. To prove measurement reproducibility, two measurements were made for each DUT with 30 minute time intervals. Fig. 5.6(a) shows the initial measurements of the short, open, 50 Ω calibration standards, and a 23 Ω resistor that had 30 pH associated inductance. Fig. 5.6(b) shows the second measurement. The reproducibility in S11 magnitude was within ± 1 dB to 96 GHz.

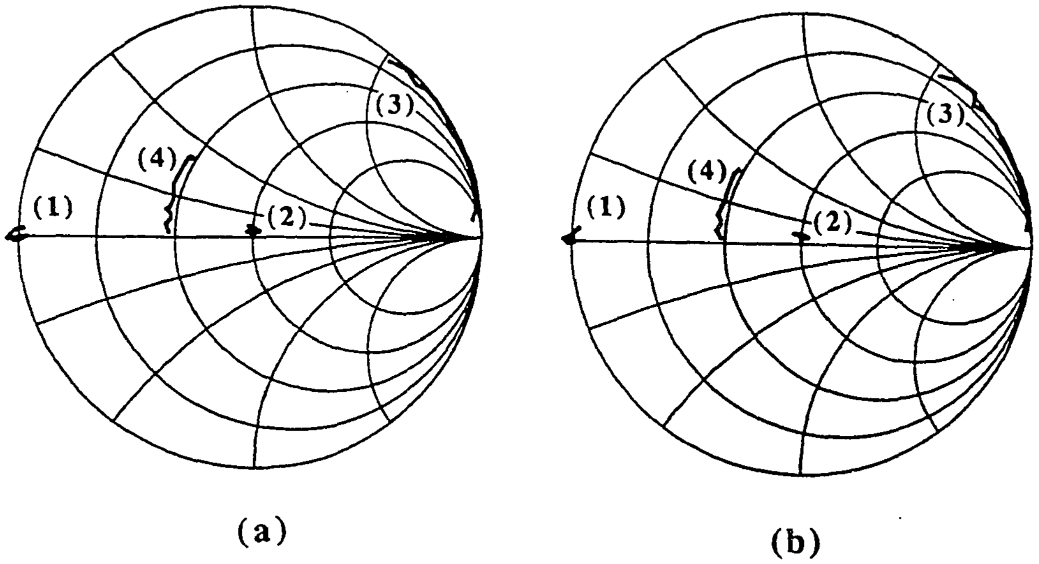

Figure 5.6. S11 measurements of (1) short, (2) load, (3) open, and (4) 23 Ω resistor from 8-96 GHz: (a) initial measurements, and (b) measurements performed 30 minutes later.

5.2.2. Second Generation Results

The first generation active probes suffered from high losses of the long alumina probe tips and from bias tee layout parasitics. To improve the active probe bandwidth, the second generation probe tips were fabricated on quartz and were much shorter (2 mm) than the first generation probe tips. In addition, the bias tee was not implemented in this generation of NWA ICs. The probe body was also re-designed to reduce its size to be comparable to and compatible with commercial microwave probes so that commercial probes could be used, if they were needed, along with the active probes. In measuring the probe step response, an NLTL on the NWA IC was driven with a 10 GHz sinusoidal input and generated a shockwave stimulus signal. The output waveform of the active probe subject to an open circuit is shown in Fig. 5.7. This output waveform, the sum of the incident and reflected signals, had an incident signal falltime of 2.6 ps and a reflected signal falltime of 4 ps. The corresponding -3-dB bandwidth for this probe was then 90 GHz, which included the convolved contributions of the NLTL pulse generator falltime, the capacitance charging time of the two sampling circuits, the probe tip losses, and the inductance of bond wires connecting the probe tip to the NWA IC. In addition to the major reflection edge from the open circuit, two other prominent features can be observed in the waveform. The first is the reflection from the bond wire inductance as indicated in Fig. 5.7. The reflection occurs at about 13 ps from the incident edge, corresponding to the round-trip delay between the directional sampling circuit and the NWA IC to probe tip interface. As discussed in Chapter 3, SPICE simulation can be used to determine the bond wire inductance by applying a similar input shockwave to the directional sampling circuit which incorporates the bond wires and varying the bond wire length to yield an output waveform that matches the measured waveform. An inductance of 60 pH was found by this procedure, corresponding to a CPW bond wire connection bandwidth of 265 GHz. The second feature is the fast falling edge immediately following the inductive reflection. The magnitude of this fast falling edge is about one third of that of the incident edge, indicating a high to low impedance mismatch from the NWA IC to the probe tip. We will come back to this point in the next sub-section.

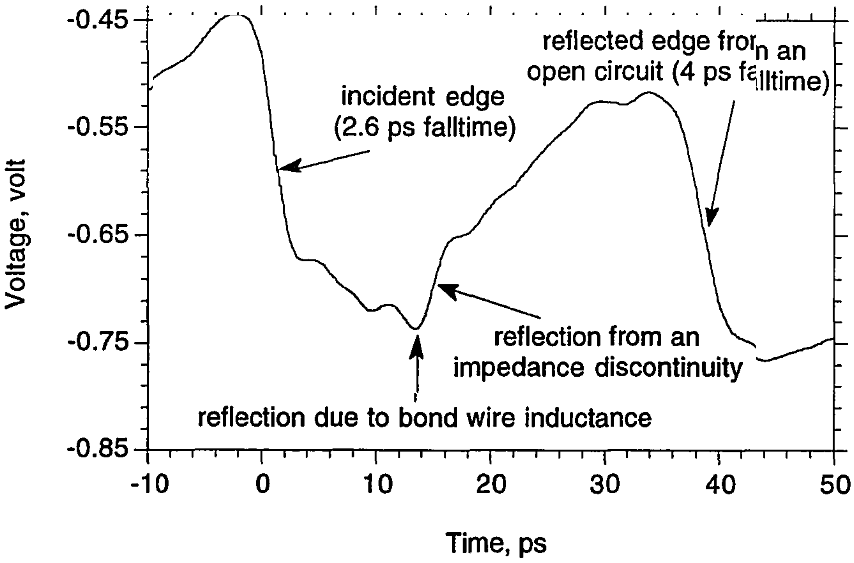

Figure 5.7. Step response of the second generation of active probes.

The measurement setup was similar to that shown in Fig. 5.3 except that no IF signal processing electronics were employed. Both LRL and LRM calibration techniques were implemented for this generation of probes. While LRL transmission line calibration standards were fabricated at UCSB, the LRM calibration standards were purchased from Cascade Microtech Inc. [53]. Both the LRL and LRM calibration mathematical procedures were implemented with C and some example codes are attached in Appendix C.

As discussed in Chapter 4, the measurement accuracy using LRL calibration relies on accuracy in the determination of the transmission line parameters (propagation constant and loss coefficient) of the line standards. To verify the accuracy of the calibration, the system was first calibrated with LRL (three line standards are required to cover the 10-150 GHz frequency range), and the calibration standards were remeasured. Fig. 5.8 shows the transmission measurements of a 1.6 ps transmission line. It can be noted that the line parameters can only be determined accurately to about 100 GHz, beyond which larger errors in magnitude and phase of S21 are observed.

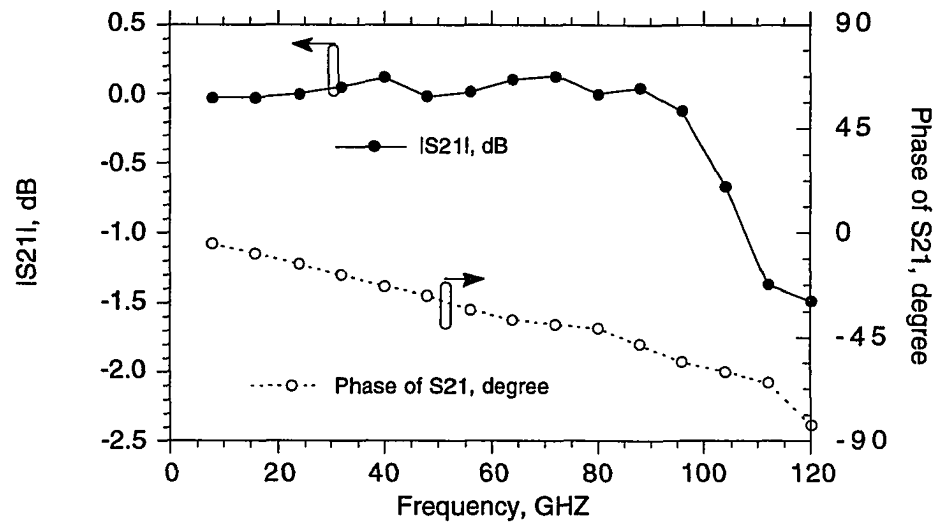

Figure 5.8. 2-port measurements of a 1.6 ps transmission line with LRL calibration.

With LRM calibration, more accurate measurements were obtained. Shown in Fig. 5.9 are the S-parameters of a 25-ps transmission line fabricated on an alumina substrate. The measurement reproducibility of the data was verified by taking 3 different measurements at 30 minute time intervals. Fig. 5.9(a) is a plot of the magnitude of S21 in dB. The data taken at the 3 different times are all plotted on the same graph to show that the deviation is less than ± 0.3 dB. Fig. 5.9(b) shows the phase of S21 for the 3 measurements and a comparison to the expected phase assuming a relative dielectric constant of 9.8 for the alumina substrate. Fig. 5.9(c) shows the magnitude in dB of S11. The return loss is better than 15 dB to 100 GHz. Fig. 5.19 shows the S-parameters of a nominal 50 Ω 6-dB attenuator. Fig. 5.10(a) is a plot of |S21| and Fig. 5.10(b) is plot of |S11|, which show good agreement with measurements taken on a HP 8510 vector network analyzer to 40 GHz. Again, the transmission measurements are reproducible within ± 0.3 dB to 120 GHz and the return loss is better than 15 dB to 100 GHz. For both DUTs, the return loss degrades to about 10 dB at 120 GHz.

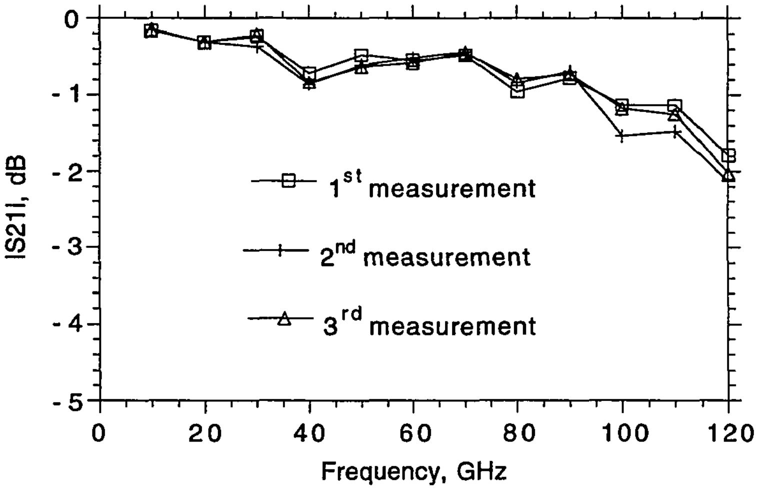

(a)

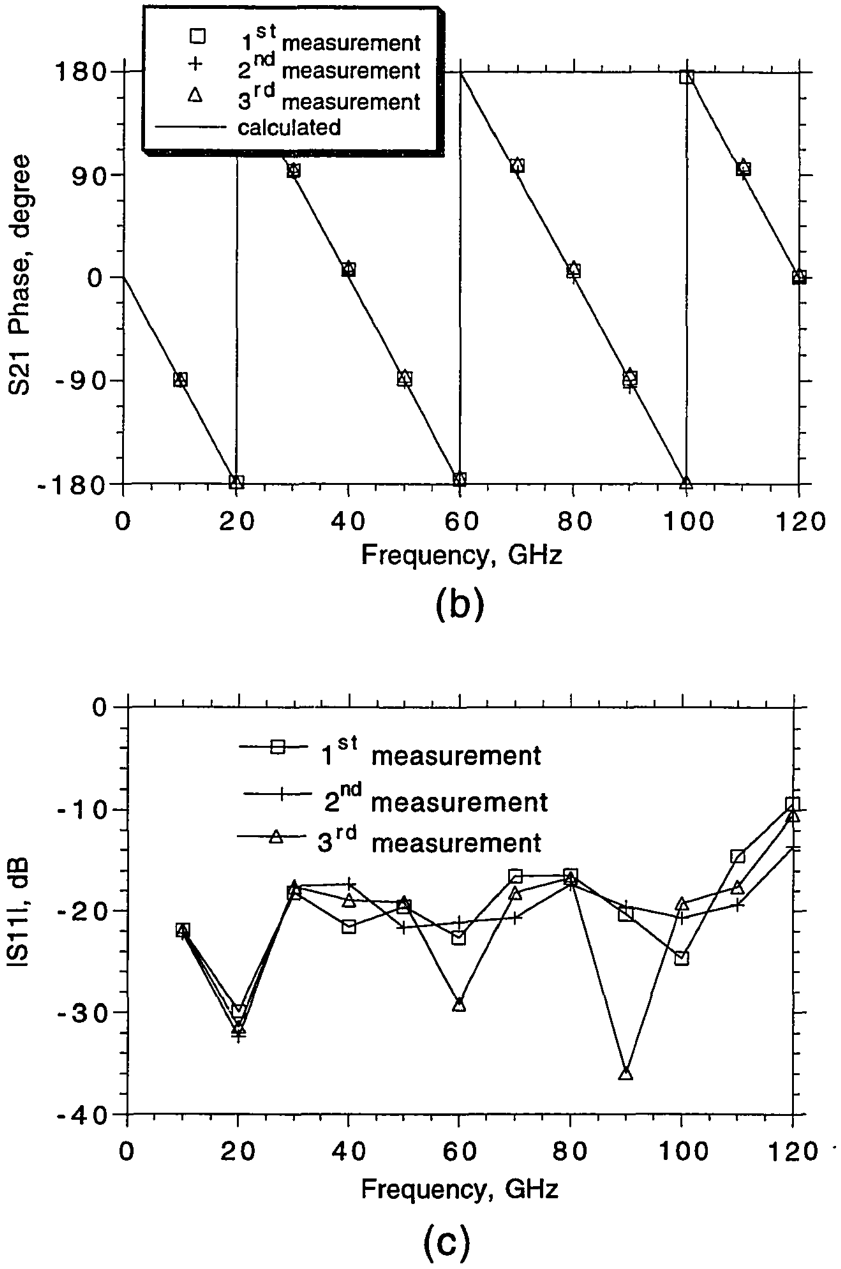

Figure 5.9. 2-port S-parameter measurements (taken at three different times with 30 minute time intervals) of a nominal 50 Ω 25-ps transmission line: (a) dB plot of the magnitude of S21, (b) calculated and measured phase of S21, and (c) dB plot of the magnitude of S11.

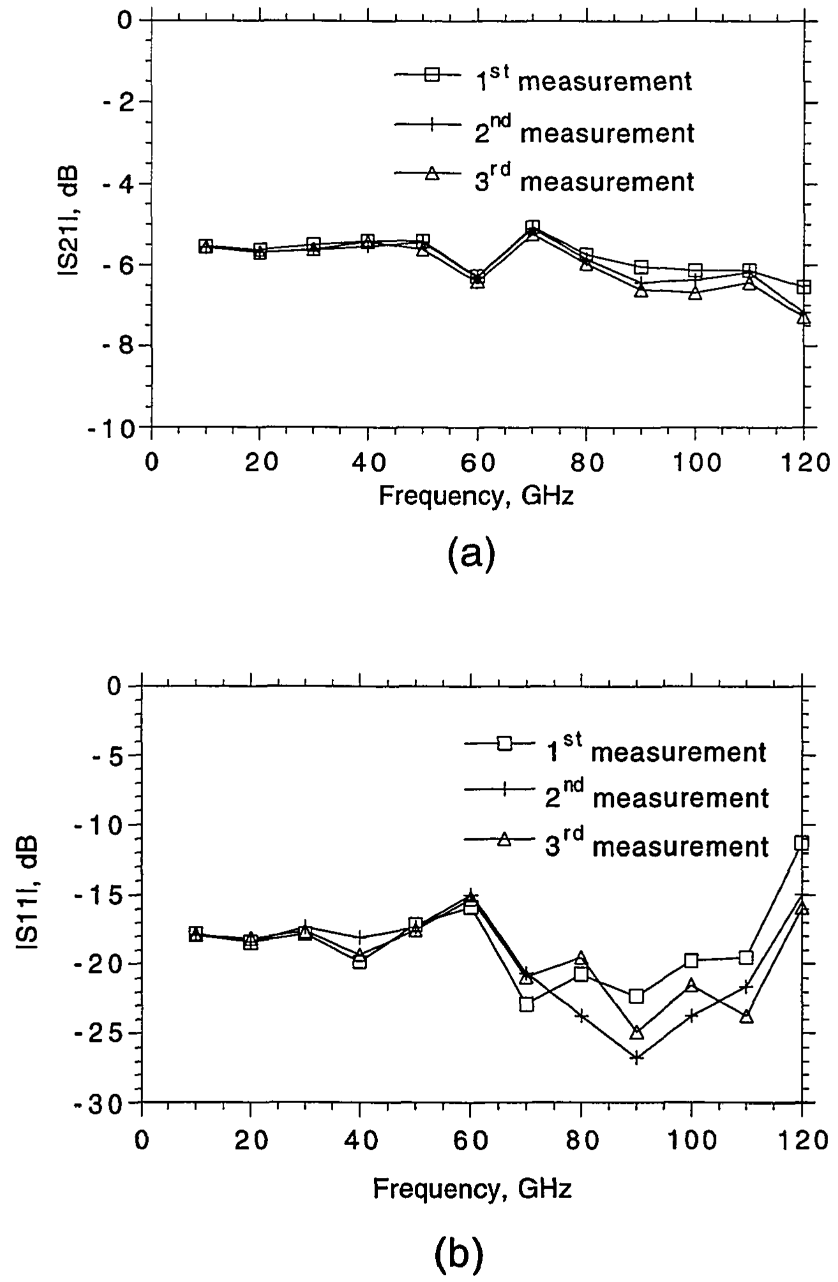

Figure 5.10. 2-port measurements (taken at three times with 30 minute time intervals) of a nominal 6-dB attenuator: (a) dB plot of the magnitude of S21, and (b) dB plot of the magnitude of S11.

5.2.3. Third Generation Results

The return loss measurements of nominally 50 Ω DUTs in the second generation results showed degradation beyond 100 GHz, which could be limited by the measurement system directivity. The broadband reflection observed in the second generation probe step response measurement indicated a significant impedance mismatch between the NWA ICs and the probe tips and further suggested that uncorrected system directivity was degraded due to this impedance mismatch. To investigate this impedance mismatch, a series of HP8510 S-parameter measurements were done on several 50 Ω transmission lines fabricated on the same quartz substrate with the probe tips. These transmission lines were designed to be used in the LRL calibration procedures. These lines had the same dimensions as that of the probe tips, and one set of the lines incorporated air bridges to suppress undesired slot line modes on the CPW lines, and thus resembled the quartz probe tips. Fig. 5.11 shows the magnitude of S11 of two 2400-μm long CPW lines, one with air bridges and one without. It can be noted that the return loss of the line with air bridges is about 20 dB worse than that of the line without air bridges, indicating significant loading by the capacitance between the air bridge and the center conductor of the CPW line. Using Libra, the characteristic impedance, the effective relative dielectric constant, the line inductance and capacitance were extracted from the measured S-parameters. The resulting capacitance per air bridge was ≈ 35 fF. For the second generation probe tips, the air bridge and the CPW center conductor cross-over area was 4000 μm^2. Using a simple parallel-plate capacitance formula and assuming air bridge height of 2 μm, the air bridge capacitance was calculated to be 18 fF. The measured 35 fF capacitance was twice the calculated value, and this was attributed to polyimide trapped underneath the air bridges (the polyimide layer was spun on the quartz substrate as a protective layer for substrate sawing). With the measured 35 fF air bridge capacitance, the measured (and calculated) characteristic impedance became only 30 Ω, resulting in a 25% reflection for a signal coming from a 50 Ω transmission line. This verified the broadband reflection observed from the probe response measurements (Fig. 5.3). In addition to the degradation in system directivity due to dramatic reduction in probe tip impedance, the Bragg frequency (inherent in any periodic structures) was also significantly reduced. The Bragg frequency was calculated to be approximately 180 GHz. Using Libra, a quartz line periodically loaded with 35 fF capacitors were simulated and the resulting S-parameters verified the above Bragg frequency calculation.

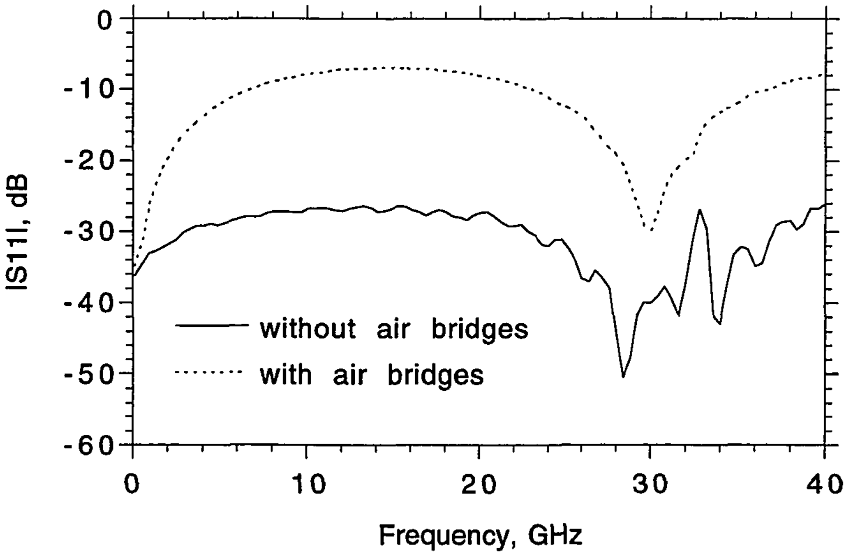

Figure 5.11. Return losses of two 2400-μm long quartz CPW lines: one is periodically loaded with air bridges and one is not loaded.

The third generation probe tips were designed with 5 times smaller air bridges. Libra simulation predicted that a 5 times reduction in air bridge capacitance would improve the CPW line return loss by 10-15 dB and push the Bragg frequency to beyond 300 GHz. Fig. 5.12 shows the return loss of a new 2400-μm air bridge loaded CPW line. Comparing to that in Fig. 5.11, an improvement of > 10 dB can be noted.

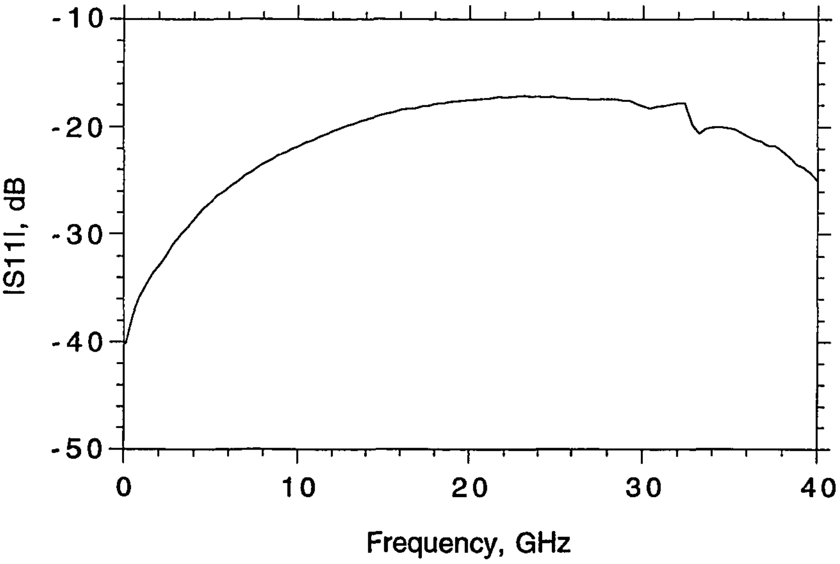

Figure 5.12. Measured return loss of a 2400-μm long quartz CPW line loaded periodically with 5 times smaller air bridges than that shown in Fig. 5.11.

The step response of the third generation probes are shown in Fig. 5.13. Comparing to the step response of the second generation probes, the incident edge falltime is ≈ 2.5 ps; only reflection arising from ribbon bond inductance is observed; the falltime of the reflection from the open circuit is now ≈ 3 ps. The corresponding -3-dB bandwidth of the active probe (for network measurement) is 110 GHz.

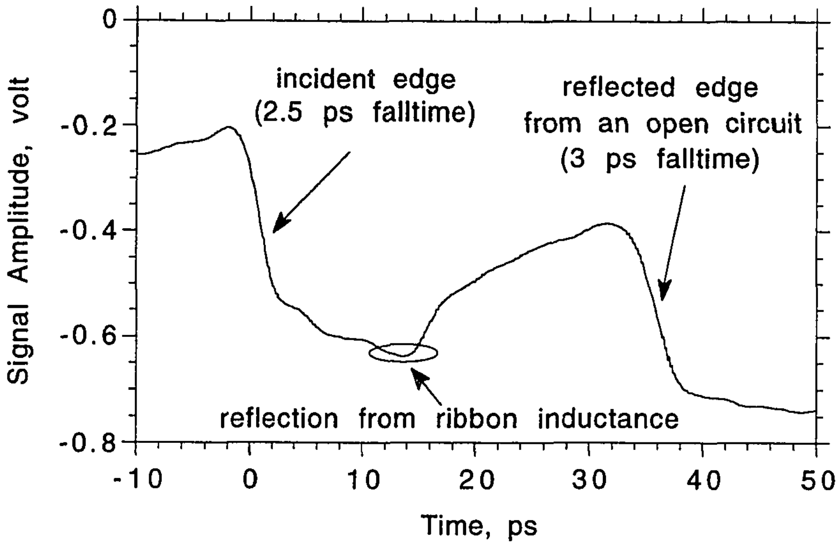

Figure 5.13. Step response of the third generation of the active probes.

The system configuration was as shown in Fig. 5.3, which included the IF signal processing electronics. Because the IF bandwidth was increased to the MHz range, the IF fundamental frequency was at 10 KHz, reducing phase noise aliasing. In addition, the summing circuit produced the approximate incident and reflected waves before being acquired by the digitizing oscilloscope, decreasing the effect of quantization noise on system directivity. Currently, the IF bandwidth is ≈ 1 MHz, the IF fundamental frequency is 10 KHz, and the number of digitizing data points is 512. Consequently, the digitizing oscilloscope's sampling frequency is about 5 times of the IF signal bandwidth, and the Nyquist criterion is satisfied. In this system, the microwave synthesizers which drove the NLTLs on the active probes were controlled via a GPIB interface by a work-station controller, so that the NLTL drive frequencies could be automatically incremented to yield much more frequency data points than in previous experiments.

The calibrated measurements were obtained with the LRL calibration procedure. To verify the performance of the vector network analyzer (VNA), the VNA was calibrated and the 1-ps through line calibration standard was subsequently remeasured. The measured and calculated S-parameters are shown in Fig. 5.14. Two measurements were performed 30 minutes apart with the same calibration. As shown in Fig. 5.14(a), the accuracy and reproducibility in transmission measurement are within ±0.3 dB to 160 GHz, and degrade to ±1 dB around 200 GHz; the phase accuracy, also shown in Fig. 5.14(a), is within 0.1 ps to 200 GHz; the return loss, shown in Fig. 5.14(b), is less than -30 dB to 160 GHz, and becomes -10 dB around 200 GHz. However, when the probes were raised (open circuit termination), the measured S-parameters (not shown) had as much as 1 dB error above 100 GHz. While measurement reproducibility is limited by phase noise, quantization errors, and probe crosstalk, measurement accuracy includes the effect of errors in the calibration standards. S-parameter measurements of the calibration standards themselves give good indications about system reproducibility (hence system phase noise, quantization errors, and probe coupling) regardless the correctness of the models for the calibration standards. Therefore, because less accurate measurements were obtained for an open circuit load than for the 1-ps through line (a pre-defined standard), errors in the calibration standards themselves are currently the dominant source of measurement error.

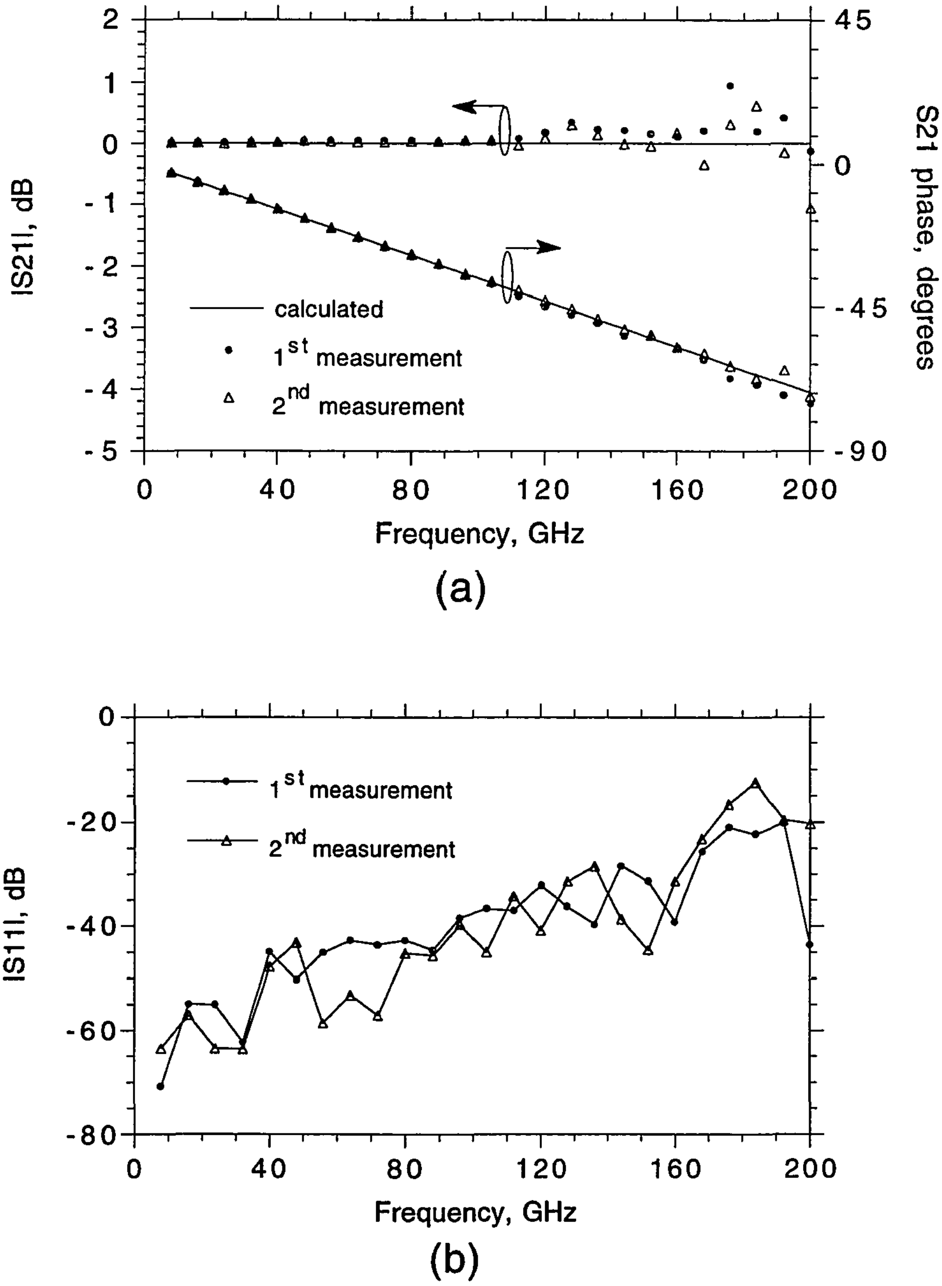

Figure 5.14. 2-port S-parameter measurements (taken at 30 minute time intervals) of a 1-ps through line calibration standard: (a) magnitude and phase of S21, and (b) magnitude of S11.

Several other passive devices were also measured with this VNA. Shown in Fig. 5.15 is the measured S11 magnitude of a 50 Ω load used in the LRL calibration. According to an application note from Cascade Microtek Inc., a 7.5 pH series inductance should be added to the model for this 50 Ω match load, and the calculated S11 magnitude thus obtained shows good agreement with the measured data. Shown in Fig. 5.16 are the measured S11 and S21 magnitudes of a 40 ps transmission line. The microwave synthesizer frequencies were automatically incremented via a GPIB interface, and the resulting measurements had much more data points than previous measurements. However, there are spikes in these measurements arising from inadequate drive power for the stimulus NLTLs at the corresponding fundamental frequencies.

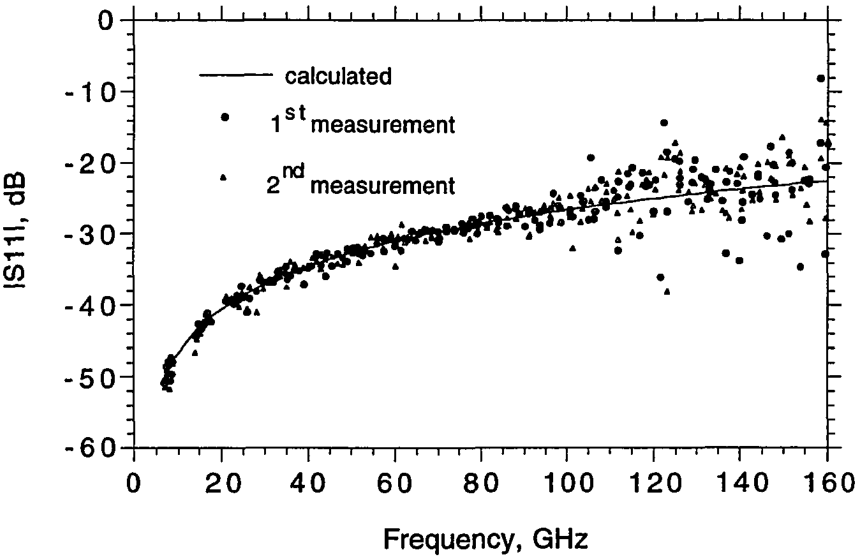

Figure 5.15. Measured and calculated S11 magnitude of a 50 Ω load in series with a 7.5 pH inductor (two measurements were taking 30 minutes apart).

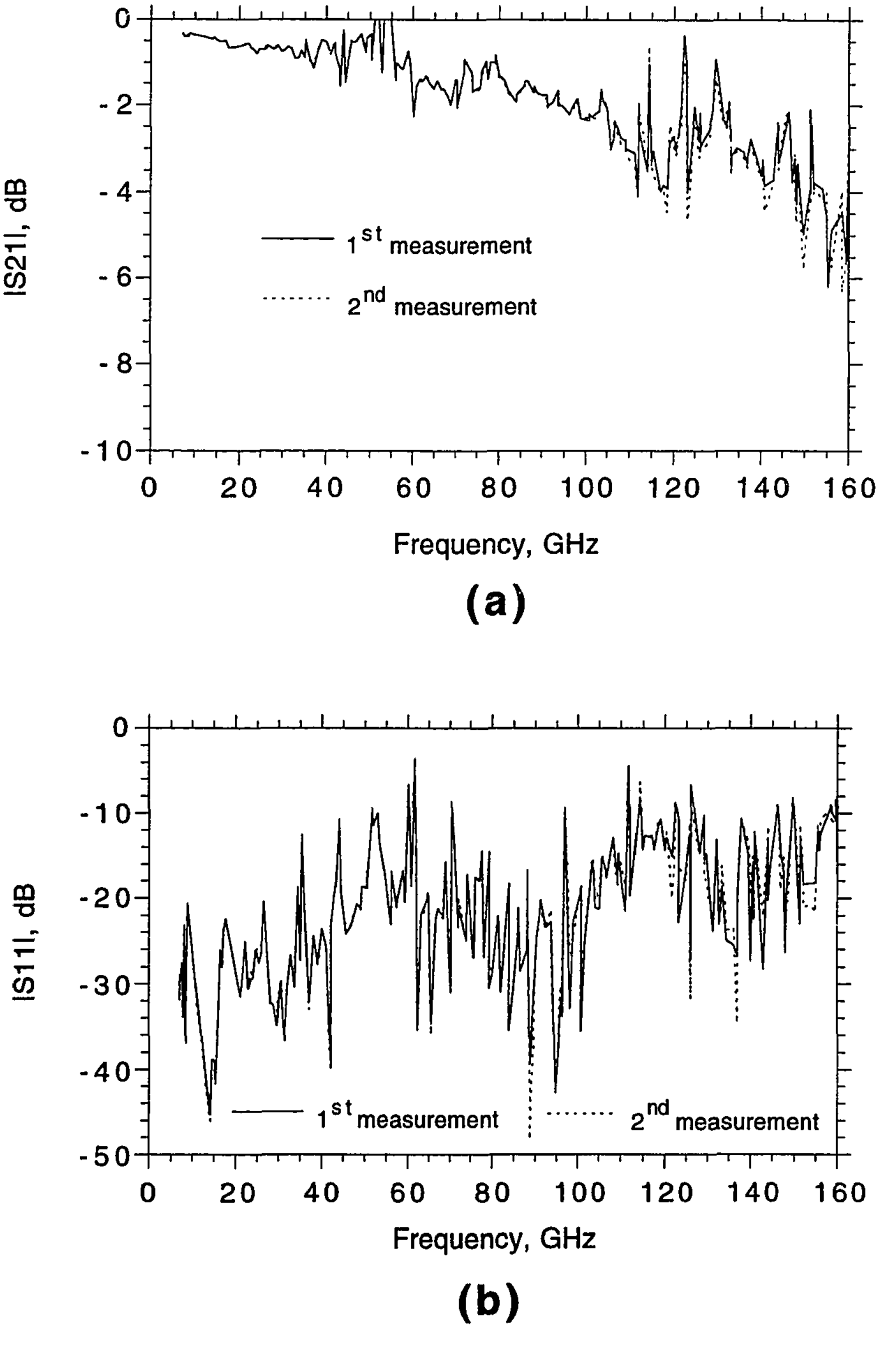

Figure 5.16. S-parameter measurements (taken at 30 minute time intervals) of a 40-ps 50 Ω transmission line: (a) magnitude of S21, and (b) magnitude of S11.

With this VNA, we measured 3 MMICs fabricated with a 0.16 µm pseudomorphic MODFET technology. The S-parameters were obtained with NLTL drive frequencies varied from 7 to 8 GHz in 0.2 GHz steps. The first MMIC was a 3-stage reactively-matched low noise amplifier (LNA) [54]. This MMIC was measured with the second generation active probes before fabrication of the third generation active probes. Fig. 5.17 shows the S-parameters measured with the LNA biased at a drain voltage of 4.2 V and a drain current of 75 mA. The LNA had 27 dB gain at 67 GHz and 20 dB gain at 76-77 GHz, the frequency band of interest. The input and output return losses at 77 GHz were better than -14 and -16 dB, respectively. The reverse isolation (not shown) was greater than 28 dB over the full 20-100 GHz band. S-parameter measurements of the LNA under identical bias conditions were also performed on a similar LNA chip with a commercial coaxial 50 GHz network analyzer extended to 78 GHz by a waveguide test set [55].

The other two MMICs were measured with the third generation active probes. The second MMIC was a 5-stage traveling-wave amplifier (TWA) [56]. Fig. 5.18 shows the gain and return losses of the TWA measured both by the active probes and by the commercial network analyzer. The gain of the TWA was typically 8 dB over the full 7-80 GHz band, and dropped off rapidly beyond 80 GHz; the input and output matching was better than -5 dB over the full 7-80 GHz. The third MMIC was a medium power amplifier (MPA) that was designed to provide gain from 60-80 GHz. Fig. 5.19 shows the gain and return losses of the MPA measured by the active probes and by the commercial network analyzer. The MPA had more than 8 dB gain in the 60-80 GHz band, and, as measured by the active probes, the gain was greater than 5 dB to 90 GHz; the return losses were better than -8 dB in the 65-85 GHz band.

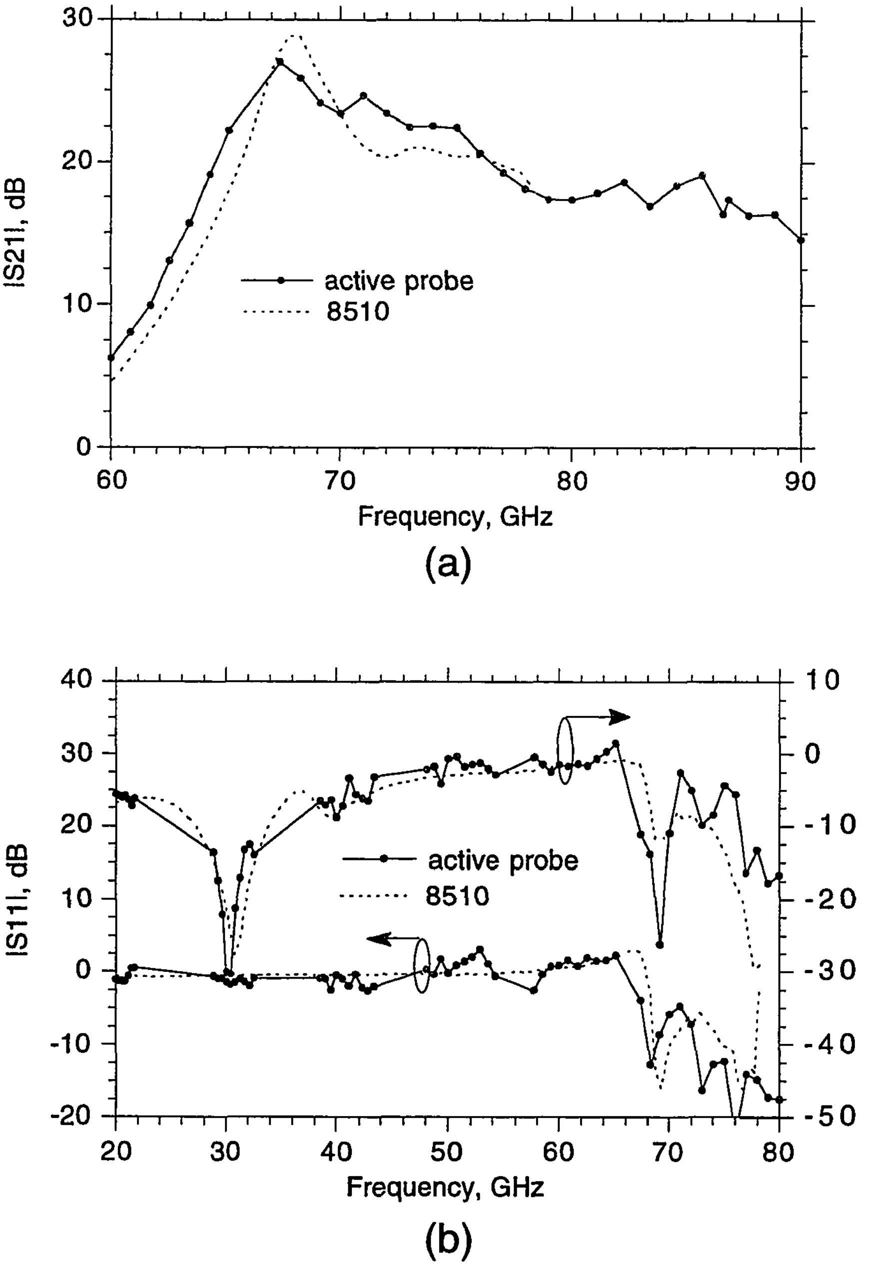

Figure 5.17. S-parameter measurements of a 3-stage low noise amplifier: (a) gain, and (b) return losses.

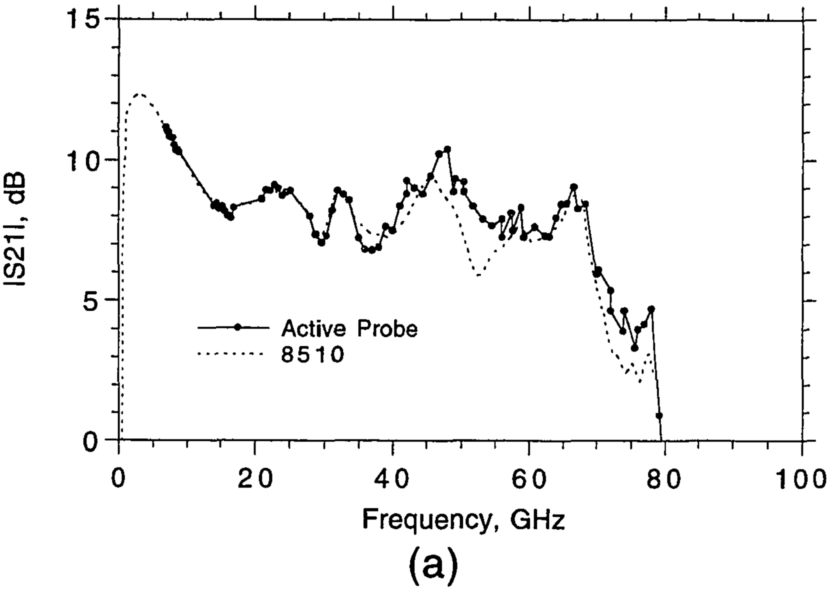

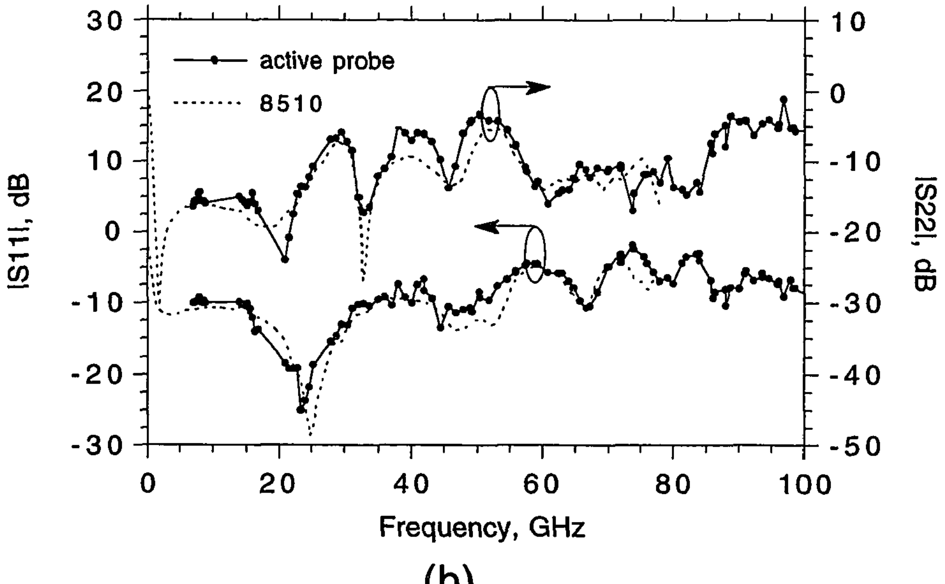

Figure 5.18. S-parameter measurements of a 5-stage traveling-wave amplifier: (a) gain, and (b) return losses.

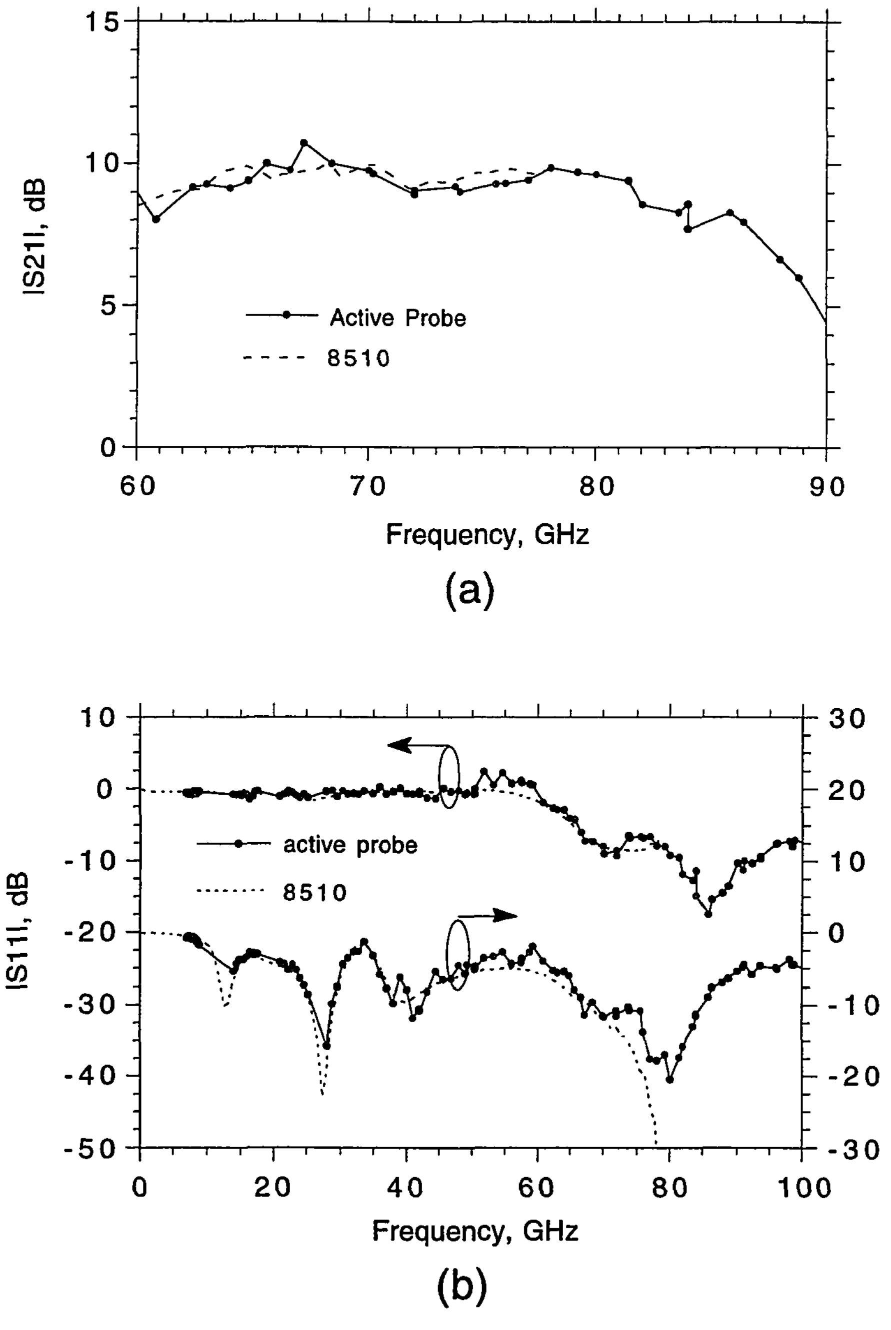

Figure 5.19. S-parameter measurements of a medium power amplifier: (a) gain, and (b) return losses.

As is apparent from these MMIC S-parameter measurements, good agreement between those measured by the active probes and by the commercial network analyzer was obtained in the 7-80 GHz band. It can also be noted that agreement between measurements with the two different measurement systems is better for the third generation active probes than for the second generation ones due to improvement in probe performance. Discrepancies between these measurements could be attributed to several reasons. First, the MMIC bias conditions with the commercial network analyzer were slightly different from those with the active probes because circuit oscillation occurred when the MMICs were subject to the same bias conditions as those with the active probes. Second, not the same circuits on the wafer were measured with these two measurement systems, and circuit-circuit variations across the wafer contribute to the measurement discrepancies. Beyond 80 GHz, the MMIC could only be measured by the active probes. For these measurements, 128 averages were used. Thanks to the much higher IF frequencies, the digitizing oscilloscope averaged quite fast. It took approximately 1 hour to do the calibration and measure one DUT with 10 increments of NLTL drive frequencies.

5.3. Network Measurements With Alternative System Configurations

As discussed in Chapter 4, one major limitation on the network measurement system directivity and dynamic range arises from the quantization noise of the digitizing oscilloscope. To improve the digitizing resolution of the system, one alternative system configuration used four lock-in amplifiers, in place of the digitizing oscilloscope, to measure the four IF signals. With the lock-in amplifiers, each harmonic signal in the IF time waveform was measured with the full resolution of the A/D converters in the lock-in amplifiers (currently 13 bits), resulting in significant improvement in signal/quantization noise ratio, especially at higher frequencies. Fig. 5.20 shows the system setup with the lock-in amplifiers. The RF portion of the setup was identical to that using the digitizing oscilloscope (Fig. 5.3). In measuring the IF signals, the lock-in amplifiers autoscaled their measurement range for each harmonic in the IF signals to allow full resolution for that harmonic. The IF fundamental frequency was 1 KHz. A low-frequency synthesizer provided the reference signal for the lock-in amplifiers. Signal phase drift arising from the frequency synthesizers were minimized by subtracting the phase angles of the incident signal to those of the other three IF signals. The system noise (phase noise, etc.) on each harmonic of the IF signals was reduced

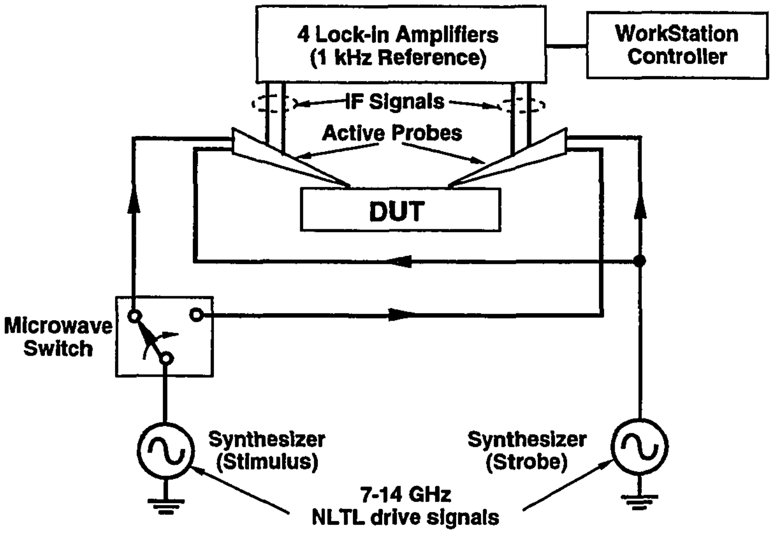

Figure. 5.20. Schematics of an alternative 2-port measurement set-up using lock-in amplifiers to measure the IF signals.

with the use of moderately long time constants in the lock-in amplifiers. Currently, a time constant of 1 second is used for detection of harmonics less than 100 GHz and 3 seconds for harmonics greater than 100 GHz. The trade-off is narrower filter and longer data acquisition time.

To verify the performance of the current system configuration, a 1-ps through line was measured. These measurements were obtained with the second generation of probes. The resulting S-parameters are shown in Fig. 5.21. Two measurements were performed 30 minutes apart with the same calibration. As shown in Fig. 5.21(a), the accuracy and reproducibility in transmission measurement are within ± 0.2 dB to 120 GHz, and degrade to ± 1 dB around 160 GHz; the phase accuracy, shown in Fig. 5.21(b), is typically within 0.2 ps to 160 GHz; the return loss, shown in Fig. 5.21(c), is less than -15 dB to 130 GHz, and becomes -5 dB around 160 GHz, limited by the poor uncorrected directivity of the active probes. Fig. 5.22 shows the S-parameter measurements of a 25-ps transmission line. Similar system performance can be noted from these measurements. Beyond 160 GHz, the system performance degrades drastically due to the low Bragg frequency of this generation of probe tips.

Comparing to the second generation measurement results with the digitizing oscilloscope, this system configuration yields more accurate and reproducible (hence higher bandwidth) measurements. One major drawback of this system is the long data acquisition time. For the system to acquire 25 harmonic data points and with a time constant of 1 second, for example, it takes 2 hours to perform the calibration and measure one DUT.

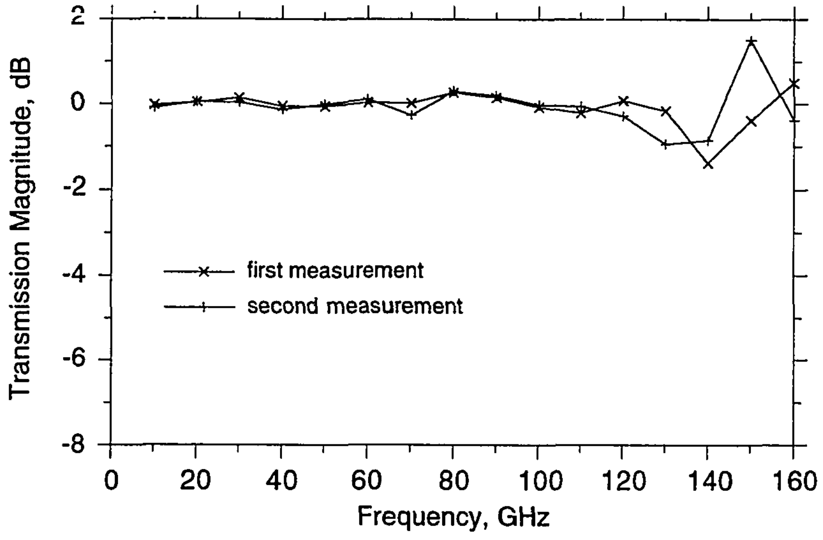
Transmission Magnitude, dB
2
0
-2
-4
-6
-8
0
20
40
60
80
100
120
140
160
Frequency, GHz
first measurement
second measurement

(a)

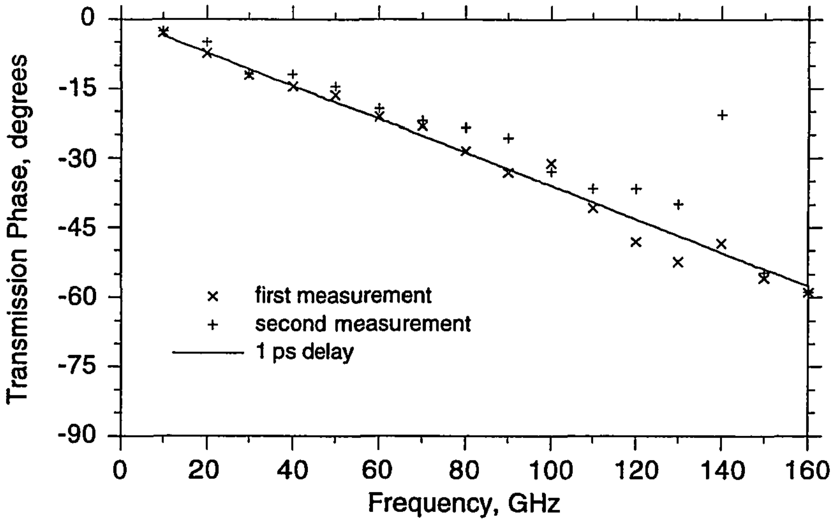
Transmission Phase, degrees
0
-15
-30
-45
-60
-75
-90
0
20
40
60
80
100
120
140
160
Frequency, GHz
× first measurement
+ second measurement
1 ps delay

(b)

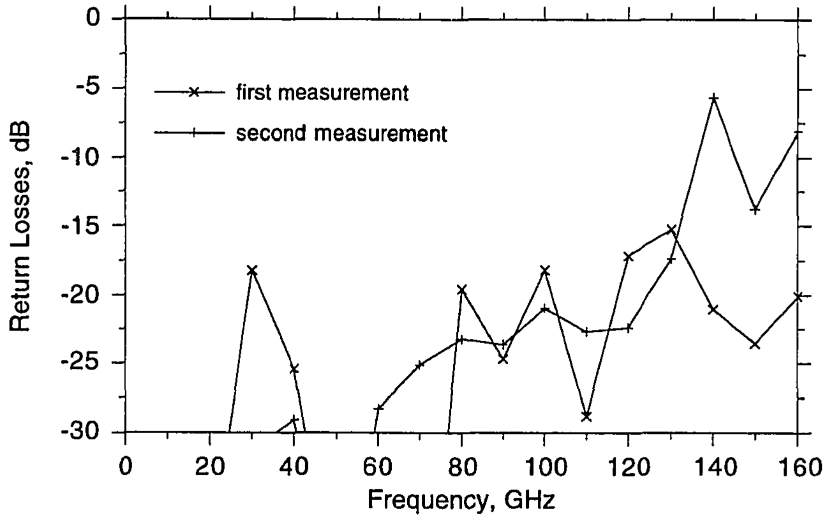

(c)

Figure. 5.21. 2-port measurements of a 1-ps through line (two measurements taken 30 minutes apart): (a) dB plot of the transmission magnitude, (b) calculated and measured transmission phase, and (c) dB plot of the return loss magnitude.

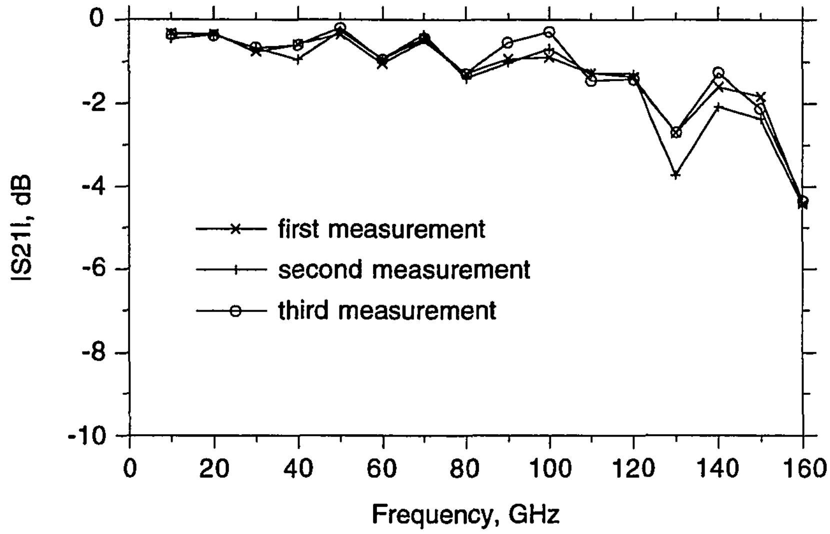

(a)

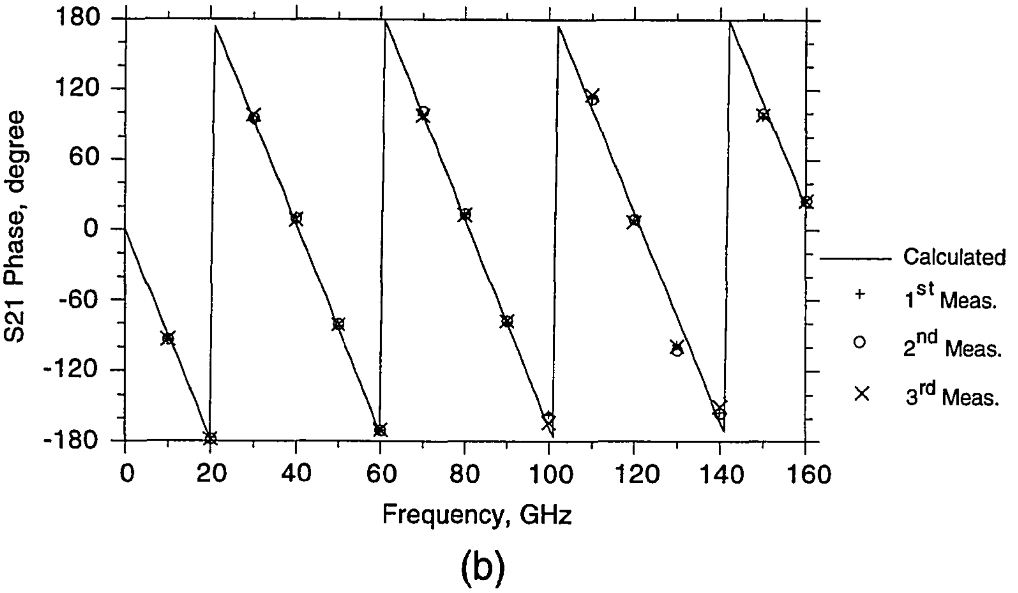

Figure 5.22. 2-port measurements of a 25-ps transmission line (three measurements taken with 30 minute time intervals): (a) dB plot of the transmission magnitude, and (b) calculated and measured transmission phase.

To eliminate the phase noise arising from the use of two microwave synthesizers, a second alternative system configuration shown in Fig. 5.23 was experimented with. In this measurement setup, only a single microwave synthesizer is used. A phase shifter (a computer-controlled mechanical delay) shifts the relative phase between the drive signals for the stimulus NLTL and the strobe NLTL on the active probes to trace out the whole period of the signal waveforms. A PIN modulator modulates the drive signal at 10 KHz and the signal voltages for each phase shift (delay time) can be synchronously detected with the lock-in amplifiers (also with a 10 KHz reference signal). If the phase shifter has no or very little timing jitter and drift, the phase noise can essentially be eliminated. Unfortunately, the current mechanical phase shifter has significant timing errors. Waveforms measured with subsequent scans do not reproduce well, and waveforms for the same scan are not periodic. We conclude that it is difficult for systems incorporating mechanical phase shifters to produce accurate and reproducible network measurements due to the lack of commercial high precision phase shifters (which require precise travel distance and well-controlled effective dielectric constant).

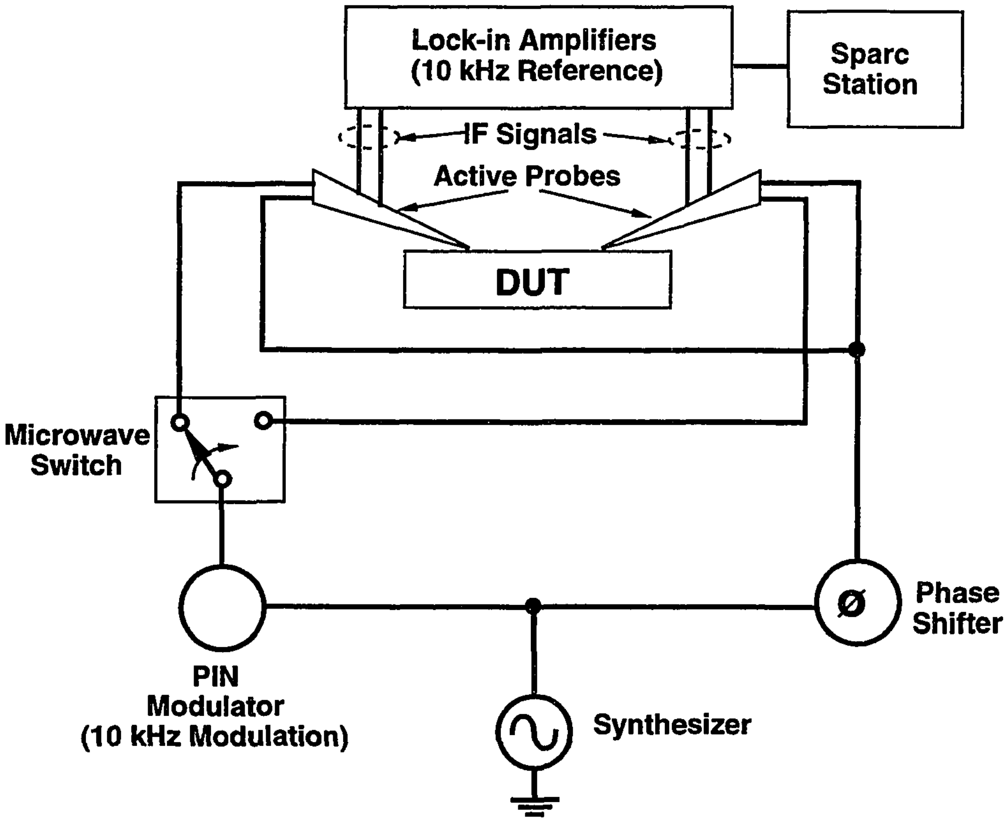

Figure 5.23. Schematics of a second alternative network measurement setup using a single microwave synthesizer and a mechanical delay.

Chapter 6

Summary and Future Directions

Nonlinear transmission line pulse generators are capable of generating large amplitude electrical transients with very fast transitions. As one of the application of the NLTL technology, the work presented in this dissertation deals with the design and fabrication of very high speed sampling circuits and active probes for millimeter-wave on wafer waveform and network measurements. With NLTLs as the strobe signal generators, 275 GHz GaAs sampling circuits were fabricated using a simple 3-mask process steps with 3-µm design rules. These sampling circuits showed clean step response due to relatively clean circuit layout. The NLTL output waveforms showed transition times of ≈ 2 ps, hence containing significant harmonic power to 200 GHz. Using a second NLTL as the stimulus signal source and incorporating a 6-dB attenuator as the directional device, integrated circuits for network analysis were fabricated. These NWA ICs showed 2.3 ps step response time, corresponding to 150 GHz -3-dB bandwidth. Mounting the NWA ICs on wafer probes directly adjacent to low-loss CPW probe tips, signal delivery to and detection from DUTs were made possible at millimeter-wave frequencies.

Three generations of active probes were fabricated. The first generation active probes had NWA ICs incorporating bias tees and 5 mm long alumina probe tips. These probes suffered from high probe tip losses due to high dielectric constant of the alumina substrates (= 9.8) and from layout parasitics of the bias tees. The resulting -3-dB bandwidth of these probes were only ≈ 55 GHz. The second generation active probes had 2 mm long quartz (= 3.8) probe tips, hence much lower probe tip losses. However, due to significant capacitive loading from the air bridges connecting the CPW ground planes, the probe tip impedance was only ≈ 30 Ω and significantly degrade the active probe directivity. The third generation active probes had probe tips with much smaller air bridges, hence smaller capacitive loading. The -3-dB bandwidths of these probes were > 110 GHz, more than twice the bandwidths of the first generation active probes.

While waveform measurement time resolution (smallest measurable transition time) is mainly limited by the active probe -3-dB bandwidth, network measurement accuracy and reproducibility are limited collectively by various sources of noise in the system, errors in the models of the calibration standards, and the active probe bandwidth. With the basic network measurement system configuration (Fig. 5.3) where two microwave synthesizers were used to drive the NLTLs on the active probes and a 8-bit digitizing oscilloscope was used to acquire the IF waveforms, five major sources of system noise (or errors) were identified. The first one was the phase noise arising from the timing jitter between the two microwave synthesizers. The phase noise was reduced with higher IF signal frequencies (harmonics of 10 KHz), which was made possible with buffer circuits to increase the IF signal bandwidth. The second source of noise came from the 8-bit sampling oscilloscope. For a sawtooth waveform, the signal/quantization noise ratio was found to be ≈ 20 dB at 200 GHz. The third source of noise was the sampling circuit noise. The sampling circuit noise figure was measured to be ≈ 65 dB and was of minor importance comparing to other sources of noise. The fourth source of noise arisen from crosstalk between active probes. About

-40 dB probe coupling was observed when the probes were brought with 200-µm of each other. Finally, errors in models of the calibration standards limit the measurement accuracy. SOL, LRL, and LRM calibration methods were implemented. LRM calibration resulted in the most accurate measurements. However, the 50 Ω match load standard was not verified above 75 GHz and can contribute significant measurement errors beyond 75 GHz.

Both waveform and network measurements were presented. For waveform measurements, waveforms with transition times in the order of 2-3 ps were measured. The evolution of the network measurements were described by three generations of results, which corresponded to the three generations of active probes. The first generation results were 1-port measurements to 96 GHz with SOL calibration. The measurement accuracy and reproducibility were ± 1dB. The second generation results were 2-port measurements to 120 GHz using LRM calibrations. LRL calibration was also implemented but had less satisfactory results. The third generation system performance was demonstrated with 2-port measurements of a 1-ps through line to 200 GHz. Much better measurement accuracy and reproducibility as well as system directivity were obtained comparing to those of the previous systems. With this system, three MMICs which operate from DC-100 GHz are characterized. The S-parameters showed good agreement with those measured by a commercial network analyzer from 7-78 GHz. Although very reproducible and accurate measurements on calibration standards (i.e. the 1-ps through line) were obtained to 200 GHz, measurements of other DUTs (such as an open circuit) showed larger errors above 100 GHz. Currently, the most dominant measurement errors can be attributed to the errors in the models of the calibration standards, and the second most important source of errors arises from quantization noise.

Alternative network measurement configurations, which addressed or attempted to address some of the limitations of the basic system configuration (Fig. 5.3), were explored. The first alternative system configuration used lock-in amplifiers, in place of the digitizing oscilloscope, to measure each harmonic signal separately with a full 13-bit resolution. This significantly improved the signal to quantization noise ratio. The resulting S-parameter measurements showed moderate improvement over those with the basic system configuration. One major drawback of this system configuration was the exceedingly long data acquisition time. A second alternative system configuration used a single microwave synthesizer to provide the NLTL drive signals and used a mechanical delay to shift the RF signal so that the entire period of the signal waveforms could be traced out. This attempted to address the system phase noise problem of the system with two microwave synthesizers but was a total failure due to poor timing precision of the commercially available mechanical delay lines.

The measurement accuracy is currently limited by the errors in the models of the calibration standards. Fig. 6.1(a) shows the 1-ps transmission line and the 50 Ω match load on a commercial calibration standard substrate. In the LRM calibration, the 1 ps CPW through line is defined as a lossless, dispersionless transmission line, which is still a good approximation to 200 GHz. For higher frequencies, the non-ideality must be incorporated into the model for the 1 ps through line. The 50 Ω standard is modeled as a perfect 50 Ω in series with a variable inductor whose inductance depends on the amount of probe-standard overlap [51]. This model is not verified beyond 75 GHz. Use of offset calibration standards and offset DUTs (Fig. 6.1(b)) results in similar probe to calibration standard/DUT launching characteristics and can improve calibration standard (hence measurement) accuracy [57].

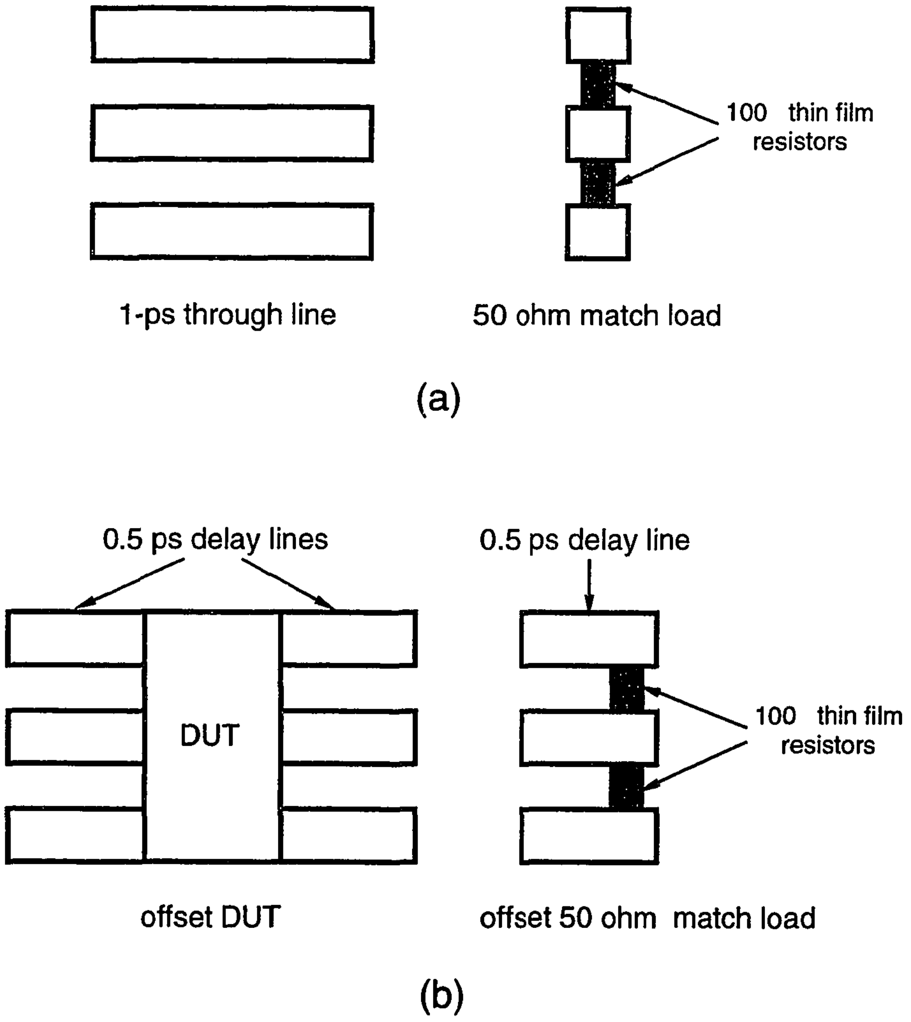

Figure 6.1. Schematic diagrams of (a) the 1-ps through line and the 50 Ω match load on a commercial calibration standard substrate, and (b) the offset DUT and the offset 50 Ω match load.

Other sources of system noise can be dealt with using better data acquisition instruments. The system phase noise can be further reduced with low phase noise synthesizers. The quantization noise can be reduced with high resolution digitizing oscilloscopes or A/D converters. The probe crosstalk can be reduced with a better shielded and grounded probe body design to minimize electromagnetic interference effects.

The waveform and network measurement bandwidth is ultimately limited by the active probe bandwidth as the mm-wave signals are attenuated beyond the -3 dB bandwidth of the active probe. The bandwidth limits of the active probes arise from the NWA ICs, the probe tips, and the interconnection between the ICs and the tips. The current NWA ICs use 275 GHz-bandwidth sampling circuits and 1.8 ps NLTLs. 725 GHz bandwidth sampling circuits and 0.48 ps NLTLs have been fabricated [27] and sampling circuits and NLTL with still higher bandwidth are currently being pursued by Scott Allen; using these, the NWA IC bandwidth can be extended to at least 400 GHz. The bandwidth of the active probes would then be limited by the probe tips and the interconnection bandwidth, currently 260 GHz. Probe tip losses and bond inductances can be reduced through use of beam lead technology to mount NWA ICs close to probe tip contact points (Fig. 6.2), thereby minimizing both the CPW probe tip length and eliminating bond wire inductance.

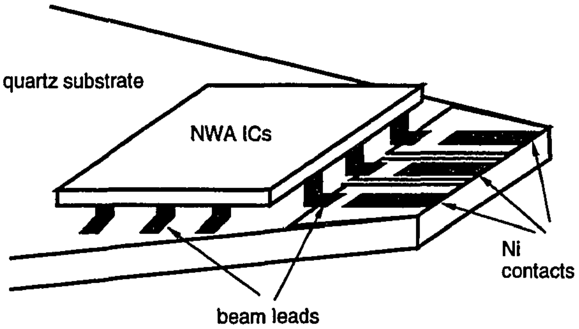

Figure 6.2. Schematic diagram of an active probe fabricated with beam lead technology.

The beam leads can be fabricated with a similar process as that for fabrication of air bridges and can be incorporated into the normal 6-mask process for the NWA ICs. After all 6-mask steps, the wafer is first thinned down to ≈ 4 mils (100 μm). A photolithographic step is then used, on the backside of the wafer, to define the etch lines for individual chips. These chips can then be separated from each other by a chemical etch. The NWA ICs now have beam leads around their peripheries and can be mounted up-side-down onto the quartz probe tips (Fig. 6.2). Because the ICs are thin, they can be mounted very close to the tip contact area without touching the DUT when the probe is in contact with the DUT. The most critical issue in beam lead fabrication is their adhesion on the ICs. It was found that bead leads adhere much better on ohmic contact pads [58].

The bias tees currently suffer from layout parasitics arising from the long isolation resistor. The bias tees were measured with the active probes. While the transmission characteristics ($|S21|$ and $|S12|$) were relatively flat (from -3.5 dB at 8 GHz gradually down to -6 dB at 160 GHz), the return losses ($|S11|$ and $|S22|$) degraded from ≈ -20 dB at 8 GHz to ≈ -5 dB beyond 130 GHz. This would severely limit the directivity of the active probes at high frequencies. One way to solve this problem is to implement the isolation resistor with a thin film which has higher sheet resistivity than the N^+ layer sheet resistance of the current GaAs wafer. One common choice is Tantalum nitride. Although this introduces one more process step, much cleaner bias tee layout can be obtained, hence reducing layout parasitics.

However, comparing to the conventional frequency-domain network analysis, the time-domain method has several inherent disadvantages. First, intermodulation effects limit measurement accuracy and dynamic range. In conventional frequency-domain network measurements, a sinusoidal stimulus signal (Fig. 6.3(a)) is applied to the DUT, and the response signal of the DUT at the same frequency (f_0) is measured. Due to nonlinearities in the DUT, some harmonic power will be generated, in response to the single frequency stimulus signal, at the Fourier harmonics of f_0 (Fig 6.3(b)). Because a commercial network analyzer only measures the DUT response at f_0, the spurious harmonic signals do not affect the measurement accuracy and dynamic range. On the contrary, for the network measurement system using active probes, the stimulus signal is a time-domain sawtooth waveform which contains harmonic power at multiple Fourier harmonics of the NLTL drive frequency f_0 (Fig. 6.3(c)). Due to nonlinearities in the DUT, spurious signals are generated at harmonics and sub-harmonics of f_0 (arising from intermodulation products of the stimulus harmonic signals) and superimposed on the desired DUT response signals (Fig. 6.3(d)). Because the magnitude and phase of these spurious signals depend on the particular DUT, they cannot be eliminated (or corrected) by the calibration procedure. Moreover, this problem is compounded by the fact that DUT nonlinearities depend on the amplitude of the applied stimulus signals which cannot be readily controlled in the active probe measurement system.

Second, the signal to quantization noise ratio is inherently poorer in the active probe system than the frequency-domain network analyzers for a given quantizer (digitizing oscilloscope). In the conventional frequency-domain network analyzer, the stimulus signal to and the response signal from the DUT at each frequency are digitized with the full digitizer resolution. On the other hand, in the active probe system, the sawtooth stimulus signal contains a series of Fourier harmonic signals whose power

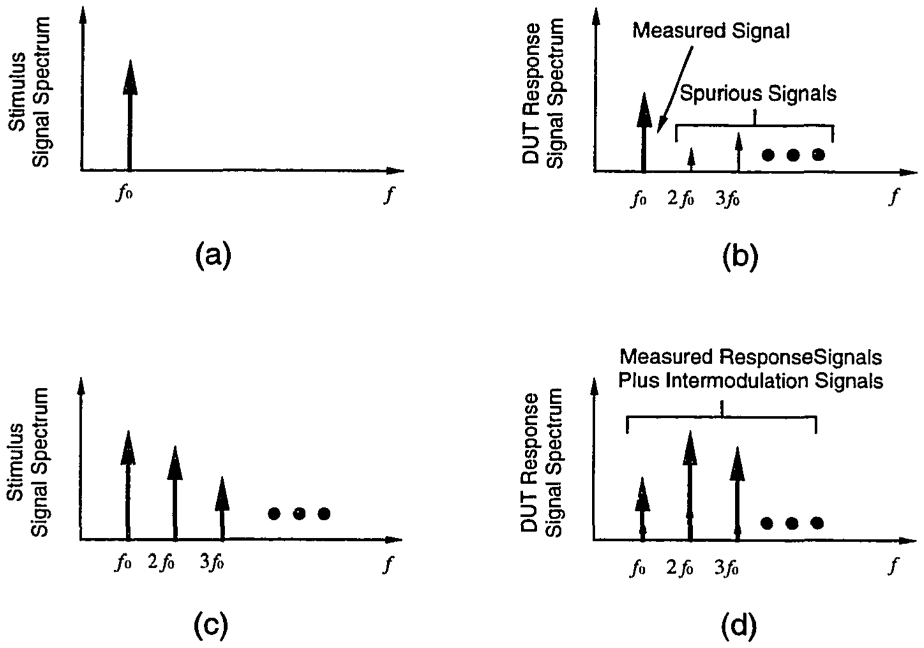

Figure 6.3. Comparision of stimulus and measured signal spectrums of the frequency-domain ((a) and (b)) and time-domain network analyzers ((c) and (d)): (a) & (c) stimulus signal spectrum, and (b) & (d) measured DUT response and spurious signal spectrum.

varies as $1/n^2$ (where n is the Fourier harmonic number). As discussed in chapter 4, assuming the quantization noise is uncorrelated from sample to sample and uniformly distributed in the quantization interval, the quantization noise is white, hence the signal to quantization noise ratio decreases as frequency increases. Alternatively, this can be viewed as higher frequency signals being digitized with smaller resolution. It should be emphasized that although a pulsed stimulus signal has relatively constant harmonic signal amplitudes (hence these signals are quantized with approximately the same resolution), the quantization resolution is smaller than the full resolution of the quantizer, because the peak amplitude of the pulse train is much larger than that of its harmonic components.

Third, the stimulus signal amplitudes cannot be controlled readily in the active probe measurement system, which further deteriorates the intermodulation problem and limit system dynamic range. Currently, a 25 dB attenuator and a 6-dB attenuator (the directional device in the NWA IC) attenuate the ≈ 5 volt NLTL output signal to 140 mV for the DUT. Because the signal amplitudes decrease as $1/n$ for a sawtooth waveform, there is a variation of 26 dB in signal amplitudes over 20 harmonics in the stimulus signal. Consequently, in S-parameter measurements of a high-gain, small signal amplifier, the large stimulus signal amplitudes at lower frequencies may cause saturation of the DUT which introduces transmission measurement error due to DUT nonlinearities (hence intermodulation effects), while the small stimulus signal amplitudes at higher frequencies may result in inaccurate return loss measurements of the same DUT because the reflected signal from a well-matched DUT may be comparable to or smaller than the system noise levels. In addition, the large variation in the stimulus signal amplitudes over frequency places an additional limit on the system dynamic range and measurement accuracy because of saturation of the measurement system itself (the directional sampling circuits on the NWA ICs) for large stimulus signals and because of small DUT response signals garbled up by system noise for small stimulus signals. A pulsed signal has a relatively constant signal spectrum and its use as the stimulus signal should alleviate this problem somewhat.

Despite its inherent disadvantages of the time-domain network measurement method comparing to the conventional frequency-domain method, the active probe system provides a convenient tool for characterization of MMICs because of the availability of very high frequency stimulus signal power from the NLTLs and the successful implementation of a very high frequency signal path between the stimulus signal source, the measurement port, and the DUT. An NLTL pulse generator is a much less expensive stimulus signal generator than a DC-200 GHz microwave synthesizer. With the anticipated improvements in calibration standard accuracy and active probe bandwidth, and significant reduction in system noise, on-wafer waveform and network measurements in sub-millimeter-frequencies are feasible.

Bibliography

[1] U. K. Mishra, A. S. Brown, and S. E. Rosenbaum, "DC and RF performance of 0.1 μm gate length AlInAs-GaInAs pseudo-morphic HEMT's", Technical Digest, 1988 International Electron Device Meeting, Dec. 4-11, San Francisco.

[2] L. D. Nguyen, A. S. Brown, M. A. Thompson, L. M. Jelloian, L. E. Larson, and M. Matloubian, "650-A self-aligned-gate pseudomorphic $Al_{0.48}In_{0.52}As / Ga_{0.20}In_{0.80}As$ high electron mobility transistors", IEEE Elect. Dev. Lett., vol. 13, no. 3, March 1992, pp. 143-145.

[3] P. Ho, M. Y. Kao., P. C. Chao, K. H. G. Duh, J. M. Ballinger, S. T. Allen, A. J. Tessmer, and P. M. Smith, "Extremely high gain 0.15 μm gate-length InAlAs/InGaAs/InP HEMTs", Elect. Lett., 14 Feb. 1991, vol. 27, no. 4, pp. 325-327.

[4] H. Wang, T. N. Ton, K. L. Tan, D. Garske, G. S. Dow, J. Berenz, M. W. Popieszalski, and S. K. Pan, "A D-band monolithic low-noise amplifier", proceedings, 1992 IEEE GaAs IC Symposium, Miami Beach, Florida, Oct. 4-7.

[5] R. Majidi-Ahy, C. Nishimoto, M. Riaziat, M. Glenn, S. Silverman, S. Weng, Y. Pao, G. Zdasiuk, S. Bandy and Z. Tan, "100 GHz High-Gain InP MMIC Cascode Amplifier", 1990 GaAs IC Symposium, Oct. 7-10, New Orleans.

[6] R. Majidi-Ahy, C. Nishimoto, M. Riaziat, M. Glenn, S. Silverman, S. Weng, Y. Pao, G. Zdasiuk, S. Bandy and Z. Tan, "5-100 GHz InP coplanar waveguide MMIC distributed Amplifier", IEEE Trans. MTT, vol. 38, no. 12, Dec. 1990.

[7] Tektronix Incorporated, P. O. Box 500, Beaverton, Oregon 97077.

[8] Wiltron Company, 490 Jarvis Drive, Morgan Hill, CA 95037.

[9] S. M. J. Liu and G. G. Boll, "A new probe for W-band on-wafer measurements", Symposium Digest, IEEE MTT-S, June 14-18, 1993, Atlanta.

[10] E. M. Godshalk, "A W-band wafer probe", Symposium Digest, IEEE MTT-S, June 14-18, 1993, Atlanta.

[11] AB Millimeter, 52 Rue Lhomond, 75005 Paris, France.

[12] J. L. Moll and S. A. Hamilton, "Physical modeling of the step recovery diode for pulse and harmonic generation circuits," Proc. IEEE. Vol. 57, pp. 1250-1269, July 1969.

[13] J. Merkelo and R. D. Hall, "Broad-band thin-film signal sampling circuit," IEEE J. of Solid-State Circuits, vol. SC-7, pp. 50-54, Feb. 1972.

[14] S. E. Moore, B. E. Gilchrist, and J. G. Galli, "Microwave sampling effective for ultra-broadband frequency conversion," Microwave Syst. News, pp. 113-120, Feb. 1986.

[15] Microwaves & RF, pp. 167, March 1993.

[16] R. L. Fork, C. H. Brito-Cruz, P. C. Becker, and C. V. Shank, Optics Letters, 12, 483, 1987.

[17] U. D. Keil and D. R. Dykaar, "Electrooptic sampling at 150 fs", proceedings, 1993 OSA conference on Ultrafast Electronics and Optoelectronics, January 25-27, San Francisco, CA.

[18] D. H. Auston, "Impulse response of photoconductors in transmission lines", IEEE J. Quant. Elect., vol. 19, no. 4, April 1983.

[19] J. Nees, S. Williamson, J. Kim, and S. Gupta, "Picosecond detector, optical

temperal analyzer, and free-standing circuit probe", proceedings, 1993 OSA conference on Ultrafast Electronics and Optoelectronics, Jan. 25-27, San Francisco, CA.

[20] J. Kim, J. Son, S. Wakana, J. Nees, S. Williamson, J. Whitaker, Y. Kwon, and D. Pavlidis, "Time-domain network analysis of MM-wave circuits based on a photoconductive probe sampling technique", Symp. Dig., 1993 MTT-s, June 14-18, Atlanta, Georgia.

[21] M. D. Feuer, S. C. Shunk, P. R. Smith, J. J. Law, C. A. Law, C. A. Burrus, and M. C. Nuss, "Highly reproducible optoelectronic wafer probes with fiber input", proceedings, 1993 OSA conference on Ultrafast Electronics and Optoelectronics, January 25-27, San Francisco, CA.

[22] N. Katzenellenbogen and D. R. Grischkowsky, "Efficient generation of 380 fs pulses of THaz radiation by ultrafast laser pulse excitation of a biased metal-semiconductor interface", Appl. Phys. Lett., vol. 58, no. 3, pp. 222-224, January, 1991.

[23] J. A. Valdmanis, G. Mourou, and C. W. Gabel, "Picosecond electrooptic sampling system", Appl. Phys. Lett., vol. 41, pp. 211-212, 1982.

[24] K. J. Weingarten, M. J. W. Rodwell, and D. M. Bloom, "Picosecond optical sampling of GaAs integrated circuits", IEEE J. of Quant. Elect., vol. 24, no. 2, February, 1988.

[25] H. Cheng and J. F. Whitaker, "300-GHz-bandwidth network analysis using time-domain electrooptic sampling", Symp. Dig., 1993 MTT-s, June 14-18, Atlanta, Georgia.

[26] A. Yariv and P. Yeh, Optical Waves in Crystals, Wiley-Interscience, New York, 1984.

[27] S. T. Allen, U. Bhattacharya, and M. J. W. Rodwell, "725 GHz sampling circuits integrated with nonlinear transmission lines", to be presented in the 1994 Device Research Conference, June 20-23, Boulder, Colorado.

[28] M. J. W. Rodwell, M. Kamegawa, R. Yu, M. Case, E. Carman, and K. S. Kiboney, "GaAs Nonlinear Transmission Lines for Picosecond Pulse Generation and Millimeter-Wave Sampling", IEEE Trans. on Microwave Theory and Techniques, Vol. 39, No.7, July 1991.

[29] S. T. Allen, U. Bhattacharya, and M. J. W. Rodwell, "4 THz sidewall-etched varactors for sub-mm-wave sampling circuits," Technical Digest, 1993 GaAs IC Symposium, Oct. 10-13, San Jose.

[30] M. S. Shakouri, A. Black, B. A. Auld, and D. M. Bloom, "500 GHz MMIC sampling wafer probe," Electronic Letters, vol. 29, no. 6, pp. 557-558, March 18, 1993.

[31] J. M. L. Jannsen, "A cathod ray oscillograph for periodic phenomena of higher frequencies", Philips Research Reports, pp. 205, June 1950.

[32] R. Carlson, "Sampling oscillography", IRE WESCON Records, Part 8, pp. 45-51, 1957.

[33] H. Wallman and G. E. Valley, Jr., "Vacuum Tube Amplifiers", McCraw-Hill, New York, 1948.

[34] Mark J. W. Rodwell, "Picosecond electrical wafefront generation and picosecond optoelectronic instrumentation", Ph. D. dissertation, Standford University, Dec. 1987.

[35] Michael Case, "Nonlinear transmission lines for picosecond pulse, impulse and millimeter-wave harmonic generation", Ph. D. dissertation, University of California, Santa Barbara, July 1993.

[36] C. J. Madden, R. A. Marsland, M. J. W. Rodwell, D. M. Bloom, and Y. C. Pao, "Hyperabrupt-doped GaAs nonlinear transmission lines for picosecond shockwave generation", Applied Physics Letters, vol. 54, no. 11, pp. 1019-1021, March 13, 1989.

[37] Y. Konishi, M. Kamegawa, M. Case, R. Yu, S. Allen, and M. J. W. Rodwell, "A broadband free-space millimeter-wave vector transmission measurement system," to be published in IEEE Transactions on Microwave Theory and Techniques.

[38] M. J. W. Rodwell, D. M. Bloom, and K. J. Weingarten, "Subpicosecond laser timing stabilization", IEEE Journal of Quantum Electronics, vol. 25, no. 4, April, 1989.

[39] Cascade Microtech Inc., P. O. Box 1589, Beaverton, OR 97075-1589.

[40] R. K. Hoffmann, "Handbook of microwave integrated circuits," Artech House Inc., 1987.

[41] D. B. Rutledge, D. P. Neikirk, and D. P. Kasilingam, "Integrated-Circuit Antennas" in Infrared and Millimeter Waves, Ed. by K. J. Button, Vol. 10, pp. 1-90, New York: Academic Press, 1984.

[42] M. Caulton, "Lumped elements in microwave integrated circuits," in Advances in Microwaves, Ed. by Leo Young and H. Sobol , pp. 143-167, Academic Press, 1974.

[43] A. Fettweis, "Steady-state analysis of circuits containing a periodically-operated switch", IRE Trans. on Circuit Theory, Sept. 1959.

[44] D. L. Fried, "Analog sample-data filters", IEEE Journal of Solid-State Circuits, August, 1973.

[45] D. Rubin, "De-embedding mm-wave MICs with TRL", Microwave Journal, June, 1990.

[46] J. Fitzpatrick, "Error models for systems measurement", Microwave Journal, May 1978.

[47] M. A. Maury Jr. and G. R. Simpson, "LRL calibration of vector automatic network analyzers", Microwave Journal, May 1987.

[48] H. J. Eul and B. Schiek, "Thru-Match-Reflect: One Result of A Rigorous Theory for De-embedding and Network Analyzer Calibration," Proceedings of the 18th European Microwave Conference, Stockholm, Sweden, 1988.

[49] S. Lauizenhiser, A. Davidson, and K, Jones, "Improve accuracy of on-wafer tests via LRM calibration", Microwave Journal, Jan 1990.

[50] R. A. Soares, P. Gouzien, P. Legaud, and G. Follot, "A unified mathematical approach to two-port calibration techniques and some applications", IEEE Trans. on Microwave Theory and Techniques, vol. 37, no. 11, Nov. 1989.

[51] A. Davidson, K. Jones, and E. Strid, "LRM and LRRM calibrations with automatic determination of load inductance", Application Note, Cascade Microtech, 14255 SW Brigadoon Ct., Beaverton, OR 97005.

[52] R. Y. Yu, Y. Konishi, S. Allen, M. Reddy, and M. J. W. Rodwell, "A traveling-wave resonant tunnel diode pulse generator," submitted to Microwave and Guide

Wave Lett. for publication.

[53] Specification Sheet for Calibration Kit 25, Cascade Microtech, Inc., PO Box 1589, Beaverton, OR, 97075-1589.

[54] M. Schlechtweg, P. Tasker, W. Reinert, J. Braunstein, W. Haydl, A. Hulsmann, and K. Kohler, "High gain 70-80 GHz MMIC amplifiers in coplanar waveguide technology," Electronics Lett., vol. 29, no. 12, June 1993, pp. 1119-1120.

[55] P. J. Tasker, M. Schlechtweg, and J. Braunstein, "On-wafer single contact S-parameter measurements to 75 GHz: calibration and measurement system," 23rd European Microwave Conf., Madrid, 1993.

[56] J. Braunstein, M. Schlechtweg, P. J. Tasker, W. Reinert, A. Julsmann, K. Kohler, W. Bronner, R. Bosch, and W. Haydl, "High performance narrow and wide bandwidth amplifiers in CPW-technology up to W-band," Technical Digest, 1993 GaAs IC Symposium, Oct. 10-13, San Jose.

[57] S. M. J. Liu, K. H. G. Duh, S. C. Wang, O. S. A. Tang, and P. M. Smith, "75-110 GHz InGaAs/GaAs HEMT high gain MMIC amplifier", Tech. Digest, GaAs IC Symposium, San Jose, Oct. 10-13, 1993.

[58] Philip Canfield, Private Communication, Hewlett Packard Company, Santa Rosa, California.

Appendix A. MWSPICE Netilists for the Sampling Circuits and the NWA ICs

The following are the MWSPICE netlists which contains the optimal values for all the components used in the sampling circuits and the NWA ICs.

Netlist #1: Sampling circuit strobe circuit simulation.

```
**********************************************************************
* simulation of strobe circuit with two 3 µm x 3 µmdiodes
VS 1 0 PULSE(12 0 5P 3P)
V1 5 10 1.65
D1 6 5 DMOD
D2 6 5 D2
RS 1 2 50
C2 3 0 15F
C1 4 3 120F
R1 4 3 40
Rd 7 6 18.2
Rd1 7 8 18.2
D3 12 8 DMOD
D4 12 8 D2
R3 4 13 13.5
R4 14 0 0.01
R5 4 9 13.5
R6 9 10 3.6
R7 10 11 3.6
R8 9 12 200
R9 12 0 0.01
R10 15 16 10
T3 11 12 16 15 Z0=100 TD=1.5P K=1 A=0 F=1MEG
*4 12 0 0 16 Z0=100 TD=1.5P K=1 A=0 F=1MEG
T1 13 14 14 14 Z0=100 TD=1.5P K=1 A=0 F=1MEG
T2 2 0 0 3 Z0=50 TD=15P K=1 A=0 F=1MEG
.MODEL DMOD D IS=4.5F RS=0.00 CJO=0.0000F VJ=1.008 M=0.708 BV=15.36
.MODEL D2 D IS=0 CJO=12.057F VJ=1.008 M=0.708 BV=15.36
.TRAN .1P 100P 0 .1P
.FILE TRAN V(2) V(9) V(7) I(D1) V(4) V(10)
.END
**********************************************************************
```

Netlist #2: Sampling circuit signal line bandwidth simulation.

```
**********************************************************************
This program calculates the RF line roll off (no attenuation)
VS 1 0 PULSE(.05 -.05 1p .01p)
V1 3 0 -1
v2 0 4 -1
```

```
D1 3 7 DMOD
D2 7 4 DMOD
RS 1 2 50
R1 5 6 50
R2 6 0 2.5
R3 9 0
.MODEL DMOD D IS=1.5F RS=6.03 CJO=6.96F VJ=1.518 M=0.916 BV=10
.TRAN .1P 04P 0 .01p
.FILE TRAN V(2) I(D1) I(D2)
.END
*****************************************************************
```

Netlist #3: NWA IC strobe circuit simulation.

```
*****************************************************************
* simulation of strobe line for 2 micron by 3 micron diodes
VS 1 0 PULSE(12 0 5P 2p)
V1 7 5 2.04
D1 15 7 DMOD
D2 15 7 D2
RS 1 2 50
*C1 3 6 15F
*RC1 6 0 5.9
C2 4 3 30F
RC2 4 5 3
R1 5 3 50
Rd1 8 15 22.867
Rd2 8 9 22.867
D3 0 9 DMOD
D4 0 9 D2
V2 11 5 2.04
D5 12 11 DMOD
D6 12 11 D2
Rd3 12 13 22.867
Rd4 13 14 22.867
D7 0 14 DMOD
D8 0 14 D2
RA1 5 10 133.86
RA2 10 0 133.86
T1 5 0 0 0 Z0=100 TD=1P K=1 A=0 F=1MEG
T2 5 0 0 0 Z0=100 TD=1P K=1 A=0 F=1MEG
T3 2 0 0 3 Z0=50 TD=15P K=1 A=0 F=1MEG
*.MODEL DMOD D IS=4.5F RS=0.00 CJO=0.0000F VJ=1.008 M=0.708 BV=15.36
.MODEL DMOD D IS=3F RS=0 CJO=0 VJ=1.008 M=0.708 BV=15.36
*.MODEL D2 D IS=0 CJO=12.057F VJ=1.008 M=0.708 BV=15.36
.MODEL D2 D IS=0 CJO=8.0505F VJ=1.008 M=0.708 BV=15.36
.TRAN .1P 100P 0 .1P
.FILE TRAN V(2) V(8) V(13) I(D1) I(D5)
.END
```

```
********************************************************************
```

Netlist #4: NWA IC signal line bandwidth simulation.

```
********************************************************************
signal line fall time, 2 micron by 3 micron.
VS 1 0 PULSE (.05 -.05 1P 2.5P)
RS 1 2 50
T1 2 0 0 3 Z0=50 TD=0.5P K=1 A=0 F=1MEG
R1 3 7 16.6
R2 7 0 67
R3 7 8 16.6
D1 5 3 DMOD
D2 3 6 DMOD
V1 5 0 -1
V2 6 0 1
D3 9 8 DMOD
D4 8 10 DMOD
V3 9 0 -1
V4 10 0 1
RT 8 0 50
*.MODEL DMOD D IS=4.5F RS=15.7 CJO=12.057F VJ=1.008 M=0.708 BV=15.36
.MODEL DMOD D IS=3F RS=22.867 CJO=8.0505F VJ=1.008 M=0.708 BV=15.36
.TRAN .1P 6P 0 .01P
.FILE TRAN V(3) V(8) V(2) I(D1) I(D2) I(D3) I(D4)
.END
********************************************************************
```

Appendix B: Detailed Process Flow Sheets

Appendix B.1. Process Flow Sheets For Sampling Circuits and Netwok Aanlyzer ICs

This section shows the standard process steps used in Rodwell group for fabrication of the sampling circuits (the first three masks for the 3-mask sampling circuits) and the NWA ICs. The smallest features are 2 μms.

I. Self-Aligned Ohmic Contacts (Mask Layer 1, Ohmic, Dark-Field)

A. Solvent Cleaning

Cleanliness Caution: New bottles of solvents out of the cabinet are dirty. Wipe down with a towel and change your gloves before getting near your wafer.

Safety Note: Keep hot solvents well under the splash guards. Always have tweezers in a heated solvent to provide a boiling surface and prevent eruptions.

1. Check the resistivity of the D.I. water. It should be > 17MΩ.
2. Hot TCA 5 min.
3. Cold ACE 5 min.
4. Hot METH 5 min.
5. Hot ISO 5 min.
6. Running DI 3 min.
7. Blow dry with N_2
8. Dehydration bake, 120°C, 30 min. in petri dish without cover

B. Photoresist Application

Safety Note: The vapors from photoresist are extremely harmful. Never breathe if you put your head under the hood.

1. Cool down after dehydration, 10 min.
2. Use our own spinner bowl and our chuck without the O-ring
3. Wafer on spinner chuck with vacuum, blow with N_2
4. Apply AZ P4210 with syringe and filter to cover wafer
5. Spin at 5.5 krpm for 30 sec.
6. Soft Bake, 90 °C, 30 min. in petri dish without cover
7. Clean the bowl and chuck with ACE (wear a Silver Shield glove)

C. Exposure

1. Cool down after soft bake, 10 min.
2. Use exposure of 7.5 mW for 10.5 sec. (79 mJ)
3. Use hard-contact (HP mode) and use our own O-ring

D. Development

1. 2 beakers of AZ 400K : DI :: 1:4 in temperature control bath (20 °C)
2. 1 beaker of toluene in temp. control bath (can be recycled) with cover
3. 10 min. toluene soak
4. Blow off toluene with N_2
5. Develop in first beaker for 60 sec.
6. Develop in second beaker for 30 sec.
7. Rinse in running DI water for 3 min.
8. Blow dry with N_2

E. Oxygen Plasma Descum of Photoresist

1. 300mT of O_2
2. power = 100W at high frequency (13.56 MHz)
3. run for 15 seconds

F. Recess Etch

Safety Note: Wear Silver Shield gloves or equivalent when handling bottles of concentrated acids or bases. Wear face shield at all times while at acid hood.

1. Mix etchant
    a. $NH_4OH : H_2O_2 : H_2O :: 5.8 : 1 : 83$
    b. 21 ml : 3.6 ml : 300 ml (graduated cylinder, pipette, cylinder)
    c. Use magnetic stirrer bar to agitate solution ≈ 30 min. before etch
2. Mix a dilute slution of $NH_4OH : H_2O :: 1 : 10$
3. Dektak wafer, measure photoresist thickness
4. Dip in dilute NH_4OH for 20 sec.
5. Rinse in DI for 3 min.
6. Etch in $NH_4OH : H_2O_2 : H_2O$ solution for 20 or 30 seconds
    Etch rate: Masa sees 53Å/sec
    Scott sees 70Å/sec
7. Rinse in running DI for 3 min.
8. Blow dry with N_2
9. Use Dektak to determine etch depth and rate
10. Etch to get to N+ region, repeating steps 6 to 9, rotating wafer 180° after every 30 sec of etching

G. Evaporation

1. Place wafer in E-Beam mount
2. Use aluminum ring to mask wafer edges. Only tighten the screws enough to barely hold the wafer. If the ring comes down tightly against the wafer, the wafer will crack.
3. Make sure the crystal monitor reads <18; change if necessary
4. Pump down to at least 2×10^{-6} torr
5. Deposit material:

Material	Thickness(Å)	Dep. Rate (Å/sec)	Approx. Vernier
a. Ge	108	2-3	1.75
b. Au	102	2-3	1.90
c. Ge	63	2-3	1.75

If the thicknesses have not been quite right, adjust the last Au thickness to give the correct stochiometric ratio of Ge:Au = 1: 1.977

d. Au	236	2-3	1.90
e. Ni	100	2-3	1.75
f. Au	3000	5	1.95

(use 2 steps; allow wafer to cool for 5 min. between)

H. Liftoff (in order of severity) <u>-->> DO NOT LET ACE DRY ON WAFER! <<--</u>

1. Beaker of ACE with magnetic stirrer bar at setting of 3-4 (usually takes ≈ 20 min.)
2. ACE squirt bottle
3. If the liftoff is stubborn, leave the wafer soaking in ACE overnight. Because ACE evaporates quickly, seal the top of the beaker with foil.
4. Only as a last resort: Beaker of ACE in ultrasonic. Ultrasonic will weaken your wafer and it might not survive further process steps.
5. Rinse in METH then ISO with squirt bottle
6. Rinse in running DI water for 3 min.
7. Blow dry with N_2

I. Rapid Thermal Anneal

Safety Note: A wafer that is removed from the RTA is contaminated with arsenic. Rinse your wafer thoroughly under running DI. Also, if you have used our own Si wafer, rinse it thoroughly as well before putting it away.

1. Program RTA for the following:
    a. delay 20 sec.
    b. ramp 30 °C/sec. to 400 °C
    c. sustain 60 sec. 400 °C
    d. delay 150 sec. to cool
2. Place wafer in center of Si holder
3. Run Program
4. Rinse wafer in DI for 2 min.
5. Inspect under microscope. You should be able to see the change in the surface. If there was no change, run the program again at 10° higher temperature for 30 more seconds.
6. Measure TLM pattern, should get $R_C \approx 20\ \Omega\bullet\mu m$, $R_{SH} \approx 4\ \Omega/sq$
7. If you don't get typical values ± 50%, consider changing program

II. Ion Implantation Mask (Mask Layer 2, Isolation, Dark-Field)

A. Solvent Cleaning

Cleanliness Caution: New bottles of solvents out of the cabinet are dirty. Wipe down with a towel and change your gloves before getting near your wafer.
Safety Note: Keep hot solvents well under the splash guards. Always have tweezers in a heated solvent to provide a boiling surface and prevent eruptions.

1. Check the resistivity of the D.I. water. It should be > 17MΩ.
2. Hot TCA 5 min.
3. Cold ACE 5 min.
4. Hot METH 5 min.
5. Hot ISO 5 min.
6. Running DI 3 min.
7. Blow dry with N_2
8. Dehydration bake, 120°C, 30 min. in petri dish without cover

B. Silicon Dioxide Application

1. Clean the chamber as recommended on the instructions
    a. 300mT of CF_4 at 300W for 20 min.
2. Before turning off the CF_4, set the RF power to 4 Watts
    a. Switch the power toggle switch to "Low"
    b. Turn on the multimeter and set it to read on the 200 mV scale
    c. Adjust the power until the meter reads 4.0
    d. Turn off power, then turn off CF_4
3. Vacuum the chamber for 30 min. and then purge twice
4. Vent the chamber and load the wafer
5. Set the heater to 270°C
6. Turn on the gases according to the directions and set as follows:
    a. N_2O: flow rate =25.0 sccm; set point ≈25.3
    b. SiH_4: flow rate = 70.0 sccm; set point ≈ 71.3
7. Set the controller to auto and set chamber pressure to 770mT
8. Turn on RF power and set to 5W. (The power fluctuates a lot, so monitor it carefully and keep it as close to 5W as possible.)
9. Run for 10 minutes

10. Shut down the system according to the directions
11. Allow the stage to cool to less than 100°C before removing wafer
12. Use ellipsometer to measure film thickness and index
    a. Thickness should be ≈1000Å
    b. Index should be ≈1.49
13. Proceed with polyimide application immediately

C. Polyimide Application

Safety Note: The vapors from polyimide are extremely harmful. Never breathe if you put your head under the hood.

1. Mix adhesion promoter in a dropper bottle
    a. One part QZ 3289 concentrate
    b. Nine parts QZ 3290 dilutant
2. Use our own bowl and chuck without O-ring
3. Wafer on spinner chuck with vacuum
4. Blow off with N_2
5. Apply adhesion promoter to cover wafer
6. Spin at 5 krpm for 30 sec.
7. Let evaporate for 2 min. on chuck then blow off with N_2
8. Apply Probromide 284 to cover wafer with syringe and filter
9. Spin at 6 krpm for 30 sec. (gives ≈ 1.4 µm film)
10. Clean the bowl and chuck with ACE (wear a Silver Shield glove)
11. Hard bake polyimide in petri dish without cover
    Using programmable oven:
    a. 90°C for 30 min.
    b. ramp to 170°C at 5°C per min.
    c. hold at 170°C for 40 min.
    d. ramp to 240°C at 2°C per min.
    e. hold at 240°C for 20 min.
    f. ramp to 170°C at 2°C per min
    Using discrete temperature ovens:
    a. 90°C oven for 40 min.
    b. 170°C oven for 40 min. (use oven back in E-beam area)
    c. ramp to 240°C oven, hold for 20 min. (= 50 min. total)
    d. ramp down to 170°C (takes about 30 min.)

D. Oxygen Plasma

1. Set for 100 W, 300 mTorr of O_2
2. Run for 1 min. (etches ≈ 0.4 µm of polyimide)

E. Photoresist Application

Safety Note: The vapors from photoresist are extremely harmful. Never breathe if you put your head under the hood.

1. Cool down after dehydration, 10 min.
2. Use our own spinner bowl and our chuck without the O-ring
3. Wafer on spinner chuck with vacuum, blow with N_2
4. Apply AZ P4210 with syringe and filter to cover wafer
5. Spin at 5.5 krpm for 30 sec.
6. Soft Bake, 90 °C, 30 min. in petri dish without cover
7. Clean the bowl and chuck with ACE (wear a Silver Shield glove)

F. Exposure

1. Cool down after soft bake, 10 min.
2. Use exposure of 7.5 mW for 10.5 sec. (79 mJ)
3. Use hard-contact (HP mode) and use our own O-ring

G. Development

1. 2 beakers of AZ 400K : DI :: 1:4 in temperature control bath (20 °C)
2. 1 beaker of toluene in temp. control bath (can be recycled) with cover
3. 10 min. toluene soak
4. Blow off toluene with N_2
5. Develop in first beaker for 60 sec.
6. Develop in second beaker for 30 sec.
7. Rinse in running DI water for 3 min.
8. Blow dry with N_2
9. Dektak photoresist to make sure it is 1.8μm thick

H. Evaporation

1. Place wafer in E-Beam mount
2. Use aluminum ring to mask wafer edges. Only tighten the screws enough to barely hold the wafer. If the ring comes down tight against the wafer, the wafer will crack.
3. Use boom to lower sample, increasing deposition rate by a factor of ≈3.1
4. Make sure the crystal monitor reads <18; change if necessary
5. Pump down to at least 2 X 10^{-6} torr
6. Deposit material:

Material	Thickness(Å)	Dep. Rate (Å/sec)	Approx. Vernier
a. Ti	200÷3.1=65	2-3	1.75
b. Au	16,000÷3.1=5160	5-7	1.90

(use 2 steps; allow wafer to cool for 8 min. between)

I. Liftoff (in order of severity) <u>-->> DO NOT LET ACE DRY ON WAFER! <<--</u>

1. Beaker of ACE with magnetic stirrer bar at setting of 3-4 (usually takes ≈ 20 min.)
2. ACE squirt bottle
3. If the liftoff is stubborn, leave the wafer soaking in ACE overnight. Because ACE evaporates quickly, seal the top of the beaker with foil.
4. Do not use ultrasonic or other mechanical means for this liftoff. It will cause some of the isolation pads to come off the polyimide.
5. Rinse in METH then ISO with squirt bottle
6. Rinse in running DI water for 3 min.
7. Blow dry with N_2

J. Polyimide Post Bake (in petri dish without cover)

Using programmable oven:

a. 170°C for 15 min.
b. ramp to 240°C at 2°C per min.
c. hold at 240°C for 30 min.
d. ramp to 170°C at 2°C per min

Using discrete temperature ovens:

a. 170°C oven for 15 min. (use oven in E-beam area)
b. ramp to 240°C oven, hold for 30 min. (≈ 65 min. total)
c. ramp to 170°C (takes about 30 min.)

K. Polyimide Etch

1. 10 min. cool down
2. Set O_2 plasma for 100 W, 300 mTorr of O_2 only
3. Run for ≈ 8 min. to remove all polyimide from exposed areas
4. Inspect under microscope
4. Run longer if necessary in 30 or 60 sec. steps

L. Ion Implantation

1. First call, then send via Federal Express to:

   Myriam Brors
   IICO Corp.
   3050 Oakmead Village Drive
   Santa Clara, Ca 95051
   (408) 727-2547

2. Typical implant (Change implant profile to fit your epi structure)

Implantation Species	Dose	Energy	Off Angle
Proton (H^+)	1.7×10^{15} cm^{-2}	180 keV	7°
Proton (H+)	4×10^{14} cm^{-2}	110 keV	7°

   keep beam current ≈ 100 μA to minimize heating

M. Strip Polyimide

1. Put wafer in suspended holder and heat polyimide thinner ≈ 90°C (Set temp control to 2.5 to maintain 90°C)
2. Allow wafer to soak in hot thinner for ≈ 60 min. with stirrer bar = 3-4
3. Put wafer in room temperature polyimide stripper for 10 min.
4. If some Au remains, put back in hot thinner for 60 min. as in steps 1 & 2
5. Put hot thinner into ultrasonic bath and run for 1 min.
   a. By this time, all pieces of gold should be gone; goto 6.
   b. If some gold pads remain, goto step 3
6. Put in room temperature stripper for 10 min.
7. Put back in hot thinner with stirrer bar for 10 min.
8. Follow with ACE, METH, ISO in squirt bottles
9. Rinse in running DI for 3 min.
10. Inspect under microscope
11. If more gold remains, repeat entire process, steps 1 to 9

N. Oxygen Plasma Clean

1. Set O_2 plasma for 300 mTorr and 300 W
2. Run for 10 minutes
3. Inspect under microscope
4. If any scum remains, run in plasma for longer. **IMPORTANT:** Any scum left on the oxide surface will still be left on your wafer surface after oxide removal. Make sure that you have a pure surface before proceeding.

O. Silicon Dioxide Removal

Safety Note: When working with HF, always wear a new pair of our own yellow safety gloves. Wear a face shield at all times when working near the HF hood, and keep glassware away.

1. Put wafer in straight Buffer HF for 2 min.
2. Rinse in running DI for 3 min.
3. Inspect under microscope
4. Etch again in 30 sec. intervals as necessary

III. Schottky Contacts and Interconnect Metal (Mask Layer 0, Dark-Field)

A. Solvent Cleaning

Cleanliness Caution: New bottles of solvents out of the cabinet are dirty. Wipe down with a towel and change your gloves before getting near your wafer.

Safety Note: Keep hot solvents well under the splash guards. Always have tweezers in a heated solvent to provide a boiling surface and prevent eruptions.

1. Check the resistivity of the D.I. water. It should be > 17MΩ.
2. Hot TCA 5 min.
3. Cold ACE 5 min.
4. Hot METH 5 min.
5. Hot ISO 5 min.
6. Running DI 3 min.
7. Blow dry with N_2
8. Dehydration bake, 120°C, 30 min. in petri dish without cover

B. Photoresist Application

Safety Note: The vapors from photoresist are extremely harmful. Never breathe if you put your head under the hood.

1. Cool down after dehydration, 10 min.
2. Use our own spinner bowl and our chuck without the O-ring
3. Wafer on spinner chuck with vacuum, blow with N_2
4. Apply AZ P4210 with syringe and filter to cover wafer
5. Spin at 5.5 krpm for 30 sec.
6. Soft Bake, 90 °C, 30 min. in petri dish without cover
7. Clean the bowl and chuck with ACE (wear a Silver Shield glove)

C. Exposure

1. Cool down after soft bake, 10 min.
2. Use exposure of 7.5 mW for 10.5 sec. (79 mJ)
3. Use hard-contact (HP mode) and use our own O-ring

D. Development

1. 2 beakers of AZ 400K : DI :: 1:4 in temperature control bath (20 °C)
2. 1 beaker of toluene in temp. control bath (can be recycled) with cover
3. 10 min. toluene soak
4. Blow off toluene with N_2
5. Develop in first beaker for 60 sec.
6. Develop in second beaker for 30 sec.
7. Rinse in running DI water for 3 min.
8. Blow dry with N_2

E. Oxygen Plasma Descum of Photoresist

1. 300mT of O_2
2. power = 100W at high frequency (13.56 MHz)
3. run for 15 seconds

F. Evaporation

Safety Note: Wear Silver Shield gloves or equivalent when handling bottles of concentrated bases. Wear face shield at all times while at acid hood.

1. Mix a dilute soultion of $NH_4OH : H_2O$ :: 1 : 10
2. Dip in dilute NH_4OH for 20 sec.
3. Rinse in DI for 3 min.
4. Blow dry with N_2
5. Place wafer in E-Beam mount
6. Use aluminum ring to mask wafer edges. Only tighten the screws enough to barely hold the wafer. If the ring comes down tight against the wafer, the wafer will crack.
7. Use boom to lower sample, increasing deposition rate by a factor of ≈3.1
8. Make sure the crystal monitor reads <18; change if necessary
9. Pump down to about 7×10^{-7} torr
10. Deposit material:

Material	Thickness(Å)	Dep. Rate (Å/sec)	Approx. Vernier
a. Ti	200÷3.1=65	2-3	1.75
b. Pt	500÷3.1=165	2-3	2.15
c. Au	10,000÷3.1=3230	4-6	1.95

(use 2 steps; allow wafer to cool for 5 min. between)

G. Liftoff (in order of severity) -->> DO NOT LET ACE DRY ON WAFER! <<--

1. Beaker of ACE with magnetic stirrer bar at setting of 3-4 (usually takes ≈ 20 min.)
2. ACE squirt bottle
3. If the liftoff is stubborn, leave the wafer soaking in ACE overnight. Because ACE evaporates quickly, seal the top of the beaker with foil.
4. Only as a last resort: Beaker of ACE in ultrasonic. Ultrasonic will weaken your wafer and it might not survive further process steps.
5. Rinse in METH then ISO with squirt bottle
6. Rinse in running DI water for 3 min.
7. Blow dry with N_2

IV. Silicon Nitride Capacitors (Mask Layer 3, Nitride, Dark-Field)

A. Solvent Cleaning

Cleanliness Caution: New bottles of solvents out of the cabinet are dirty. Wipe down with a towel and change your gloves before getting near your wafer.

Safety Note: Keep hot solvents well under the splash guards. Always have tweezers in a heated solvent to provide a boiling surface and prevent eruptions.

1. Check the resistivity of the D.I. water. It should be > 17MΩ.
2. Hot TCA 5 min.
3. Cold ACE 5 min.
4. Hot METH 5 min.
5. Hot ISO 5 min.
6. Running DI 3 min.
7. Blow dry with N_2
8. Dehydration bake, 120°C, 30 min. in petri dish without cover

B. Oxygen Plasma and Ammonium Hydroxide Surface Prep

1. Set Plasma Etch system for 100 W, 300 mTorr of O_2
2. Run for 1 min.
3. Mix a dilute solution of $NH_4OH : H_2O :: 1 : 10$
4. Dip in dilute NH_4OH for 20 sec.

C. Nitride Deposition

1. Cleaning chamber
    a. Put selection switch "PEIIA/PEIIB" to "PEIIA"
    b. Open CF_4 tank
    c. Vacuum chamber < 50 mTorr
    d. Sw gas #1 on, adjust 300 mTorr
    e. RF on, adjust power to 300W, allow 5 to 20 min. (for 1 hour deposition)
    f. Sw gas #1 off, RF power back to 0, RF Sw off, Close CF_4 tank
    g. If different kind of film is used before, clean the chamber and
    h. deposit desired film on test wafer and pre-coat chamber
2. Loading Sample

- a. Turn on PEII-A and PEII-B (Both should be always on)
- b. Put selection switch "PEIIA/PEIIB" to "PEIIB"
- c. Open desired gas tank, SiO_2=Silane+N_2O,SiN=Silane+N
- d. Sol'n close, Vent open
- e. Load sample
- f. Don't put sample close to the center hole. You may lose your
- g. sample.
- h. Vent close, Sol'n open, wait pressure < 50 mTorr
- i. Turn on Heater, check and adjust set point, wait for desired temperature
- j. SiN --> 285°C
- k. takes 20 min, (5 min in series run)

3. Set controller (for SiN)
   - a. Set the SW on rear panel of PEIIA to "DEP"
   - b. PEIIA Gas#1 SW (CF_4) on
   - c. PEIIB SW on front panel N_2 (#3) and SiH_4 (#2) on, See green
   - d. LED on.
   - e. PEIIB SW on rear panel N_2 (#3) and SiH_4 (#2) on
   - f. Set display channel to 3(N_2)
   - g. Set flow rate dial #1 to 0.71 (always), make sure the flow rate is 25.0
   - h. Set display channel to 2 (SiH_4)
   - i. Set flow rate dial #1 to 1.40 (always), make sure the flow rate is 45.0 If not, adjust trimmer with screw driver
   - j. Set valve controller "auto," wait until pressure become 660 mTorr adjust "setpoint" on exhaust valve controller
   - k. RF power on, Adjust power to 3 W, Start timer ,
5. Open chamber
   - a. Decrease RF power, RF power off
   - b. Set valve controller to "manual"
   - c. PDIIB SW of N_2 and SiH_4 on rear panel off, wait pressure < 0.01 Torr
   - d. PDIIB only N_2 on, wait until pressure become stabilize then turn off N_2 gas
   - e. Repeat that procedure 2 times, vent SiH_4 completely
   - f. Sol'n valve close, vent open
6. Shut down procedure
   - a. Set valve controller to "manual"
   - b. Valve controller power off
   - c. PDIIB 2 SW of N_2 and SiH_4 on rear panel off
   - d. Heater sw off
   - e. PDII main power off
   - f. N_2O gas SiH_4 gas close
7. Use ellipsometer to measure film thickness and index
   - a. Thickness should be ≈ 850Å
   - b. Index should be ≈2.05

D. Photoresist Application

Safety Note: The vapors from photoresist are extremely harmful. Never breathe if you put your head under the hood.

1. Cool down after dehydration, 10 min.
2. Use our own spinner bowl and our chuck without the O-ring
3. Wafer on spinner chuck with vacuum, blow with N_2
4. Apply AZ P4210 with syringe and filter to cover wafer
5. Spin at 5.5 krpm for 30 sec.
6. Soft Bake, 90 °C, 30 min. in petri dish without cover
7. Clean the bowl and chuck with ACE (wear a Silver Shield glove)

E. Exposure
1. Cool down after soft bake, 10 min.
2. Use exposure of 7.5 mW for 10.5 sec. (79 mJ)
3. Use hard-contact (HP mode) and use our own O-ring

F. Development
1. 2 beakers of AZ 400K : DI :: 1:4 in temperature control bath (20 °C)
2. 1 beaker of toluene in temp. control bath (can be recycled) with cover
3. 10 min. toluene soak
4. Blow off toluene with N_2
5. Develop in first beaker for 60 sec.
6. Develop in second beaker for 30 sec.
7. Rinse in running DI water for 3 min.
8. Blow dry with N_2

G. Etch Nitride
1. Set Plasma Etch system for 100 W, 300 mTorr of CF_4
2. Run for 6 min.

H. Remove Photoresist
1. Use beaker of ACE with stirrer bar

V. Air Bridges and Posts (Mask Layers 4 & 5, Post & AB, both Dark-Field)

NOTE: You must proceed from steps A. to I. without stopping!

A. Solvent Cleaning

Cleanliness Caution: New bottles of solvents out of the cabinet are dirty. Wipe down with a towel and change your gloves before getting near your wafer. **Safety Note:** Keep hot solvents well under the splash guards. Always have tweezers in a heated solvent to provide a boiling surface and prevent eruptions.

1. Check the resistivity of the D.I. water. It should be > 17MΩ.
2. Hot TCA 5 min.
3. Cold ACE 5 min.
4. Hot METH 5 min.
5. Hot ISO 5 min.
6. Running DI 3 min.
7. Blow dry with N_2
8. Dehydration bake, 120°C, 30 min. in petri dish without cover

B. Photoresist Application

Safety Note: The vapors from photoresist are extremely harmful. Never breathe if you put your head under the hood. Always hold your breath when you open the refrigerator that has the large bottles of photoresist.

1. Cool down after dehydration, 10 min.
2. Use our own bowl and chuck without O-ring
2. Wafer on spinner chuck with vacuum, blow with N_2
3. Apply AZ P4330-RS with syringe and filter to cover wafer

4. Spin at 6 krpm for 30 sec.
5. Soft Bake, 90°C, 30 min. in petri dish without cover
7. Clean the bowl and chuck with ACE (wear a Silver Shield glove)

C. Exposure #1: **Post Mask**
   1. Cool down after soft bake, 10 min.
   2. Set exposure of 7.5 mW for 12.5 sec. (94 mJ)
   3. Use hard-contact (HP mode) and use our own O-ring

D. Development
   1. Mix AZ400 : DI H_2O :: 1 : 4
   2. 2 beakers of diluted developer in temperature control bath (20 °C)
   3. Develop in first beaker for 45 sec.
   4. Develop in second beaker for 15 sec.
   5. Rinse in running DI water for 3 min.
   6. Blow dry with N_2
   7. Oxygen plasma descum
      a. 300mT of O_2
      b. power = 100W at high frequency (13.56 MHz)
      c. run for 15 seconds
   8. Post Bake in 120° C oven for 30 min. in petri dish without cover

E. Gold Etch

Safety Note: Wear Silver Shield gloves or equivalent when handling bottles of concentrated acids. Wear face shield at all times while at acid hood.

   1. Mix new etchant every time: $KI_2/I_2/H_2O$: H_2O, 1 : 5
   2. Etch for 5 sec.
   3. Rinse in running DI for 3 min.

F. Sputter Flash Layer (Tom ex. 8668)
   1. Loading Sample
      a. Use special sample holder for Ti/Au, (stored in the right cabinet under the table at your left hand side.)
      b. Mount your sample on the holder
      c. Turn off ion gage (IG1, on the second panel from the top)
      d. Flip toggle switch to "Vent" (on the second panel from the top)
      e. Wait 40 sec, open the chamber door
      f. Mount sample holder on the turn table
      g. Rotate the turn table and put the sample over the Ti gun (#4, right hand side)
      h. Close the chamber door
      i. Flip the toggle switch to "Pump"
      j. Capacitance manometer turns on automatically (first panel from the top)
      k. Make sure ion gage turns on below 20 mTorr
      l. Pump down to less than $5x10^{-6}$ (Wait for 30 ~ 40 min)
   2. Set up
      a. Zero the capacitance manometer (Use screw driver, coarse and fine)
      b. Write down base pressure
      c. Turn off filament with switch IG1
      d. Turn on Argon, Gas selector (Adjust flow rate to 25)
      e. Turn on orifice
      f. Adjust pressure (use micrometer on the backside of the chamber) to 10 mT (See Cap. manometer)

    - g. Check DC power supply on
    - h. Key on power supply to "Prog",
      (at "Lock, you can not change setting)
  - 3. Ti Layer
    - a. Adjust power level to 0.1 kW
      (Push "Level" and turn "Modify" knob)
    - b. Check ramp time 1 min, (Push "Level" and turn "Modify" knob)
    - c. Set timer for 1 min. and 30 sec. for 100 Å thick Ti (growth rate is 70 Å/min under this condition)
    - d. Set S-Gun to No. 4
    - e. Turn on plasma ("Output" on)
    - f. Open shutter, Start timer
    - g. Close shutter when done
    - h. Turn off plasma
  - 4. Au Layer
    - a. Set S-Gun to No. 2
    - b. Rotate the sample holder to Au gun (#2)
      (Rotate knob 360° with screw driver)
    - c. Adjust power level (0.2 kW)
    - d. Set timer for 3 minutes and 10 seconds for 2000 Å thick Au
      (deposition rate is 643 Å/min)
    - e. Turn on plasma
    - f. Open shutter
    - g. Close shutter when done
    - h. Turn off plasma
  - 5. Ti Layer
    - a. Set back to Ti gun (#4)
    - b. Rotate the sample holder back to Ti gun (#4)
    - c. Adjust power level back to 0.1 kW
    - d. Set timer for 4 minutes and 30 seconds for 300 Å thick Ti
    - e. Turn on plasma
    - f. Open shutter
    - g. Close shutter when done
  - 6. Shut off
    - a. Turn off plasma
    - b. Mass flow control (Argon) off
    - c. Orifice off
    - d. Flip the toggle switch to "Vent"
    - e. Take out samples
    - f. Vacuum the system
    - g. Flip the toggle switch to "Pump"

G. Photoresist Application

Safety Note: The vapors from photoresist are extremely harmful. Never breathe if you put your head under the hood.

1. Immediately take wafer from sputtering machine to photoresist bench
2. Use our own bowl and chuck without O-ring
3. Wafer on spinner chuck with vacuum, blow with N_2
4. Apply AZ P4330-RS with syringe and filter to cover wafer
5. Spin at 6 krpm for 30 sec.
6. Soft Bake, 90 °C, 30 min. in petri dish without cover
7. Clean the bowl and chuck with ACE (wear a Silver Shield glove)

H. Exposure #2: **AB Mask**

1. Cool down after soft bake, 10 min.
2. Use exposure of 7.5 mW for 14 sec. (105 mJ)
3. Use hard-contact (HP mode) and use our own O-ring

I. Development

1. Mix AZ 400K : DI :: 1:4
2. 2 beakers of diluted developer in temperature control bath (20 °C)
3. Develop in first beaker for 45 sec.
4. Develop in second beaker for 15 sec.
5. Rinse in running DI water for 3 min.
6. Blow dry with N_2
7. Oxygen plasma descum
    a. 300mT of O_2
    b. power = 100W at high frequency (13.56 MHz)
    c. run for 15 seconds
8. Post Bake in 120° C oven for 30 min. in petri dish without cover

J. Plating Preparation

1. Clean tweezers, anode, thermometer and magnet with ISO and DI water
2. Rinse wafer in running DI for 3 min.
3. Heat 800 ml of plating solution in beaker with short stirrer bar to 45°C (temp setting = 2.0 to maintain 45°C)

K. Titanium Etch

Safety Note: When working with HF, always wear a new pair of our own yellow safety gloves. Wear a face shield at all times when working near the HF hood, and keep glassware away.

1. Dektak photoresist and record initial thickness
2. Use a swab with ACE to remove the photoresist on one edge of the wafer. This is used to make the electrical contact.
3. Mix HF : DI H_2O, 1 : 20
4. Etch top layer of Ti ≈ 30 sec. (10 sec. after surface appears gold)
5. Rinse in running DI for 3 min.

L. Gold Plating

1. The plating rate depends on the size of the wafer and the number of air bridges on it, as well as the age of the plating solution. Start with a plating current of 50μA for a 2 inch wafer, or scale down proportionally for smaller pieces.
2. Plate for 15 minutes with stirrer bar set to 3 and T=45°C.
3. Rinse in running DI for 3 minutes
4. Blow dry with N_2
5. Dektak the photoresist and calculate how much the depth has changed
6. Adjust the current to get a plating rate of 1.8μm/hr.
7. Repeat steps 2 to 6 to keep close track of the plating rate
8. Plate until the top of the air bridges are even with the photoresist, for a total thickness of 3μm

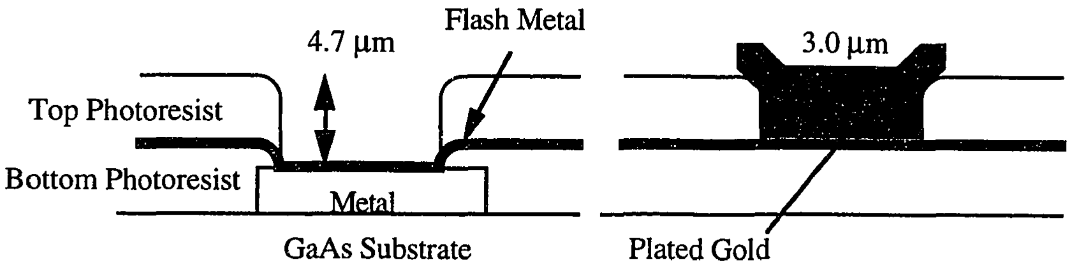

M. First Photoresist Layer Removal
  1. Flood expose top layer for 60 sec.
  2. 2 beakers of AZ 400K:DI, 1 : 1
  3. Develop in first beaker for 60 sec.
  4. Develop in second beaker for 30 sec.
  5. Rinse in running DI water for 3 min.
  6. Blow dry with N_2

N. Etch First Titanium Layer
  1. Use HF : DI H_2O, 1 : 20 from before
  2. Etch for ≈ 30 sec. with moderate agitation
  3. Etch for 10 seconds after gold appears
  4. Rinse in running DI water for 3 min.
  5. Blow dry with N_2

O. Etch Gold Layer
  1. Mix new etchant: $KI_2/I_2/H_2O$: DI, 1:1
  2. Etch initially for 5 sec., using stirrer bar
  3. Rinse in running DI for 3 min.
  4. Blow dry with N_2
  5. Inspect under microscope
  6. If some Au is still left, etch for another 3 sec.
  7. Repeat steps 2 through 6 as necessary, rotating the wafer each time

P. Etch Bottom Titanium Layer
  1. use HF : DI H_2O, 1 : 20 from before
  2. Etch for ≈ 30 sec. with moderate agitation
  3. Etch for 10 seconds after gold appears
  4. Rinse in running DI water for 3 min.
  5. Blow dry with N_2

Q. Remove Bottom Photoresist Layer
  1. Use ACE in beaker with stirrer bar for 3 min.
  2. Follow with ACE, METH, ISO in squirt bottles
  3. Rinse in running DI for 3 min.
  4. Blow dry with N_2

Appendix B.2. Process flow sheets for fabrication of quartz probe tips

This process flow is used to fabricate the quartz probe tips and the signal routing substrates for the active probes. This process flow applies to 5-µm minimum features (lines and gaps), and applicability for smaller features is not varified. We have purchased quartz substrates from two different vendors:

(1) Valley Design Corporation, 63 power Rd., Westford, MA 01886-4110, Tel. (508)692-1971

(2) Continental Glass Engineering, 2636 So. Hill St., Los Angeles, CA 90007, Tel. (213)748-7227

Valley Design Corporation offers high quality (i.e. very accurate dimensions) substrates. Continental Glass Engineering provides substrates with a much lower price (as much as 6 times less than Valley Design Corp.), but the dimensions of the substrates have been very inaccurate (errors > 10%). So depending on the application, it may be advantageous to use one vendor over the other.

I. Transmisison Line Metal (Mask Layer 1, Dark Field)

Because quartz substrates have usually undergone machine shop type processing, the surfaces of the substrates are extremely dirty, so extra effort in substrate cleaning is required.

A. Preliminary Cleaning
   1. Use Lab Clean or Windex (usually available in the clean room) and foam swabs to clean (wipe) the surface of the substrate.
   2. DI rinse for 3 min.
   3. Inspect under the microscope. If any dirts remain, repeat steps 1 and 2.

B. Solvent Cleaning

Cleanliness Caution: New bottles of solvents out of the cabinet are dirty. Wipe down with a towel and change your gloves before getting near your substrate.

Safety Note: Keep hot solvents well under the splash guards. Always have tweezers in a heated solvent to provide a boiling surface and prevent eruptions.
   1. Check the resistivity of the D.I. water. It should be > 17MΩ.
   2. Hot TCA 5 min.
   3. Cold ACE 5 min.
   4. Hot METH 5 min.
   5. Hot ISO 5 min.
   6. Running DI 3 min.
   7. Blow dry with N_2
   8. Dehydration bake, 120°C, 30 min. in petri dish without cover

C. Photoresist Application

Safety Note: The vapors from photoresist are extremely harmful. Never breathe if you put your head under the hood.
   1. Cool down after dehydration, 10 min.
   2. Use our own spinner bowl and our chuck without the O-ring
   3. Substrate on spinner chuck with vacuum, blow with N_2
   4. Apply HMDS to cover substrate
   5. Spin at 5.5 krpm for 30 sec.
   6. Apply AZ P4210 with syringe and filter to cover substrate
   7. Spin at 5.5 krpm for 30 sec.
   8. Soft Bake, 90 °C, 30 min. in petri dish without cover
   9. Clean the bowl and chuck with ACE (wear a Silver Shield glove)

D. Exposure
   1. Cool down after soft bake, 10 min.
   2. Wipe edge bead off with q-tip (expecially at the corners)
   3. Use exposure of 7.5 mW for 10.5 sec. (79 mJ)
   4. Use soft-contact mode

E. Development

    1. 2 beakers of AZ 400K : DI :: 1:4 in temperature control bath (20 °C)
    2. 1 beaker of toluene in temp. control bath (can be recycled) with cover
    3. 10 min. toluene soak
    4. Blow off toluene with N_2
    5. Develop in first beaker for 60 sec.
    6. Develop in second beaker for 30 sec.
    7. Rinse in running DI water for 3 min.
    8. Blow dry with N_2

F. Oxygen Plasma Descum of Photoresist
    1. 300mT of O_2
    2. power = 100W at high frequency (13.56 MHz)
    3. run for 15 seconds

G. Evaporation
    1. Mount substrate in E-Beam mount
    7. Use boom to lower sample, increasing deposition rate by a factor of ≈3.1
    8. Make sure the crystal monitor reads <18; change if necessary
    9. Pump down to about 1 X 10^{-6} torr
    10. Deposit material:

Material	Thickness(Å)	Dep. Rate (Å/sec)	Approx. Vernier
a. Ti	200÷3.1=65	2-3	1.75
b. Au	10,000÷3.1=3230	4-6	1.95

(use 2 steps; allow substrate to cool for 5 min. between)

G. Liftoff (in order of severity) DO NOT LET ACE DRY ON SUBSTRATE!
    1. Beaker of ACE with magnetic stirrer bar at setting of 3-4 (usually takes ≈ 20 min.)
    2. ACE squirt bottle
    3. If the liftoff is stubborn, leave the substrate soaking in ACE overnight. Because ACE evaporates quickly, seal the top of the beaker with foil.
    4. Only as a last resort: Beaker of ACE in ultrasonic. Ultrasonic will weaken your substrate and it might not survive further process steps.
    5. Rinse in METH then ISO with squirt bottle
    6. Rinse in running DI water for 3 min.
    7. Blow dry with N_2

II. Air Bridges and Posts (Mask Layers 2 & 3, Post & AB, both Dark-Field)

NOTE: You must proceed from steps A. to I. without stopping!

A. Solvent Cleaning

Cleanliness Caution: New bottles of solvents out of the cabinet are dirty. Wipe down with a towel and change your gloves before getting near your substrate.

Safety Note: Keep hot solvents well under the splash guards. Always have tweezers in a heated solvent to provide a boiling surface and prevent eruptions.

    1. Check the resistivity of the D.I. water. It should be > 17MΩ.
    2. Hot TCA 5 min.
    3. Cold ACE 5 min.
    4. Hot METH 5 min.
    5. Hot ISO 5 min.
    6. Running DI 3 min.
    7. Blow dry with N_2

8. Dehydration bake, 120°C, 30 min. in petri dish without cover

B. Photoresist Application

Safety Note: The vapors from photoresist are extremely harmful. Never breathe if you put your head under the hood. Always hold your breath when you open the refrigerator that has the large bottles of photoresist.

1. Cool down after dehydration, 10 min.
2. Use our own bowl and chuck without O-ring
2. Substrate on spinner chuck with vacuum, blow with N_2
3. Apply HMDS to cover substrate
4. Spin at 6 krpm for 30 sec.
5. Apply AZ P4330-RS with syringe and filter to cover substrate
6. Spin at 6 krpm for 30 sec.
7. Soft Bake, 90°C, 30 min. in petri dish without cover
8. Clean the bowl and chuck with ACE (wear a Silver Shield glove)

C. Exposure #1: **Post Mask**

1. Cool down after soft bake, 10 min.
2. Wipe edge bead off with q-tip (expecially at the corners)
3. Set exposure of 7.5 mW for 12.5 sec. (94 mJ)
4. Use soft-contact mode

D. Development

1. Mix 2 beakers of AZ400 : DI H_2O = 1 : 4
2. Place the diluted developer in temperature control bath (20 °C)
3. Develop in first beaker for 45 sec.
4. Develop in second beaker for 15 sec.
5. Rinse in running DI water for 3 min.
6. Blow dry with N_2
7. Oxygen plasma descum
    a. 300mT of O_2
    b. power = 100W at high frequency (13.56 MHz)
    c. run for 15 seconds
8. Post Bake in 120° C oven for 30 min. in petri dish without cover

E. Gold Etch

Safety Note: Wear Silver Shield gloves or equivalent when handling bottles of concentrated acids. Wear face shield at all times while at acid hood.

1. Mix new etchant every time: $KI_2/I_2/H_2O$: H_2O, 1 : 5
2. Etch for 5 sec.
3. Rinse in running DI for 3 min.

F. Sputter Flash Layer (Tom ex. 8668)

1. Loading Sample
    a. Use special sample holder for Ti/Au, (stored in the right cabinet under the table at your left hand side.)
    b. Mount your sample on the holder
    c. Turn off ion gage (IG1, on the second panel from the top)
    d. Flip toggle switch to "Vent" (on the second panel from the top)
    e. Wait 40 sec, open the chamber door
    f. Mount sample holder on the turn table
    g. Rotate the turn table and put the sample over the Ti gun (#4, right hand side)
    h. Close the chamber door
    i. Flip the toggle switch to "Pump"
    j. Capacitance manometer turns on automatically

(first panel from the top)
    - k. Make sure ion gage turns on below 20 mTorr
    - l. Pump down to less than $5x10^{-6}$ (Wait for 30 ~ 40 min)
2. Set up
    - a. Zero the capacitance manometer
      (Use screw driver, coarse and fine)
    - b. Write down base pressure
    - c. Turn off filament with switch IG1
    - d. Turn on Argon, Gas selector (Adjust flow rate to 25)
    - e. Turn on orifice
    - f. Adjust pressure (use micrometer on the backside of the chamber) to 10 mT (See Cap. manometer)
    - g. Check DC power supply on
    - h. Key on power supply to "Prog",
      (at "Lock, you can not change setting)
3. Ti Layer
    - a. Adjust power level to 0.1 kW
      (Push "Level" and turn "Modify" knob)
    - b. Check ramp time 1 min, (Push "Level" and turn "Modify" knob)
    - c. Set timer for 1 min. and 30 sec. for 100 Å thick Ti (growth rate is 70 Å/min under this condition)
    - d. Set S-Gun to No. 4
    - e. Turn on plasma ("Output" on)
    - f. Open shutter, Start timer
    - g. Close shutter when done
    - h. Turn off plasma
4. Au Layer
    - a. Set S-Gun to No. 2
    - b. Rotate the sample holder to Au gun (#2)
      (Rotate knob 360° with screw driver)
    - c. Adjust power level (0.2 kW)
    - d. Set timer for 3 minutes and 10 seconds for 2000 Å thick Au
      (deposition rate is 643 Å/min)
    - e. Turn on plasma
    - f. Open shutter
    - g. Close shutter when done
    - h. Turn off plasma
5. Ti Layer
    - a. Set back to Ti gun (#4)
    - b. Rotate the sample holder back to Ti gun (#4)
    - c. Adjust power level back to 0.1 kW
    - d. Set timer for 4 minutes and 30 seconds for 300 Å thick Ti
    - e. Turn on plasma
    - f. Open shutter
    - g. Close shutter when done
6. Shut off
    - a. Turn off plasma
    - b. Mass flow control (Argon) off
    - c. Orifice off
    - d. Flip the toggle switch to "Vent"
    - e. Take out samples
    - f. Vacuum the system

g. Flip the toggle switch to "Pump"

G. Photoresist Application

Safety Note: The vapors from photoresist are extremely harmful. Never breathe if you put your head under the hood.

1. Immediately take substrate from sputtering machine to photoresist bench
2. Use our own bowl and chuck without O-ring
3. Substrate on spinner chuck with vacuum, blow with N_2
4. Apply AZ P4330-RS with syringe and filter to cover substrate
5. Spin at 6 krpm for 30 sec.
6. Soft Bake, 90 °C, 30 min. in petri dish without cover
7. Clean the bowl and chuck with ACE (wear a Silver Shield glove)

H. Exposure #2: **AB Mask**

1. Cool down after soft bake, 10 min.
2. Use exposure of 7.5 mW for 14 sec. (105 mJ)
3. Use soft-contact mode

I. Development

1. Mix 2 beakers of AZ 400K : DI = 1:4
2. Place the diluted developer in temperature control bath (20 °C)
3. Develop in first beaker for 45 sec.
4. Develop in second beaker for 15 sec.
5. Rinse in running DI water for 3 min.
6. Blow dry with N_2
7. Inspect under microscope. If photoresist scum remains in the post holes, develop for another 30 sec.
8. Repeat step 7 until no PR scum left in the post holes
9. Oxygen plasma descum
    a. 300mT of O_2
    b. power = 100W at high frequency (13.56 MHz)
    c. run for 15 seconds
10. Post Bake in 120° C oven for 30 min. in petri dish without cover

J. Plating Preparation

1. Clean tweezers, anode, thermometer and magnet with ISO and DI water
2. Rinse substrate in running DI for 3 min.
3. Heat 800 ml of plating solution in beaker with short stirrer bar to 45°C (temp setting = 2.0 to maintain 45°C)

K. Titanium Etch

Safety Note: When working with HF, always wear a new pair of our own yellow safety gloves. Wear a face shield at all times when working near the HF hood, and keep glassware away.

1. Dektak photoresist and record initial thickness
2. Use a swab with ACE to remove the photoresist on one edge of the substrate. This is used to make the electrical contact.
3. Mix HF : DI H_2O, 1 : 20
4. Etch top layer of Ti ≈ 30 sec. (10 sec. after surface appears gold)
5. Rinse in running DI for 3 min.

L. Gold Plating

1. The plating rate depends on the size of the substrate and the number of air bridges on it, as well as the age of the plating solution. Start with a plating current of 50μA for a 2 inch substrate, or scale down proportionally for smaller pieces.
2. Plate for 15 minutes with stirrer bar set to 3 and T=45°C.

3. Rinse in running DI for 3 minutes
4. Blow dry with N_2
5. Dektak the photoresist and calculate how much the depth has changed
6. Adjust the current to get a plating rate of 1.8μm/hr.
7. Repeat steps 2 to 6 to keep close track of the plating rate
8. Plate until the top of the air bridges are even with the photoresist, for a total thickness of 3μm

M. First Photoresist Layer Removal

1. Flood expose top layer for 60 sec.
2. 2 beakers of AZ 400K:DI, 1 : 1
3. Develop in first beaker for 60 sec.
4. Develop in second beaker for 30 sec.
5. Rinse in running DI water for 3 min.
6. Blow dry with N_2

N. Etch First Titanium Layer

1. Use HF : DI H_2O, 1 : 20 from before
2. Etch for ≈ 30 sec. with moderate agitation
3. Etch for 10 seconds after gold appears
4. Rinse in running DI water for 3 min.
5. Blow dry with N_2

O. Etch Gold Layer

1. Mix new etchant: $KI_2/I_2/H_2O$: DI, 1:1
2. Etch initially for 5 sec., using stirrer bar
3. Rinse in running DI for 3 min.
4. Blow dry with N_2
5. Inspect under microscope
6. If some Au is still left, etch for another 3 sec.
7. Repeat steps 2 through 6 as necessary, rotating the substrate each time

P. Etch Bottom Titanium Layer

1. use HF : DI H_2O, 1 : 20 from before
2. Etch for ≈ 30 sec. with moderate agitation
3. Etch for 10 seconds after gold appears
4. Rinse in running DI water for 3 min.
5. Blow dry with N_2

Q. Remove Bottom Photoresist Layer

1. Use ACE in beaker with stirrer bar for 3 min.
2. Follow with ACE, METH, ISO in squirt bottles
3. Rinse in running DI for 3 min.
4. Blow dry with N_2

III. Nickle Contacts (Mask Layers 4, Dark-Field)

The Ni plating solution (Ni-sulfamate-ready to use) was purchased from Technic Inc., 1170 Hawk Circle, Anaheim, CA 92807, Tel. (714)632-0200.

A. Solvent Cleaning

Cleanliness Caution: New bottles of solvents out of the cabinet are dirty. Wipe down with a towel and change your gloves before getting near your substrate.

Safety Note: Keep hot solvents well under the splash guards. Always have tweezers in a heated solvent to provide a boiling surface and prevent eruptions.

1. Check the resistivity of the D.I. water. It should be > 17MΩ.
2. Hot TCA 5 min.

3. Cold ACE 5 min.
4. Hot METH 5 min.
5. Hot ISO 5 min.
6. Running DI 3 min.
7. Blow dry with N_2
8. Dehydration bake, 120°C, 30 min. in petri dish without cover

B. Photoresist Application

Safety Note: The vapors from photoresist are extremely harmful. Never breathe if you put your head under the hood. Always hold your breath when you open the refrigerator that has the large bottles of photoresist.

1. Cool down after dehydration, 10 min.
2. Use our own bowl and chuck without O-ring
2. Substrate on spinner chuck with vacuum, blow with N_2
3. Apply HMDS to cover substrate
4. Spin at 6 krpm for 30 sec.
5. Apply AZ P4330-RS with syringe and filter to cover substrate
6. Spin at 6 krpm for 30 sec.
7. Soft Bake, 90°C, 30 min. in petri dish without cover
8. Clean the bowl and chuck with ACE (wear a Silver Shield glove)

C. Exposure

1. Cool down after soft bake, 10 min.
2. Wipe edge bead off with q-tip (expecially at the corners)
3. Set exposure of 7.5 mW for 12.5 sec. (94 mJ)
4. Use soft-contact mode

D. Development

1. Mix 2 beakers of AZ400 : DI H_2O = 1 : 4
2. Place the diluted developer in temperature control bath (20 °C)
3. Develop in first beaker for 45 sec.
4. Develop in second beaker for 15 sec.
5. Rinse in running DI water for 3 min.
6. Blow dry with N_2
7. Oxygen plasma descum
    a. 300mT of O_2
    b. power = 100W at high frequency (13.56 MHz)
    c. run for 15 seconds
8. Post Bake in 120° C oven for 30 min. in petri dish without cover

E. Gold Etch

Safety Note: Wear Silver Shield gloves or equivalent when handling bottles of concentrated acids. Wear face shield at all times while at acid hood.

1. Mix new etchant every time: $KI_2/I_2/H_2O$: H_2O, 1 : 5
2. Etch for 5 sec.
3. Rinse in running DI for 3 min.

F. Plating Preparation

1. Clean tweezers, anode, thermometer and magnet with ISO and DI water
2. Rinse substrate in running DI for 3 min.
3. Heat 800 ml of plating solution in beaker with short stirrer bar to 45°C (temp setting = 2.0 to maintain 45°C)

G. Nickle Plating

1. The plating rate depends on the size of the substrate and the number of contacts on it, as well as the age of the plating solution. Start with a

plating current of 8 mA for a 2 inch substrate, or scale down proportionally for smaller pieces.

    2. Plate for 15 minutes with stirrer bar set to 3 and T=45°C.
    3. Rinse in running DI for 3 minutes
    4. Blow dry with N_2
    5. Dektak the photoresist and calculate how much the depth has changed
    6. Adjust the current to get a plating rate of ≈ 2 μm/hr.
    7. Repeat steps 2 to 6 to keep close track of the plating rate
    8. Plate until the desire thickness is achieved

H. Remove Photoresist Layer

    1. Use ACE in beaker with stirrer bar for 3 min.
    2. Follow with ACE, METH, ISO in squirt bottles
    3. Rinse in running DI for 3 min.
    4. Blow dry with N_2

Appendix B.3. Quartz probe tipe lapping procedure

The quartz probe tips are angle-lapped to provide better visibility for the probe contact points. The lapping abrasive powders are the Silicon Carbide-1000 grit for lapping and the Alumina Micropolisher (0.3 or 1.0 μm) for polishing. Both of these products are from Buehler Ltd., 9297 Jeronimo Rd., #107B, Irvine, CA 92718, Tel. (714)458-8885. The lapping fixture is as shown in Fig. B.1.

1. Lapping preparation

a. Rinse the lapping fixtures in running water for 3 min.
b. Heat the brass fixture 120°C using a hot plate
c. Wax (with crystal wax) 3 pieces of quartz (of the probe tip thickness) around the periphery of the brass fixture (Fig. B.1(a))
d. Wax probe tips in the 45° angle slots of the brass fixture, and align the tips almost flash with the edge of the slot (Fig. B.1(b))
e. Mount the lapping fixture to the lapping handle

2. Lapping

a. Mix silicon carbide with water on the lapping plate, and rotate the lapping fixture with the handle. Lapping rate is ≈ 3 mils per 100 laps.
b. Inspect the tips (on the fixture) periodically, and more often when it is close to desired thickness (2 mils).
c. When the tip contact end is 2 mil thick (Fig. B.1(c)), stop!

3. Polishing

a. Mix the Alumina powder with water on the designated plate.
b. Rotate the lapping fixture with the handle, and inspect under the microscope. It usually takes about 300 laps to achieve very flat (shiny and transparent) surface. The material loss should be less than 1 mil.

4. Removing the probe tips

a. Remove the brass fixture from the lapping handle, and soak in ACE for 4 hours (or longer for bigger probe tips).
b. When the crystal wax dissolves in ACE, slide the probe tips out of the slots with a tweezer.

c. Rinse the tips in ISO and water
d. Rinse the brass fixture, the handle, and the lapping plates

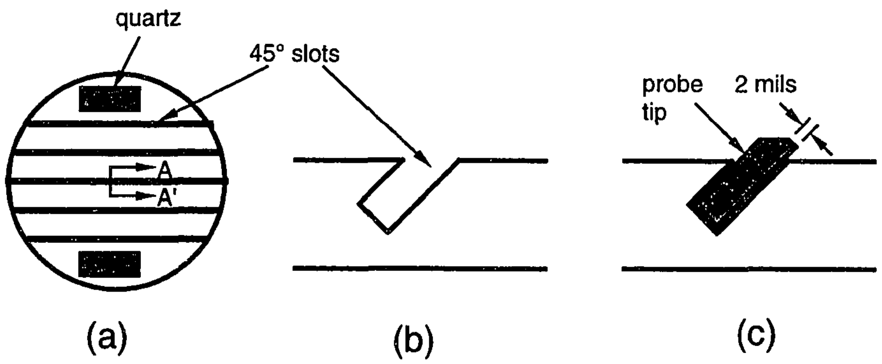

Figure B.1. Angle lapping fixture for quartz probe tips: (a) top view of the lapping fixture, (b) cross sectional view of AA', and (c) final shape of the lapped probe tips.

Appendix C. Example C Programs for System Control and Measurement De-embedding for the Active Probe Measurement System

There are over 50 C programs developed for system control and measurement de-embedding for the active probe system. For waveform measurements, the program "scope2.c" can be used. With this program, the IF signals measured by the sampling circuits are digitized, by a digitizing scope, and saved in data files for subsequent data processing. For network measurements, the programs were broken down into two modules: one for data acquisition and the other for measurement calibration. In the data acquistion modules, the time waveforms for the calibration standards and the DUTs are measured, transformed into frequency domain, and saved into data files. In the measurement calibration modules, the data files obtained with the data acquisition modules are manipulated and the corrected S-parameters are calculated. In this appendix, some example C programs (the most often used ones) for the acitve probe measurement system is listed. For example, program "ACQUIRE6.c" is the data acquisition modules; programs "1portNWA8.c" , "TWOPORT2.c", and "LRM2port8.c" are the SOL, LRL, and LRM measurement calibration modules, respectively. For the active probe system using lock-in amplifiers, the program "acquirelc.c" is used to acquire the data. Programs "matrix.c", "lockin2d.c" contain subroutines needed in the main program modules.

```
/*******************************************************************/
/* Program: scope2.c.  Copy right: Rodwell group, ECE Dept.. UC Santa Barbara. */
/*******************************************************************/
/*******This program acquires the digitized data from hp54503 scope*****/
/*******************************************************************/
/********* The acquire subroutine returns digitized data from the scope.*******/
/****The waveform on the channel is first averaged as many times as the user***/
/****wishes and then digitized.  The data is stored in an array IF[4][2050]***/
/********Ch#2 data in IF[2][1 to 1025], Ch#3 data in IF[3][1 to 1025], ********/
/******************* Ch#4 data in IF[4][1 to 1025].***********************/
/*******************************************************************/
void acquire(IF)
float  IF[4][2050];

{
int i,j,k,m,points,count;
char rd[16384],wrt[128],temp[128],chno[1];
float  xref, yref,xinc,xorg,yinc,yorg,x,y;
extern float vdc,vpp;
extern int chnos,scope;
extern char ch[5];
        switch (chnos) {
                case 1:
```

```
                if(ibwrt(scope,"DIG CHAN1",9) & ERR) err ();
                        break;
                case 2:
                        if(ibwrt(scope,"DIG CHAN1,CHAN2",15)&ERR) err();
                        break;
                case 3:
                        if(ibwrt(scope,"DIG CHAN1,CHAN2,CHAN3",21)&ERR)
err();
                        break;
                default:
        if(ibwrt(scope,"DIG CHAN1,CHAN2,CHAN3,CHAN4",27)&ERR) err();
          break;
                }

        for (k=1;k<=chnos;k++)
        {
                sprintf(chno,"%d",k);
                strcpy(wrt,"WAV:SOUR CHAN");
                strcat (wrt,chno);
                if (ibwrt(scope,wrt,14) & ERR) err ();
                if (ibwrt(scope,"WAV:PRE?",8) & ERR) err ();
                if (ibrd(scope,rd,256) & ERR) err ();
                i=j=0;
                for (count=1;count<=10;) {
                if (rd[i] != ',' && rd[i] !='\0')
                        temp[j++]=rd[i++];
                else if (rd[i] == ',' || rd[i] == '\0') {
                        temp[j]='\0';
                        switch (count) {
                                case 3:
                                        points=atoi(temp);
                        break;

                                case 8:
                                        yinc=atof(temp);
                                        break;
                                case 9:
                                        yorg=atof(temp);
                                        break;
                                case 10:
                                        yref=atof(temp);
                                        break;
                                default:
                                        break;
                        }
                        i++;
                        j=0;
                        count++;
```

```
                }
        }

/*********************** Retrieve data **************************/
        if (ibwrt(scope,"WAV:DATA?",9) & ERR) err();
        if (ibrd(scope,rd,16384) & ERR) err();
        i=j=0;
        for (count=0;count<points;) {
                if (rd[i] != ',' && rd[i] != '\0')
                        temp[j++]=rd[i++];
                else if (rd[i] == ',' || rd[i] == '\0') {
                        temp[j]='\0';
                        y=((atof(temp)-yref)*yinc)+yorg;
                        IF[k-1][count+1]=y;
                        i++;
                        j=0;
                        count++;
                }
        }

}                                       /*end k*/
}

/*********************************************************************/
/***************This subroutine autoscales input waveforms.***************/
/***The waveform on the scope is first measured. Vmax and Vmin are then used***/
/***to calculate Vdc and Vp-p.  The Y-axis range and the offset are adjusted**/
/**fill 90% of the scope's screen. This will reduce the effect of quantization*/
/*************************noise.**********************************/
/*********************************************************************/


void autoscale (l)
   int l;
{
      char  temp[128],wrt[128],rd[128] ;
         char chan[1];
         int i,len;
      void delay();
      extern float vdc,vpp;
      extern int scope;
      extern char ch[5];
      float vmax,vmin;
      sprintf(chan,"%d",l);
      strcpy(wrt,"MEAS:SOUR CHAN");
      strcat(wrt,chan);
      if (ibwrt(scope,wrt,15) & ERR) err();
      if (ibwrt(scope,"MEAS:VMIN?",10) & ERR) err();
```

```
        delay(15);
        if (ibrd(scope,rd,128) & ERR) err();
        delay(15);
        vmin=atof(rd);
        if (ibwrt(scope,"MEAS:VMAX?",10) & ERR) err();
        delay(15);
        if (ibrd(scope,rd,128) & ERR) err();
        delay(15);
        vmax=atof(rd);
        vdc=(vmin+vmax)/2;
        vpp=1.1*(vmax-vmin);
        sprintf(temp,"%e",vdc);
        sprintf(chan,"%d",l);
        strcpy(wrt,"CHAN");
        strcat(wrt,chan);
        strcat(wrt,":OFFS ");
        strcat(wrt,temp);
        len=strlen(wrt);
        if (ibwrt(scope,wrt,len) & ERR) err();
        delay(15);
        sprintf(temp,"%e",vpp);
        sprintf(chan,"%d",l);
        strcpy(wrt,"CHAN");
        strcat(wrt,chan);
        strcat(wrt,":RANG ");
        strcat(wrt,temp);
        len=strlen(wrt);
        if(ibwrt(scope,wrt,len) & ERR) err();
        delay(30);


}

/******************************************************************/
/***************************A simple delay****************************/
/******************************************************************/
 void delay(n)
int n;
{
            int i=0;
            while (i<n*10000)
            {
            i++;
            }
}
/******************************************************************/
/************************ HPIB errors**********************************/
/******************************************************************/
```

```
err ()
{
        printf("\nThere was a problem in executing an hpib command.\n");
        exit (0);
}
/***************************** END *****************************/


/******************************************************************/
/* Program: ACQUIRE6.c.  Copy right: Rodwell Group, ECE Dept. UCSB.      */
/*****************************************************************/
/******************************************************************/
/*This program acquires the waveforms for calibrating the 2port measurements*/
/*By Ruai Yu.  First version . 12/25/91.*/
/*Two-port NWA Calibration, Measurement, and Switching Routines.*/
/*Revised by J. Pusl 5/92. Second version.*/
/*filename=/home/rlab/pusl/cprog/nwa.c*/
/*Revised by Madhukar Reddy 7/92. Third version.*/
/*filename=/home/rlab/madhu/2port/2port6.c*/
/******************************************************************/
/******************************************************************/
/*****************Include the following standard libraries******************/
#include <math.h>
#include <stdio.h>
#include <ctype.h>
#include <string.h>
/******************************************************************/
/*****************Include the following user created libraries***************/

#include "complex.h"

#include "ugpib.h"
#include "scope2.c"
/******************************************************************/
#define PI 3.141592654


/*GLOBAL VARIABLES*/
float vdc,vpp;
int scope,SWITCH,len,chnos;
char ch[5],trigch[5];

main ()
{
fcomplex S[100][7][5],SDE[100][5],A[5],IA[5],GammaA[100],GammaB[100];
fcomplex CFFT[7][2][4][100],a1[7][2][100],b1[7][2][100];
fcomplex a2[7][2][100],b2[7][2][100];
```

```
fcomplex T1,T2,ONE,TWO,THREE;
float L[6],time;
int i,j,k,l,m,n=1,s,dps,avgs,nhs,stim;
char filename[64],wrt[64],file[64],file1[64],temp1[10];
char temp2[10],temp3[10],temp[10],option[10],temp5[10],temp6[10];
float freq,rffreq,re,im,mag,phase,FFT[7][2][4][2050];
struct device device;
FILE *fp ;

chnos=4;

ONE.r=1;ONE.i=0;
TWO.r=2;TWO.i=0;
THREE.r=3;THREE.i=0;

/*******Ask user to calibrate the system and take the S-parameters*******/
printf("You must have the following set-up:\n");
printf("Scope channel: 1=port1in, 2=port1out,3=port2in,4=port2out\n");
/*Measure all the Cal Standards and Device Under Test (DUT).*/


printf ("\nPlease enter the RF frequency in GHz:");
scanf("%f",&rffreq);
nhs=floor(370.0/rffreq);
printf("\nPlease enter # of data points (power of 2)\n");
scanf("%d",&dps);
printf("\nPlease enter # of averages \n");
scanf("%d",&avgs);
printf("There are 4 measurements to be made:  \n");
printf("1) 1 ps Through Line -Enter 1 for measurement #\n");
printf("2) 50 Ohm Matched Load- Enter 2 for measurement #\n");
printf("3) Open or Short as a reference Load-Enter 3 for measurement #\n");
printf("4) DUT Enter 4 for Measurement #\n");
/*****************Set up the instruments*******************************/
/*The RF switch is the HP 11713*/
 printf ("please enter the measurement number!\n");
 scanf("%d",&l);
 if (l>3) {
   i=4;
   }
 else {
   i=l;
   }
 printf("Ready for Measurement #%d, and press any key to proceed!\n",i);
 scanf("%s",wrt);
 SWITCH=ibfind("hp11713");
 if (SWITCH<0)
 {
```

```
  printf ("\nCannot find hp11713 switch.\n");
  err ();
}

if (ibllo(SWITCH) & ERR) err();

/*The scope is the HP 54503.  Set it up.  */

scope=ibfind("hp54503");
if (scope < 0)
{
  printf ("\nCannot find hp54503 scope.\n");
  err ();
}
ioctl(scope,IBGET,&device);
device.d_tmo=T300s;
ioctl(scope,IBSET,&device);

if (ibllo(scope) & ERR) err ();
if (ibwrt(scope,"BEEP",4) & ERR) err ();
if (ibwrt(scope,"EOI ON",6) & ERR) err ();
if (ibwrt(scope,"SYST:HEAD OFF",13) & ERR) err ();
if (ibwrt(scope,"WAV:FORM ASC",12) & ERR) err();

sprintf(temp,"%d",dps);
strcpy(wrt,"ACQ:POIN ");
strcat(wrt,temp);
len=strlen(wrt);
if (ibwrt(scope,wrt,len) & ERR) err();
strcpy(file1,"calt");
sprintf(wrt,"%d",i);
strcat(file1,wrt);
if (i>3) {
 printf ("Please enter the name of the file for the dut\n");
 scanf("%s",file1);
 strcpy(temp6,file1);
 strcat(file1,"t");
 }

 for (m=1;m<=2;m++) {
   if(m==1) {
     if (ibwrt(SWITCH,"B0",2) & ERR) err();
     stim=1;
     }
    else {
      if (ibwrt(SWITCH,"A0",2) & ERR) err();
      stim=3;
    }
```

```
    delay(15);
    if (ibwrt(scope,":AUT",4) & ERR) err();
    delay(100);
    sprintf(temp,"%d",stim);
    strcpy(wrt,":TRIG:SOUR CHAN");
    strcat(wrt,temp);
    len=strlen(wrt);
    if (ibwrt(scope,wrt,len) & ERR) err();
    delay(15);
    if (ibwrt(scope,":TIM:MODE AUTO;RANG 0.05MS;REF CENT;DEL 0MS",43)
& ERR) err ();
    delay(15);
    if (ibwrt(scope,":TRIG:CENT;MODE EDGE;SLOP POS;HOLD
TIME,0.045MS;SENS LOW",56) & ERR) err ();
    delay (25);
    for(k=1;k<=chnos;k++) {
     delay(60);
     autoscale(k);
      }
sprintf(temp,"%d",avgs);
strcpy(wrt,"ACQ:COUN ");
strcat(wrt,temp);
len=strlen(wrt);
if (ibwrt(scope,"ACQ:TYPE AVER",13) & ERR) err();
if (ibwrt(scope,wrt,len) & ERR) err();
acquire (FFT[i-1][m-1]);
/*strcpy(file,file1);
sprintf(wrt,"%d",m);
strcat(file,wrt);
strcpy(temp3,file);
for (k=1;k<=4;k++) {
strcpy(file,temp3);
sprintf(temp,"%d",k);
strcat(file,temp);
fp=fopen (file,"w");
for (j=1;j<=dps;j++) {
     time=(j-1)*1000/(rffreq*dps) ;
     fprintf(fp,"%le %le\n",time,FFT[i-1][m-1][k-1][j]);
}
fclose(fp);
}*/
}
/*Release GPIB control of the instruments.*/
   if (ibwrt(scope,"RUN",3) & ERR) err();
   if (ibwrt(scope,"BEEP",4) & ERR) err();
   if (ibloc(scope) & ERR) err();
   if (ibonl(scope,0) & ERR) err();
   if (ibloc(SWITCH) & ERR) err();
```

```
   if (ibonl(SWITCH,0) & ERR) err();
s=dps/2;
  for (m=1;m<=2;m++){
   for (k=1;k<=4;k++)  {
    realft(FFT[i-1][m-1][k-1],s,1);
    n=3;
    for (j=2;j<=nhs;j++)    {
       CFFT[i-1][m-1][k-1][j-1].r=FFT[i-1][m-1][k-1][n];
       CFFT[i-1][m-1][k-1][j-1].i=FFT[i-1][m-1][k-1][n+1];
       n+=2;
       }
    }
   }

    strcpy(file,"calf");
    sprintf(wrt,"%d",i);
    strcat(file,wrt);
    if (i>3) {
    strcpy(file,temp6);
    strcat(file,"f");
    }
    strcpy(temp5,file);
   for (m=1;m<=2;m++) {
    strcpy(file,temp5);
    sprintf(wrt,"%d",m);
    strcat(file,wrt);

    strcpy(temp3,file);
    for (k=1;k<=4;k++) {
      strcpy(file,temp3);
      sprintf(temp,"%d",k);
      strcat(file,temp);
      fp=fopen (file,"w");
      for (j=2;j<=nhs;j++) {
        freq=(j-1)*rffreq;
        mag=sqrt(CFFT[i-1][m-1][k-1][j-1].r*CFFT[i-1][m-1][k-1][j-1].r+CFFT[i-
1][m-1][k-1][j-1].i*CFFT[i-1][m-1][k-1][j-1].i);

  fprintf (fp,"%e %e %e\n",freq,CFFT[i-1][m-1][k-1][j-1].r,CFFT[i-1][m-1][k-1][j-
1].i );
      }
      fclose(fp);
    }
   }
  }

/*****************End of Main****************************************/
```

```
/*****************************************************************/



/*****************************************************************/
/* Program: acquirelcd.c.  Copy right: Rodwell Group, ECE Dept., UCSB.        */
/*****************************************************************/
/*****************************************************************/
/*This program acquires the waveforms, using lock-in amplifiers, for calibrating the
2port measurements*/
/*It uses double precesion numbers and has different dynamic reserve and time
constant above 150 GHz */
/*By Ruai Yu.  First version . 12/25/91.*/
/*Two-port NWA Calibration, Measurement, and Switching Routines.*/
/*Revised by J. Pusl 5/92. Second version.*/
/*filename=/home/rlab/pusl/cprog/nwa.c*/
/*Revised by Madhukar Reddy 7/92. Third version.*/
/*revised by Ruai Yu, 5/28/93 */
/*filename=/home/rlab/madhu/2port/2port6.c*/
/*****************************************************************/
/*****************************************************************/
/*****************Include the following standard libraries*****************/
#include <math.h>
#include <stdio.h>
#include <ctype.h>
#include <string.h>
#include <sys/timeb.h>
#include <stdlib.h>
/*****************************************************************/
/*****************Include the following user created libraries***************/

#include "dcomplex.h"

#include "ugpib.h"
/*****************************************************************/
#define PI 3.141592654

extern int ftime();

/*GLOBAL VARIABLES*/
int scope,HP3325,SR530[5],SWITCH,len,chnos,nhs,stim;
static struct timeb tp0,tp1;
char ch[5],trigch[5];

void delay ();
void autosen ();
void acquire ();
```

```
#include "lockin1d.c"  /* This program contains the data acquisition routines with
lock-ins. */

main ()
{
dcomplex S[100][7][5],SDE[100][5],A[5],IA[5],GammaA[100],GammaB[100];
dcomplex CFFT[4][2][4][100],a1[7][2][100],b1[7][2][100];
dcomplex a2[7][2][100],b2[7][2][100];
dcomplex T1,T2,ONE,TWO,THREE;
double L[6],time;
int i,j,k,l,m,n=1,p,s;
char filename[64],wrt[64],file[64],file1[64],temp1[10];
char temp2[10],temp3[10],temp[10],option[10],temp5[10],temp6[10];
double freq,rffreq,re,im,mag,phase,FFT[4][2][5][100][3],angle;
struct device device;
FILE *fp ;

chnos=4;

ONE.r=1;ONE.i=0;
TWO.r=2;TWO.i=0;
THREE.r=3;THREE.i=0;

/*******Ask user to calibrate the system and take the S-parameters*******/
printf("You must have the following set-up:\n");
printf("lockin: 1=port1in, 2=port1out,3=port2in,4=port2out\n");
/*Measure all the Cal Standards and Device Under Test (DUT).*/


printf ("\nPlease enter the RF frequency in GHz:");
scanf("%lf",&rffreq);
nhs=floor(200.0/rffreq);
printf ("\nThe IF frequency must be 1 KHz.\n");
printf("There are 4 measurements to be made: \n");
printf("1) 1 ps Through Line -Enter 1 for measurement #\n");
printf("2) 50 Ohm Matched Load- Enter 2 for measurement #\n");
printf("3) Open or Short as a reference Load-Enter 3 for measurement #\n");
printf("4) DUT Enter 4 for Measurement #\n");
/*****************Set up the instruments*******************************/
/*The RF switch is the HP 11713*/
 printf ("please enter the measurement number!\n");
 scanf("%d",&l);
 if (l>3) {
   i=4;
   }
 else {
   i=l;
```

```
    }
   printf("Ready for Measurement #%d, and press any key to proceed!\n",i);
  scanf("%s",wrt);

 SWITCH=ibfind("hp11713");
 if (SWITCH<0)
 {
   printf ("\nCannot find hp11713 switch.\n");
   err ();
 }

 if (ibllo(SWITCH) & ERR) err();


 /************** address HP3325 *****************/

 HP3325=ibfind("hp3325");
 if (HP3325<0)
 {
         printf("\nCannot find hp3325.\n");
         err ();
 }

 /************** address all four lock-ins *************************/

 SR530[1]=ibfind("sr530");
 if (SR530[1]<0)
 {
         printf("\nCannot find sr530 lock-in.\n");
         err ();
 }

 SR530[2]=ibfind("sr510a");
 if (SR530[2]<0)
 {
         printf("\nCannot find sr510a lock-in.\n");
         err ();
 }

 SR530[3]=ibfind("sr510b");
 if (SR530[3]<0)
 {
         printf ("\nCannot find sr510b lock-in.\n");
         err ();
 }

 SR530[4]=ibfind("sr510c");
 if (SR530[4]<0)
```

```
{
        printf("\nCannot find sr510c lock-in.\n");
        err ();
}

/****************** initialize the lock-in's ******************/
for (p=1;p<=4;p++)
if (ibwrt(SR530[p],"Z",1) & ERR) err ();
delay (5.0); /* wait for the error signal to die down */

for (p=1;p<=4;p++)
if (ibwrt(SR530[p],"I1",2) & ERR ) err ();

for (p=1;p<=4;p++)
if (ibwrt(SR530[p],"L1,1",4) & ERR) err ();

for (p=1;p<=4;p++)
if (ibwrt(SR530[p],"L2,1",4) & ERR) err ;

for (p=1;p<=4;p++)
if (ibwrt(SR530[p],"B1",2) & ERR) err ();

for (p=1;p<=4;p++)
if (ibwrt(SR530[p],"S2",2) & ERR) err ();

/********************** initialize hp3325 ********************/

if (ibwrt(HP3325,"*RST",4) & ERR) err ();
if (ibwrt(HP3325,"AM1VO",5) & ERR) err ();

if (i<=3) {
        strcpy(file1,"calf");
        sprintf(wrt,"%d",i);
        strcat(file1,wrt);
        }
else  {
        printf ("Please enter the name of the file for the dut\n");
        scanf("%s",file1);
        strcat(file1,"f");
        }

for (m=1;m<=2;m++) {
   if(m==1)  {
     if (ibwrt(SWITCH,"B0",2) & ERR) err();
     stim=1;
     }
    else {
      if (ibwrt(SWITCH,"A0",2) & ERR) err();
```

```
      stim=3;
    }
delay (5.0);
acquire (FFT[i-1][m-1]);
}

/*Release GPIB control of the instruments.*/
  /* if (ibwrt(scope,"RUN",3) & ERR) err();
   if (ibwrt(scope,"BEEP",4) & ERR) err();
   if (ibloc(scope) & ERR) err();
   if (ibonl(scope,0) & ERR) err();
   if (ibloc(SWITCH) & ERR) err();
   if (ibonl(SWITCH,0) & ERR) err();*/

for (m=1;m<=2;m++) {
         strcpy(temp1,file1);
    sprintf(wrt,"%d",m);
    strcat(temp1,wrt);
    for (k=1;k<=4;k++) {
      strcpy(file,temp1);
      sprintf(temp,"%d",k);
      strcat(file,temp);
      fp=fopen (file,"w");
      for (j=1;j<=nhs;j++) {
        freq=j*rffreq;
          angle=2*PI*FFT[i-1][m-1][k][j][2]/360;
CFFT[i-1][m-1][k-1][j-1].r=FFT[i-1][m-1][k][j][1]*cos(angle);
CFFT[i-1][m-1][k-1][j-1].i=FFT[i-1][m-1][k][j][1]*sin(angle);
 fprintf (fp,"%le %le %le\n",freq,CFFT[i-1][m-1][k-1][j-1].r,CFFT[i-1][m-1][k-1][j-
1].i );
      }
      fclose(fp);
    }
  }
 }


/*****************End of Main****************************************/
/*******************************************************************/



/*******************************************************************/
/* file name: 1portNWA8.c.  Copy right: Rodwell Group, ECE Dept., UCSB.       */
/*******************************************************************/
/*This program provides control and de-embedding functions for the NWA system to
perform one port measurement with different matrix element normalization*/
/*By Ruai Yu.  First version. 2/14/91.*/
```

```
/*Revised by Madhukar Reddy. 7/15/92.*/
/*filename = /home/rlab/madhu/gpib/1portNWA.c
/*Compile it as follows:
cc  <filename.c>  -L/usr/local/lib -lcomplex -lfourier -lgpib -I/usr/local/include -lm
/******************************************************************/
/******************************************************************/
/**********This program calculates S11 of a 1-Port Network from the**********/
/*******measured time domain waveforms.  The waveforms displayed in********/
/**********HP 54503 scope are first acquired using the autoscale and***********/
/**********acquire subroutines.  The waveforms are first digitized ************/
/**********and the data is acquired in an array of size 2050. The *************/
/**********data is stored in locations starting 1 to 1025 (1024 points)********/
/**********The data is then sent to an FFT subroutine where the DFT ***********/
/**********of the waveform is calculated.  The frequency domain data**********/
/**********is stored in the same array.  The real part of the ith *************/
/**********harmonic is stored in the i+3 location and the imaginary part*******/
/**********in the i+4 location.  For example if the fundamental frequency******/
/**********is 10GHz, the 2nd harmonic component(i.e 20GHz) has a real part****/
/**********in FFT[5] and the imaginary part in FFT[6].  The frequency data*****/
/**********is then utilized in finding the de-embedding functions for the******/
/********NWA system.  S11 of the 1-Port Network(DUT) can then be calculated**/
/******************************************************************/
/*******Include the following standard libraries******/

#include <math.h>
#include <stdio.h>
#include <string.h>
#include <ctype.h>

/******************************************************************/
/*******The following user created libraries should be included.***************/
/****The ugpib.h library supports functions which enable programming of*** ****/
/*******the HP54503 scope using the general purpose interface bus************/
/****The complex.h library is included for the complex algebraic functions*****/
/****The fourier.h library contains the fourier transform function*************/
/****The scope.h library enables autoscaling and acquiring of the time*********/
/*******waveforms on the scope.****************************************/
/****The matrix.h library supports matrix algebra****************************/
/******************************************************************/
#include "ugpib.h"
#include "complex.h"
#include "scope2.c"
#include "fourier.h"
#include "matrix.c"
/******************************************************************/
/*****Decalaration of functions and external variables************************/

void SOL ();
```

```
fcomplex Cdiv1 ();
float vdc,vpp;
int scope,len,chnos;
char ch[5];

/*************************** BEGIN OF MAIN ************************/

main ()
{
fcomplex  S11,CFFT[50][3][5],Gs[50],Go[50],Gl[50],A1,A2,A3;
fcomplex T1,T2,SA1[50],SA2[50],SA3[50];
int i,j,k,n,p=1,points,count,dps,s;
char fent[64],file[64],file1[64],file2[64],temp[10],wrt[100];
float time,freq,f,w,Ls,C,Ll,FFT[4][4][2050];
float SR,SI,SR1,SI1,SR2,SI2,SR3,SI3,MAG,PHASE;
struct device device;
FILE *fp ;

/**************** Measurement Set up********/

printf("this program will find S11 using the NWA chip\n");
printf("you must have the following set-up:\n");
printf("scope channel 1=port_in, 2=port_out\n");
printf("scope triger=channel 1.\ntimebase=0.1ms.\n");
printf("IF frequency=10 KHz.\n");
printf("please enter the RF frequence in GHz.\n");
scanf("%f",&f);
printf("\nPlease enter # of data points (power of 2)\n");
scanf("%d",&dps);

/*****************Initializing the scope ******************************/
/*measure all the Cal Standards and Device Under Test.*/

printf ("Ready to perform calibration.\n");
printf("Perform Calibration in the following order:\n");
printf ("Cal #1=short;                    Cal #2=open;            Cal #3=load.\n");

chnos=2;
scope=ibfind("hp54503");
if (scope < 0)
{
  printf ("\nCannot find hp54503 scope.\n");
  err ();
}
ioctl(scope,IBGET,&device);
device.d_tmo=TNONE;
ioctl(scope,IBSET,&device);
if (ibllo(scope) & ERR) err ();
```

```
if (ibwrt(scope,"BEEP",4) & ERR) err ();
if (ibwrt(scope,"EOI ON",6) & ERR) err ();
if (ibwrt(scope,"SYST:HEAD OFF",13) & ERR) err ();
if (ibwrt(scope,"WAV:FORM ASC",12) & ERR) err();
sprintf(temp,"%d",dps);
strcpy(wrt,"ACQ:POIN ");
strcat(wrt,temp);
len=strlen(wrt);
if (ibwrt(scope,wrt,len) & ERR) err();
if (ibwrt(scope,"ACQ:TYPE AVER",13) & ERR) err();
if (ibwrt(scope,"ACQ:COUN 256",12) & ERR) err();

/*******************************************************************/

/********Measure the Calibration standards and the Device Under
Test(DUT)in****/
/********the following order. 1-Short; 2-Open; 3-50 ohm Load; 4-
DUT;***********/
/*******************************************************************/
strcpy(file1,"calt");
strcpy(file2,"calf");

for (i=1;i<=3;i++)  {
  printf ("please measure Cal Standard#%d, and press any key to proceed!\n",i);
  scanf("%s",temp);
if (ibllo(scope) & ERR) err ();
    if (ibwrt(scope,":AUT",4) & ERR) err();
  delay(50);
  if (ibwrt(scope,":TIM:MODE TRIG;RANG 0.1MS;REF CENT;DEL 0MS",42) &
ERR) err();
  delay(15);
  if (ibwrt(scope,":TRIG:MODE EDGE;SLOP POS;HOLD TIME,0.19MS;SENS
LOW",50) & ERR) err ();
  delay(15);
if (ibwrt(scope,"ACQ:TYPE AVER",13) & ERR) err();
if (ibwrt(scope,"ACQ:COUN 256",12) & ERR) err();
delay(30);
  for(k=1;k<=chnos;k++) {
    delay(50);
    autoscale(k);
  }
  acquire (FFT[i-1]);

/*save the time waveforms if desired*/
/*  for (k=1;k<=2;k++)  {
  sprintf(wrt,"%d",i);
  strcpy(file,file1);
  strcat(file,wrt);
```

```
  sprintf(temp,"%d",k);
  strcat(file,temp);
  fp=fopen(file,"w");
  for (j=1;j<=1024;j++)
        fprintf(fp,"%e\n",FFT[i-1][k-1][j]);
  fclose(fp);
  }*/

      if (ibwrt(scope,"RUN",3) & ERR) err();
      if (ibwrt(scope,"BEEP",4) & ERR) err();
      if (ibloc(scope) & ERR) err();
}

/***Fourier transform the cal standard time waveforms.*/
s=dps/2;
for (i=1;i<=3;i++) {
  for (k=1;k<=2;k++)  {
    realft(FFT[i-1][k-1],s,1);
    n=1;
    for (j=1;j<=50;j++)    {
      CFFT[j-1][k][i].r=FFT[i-1][k-1][n];
      CFFT[j-1][k][i].i=FFT[i-1][k-1][n+1];
      n+=2;
    }

/*save the frequency waveforms.*/
/*sprintf(wrt,"%d",i);
strcpy(file,file2);
strcat(file,wrt);
sprintf(temp,"%d",k);
strcat(file,temp);
fp=fopen (file,"w");
for (j=1;j<=50;j++) {
     freq=(j-1)*f;
     SR=CFFT[j-1][k][i].r;
     SI=CFFT[j-1][k][i].i;
     fprintf(fp,"%le %le %le\n",freq,SR,SI);
     }
     fclose(fp); */

  }
}

printf ("Calibration completed.  Measure DUT next\n");

dut:            /*Label for goto dut statement*/

printf  ("please measure Device Under Test, and press any key to proceed!\n",i);
```

```
scanf("%s",temp);
printf("\nplease enter the filename for data storage\n");
scanf ("%s",fent);
if (ibllo(scope) & ERR) err ();
 if (ibwrt(scope,":AUT",4) & ERR) err();
delay(50);
if (ibwrt(scope,":TIM:MODE TRIG;RANG 0.1MS;REF CENT;DEL 0MS",42) &
ERR) err();
delay(15);
if (ibwrt(scope,":TRIG:MODE EDGE;SLOP POS;HOLD TIME,0.19MS;SENS
LOW",50) & ERR)    err ();
delay(15);
if (ibwrt(scope,"ACQ:TYPE AVER",13) & ERR) err();
if (ibwrt(scope,"ACQ:COUN 256",12) & ERR) err();
delay(30);
for(k=1;k<=chnos;k++) {
  delay(50);
  autoscale(k);
}
acquire (FFT[3]);

/*save the time waveforms if desired.*/
/*printf("please enter the filename for saving the DUT raw data.\n");
scanf("%s",file1);
strcpy(file2,file1);
strcat(file1,"t");
strcat(file2,"f");
for (k=1;k<=2;k++) {
strcpy(file,file1);
sprintf(temp,"%d",k);
strcat(file,temp);
fp=fopen (file,"w");
for (j=1;j<=1024;j++)
      fprintf(fp,"%le\n",FFT[3][k-1][j]);
fclose(fp);
}*/

      if (ibwrt(scope,"RUN",3) & ERR) err();
      if (ibwrt(scope,"BEEP",4) & ERR) err();
      if (ibloc(scope) & ERR) err();

/*Fourier Transform of the DUT time waveforms.*/

i=4;
for (k=1;k<=2;k++)  {
  realft(FFT[i-1][k-1],s,1);
  n=1;
  for (j=1;j<=50;j++)    {
```

```
    CFFT[j-1][k][i].r=FFT[i-1][k-1][n];
    CFFT[j-1][k][i].i=FFT[i-1][k-1][n+1];
    n+=2;
  }
}
/*save the DUT frequency data.*/
/*for (k=1;k<=2;k++) {
strcpy(file,file2);
sprintf(temp,"%d",k);
strcat(file,temp);
fp=fopen (file,"w");
for (j=1;j<=50;j++) {
     freq=(j-1)*f;
     SR=CFFT[j-1][k][4].r;
     SI=CFFT[j-1][k][4].i;
     fprintf(fp,"%le %le %le\n",freq,SR,SI);
     }
     fclose(fp);
} */
if (p==20) goto calc;   /*Skip De-embedding if done already**/

/**************************De-embedding.****************************/

printf("Please enter Ls for Cal (in pH).\n");
scanf("%e",&Ls);
printf("please enter Copen for Cal (in fF).\n");
scanf("%e",&C);
printf("please enter Lload for Cal (in pH).\n");
scanf("%e",&Ll);
Ls=Ls*1E-3;
C=C*1E-6;
Ll=Ll*1E-3;
w=f*2*3.141592653589793;

/*fp=fopen("matrix","w");      */
for (j=1;j<=50;j++) {
  T1.r=-50;
  T2.r=50;
  T1.i=T2.i=(j-1)*w*Ls;
  Gs[j-1]=Cdiv1(T1,T2);
  T1.r=T2.r=1;
  T1.i=-50*(j-1)*w*C;
  T2.i=50*(j-1)*w*C;
  Go[j-1]=Cdiv1(T1,T2);
  T1.r=0;
  T2.r=100;
  T1.i=T2.i=(j-1)*w*Ll;
  Gl[j-1]=Cdiv1(T1,T2);
```

```
  SOL(&A1,&A2,&A3,CFFT[j-1],Gs[j-1],Go[j-1],Gl[j-1]);
  SA1[j-1].r=A1.r;
  SA1[j-1].i=A1.i;
  SA2[j-1].r=A2.r;
  SA2[j-1].i=A2.i;
  SA3[j-1].r=A3.r;
  SA3[j-1].i=A3.i;
     SR1=A1.r;
     SI1=A1.i;
     SR2=A2.r;
     SI2=A2.i;
     SR3=A3.r;
     SI3=A3.i;
/*     fprintf(fp,"%le %le %le %le %le %le\n",SR1,SI1,SR2,SI2,SR3,SI3); */
}
/*fclose(fp); */

/*save the results.*/

calc:
strcpy(file,fent);
strcat(file,".s1p");
fp=fopen(file,"w");
fprintf(fp,"# GHZ S MA R 50\n");
for (j=2;j<=50;j++) {
  S11=Cdiv1(Csub(Cmul(CFFT[j-1][1][4],SA2[j-1]),CFFT[j-
1][2][4]),Csub(Cmul(CFFT[j-1][2][4],SA1[j-1]),Cmul(CFFT[j-1][1][4],SA3[j-1])));
  freq=(j-1)*f;
  SR=S11.r;
  SI=S11.i;
  MAG=sqrt(SR*SR+SI*SI);
  PHASE=atan2(SI,SR)*180/3.141592653589793;
  fprintf(fp,"%le  %le  %le\n",freq,MAG,PHASE);
}
fclose(fp);
printf ("Do you want to measure other device using the same cal?");
scanf ("%s",wrt);
if (wrt[0] != 'n' && wrt[0] != 'N') {
  p=2;
  goto dut;
}
else {
  printf("Do you want to start over?");
  scanf ("%s",wrt);
  if (wrt[0] != 'n' && wrt[0] != 'N') main ();
  else {
     /*release GPIB control of the instruments.*/
     if (ibwrt(scope,"RUN",3) & ERR) err();
```

```
      if (ibwrt(scope,"BEEP",4) & ERR) err();
      if (ibloc(scope) & ERR) err();
      if (ibonl(scope,0) & ERR) err();
    }
  }
}
/**************************END OF MAIN****************************/


/*************************BEGIN SUBROUTINES*********************/

/*********************** SOL Calibration Routine ***********************/
/*This program performs the SOL calibration procedures based on the measured s-
parameteers.1/17/91*/

void SOL(A1,A2,A3,IF,Gs,Go,Gl)
fcomplex *A1,*A2,*A3,IF[3][5],Gs,Go,Gl;

{
fcomplex A,NEG;
fcomplex B[4][4],D[4][2],T[4][2];
int i,j;

NEG.r=-1.0;
NEG.i=0;

B[1][1]=Cmul(IF[2][1],Gs);
B[1][2]=Cmul(NEG,IF[1][1]);
B[1][3]=Cmul(Cmul(NEG,IF[1][1]),Gs);
B[2][1]=Cmul(IF[2][2],Go);
B[2][2]=Cmul(NEG,IF[1][2]);
B[2][3]=Cmul(Cmul(NEG,IF[1][2]),Go);
B[3][1]=Cmul(IF[2][3],Gl);
B[3][2]=Cmul(NEG,IF[1][3]);
B[3][3]=Cmul(Cmul(NEG,IF[1][3]),Gl);
D[1][1]=Cmul(NEG,IF[2][1]);
D[2][1]=Cmul(NEG,IF[2][2]);
D[3][1]=Cmul(NEG,IF[2][3]);
DET(&A,B);

for (i=1;i<=3;i++) {
  T[i][1]=B[i][1];
  B[i][1]=D[i][1];
}
DET(A1,B);
for (i=1;i<=3;i++) {
  B[i][1]=T[i][1];
  T[i][1]=B[i][2];
```

```
  B[i][2]=D[i][1];
}
DET(A2,B);
for (i=1;i<=3;i++) {
  B[i][2]=T[i][1];
  T[i][1]=B[i][3];
  B[i][3]=D[i][1];
}
DET(A3,B);

if ((A.r==0) && (A.i==0)) printf ("Calibration cannot be performed due to zero
determinant.\n");
else {
    *A1=Cdiv1(*A1,A);
    *A2=Cdiv1(*A2,A);
    *A3=Cdiv1(*A3,A);
}
}

/********************SUBROURINE Cdiv1 ****************************/
fcomplex Cdiv1(a,b)
fcomplex a,b;
{
  fcomplex c;
  float den;

        den=b.r*b.r+b.i*b.i;
        c.r=(a.r*b.r+a.i*b.i)/den;
        c.i=(a.i*b.r-a.r*b.i)/den;
        return c;
}

/*************************END OF SUBROUTINES*******************/

/******************************************************************/
/* Program: TWOPORT2.c.  Copy right: Rodwell Group, ECE Dept., UCSB.     **/
/******************************************************************/
/*This program provides de-embedding functions for the NWA system using LRL
calibration.*/
/*By Ruai Yu.  First version . 12/25/91.*/
/*Two-port NWA Calibration, Measurement, and Switching Routines.*/
/*LRL Calibration.*/
/*Revised by J. Pusl 5/92. Second version.*/
/*filename=/home/rlab/pusl/cprog/nwa.c*/
/*Revised by Madhukar Reddy 7/92. Third version.*/
/*filename=/home/rlab/madhu//gpib/2port/TWOPORT2.c*/
/******************************************************************/
/******************************************************************/
```

```
/*****************Include the following standard libraries******************/
#include <math.h>
#include <stdio.h>
#include <ctype.h>
#include <string.h>
/******************************************************************/
/*****************Include the following user created libraries**************/
#include "complex.h"
#include "fourier.h"
#include "matrix.c"
/******************************************************************/
#define PI 3.141592654

void LRL();
void Rpa();



main ()
{
fcomplex S[100][7][5],SDE[100][5],A[5],IA[5],GammaA[100],GammaB[100];
fcomplex CFFT[7][2][4][100],a1[7][2][100],b1[7][2][100];
fcomplex a2[7][2][100],b2[7][2][100];
fcomplex T1,T2,ONE,TWO,THREE,FOUR,FIVE,TWENTYONE;
float L[6];
int i,j,k,m,n=1,s,dps,nhs;
char filename[64],wrt[64],file[64],file1[64],temp1[10];
char temp2[10],temp3[10],temp[10];
float freq,rffreq,re,im,mag,phase;
float  time,FFT[7][2][4][2050];
FILE *fp ;


ONE.r=1;ONE.i=0;
TWO.r=2;TWO.i=0;
THREE.r=3;THREE.i=0;
FOUR.r=4.0;FOUR.i=0.0;
FIVE.r=5.0;FIVE.i=0.0;
TWENTYONE.r=21.0;TWENTYONE.i=0.0;
L[1]=300;
L[2]=2450;
L[3]=1080;
L[4]=585;
L[5]=460;
```

```
printf ("\nPlease enter the RF frequency in GHz:");
scanf("%f",&rffreq);
nhs=floor(370.0/rffreq);
printf("\nPlease enter # of data points (power of 2)\n");
scanf("%d",&dps);
for (i=1;i<=7;i++) {
    if(i==7) {
    printf("\nPlease enter the file name for the dut\n");
    scanf("%s",file1);
    }
    else {
    strcpy(file1,"calt");
    sprintf(wrt,"%d",i);
    strcat(file1,wrt);
    }
    strcpy(temp1,file1);
    for (m=1;m<=2;m++) {
    sprintf(wrt,"%d",m);
    strcpy(file,temp1);
    strcat(file,wrt);
    strcpy(temp3,file);
    for (k=1;k<=4;k++) {
      strcpy(file,temp3);
      sprintf(temp,"%d",k);
      strcat(file,temp);
      fp=fopen (file,"r");
      for (j=1;j<=dps;j++) {
        fscanf (fp,"%e %e\n",&time,&FFT[i-1][m-1][k-1][j]);
      }
      fclose(fp);
    }
  }
}

/*Fourier Transform cal standard time waveforms.
Count variables: i=measurement #, j=harmonic #(1-30 for 300 GHz),
            k=scope channel 1-4, m=IF port 1 or 2.        */
s=dps/2;
for (i=1;i<=7;i++) {
  for (m=1;m<=2;m++){
    for (k=1;k<=4;k++)  {
     realft(FFT[i-1][m-1][k-1],s,1);
     n=3;
     for (j=2;j<=nhs;j++)    {
        CFFT[i-1][m-1][k-1][j-1].r=FFT[i-1][m-1][k-1][n];
        CFFT[i-1][m-1][k-1][j-1].i=FFT[i-1][m-1][k-1][n+1];
        n+=2;
        }
```

```
      }
     }
   }
for (i=1;i<=7;i++) {
  for (m=1;m<=2;m++) {
    strcpy(file,"calf");
    sprintf(wrt,"%d",i);
    strcat(file,wrt);
    sprintf(wrt,"%d",m);
    strcat(file,wrt);
    strcpy(temp3,file);
    for (k=1;k<=4;k++) {
      strcpy(file,temp3);
      sprintf(temp,"%d",k);
      strcat(file,temp);
      fp=fopen (file,"w");
      for (j=2;j<=nhs;j++) {
        freq=(j-1)*rffreq;
        mag=sqrt(CFFT[i-1][m-1][k-1][j-1].r*CFFT[i-1][m-1][k-1][j-1].r+CFFT[i-
1][m-1][k-1][j-1].i*CFFT[i-1][m-1][k-1][j-1].i);
        fprintf (fp,"%e %e %e\n",freq,CFFT[i-1][m-1][k-1][j-1].r,CFFT[i-1][m-1][k-
1][j-1].i );
      }
      fclose(fp);
    }
   }
}


/*Calculate all the forward and reverse waves at the two ports for the
first 30 frequency points. 30th freq point=300 GHz for 10 GHz fundamental
T1 and T2 are the Attenuator constants for the forward and reverse waves*/

T1=Cdiv(TWO,TWENTYONE);
T2=Cdiv(FIVE,TWENTYONE);
for (j=2;j<=nhs;j++)  {
 for (i=1;i<=7;i++)  {
  for (m=1;m<=2;m++) {
    a1[i-1][m-1][j-1]=Cmul(T1,Csub(Cmul(FIVE,CFFT[i-1][m-
1][0][j-1]),Cmul(TWO,CFFT[i-1][m-1][1][j-1])));
    b1[i-1][m-1][j-1]=Cmul(T2,Csub(Cmul(FIVE,CFFT[i-1][m-
1][1][j-1]),Cmul(TWO,CFFT[i-1][m-1][0][j-1])));
    a2[i-1][m-1][j-1]=Cmul(T1,Csub(Cmul(FIVE,CFFT[i-1][m-
1][2][j-1]),Cmul(TWO,CFFT[i-1][m-1][3][j-1])));
    b2[i-1][m-1][j-1]=Cmul(T2,Csub(Cmul(FIVE,CFFT[i-1][m-
1][3][j-1]),Cmul(TWO,CFFT[i-1][m-1][2][j-1])));
    }
```

```
/*Calculate the S-parameters.*/

    A[1]=a1[i-1][0][j-1];
    A[2]=a1[i-1][1][j-1];
    A[3]=a2[i-1][0][j-1];
    A[4]=a2[i-1][1][j-1];
    Inv(A,IA);
    /*s11*/  S[j-1][i-1][1]=Cadd(Cmul(IA[1],b1[i-1][0][j-1]),Cmul(IA[3],b1[i-1][1][j-
1]));
    /*s12*/  S[j-1][i-1][2]=Cadd(Cmul(IA[2],b1[i-1][0][j-1]),Cmul(IA[4],b1[i-1][1][j-
1]));
    /*s21*/  S[j-1][i-1][3]=Cadd(Cmul(IA[1],b2[i-1][0][j-1]),Cmul(IA[3],b2[i-1][1][j-
1]));
    /*s22*/  S[j-1][i-1][4]=Cadd(Cmul(IA[2],b2[i-1][0][j-1]),Cmul(IA[4],b2[i-1][1][j-
1]));
    }
  GammaA[j-1]=Cdiv(b1[5][0][j-1],a1[5][0][j-1]);
  GammaB[j-1]=Cdiv(b2[5][1][j-1],a2[5][1][j-1]);
  }


/*De-embedding. 'SDE' are the de-embedded S-parameters.  */
  j=2.0;
  while((j-1)*rffreq<=30.0) {
    LRL(SDE[j-1],S[j-1][0],S[j-1][1],S[j-1][6],GammaA[j-1],GammaB[j-
1],L[1],L[2]);
    j++;
    }
  while((j-1)*rffreq<=90.0) {
    LRL(SDE[j-1],S[j-1][0],S[j-1][2],S[j-1][6],GammaA[j-1],GammaB[j-
1],L[1],L[3]);
    j++;
    }
  while((j-1)*rffreq<=270.0) {
    LRL(SDE[j-1],S[j-1][0],S[j-1][3],S[j-1][6],GammaA[j-1],GammaB[j-
1],L[1],L[4]);
    j++;
    }

  while((j-1)*rffreq<=370.0) {
    LRL(SDE[j-1],S[j-1][0],S[j-1][4],S[j-1][6],GammaA[j-1],GammaB[j-
1],L[1],L[5]);
    j++;
    }
/*Save the results to a file.*/
```

```
printf ("\nPlease enter the filename for data storage:");
scanf ("%s",filename);
strcat(filename,".s2p");
fp=fopen(filename,"w");
fprintf(fp,"# GHZ S RI R 50\n");
for (j=2;j<=nhs;j++) {
  freq=(j-1)*rffreq;              /*freq is in GHz now*/
  fprintf(fp,"%e  %e  %e",freq,SDE[j-1][1].r,SDE[j-1][1].i);
  fprintf(fp,"  %e  %e",SDE[j-1][2].r,SDE[j-1][2].i);
  fprintf(fp,"  %e  %e",SDE[j-1][3].r,SDE[j-1][3].i);
  fprintf(fp,"  %e  %e\n",SDE[j-1][4].r,SDE[j-1][4].i);
  }
fclose(fp);
   }
/*****************End of Main***************************************/
/******************************************************************/

/*****************Subroutines***************************************/
/******************************************************************/
/****************R-parameter from S-parameter extraction
(conversion)**********/
/******************************************************************/

void Rpa(R, SQ)
fcomplex R[5],SQ[5];
{
fcomplex temp1,NEG,ONE;
NEG.r=-1.0;
NEG.i=0.0;
ONE.r=1.0;
ONE.i=0.0;

R[1]= Cdiv((Csub(Cmul(SQ[2],SQ[3]),Cmul(SQ[1],SQ[4]))),SQ[3]);
R[2]= Cdiv(SQ[1],SQ[3]);
temp1=Cmul(NEG,SQ[4]);
R[3]= Cdiv(temp1,SQ[3]);
R[4]= Cdiv(ONE,SQ[3]);
}

/************************ End of Rpa Subroutine ***********************/
/******************************************************************/

/*********************** LRL Calibration Subroutine ********************/
/******************************************************************/

void LRL( SP, SL, SLP, SD, GammaA, GammaB,L1,L2)
fcomplex SP[5],SL[5],SLP[5],SD[5],GammaA,GammaB;
float L1,L2;
```

```
{
fcomplex
R[5],R1[5],RL[5],RLP[5],RD[5],T[5],IRL[5],A[5],B[5],ALB[5],IA[5],IB[5],X[5],Te
mp[5];
fcomplex g1,g2,G1,G2,b,c,d,x1,x2,temp,t1,t2,t3,t4,ONE,TWO,NEG,K,KL;
int j;
float phtemp,phA1,pht1,theta1,theta2;
ONE.r=1;ONE.i=0;
TWO.r=2.0;TWO.i=0.0;
NEG.r=-1;NEG.i=0;

/*Convert the S-parameters into R-parameters.*/

for (j=1;j<=4;j++) SP[j]=SL[j];
 Rpa(R,SP);
for (j=1;j<=4;j++) RL[j]=R[j];

for (j=1;j<=4;j++) SP[j]=SLP[j];
 Rpa(R,SP);
for (j=1;j<=4;j++) RLP[j]=R[j];

for (j=1;j<=4;j++) SP[j]=SD[j];
 Rpa(R,SP);
for (j=1;j<=4;j++) RD[j]=R[j];

/*calculate [T]=[RLP][RL]-1.*/
Inv(RL,IRL);
Mul(T,RLP,IRL);
/*Solve for g.*/
b=Cdiv( Cadd(T[1],T[4]),TWO);
c=Csub(Cmul(T[1],T[4]),Cmul(T[2],T[3]));
d=Csub(ONE,Cdiv(c,Cmul(b,b)));
g1=Cmul(b,Cadd(ONE,Csqrt(d)));
g2=Cdiv(ONE,g1);

/*Calculate x1 and x2.*/
if ( g1.i<0) {
 G1=g1;
 G2=g2;
 }
else    {
 G1=g2;
 G2=g1;
 }
x1=Cdiv(T[3],Csub(G1,T[4]));
x2=Cdiv(T[2],Csub(G2,T[1]));

/*Calculate the propagation constant k for the calibration line.*/
```

```
K.r=(1/(L2-L1))*log(sqrt(G2.r*G2.r+G2.i*G2.i));
K.i=(1/(L2-L1))*atan(G2.i/G2.r);
if(G2.r<0) {
 K.i=(PI+K.i*(L2-L1))/(L2-L1);
  }

KL.r=exp(K.r*L1)*cos(K.i*L1);
KL.i=exp(K.r*L1)*sin(K.i*L1);

/*Calculate A[1].*/
ALB[1]=Cdiv(RL[1],RL[4]);
ALB[2]=Cdiv(RL[2],RL[4]);
ALB[3]=Cdiv(RL[3],RL[4]);
temp=Cdiv(Csub(ALB[2],x2),Csub(ALB[1],Cmul(x2,ALB[3])));
B[3]=Cdiv(Csub(ALB[3],Cmul(ALB[1],x1)),Csub(ONE,Cmul(ALB[2],x1)));
t1=Cmul(Csub(GammaA,x2),Cadd(ONE,Cmul(temp,GammaB)));
t2=Cmul(Csub(ALB[1],Cmul(x2,ALB[3])),Cmul(KL,KL));
t3=Cmul(Cadd(GammaB,B[3]),Csub(ONE,Cmul(GammaA,x1)));
t4=Csub(ONE,Cmul(ALB[2],x1));
A[1]=Csqrt(Cdiv(Cmul(t1,t2),Cmul(t3,t4)));
temp=Cdiv(Csub(GammaA,x2),Cmul(NEG,Csub(ONE,Cmul(GammaA,x1))));
t1=Cmul(NEG,A[1]);
phA1=atan2(A[1].i,A[1].r);
pht1=atan2(t1.i,t1.r);
phtemp=atan2(temp.i,temp.r);
if (phA1<=0.0) {
  phA1=2.0*PI+phA1;
  }
if (pht1<=0.0) {
  pht1=2.0*PI+pht1;
  }
if (phtemp<=0.0) {
  phtemp=2.0*PI+phtemp;
  }
theta1=phA1-phtemp;
theta2=phtemp-pht1;
 if (fabs(theta1)>PI) {
  theta1=2.0*PI-fabs(theta1);
  }
if (fabs(theta2)>PI) {
  theta2=2.0*PI-fabs(theta2);
  }
 if (theta1>theta2) {
 A[1]=t1;

 }
/*Calculate the rest of the elements of A and B.*/
A[2]=x2;
```

```
A[3]=Cmul(A[1],x1);
A[4]=ONE;
t1=Cmul(Cmul(KL,KL),Csub(ALB[1],Cmul(x2,ALB[3])));
t2=Cmul(A[1],Csub(ONE,Cmul(ALB[2],x1)));
B[1]=Cdiv(t1,t2);
t1=Cmul(Cmul(KL,KL),Csub(ALB[2],x2));
B[2]=Cdiv(t1,t2);
B[4]=ONE;


/*Calculate the de-embedded R.*/
Inv(A,IA);
Inv(B,IB);
Mul(R1,RD,IB);
Mul(R,IA,R1);

temp=Cdiv(Cadd(KL,Cmul(A[3],Cmul(B[2],Cdiv(ONE,KL)))),RL[4]);
R[1]=Cmul(temp,R[1]);
R[2]=Cmul(temp,R[2]);
R[3]=Cmul(temp,R[3]);
R[4]=Cmul(temp,R[4]);

/*Calculate the de-embedded S-parameters.*/
SP[1]=Cdiv(R[2],R[4]);
SP[2]=Cdiv(Csub(Cmul(R[1],R[4]),Cmul(R[2],R[3])),R[4]);
SP[3]=Cdiv(ONE,R[4]);
SP[4]=Cdiv(Cmul(NEG,R[3]),R[4]);
}
/********** End of LRL Calibration Subroutine*******************/
/**********************************************************/

/***************End of 2-port NWA program**********************/



/*****************************************************************/
/* Program: LRM2port8.c.  Copy right: Rodwell Group, ECE Dept., UCSB.        */
/*****************************************************************/
/*This program provides control and de-embedding functions for the NWA system.*/
/*Two-port NWA Calibration, Measurement, and Switching Routines.*/
/*LRM Calibration.*/
/*****************************************************************/
/*****************Include the following standard libraries******************/
#include <math.h>
#include <stdio.h>
#include <ctype.h>
#include <string.h>
/*****************************************************************/
```

```
/*******************Include the following user created libraries*************/
#include "complex.h"
#include "matrix.c"
/*************************************************************/
#define PI 3.141592654

void LRM();
void Rpa();

main ()
{
fcomplex S[100][4][5],SDE[100][5],A[5],IA[5],GammaA[2][100],GammaB[2][100];
fcomplex CFFT[4][2][4][100],Gl[100],g1[100];
fcomplex a1[4][2][100],b1[4][2][100],a2[4][2][100],b2[4][2][100];
fcomplex T1,T2,T3,T4,ONE,TWO,THREE,FOUR,FIVE,TWENTYONE,NEG;
fcomplex cap,openref;
int i,j,k,m,n,r,s,dps,nhs,z;
char filename[64],wrt[64],file[64],file1[64],temp[64],temp5[64],temp6[64];
float freq,rffreq,Re,Im,mag,phase,w,Ll,C;
float  time,FFT[4][2][4][2050];
FILE *fp ;


ONE.r=1;ONE.i=0;
TWO.r=2;TWO.i=0;
THREE.r=3;THREE.i=0;
FOUR.r=4.0;FOUR.i=0.0;
FIVE.r=5.0;FIVE.i=0.0;
TWENTYONE.r=21.0;TWENTYONE.i=0.0;
NEG.r=-1;NEG.i=0;

Ll=0.0075;

printf("\nIf the dut is a 1-port enter 1. If the dut is a 2-port enter 2.\n");
scanf("%d",&z);
printf ("\nPlease enter the RF frequency in GHz:");
scanf("%f",&rffreq);
nhs=floor(300.0/rffreq);
/*printf("\nPlease enter # of data points (power of 2)\n");
scanf("%d",&dps);     */
for (i=1;i<=4;i++) {
    if (i==4) {
      printf("Please enter the filename for the dut\n");
      scanf("%s",file1);
      }
    else {
      strcpy(file1,"calf");
      sprintf(wrt,"%d",i);
```

```
       strcat(file1,wrt);
       }
     strcpy(temp5,file1);
     for (m=1;m<=2;m++) {
     strcpy(file,temp5);
     sprintf(wrt,"%d",m);
     strcat(file,wrt);
     strcpy(temp6,file);
     for (k=1;k<=4;k++) {
       strcpy(file,temp6);
       sprintf(temp,"%d",k);
       strcat(file,temp);
       fp=fopen (file,"r");
       for (j=2;j<=nhs;j++) {
         fscanf (fp,"%e %e %e\n",&time,&CFFT[i-1][m-1][k-1][j-1].r,&CFFT[i-1][m-
1][k-1][j-1].i);
         }
       fclose(fp);
      }
    }
 }
/* Set some data files to zero if the dut is a 1-port*/
if (z==1) {
  for (j=2;j<=nhs;j++) {
     CFFT[3][0][2][j-1].r=0.0;
     CFFT[3][0][2][j-1].i=0.0;
     CFFT[3][0][3][j-1].r=0.0;
     CFFT[3][0][3][j-1].i=0.0;
     CFFT[3][1][0][j-1].r=0.0;
     CFFT[3][1][0][j-1].i=0.0;
     CFFT[3][1][1][j-1].r=0.0;
     CFFT[3][1][1][j-1].i=0.0;
     }
  }

/*Calculate all the forward and reverse waves at the two ports for the
first 30 frequency points.  30th freq point=300 GHz for 10 GHz fundamental
T1 and T2 are the Attenuator constants for the forward and reverse waves*/

T1=Cdiv(TWO,TWENTYONE);
T2=Cdiv(FIVE,TWENTYONE);
for (j=2;j<=nhs;j++)  {
 for (i=1;i<=4;i++)   {
   for (m=1;m<=2;m++)  {
/*     a1[i-1][m-1][j-1]=Cmul(T1,Csub(Cmul(FIVE,CFFT[i-1][m-
1][0][j-1]),Cmul(TWO,CFFT[i-1][m-1][1][j-1]))); */
         a1[i-1][m-1][j-1]=CFFT[i-1][m-1][0][j-1];
/*     b1[i-1][m-1][j-1]=Cmul(T2,Csub(Cmul(FIVE,CFFT[i-1][m-
```

```
1][1][j-1]),Cmul(TWO,CFFT[i-1][m-1][0][j-1]))); */
        b1[i-1][m-1][j-1]=Cmul(NEG,CFFT[i-1][m-1][1][j-1]);
/*    a2[i-1][m-1][j-1]=Cmul(T1,Csub(Cmul(FIVE,CFFT[i-1][m-
1][2][j-1]),Cmul(TWO,CFFT[i-1][m-1][3][j-1]))); */
        a2[i-1][m-1][j-1]=CFFT[i-1][m-1][2][j-1];
/*    b2[i-1][m-1][j-1]=Cmul(T2,Csub(Cmul(FIVE,CFFT[i-1][m-
1][3][j-1]),Cmul(TWO,CFFT[i-1][m-1][2][j-1]))); */
        b2[i-1][m-1][j-1]=Cmul(NEG,CFFT[i-1][m-1][3][j-1]);
    }

/*Calculate the S-parameters.*/

   A[1]=a1[i-1][0][j-1];
   A[2]=a1[i-1][1][j-1];
   A[3]=a2[i-1][0][j-1];
   A[4]=a2[i-1][1][j-1];
   Inv(A,IA);
   /*s11*/  S[j-1][i-1][1]=Cadd(Cmul(IA[1],b1[i-1][0][j-1]),Cmul(IA[3],b1[i-1][1][j-
1]));
   /*s12*/  S[j-1][i-1][2]=Cadd(Cmul(IA[2],b1[i-1][0][j-1]),Cmul(IA[4],b1[i-1][1][j-
1]));
   /*s21*/  S[j-1][i-1][3]=Cadd(Cmul(IA[1],b2[i-1][0][j-1]),Cmul(IA[3],b2[i-1][1][j-
1]));
   /*s22*/  S[j-1][i-1][4]=Cadd(Cmul(IA[2],b2[i-1][0][j-1]),Cmul(IA[4],b2[i-1][1][j-
1]));
   }
  GammaA[0][j-1]=Cdiv(b1[1][0][j-1],a1[1][0][j-1]);
  GammaB[0][j-1]=Cdiv(b2[1][1][j-1],a2[1][1][j-1]);
  GammaA[1][j-1]=Cdiv(b1[2][0][j-1],a1[2][0][j-1]);
  GammaB[1][j-1]=Cdiv(b2[2][1][j-1],a2[2][1][j-1]);
  w=2*PI*(j-1)*rffreq;
  T3.r=0;
  T4.r=100;
  T3.i=T4.i=w*Ll;
  Gl[j-1]=Cdiv(T3,T4);
  g1[j-1].r=cos(w*0.001);
  g1[j-1].i=sin(w*0.001);
  }


printf("Please enter the capacitance for the open\n");
scanf("%f",&C);
/*De-embedding. 'SDE' are the de-embedded S-parameters.  */
   for (j=2;j<=nhs;j++) {
        cap.r=0.0;
        cap.i=2*PI*(j-1)*rffreq*50*C*1e-6;
        openref=Cdiv(Csub(ONE,cap),Cadd(ONE,cap));
```

```
        LRM(SDE[j-1],S[j-1][0],S[j-1][3],GammaA[0][j-1],GammaA[1][j-
1],GammaB[0][j-1],GammaB[1][j-1],Gl[j-1],g1[j-1],z,openref);
   }
/*Save the results to a file.*/

printf ("\nPlease enter the filename for data storage:");
scanf ("%s",filename);
strcat(filename,".s2p");
fp=fopen(filename,"w");
fprintf(fp,"# GHZ S RI R 50\n");
for (j=2;j<=nhs;j++) {
  freq=(j-1)*rffreq;            /*freq is in GHz now*/
  fprintf(fp,"%e  %e  %e",freq,SDE[j-1][1].r,SDE[j-1][1].i);
  fprintf(fp,"  %e  %e",SDE[j-1][2].r,SDE[j-1][2].i);
  fprintf(fp,"  %e  %e",SDE[j-1][3].r,SDE[j-1][3].i);
  fprintf(fp,"  %e  %e\n",SDE[j-1][4].r,SDE[j-1][4].i);
  }
fclose(fp);
   }
/*****************End of Main******************************************/
/**********************************************************************/

/*****************Subroutines******************************************/
/**********************************************************************/
/*************R-parameter from S-parameter extraction (conversion)**********/
/**********************************************************************/

void Rpa(R, SQ)
fcomplex R[5],SQ[5];
{
fcomplex temp1,NEG,ONE;
NEG.r=-1.0;
NEG.i=0.0;
ONE.r=1.0;
ONE.i=0.0;

R[1]= Cdiv((Csub(Cmul(SQ[2],SQ[3]),Cmul(SQ[1],SQ[4]))),SQ[3]);
R[2]= Cdiv(SQ[1],SQ[3]);
temp1=Cmul(NEG,SQ[4]);
R[3]= Cdiv(temp1,SQ[3]);
R[4]= Cdiv(ONE,SQ[3]);
}

/*********************** End of Rpa Subroutine ***********************/
/*********************************************************************/

/******************** LRM Calibration Subroutine ********************/
/*********************************************************************/
```

```
void LRM( SP, SL, SD, GA1,GA2,GB1,GB2,r1,p,z,openref)
fcomplex SP[5],SL[5],SD[5],GA1,GA2,GB1,GB2,r1,p,openref;
int z;
{
fcomplex R[5],RL[5],IRL[5],RD[5],M[5],X[5],IX[5],Temp[4][4],Temp1[4][4];
fcomplex K1,K2,K3,K4,temp1,temp2,temp3,temp4,T1[5],T2[5];
fcomplex g1,g2,x1,x2,y1,y2,y3,y4,r2,q;
fcomplex a,b,c,D,D1,D2,D3,ONE,TWO,FOUR,NEG;
float phi1,phi2,phi3,phi4,theta1,theta2;
int i,j;
ONE.r=1;ONE.i=0;
TWO.r=2.0;TWO.i=0.0;
FOUR.r=4.0;FOUR.i=0.0;
NEG.r=-1;NEG.i=0;
q=Cdiv(ONE,p);
g1=Cmul(p,p);
g2=Cdiv(ONE,g1);
/*Convert the S-parameters into R-parameters.*/

for (j=1;j<=4;j++) SP[j]=SL[j];
 Rpa(R,SP);
for (j=1;j<=4;j++) RL[j]=R[j];

for (j=1;j<=4;j++) SP[j]=SD[j];
 Rpa(R,SP);
for (j=1;j<=4;j++) RD[j]=R[j];

for (j=1;j<=4;j++) M[j]=RL[j];
/*LRM Subroutine */
K1=Cadd(M[3],Cmul(M[4],GB1));
K2=Cadd(M[1],Cmul(M[2],GB1));
K3=Cadd(M[3],Cmul(M[4],GB2));
K4=Cadd(M[1],Cmul(M[2],GB2));

temp1=Cmul(Cmul(g1,Cmul(r1,r1)),Cmul(Csub(Cmul(K1,K4),Cmul(K2,K3)),Csub(
GA2,GA1)));
temp2=Cmul(Csub(Cmul(GA2,K1),K2),Csub(K4,Cmul(GA1,K3)));
a=Cadd(temp1,temp2);
temp1=Csub(Cmul(K2,K4),Cmul(Cmul(K2,K3),GA2));
temp2=Cmul(Cmul(GA1,K1),Csub(Cmul(GA2,K3),K4));
temp3=Cmul(TWO,r1);
b=Cmul(temp3,Cadd(temp1,temp2));
temp1=Cmul(g2,Cmul(Csub(Cmul(K2,K3),Cmul(K1,K4)),Csub(GA2,GA1)));
temp2=Cmul(Csub(Cmul(GA2,K1),K2),Csub(K4,Cmul(GA1,K3)));
c=Cadd(temp1,Cmul(Cmul(r1,r1),temp2));
x1=Cmul(NEG,Cdiv(b,Cmul(TWO,a)));
x2=Cdiv(Csqrt(Csub(Cmul(b,b),Cmul(FOUR,Cmul(a,c)))),Cmul(TWO,a));
```

```
y1=Cadd(x1,x2);
y2=Csub(x1,x2);
y3=Cdiv(y1,openref);   /* Comparing the phase with an open circuit model
                                            led as a capacitor*/
y4=Cdiv(y2,openref);
phi1=atan2(y1.i,y1.r);
phi2=atan2(y2.i,y2.r);
phi3=atan2(y3.i,y3.r);
phi4=atan2(y4.i,y4.r);
if (phi3>0) {
  theta1=PI-phi3;
 }
else {
  theta1=PI+phi3;
 }
if (phi4>0) {
  theta2=PI-phi4;
 }
else {
  theta2=PI+phi4;
 }
if(theta1>theta2) {
 r2=y1;
printf ("y1 is chosen. |y1|=%f,ANG(y1)=%f;
|y2|=%f,ANG(y2)=%f.\n",20*log(sqrt(y1.r*y1.r+y1.i*y1.i)),phi1*180/PI,20*log(sqrt(
y2.r*y2.r+y2.i*y2.i)),phi2*180/PI);
 }
else {
 r2=y2;
printf ("y2 is chosen. |y1|=%f,ANG(y1)=%f;
|y2|=%f,ANG(y2)=%f.\n",20*log(sqrt(y1.r*y1.r+y1.i*y1.i)),phi1*180/PI,20*log(sqrt(
y2.r*y2.r+y2.i*y2.i)),phi2*180/PI);
 }
Temp[1][1]=r1;
Temp[1][2]=ONE;
Temp[1][3]=Cmul(NEG,Cmul(r1,GA1));
Temp[2][1]=r2;
Temp[2][2]=ONE;
Temp[2][3]=Cmul(NEG,Cmul(r2,GA2));
Temp[3][1]=Cmul(q,K1);
Temp[3][2]=Cmul(K1,Cmul(p,r1));
Temp[3][3]=Cmul(NEG,Cmul(q,K2));


for (i=1;i<=3;i++) {
   for (j=1;j<=3;j++) {
     Temp1[i][j]=Temp[i][j];
   }
```

```
}
Temp1[1][1]=GA1;
Temp1[2][1]=GA2;
Temp1[3][1]=Cmul(K2,Cmul(p,r1));

DET(&D,Temp);
DET(&D1,Temp1);
for (i=1;i<=3;i++) {
  for (j=1;j<=3;j++) {
    Temp1[i][j]=Temp[i][j];
  }
}

Temp1[1][2]=GA1;
Temp1[2][2]=GA2;
Temp1[3][2]=Cmul(K2,Cmul(p,r1));

DET(&D2,Temp1);

for (i=1;i<=3;i++) {
  for (j=1;j<=3;j++) {
    Temp1[i][j]=Temp[i][j];
  }
}
Temp1[1][3]=GA1;
Temp1[2][3]=GA2;
Temp1[3][3]=Cmul(K2,Cmul(p,r1));

DET(&D3,Temp1);
X[1]=Cdiv(D1,D);
X[2]=Cdiv(D2,D);
X[3]=Cdiv(D3,D);
X[4]=ONE;
/* If 1-port, then find S11 and S22. If 2-port then find all the S parameters*/
if (z==1) {
 Inv(X,IX);
 SP[1]=Cdiv(Cadd(Cmul(IX[1],SD[1]),IX[2]),Cadd(Cmul(IX[3],SD[1]),IX[4]));
 SP[2].r=0.0; SP[2].i=0.0;
 SP[3].r=0.0; SP[3].i=0.0;
 Mul(T1,IX,RL);
 SP[4]=Cdiv(Cadd(T1[3],Cmul(T1[4],SD[4])),Cadd(T1[1],Cmul(T1[2],SD[4])));
 SP[4]=Cmul(g2,SP[4]);
 }
else {
 Inv(RL,IRL);
 Inv(X,IX);
 Mul(T1,IX,RD);
 Mul(T2,IRL,X);
```

```
 Mul(R,T1,T2);
 R[2]=Cmul(R[2],p);
 R[1]=Cmul(R[1],Cdiv(ONE,p));
 R[4]=Cmul(R[4],p);
 R[3]=Cmul(R[3],Cdiv(ONE,p));

/*Calculate the de-embedded S-parameters for the 2-port.*/

 SP[1]=Cdiv(R[2],R[4]);
 SP[2]=Cdiv(Csub(Cmul(R[1],R[4]),Cmul(R[2],R[3])),R[4]);
 SP[3]=Cdiv(ONE,R[4]);
 SP[4]=Cdiv(Cmul(NEG,R[3]),R[4]);
  }
}
/*********** End of LRM Calibration Subroutine********************/
/***************************************************************/

/***************End of 2-port NWA program***********************/



/*****************************************************************/
/*Program: matrix.c.  Copy right: Rodwell Group, ECE Dept., UC Santa Barbara.*/
/*****************************************************************/
/* This program implements some basic functions for complex number algebra. */

/***************** Determinant of a complex matrix *********/
void DET(D,C)
fcomplex *D,C[4][4];
{
fcomplex D1,D2,D3;
D1=Cmul(C[1][1],Csub(Cmul(C[2][2],C[3][3]),Cmul(C[3][2],C[2][3])));
D2=Cmul(C[1][2],Csub(Cmul(C[2][1],C[3][3]),Cmul(C[3][1],C[2][3])));
D3=Cmul(C[1][3],Csub(Cmul(C[2][1],C[3][2]),Cmul(C[3][1],C[2][2])));
*D=Cadd(Csub(D1,D2),D3);
/*printf("D.r=%f,D.i=%f\n",(*D).r,(*D).i);*/
}

/********* Matrix inversion subroutine *********************************/

void Inv( A, IA)
fcomplex A[5],IA[5];
{
fcomplex temp,temp1,NEG;
NEG.r=-1;
NEG.i=0.0;

temp=Csub(Cmul(A[1],A[4]),Cmul(A[2],A[3]));
```

```
IA[1]=Cdiv(A[4],temp);
temp1=Cmul(NEG,A[2]);
IA[2]=Cdiv(temp1,temp);
temp1=Cmul(NEG,A[3]);
IA[3]=Cdiv(temp1,temp);
IA[4]=Cdiv(A[1],temp);
}


/******************End of Inv*****************************************/

/***********Matrix Multiplication Subroutine***************************/

void Mul(C, A, B)
fcomplex C[5],A[5],B[5];
{
C[1]=Cadd(Cmul(A[1],B[1]),Cmul(A[2],B[3]));
C[2]=Cadd(Cmul(A[1],B[2]),Cmul(A[2],B[4]));
C[3]=Cadd(Cmul(A[3],B[1]),Cmul(A[4],B[3]));
C[4]=Cadd(Cmul(A[3],B[2]),Cmul(A[4],B[4]));
}

/*************End of Mul*********************************************/


/*********Matrix Transpose Subroutine************************************/

void Tran(A,B)
fcomplex A[5],B[5];
{
A[1]=B[1];
A[2]=B[3];
A[3]=B[2];
A[4]=B[4];
}
/**********************End of Tran*************************************/



/********************************************************************/
/*Program: lockin2d.c.  Copy right: Rodwell Group, ECE Dept., UC Santa Barbara.*/
/********************************************************************/
/* This subroutine acquires the waveforms from the four lock-ins*/
/* By Ruai Yu, 11-18-92*/
/*Revised on 4-9-93 */

void acquire (v)
```

```
double v[5][100][3];
{
int i,j;
char rd[100],file[10],temp[10],wrt[10];
double deltat,tempphase;
printf("nhs=%d\n",nhs);
for (j=1;j<=nhs;j++) {
        for (i=1;i<=4;i++) if (ibwrt(SR530[i],"G24",3) & ERR) err ();
        sprintf(temp,"%d",j); /* IF requency is multiples of 1 KHz */
        strcpy(wrt,"FR");
        strcat(wrt,temp);
        strcat(wrt,"KH");
        len=strlen(wrt);
        if (ibwrt(HP3325,wrt,len) & ERR) err ();
delay (1.0); /* allow the lockin's to lock */
        for (i=1;i<=4;i++) {
                autosen (SR530[i]);
                if (ibwrt(SR530[i],"T1,7",4) & ERR) err ();
                if (ibwrt(SR530[i],"T2,2",4) & ERR) err ();
                }/* Time constant set at 1 second */

/**************** wait for 10 time-constants *****************/
delay (10.0); /* wait for 10 time constants */
for (i=1;i<=4;i++) {
        if (ibwrt(SR530[i],"Q1",2) & ERR) err ();
        if (ibrd(SR530[i],rd,15) & ERR) err ();
        v[i][j][1]=atof(rd);
        printf ("magnitude=%f, ",v[i][j][1]);
        if (i!=stim) {
        if (ibwrt(SR530[stim],"Q2",2) & ERR) err ();
        if (ibrd(SR530[stim],rd,15) & ERR) err ();
        v[stim][j][2]=atof(rd);
        if (ibwrt(SR530[i],"Q2",2) & ERR) err ();
        if (ibrd(SR530[i],rd,15) & ERR) err ();
        v[i][j][2]=atof(rd);
        if (ibwrt(SR530[stim],"Q2",2) & ERR) err ();
        if (ibrd(SR530[stim],rd,15) & ERR) err ();
        tempphase=atof(rd);
        v[i][j][2]=v[i][j][2]-(v[stim][j][2]+tempphase)/2;
        printf ("phase=%f\n",v[i][j][2]);
        } /* end if */
}
v[stim][j][2]=0;
} /* end j */
} /* end acquire */

/*************** subroutine autosen **********************/
/* This subroutine does auto sensitivity for the lock-in's */
```

```
void autosen(SR530)
int SR530;
{
float overload=0;
int i=24,len;
char wrt[100],temp[100],rd[100];

if (ibwrt(SR530,"Y4",2) & ERR) err ();
if (ibrd(SR530,rd,10) & ERR) err ();

if (ibwrt(SR530,"T1,3",4) & ERR) err (); /* set time constant to 10 ms */
if (ibwrt(SR530,"T2,0",4) & ERR) err ();

while ((overload==0) & (i>6)) {
        sprintf(temp,"%d",i);
        strcpy(wrt,"G");
        strcat(wrt,temp);
        len=strlen(wrt);
        if (ibwrt(SR530,wrt,len) & ERR) err ();
        delay (0.1); /*wait for 10 time constants */
        if (ibwrt(SR530,"Y4",2) & ERR) err ();
        if (ibrd(SR530,rd,10) & ERR) err ();
        overload=atof(rd);
        i--;
        }

if (overload==0) i--;
i=i+2;
sprintf(temp,"%d",i);
strcpy(wrt,"G");
strcat(wrt,temp);
len=strlen(wrt);
if (ibwrt(SR530,wrt,len) & ERR) err ();

} /* end subroutine */


/**************** delay by real time **************/
void delay (second)
float second;
{
float deltat=0;
ftime(&tp0);
while (deltat<second) {
ftime(&tp1);
deltat=(tp1.time+tp1.millitm/1000.0)-(tp0.time+tp0.millitm/1000.0);
}
}
```

```
/****************subroutine err****************************/
err()
{
	printf("\nThere was a problem in executing an hpib command.\n");
	exit(0);
}
```

Appendix D. Machine Drawings of the Active Probe System

This appendix includes the machine drawings for the active probe bodies, the strain relieve setup, the probe holders, and the quartz probe tip lapping fixture.

Cable Clamp

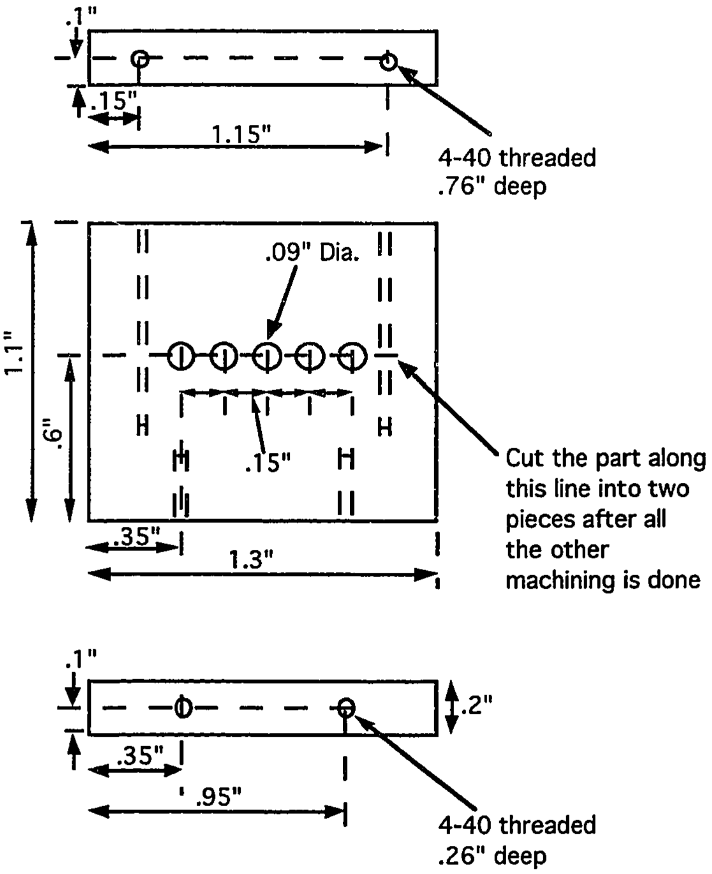

Quantity: 2
Material: Aluminum
Tolerances: .005"
Drawn By: Ruai Yu
Date: 11/29/91
Ext. 8044

Aluminum Sheet

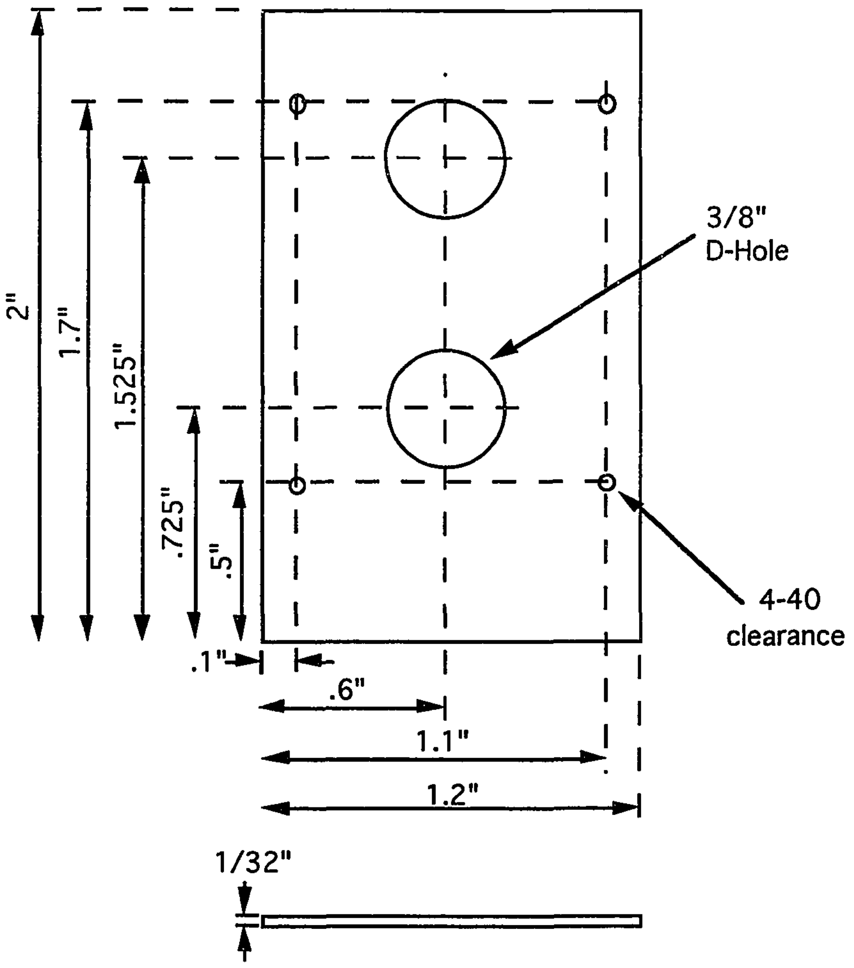

Quantity: 2
Material: Aluminum
Tolerances: .005"
Drawn By: Ruai Yu
Date: 11-29-91
Ext: 8044

K-Feedthrough Panel

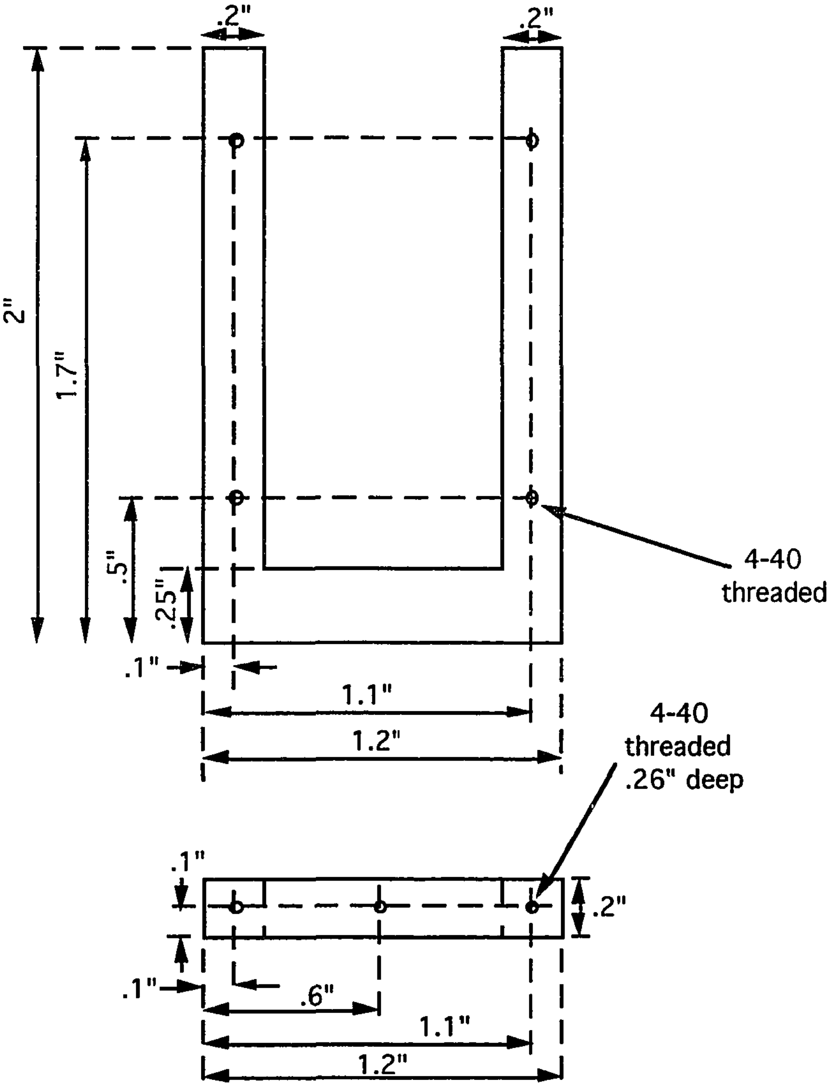

Quantity: 2
Material: Aluminum
Tolerances: .005"
Drawn By: Ruai Yu
Date: 11-19-91
Account #: 8-442530-21721-3
Ext. 8044

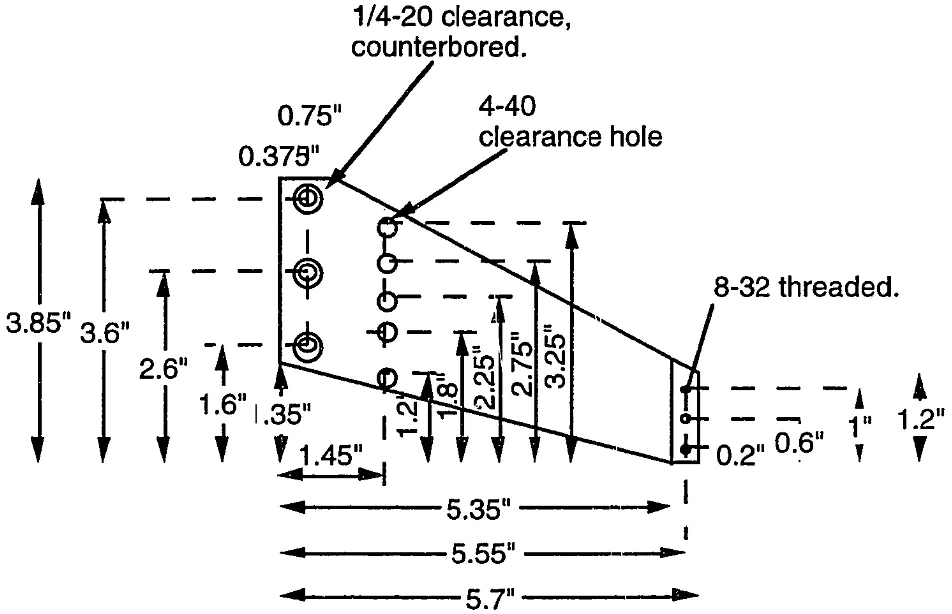

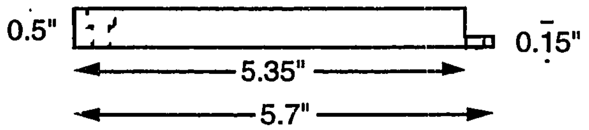

Name: 0° Probe Arm
Quantity: 2
Material: Aluminum
Tolerances: 0.005" unless otherwise specified.
Drawn By: Kirk S. Giboney
Date: 3-2-90
Modified By: Ruai Yu on 11-29-91

Side View

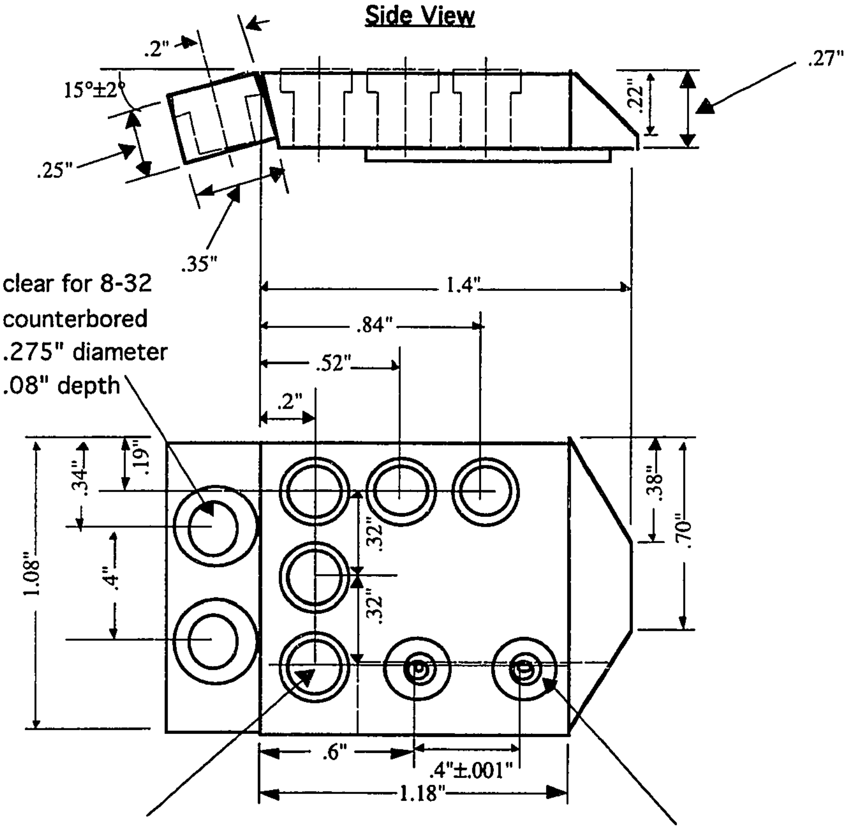

clear for 8-32
counterbored
.275" diameter
.08" depth

counterbored
.2" Diammeter
.04" depth
drill and tap for
190-32 UNF-2A

Top View

machining dimensions
are provided on a
seperate sheet

Name: Active Probe
Material: Brass
Quantity: 4
Tolerances: 0.005" except
where specified
Drawn By: Ruai Yu
Date: 4/29/92

Bottom View

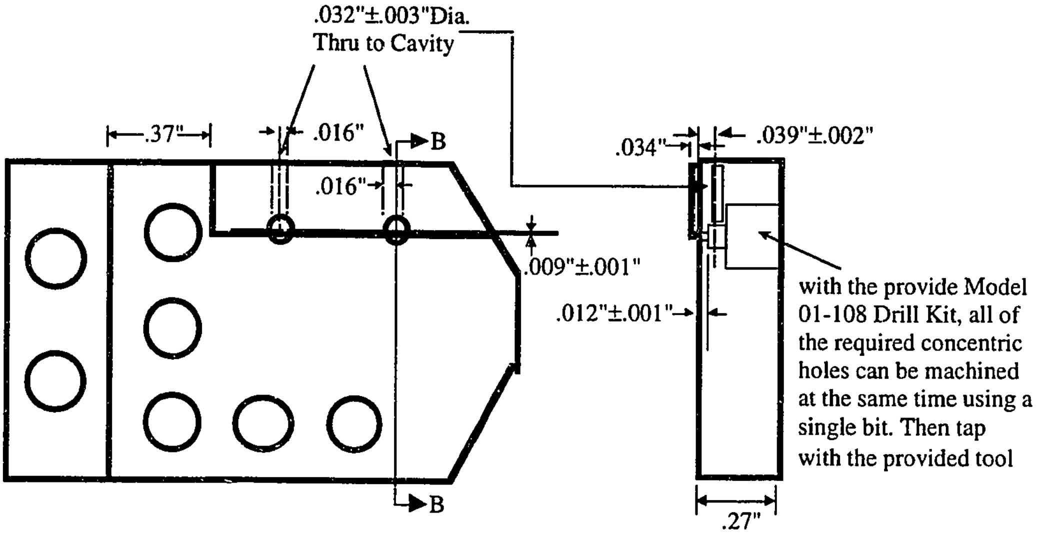

with the provide Model 01-108 Drill Kit, all of the required concentric holes can be machined at the same time using a single bit. Then tap with the provided tool

section BB

Name: Active Probe
Material: Brass
Quantity: 4
Tolerances: 0.005" except
where specified
Drawn By: Ruai Yu
Date: 4/29/92

Probe Modification

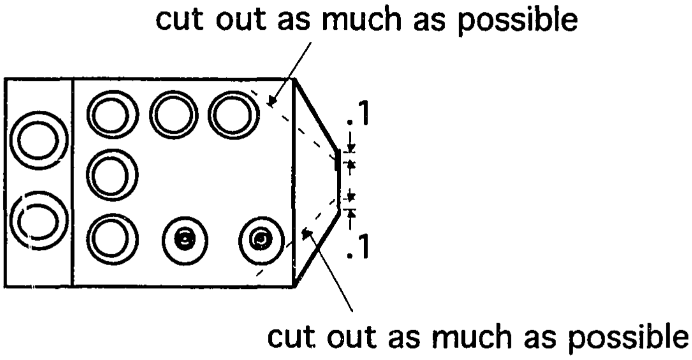

Drawn by: Ruai Yu
Quantity: 2
Date: 7/20/93
Act. #: 58-390
Ext. 8044